Exploring the synthesis and biological properties of Tobramycin-Deferiprone hybrids against *Pseudomonas aeruginosa*

By

Karan Gandhi

A thesis submitted to the Faculty of Graduate Studies of

The University of Manitoba

in partial fulfillment of the requirements of the degree of

Master of Science

Department of Chemistry

University of Manitoba

Winnipeg, Manitoba, Canada

ABSTRACT

Tetracyclines and β-lactam antibiotics are affected by multiple bacterial resistance mechanisms. One of the major resistance pathways is the alteration of the outer membrane and porin channels that prevent the entry of antibiotics into the periplasmic space. To address this issue, iron-chelators have been attached to β-lactam antibiotics to facilitate entry through a siderophore-mediated uptake system and by-pass porin channels such as cefiderocol. Alternatively, potent membrane permeabilizing agents are being developed that can disrupt the outer membrane to increase antibiotics influx, such as tobramycin-based hybrids. Several reports also suggests that the nonselective metal ion binding of tetracycline affects interactions with the target-site. Iron-chelator like deferiprone has been shown to be useful in addressing this non-selectivity by facilitating the binding of tetracycline to the target. Therefore, we hypothesize that we can utilize both properties in a hybrid molecule, i.e., membrane permeabilization and iron-chelation, to overcome tetracycline resistance against Gram-negative bacteria.

This M.Sc. thesis focuses on the development of novel hybrids of tobramycin-deferiprone. Total six hybrids and two control compounds were synthesized and tested against Gram-negative bacteria, especially; *Pseudomonas aeruginosa*, for determining antibacterial properties. Checkerboard assays were also conducted with a panel of antibiotics to determine the synergistic relationship with these hybrids. The results strengthen our hypothesis of linking tobramycin and deferiprone to achieve tetracycline potentiation because the single drug entities (control compounds) are not able to achieve comparable results like our hybrid molecules. Probable mechanism of action could be the internalization effect that renders an increased tetracycline accumulation, allowing it to illicit antimicrobial action with minimal concentration.

ACKNOWLEDGEMENTS

My deepest gratitude to my supervisor Dr. Frank Schweizer for his unwavering support and guidance throughout my M.Sc. program. His expertise in medicinal chemistry helped me to improve my critical problem solving skills and has provided a great boost to my career trajectory. The learnings that I gained by working under Dr. Schweizer's guidance has not been just theoretical but much more practical- and application-based that is going to help me in my future endeavors.

I am also grateful to have very supportive advisory committee members; Dr. George Zhanel and Dr. Nediljko Budisa, who offered me valuable suggestions and helped me to refine both technical and non-technical skills. The committee members have also motivated me to think deeper into some of the unanswered questions of antibiotic drug resistance and generating new ideas to overcome them. Also, I would like to acknowledge our collaborator Dr. Gilbert Arthur for facilitating the cytotoxicity studies in the project.

I have been fortunate to work with postdoctoral fellows; Dr. Shiv Dhiman and Dr. Ayan Mukherjee, who simplified my organic chemistry learning and provided useful tips during the synthesis and purification. Also, I appreciate the helpful and kind nature of Danyel Ramirez, Danzel Ramirez, and Rajat Arora who supported me by sharing their biology skills and for planning the next steps in the project. Thanks to Liam Berry, Joseph Rebizant, and Quinn Neale, for interesting talks on different areas of medicinal chemistry and making a friendly ambience in the lab.

Most importantly, I will be forever in-debt to my parents and teachers for always motivating me to pursue my dreams and supporting me in all walks of life.

TABLE OF CONTENTS

LIST OF TABLES

LIST OF FIGURES

Figure 4-9: Triple combination study using **27c** (8.5 μM) and ceftolozane/tazobactam (CTZ/TAZ) against β-lactamase harboring clinical isolates of *P. aeruginosa* (PA86052)

LIST OF SCHEMES

LIST OF ABBREVIATIONS

δ	chemical shifts in parts per million
Ψ	electric potential
$(Boc)_2O$	boc anhydride
AAC	aminoglycoside acetyltransferase
ANT	aminoglycoside nucleotidyltransferase
APH	aminoglycoside phosphotransferase
CCA	council of canadian academies
CDC	centers for disease control and prevention
$CDCl_3$	deuterated chloroform
CFU	colony forming units
CLSI	clinical and laboratory standards institute
COSY	correlation spectroscopy
DCM	dichloromethane
DEF	deferiprone
DMF	*N, N*-dimethylformamide
DNA	deoxyribonucleic acid
ESI-MS	electrospray ionization mass spectrometry
Et_3N	triethylamine
EUCAST	european committee on antimicrobial susceptibility testing
Exo	exotoxins
HATU	hexafluorophosphate azabenzotriazole tetramethyl uronium
HCl	hydrogen chloride

HMBC	heteronuclear multiple bond correlation
HSQC	heteronuclear single quantum coherence
IFN	interferon
IL	interleukin
J	NMR coupling constant (in hertz)
K_2CO_3	potassium carbonate
MALDI	matrix assisted laser desorption ionization
MDR	multidrug-resistant
MeOD	deuterated methanol
MeOH	methanol
MIC	minimal inhibitory concentration
NAD	nicotinamide adenine dinucleotide
NaN_3	sodium azide
NaOH	sodium hydroxide
NH_4OH	ammonium hydroxide
NLRC4	nod-like receptors family CARD domain-containing protein 4
NMR	nuclear magnetic resonance
$Pd(OH)_2/C$	palladium hydroxide on carbon
Pld	phospholipase D
PMF	proton motive force
ppm	parts per million
RND	resistance-modulation-division
ROS	reactive oxygen species

RT	room temperature
T1SS	type I secretory system
T2SS	type II secretory system
T3SS	type III secretory system
T5SS	type V secretory system
T6SS	type VI secretory system
TBAHS	tetrabutylammonium hydrogen sulfate
TBDMSCl	tert-butyldimethylsilylchloride
TBDT	tonB-dependent transporters
TLR5	toll-like receptors 5
TOB	tobramycin
XDR	extensively drug-resistant

CHAPTER ONE: INTRODUCTION AND BACKGROUND

1. INTRODUCTION

Pseudomonas aeruginosa is a Gram-negative bacterium (Family: *Pseudomonadaceae*) which has a rod-shape structure with a flagellum for its motility (1). Historically, *P. aeruginosa* had retained its position among the top five bacterial infections from 1986-1998 in the United States and the second position in Europe. The annual number of cases in the United States from 2012-2017 has been in the range of 32,600-46,000, and more than 20 cases of carbapenem-resistant *P. aeruginosa* emerged in 2018 (2). With the advent of aggressively rising Gram-negative bacterial infections, the Centers for Disease Control and Prevention (CDC), in 2019, categorized *P. aeruginosa* as a "Serious Threat" (3). The clinical presentations of *P. aeruginosa* involve severe conditions such as ventilator-associated pneumonia, urinary tract infection, intra-abdominal infection, and several others pertaining to eyes, ears, and skin tissues (4). This diversified infection range is backed up by its virulence and ubiquitous features that allow the pathogen to survive in major of the ecological settings. This makes it an opportunistic pathogen for a community spread in immunocompromised patients (1). Its survival in both aerobic and anaerobic (adapted) conditions is because of its robust energy metabolism system, which carries several terminal oxidases and denitrification enzymes that are utilized rationally in varied environmental situations (5).

Structure, Microbiology and Genome

This Gram-negative, asporogenous bacterium, which is intact at 42°C, possesses a cytoplasmic (inner) membrane with a symmetric layer and an asymmetrical outer membrane (1,6). The cytoplasmic membrane is composed of a phospholipid bilayer, and the latter is complemented by two layers, namely, lipopolysaccharide (exterior) and phospholipid (interior), that delivers an obstructed permeability network. Additionally, the exterior layer retains exchanging porins, which

allow the transfer of nutrients through them. They are made of β-sheets with lipophilic amino acids on the outer side while hydrophilic on the inner layer (6). The denitrification enzymes (NO reductase) aids in reducing nitric oxide (released by the human system) to nitrogen, and hence enable them to survive even in anaerobic conditions (5). Aside from this, the pigmented products pyoverdine (yellow-green) offers Fe^{+3} scavenging activity (for its growth), and pyocyanin (blue-green) facilitates the virulence by providing oxidant function (1,4). The biochemical evaluation provides affirmative tests for both citrate and indophenol-oxidase (4).

Its genome consists of 65-67% of cumulative guanine and cytosine content with a circular chromosome alongside numerous plasmids and a large genome of 5.5-7 Mb, which encodes several enzymes. The ubiquity feature is offered by regulatory genes, which makes up to 8% of the genome (1). In this regard, the PAO1 strain of 6.264 Mb genome size reportedly has approximately more than 500 regulatory genes. The diversity attributed by the accessory genome depends on the characteristic distribution of components like plasmids and chromosome-carrying blocks of DNA (7).

1.1 Antimicrobial resistance

The Council of Canadian Academies (CCA), in 2018, reported that approximately 26% of total bacterial infections exhibited antibiotic resistance, which was responsible for 5,400 deaths annually and affecting $2 billion economy. This number can elevate up to 40%, with almost 13,700 deaths per year in 2050, alongside significant economic loss. As a result of such situation, the focus on its prevention and the development of potential antibiotics is dramatically increasing (8). For *Pseudomonas aeruginosa*, the clinical manifestations are serious, and the condition becomes worse due to the emergence of multidrug-resistant strains that can be either *de novo* or acquired by patient-to-patient communication (9). The major risk factors associated with acquiring

multidrug-resistant *P. aeruginosa* can be linked with the prior use of antibiotics and prolonged hospital stays, especially intensive care units (ICUs) (10). This section will discuss in detail about the pathogenesis of *P. aeruginosa*, its resistance pathways, and some of the essential classes of antibiotics whose biological activity has been compromised by Gram-negative bacteria.

1.1.1 Pathogenesis

Pseudomonas aeruginosa progresses sequentially by infecting the human host cells through the release of several virulence factors like adhesins, exotoxins (ExoA, ExoS, ExoU, ExoT, and ExoY), alginate, haemophore, lipopolysaccharide, phospholipase C, phospholipase D, and proteases such as elastase (LasA and LasB) and alkaline protease. They are released from different types of secretory systems like T1SS, T2SS, T3SS, T5SS, and T6SS. Of the five systems; T1SS, T3SS and T6SS are categorized as one-step secretion systems, while T2SS and T5SS are two-step secretion systems. Moreover, the pigmented product pyocyanin is responsible for hindering electron transport mechanism and redox cycling in the host cells. All these factors contribute to specific characteristics for the propagation of infection (1,4).

Adhesins

Type IV pili and flagellum are substantial adhesins in *P. aeruginosa* responsible for binding with the host cell receptors and consequently leading to the intrusion of the released toxins from other systems that causes cell death. This successive mechanism involves interaction with the GalNAcβ1-4Gal receptor in asialoglycolipids. Moreover, for airway epithelium, binding with the apical layer occurs in the influence of N-glycans while for the basolateral, heparan sulfate proteoglycans are involved. In this regard, the function of flagella and type IV pili differs in terms of the type of motility that it offers to *P. aeruginosa* after binding to the host cell. Flagella provides

swimming motility while the later offers twitching motility (11). Flagellin monomers are considered to be essential residues for the formation of the flagellum and are responsible for generating the immune response in humans. They do so by the recognition of flagellin by Toll-like receptors 5 (TLR5) and Nod-like receptors family CARD domain-containing protein 4 (NLRC4) that further elicits an inflammatory response in the purview of pro-inflammatory cytokines production The signaling pathways mediated by TLR5 indicates that the levels of interleukin IL-1β and IL-18 are elevated during the initial stage of infection which mediates inflammatory reactions (12). Distinctively, NLRC4 under the influence of lipopolysaccharide induces such responses even in flagellin-deficient strains through the basal rod component *PscL* of the *P. aeruginosa* (1,12,13).

Type I secretion system (T1SS) and Type III secretion system (T3SS)

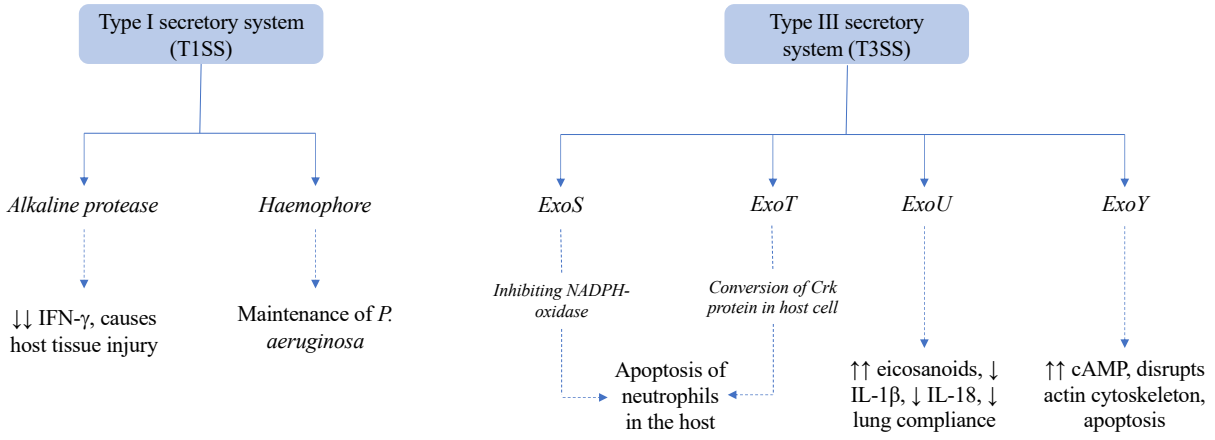

Figure 1-1: Effect of different virulence factors released from Type 1 and type III secretory systems

T1SS is involved in releasing of two major substrates; alkaline protease and haemophore (*Apr* and *Has* secretion system, respectively). Alkaline protease, which is one of the prime virulence factors,

deteriorates interferon-γ (IFN-γ) and causes host tissue injury, while haemophore is a heme acquisition protein responsible for the maintenance of *P. aeruginosa* (**Error! Reference source not found.**). On the other side, T3SS is one of the major secretory systems that release cytotoxins into the human host cells from the cytoplasm of *P. aeruginosa*. These include ExoS, ExoU, ExoT, and ExoY, which are mainly involved in the process of cell death and bacterial spread (Figure 1-1). Here, ExoS and ExoT are responsible for sustaining the *P. aeruginosa* within the host and further promoting neutrophils' apoptosis (13). This sustenance of *P. aeruginosa* within the host is due to the activity of inhibiting the phagocytic NADPH-oxidase by ExoS. Apart from this, ExoU is involved in the programmed necrosis of epithelial cells, macrophages, and neutrophils, which further results in successive infection due to compromised immunity as a result of the lower level of neutrophils. On the contrary, ExoT targets neutrophils through the conversion of Crk protein (present in the host cell) into a cytotoxin and sequentially, exalts the mitochondrial apoptosis. However, the ExoU is activated under the impetus of binding with ubiquitinylated proteins of the human host cells. Additionally, for *P. aeruginosa* releasing excessive ExoU, keratitis and acute pneumonia are the most common clinical inferences. Besides, ExoY acts by disrupting the actin cytoskeleton leading to the elevation in cAMP, which instigates apoptosis sequentially (14).

Type II secretion system (T2SS) and Type V secretion system (T5SS)

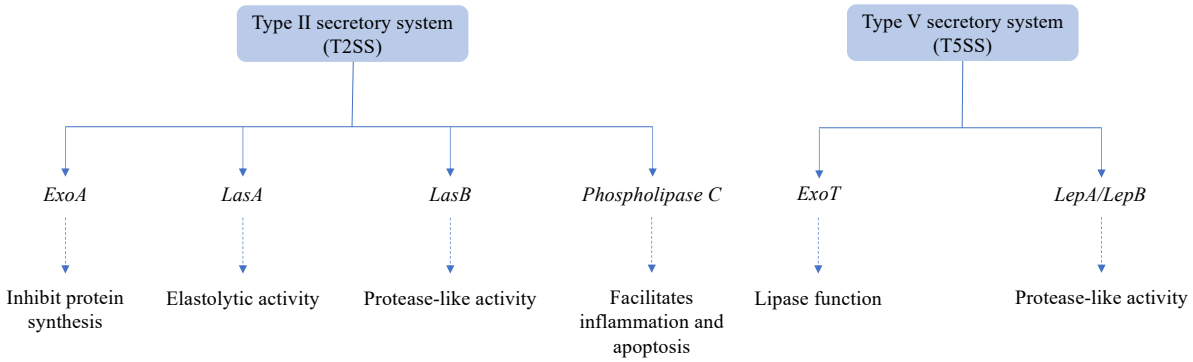

Figure 1-2: Effect of different virulence factors released from Type II and V secretory systems

ExoA and elastase B (LasB) are released from the type II secretory system where ExoA is involved in halting protein synthesis and induces apoptosis (Figure 1-2). Particularly, ExoA binds with α_2-macroglobulin receptors present in the serum of the host. Further, the A subunit gets liberated into the cytoplasm, which transfers adenosine diphosphate-ribose to elongation factor-2 from nicotinamide adenine dinucleotide (NAD), and this offers the protein synthesis inhibitory activity (1). Elastase B, a zinc metalloproteinase (LasB) belonging to the exoproteases category, acts on the extracellular matrix by hydrolysis mechanism and further breaks through the junctions between the endothelial and epithelial layers (1,15). Apart from ExoA and LasB, virulence factor LasA enhances the elastolytic activity, and phospholipase C regulates multiple processes of inflammation and apoptosis. The two-step secretion occurs via periplasm, which then translocates the substrates/products with the help of auto-transporter proteins. With a similar approach, T5SS secretes EstA and LepA/LepB that exhibits a lipase activity and protease-like function, respectively (Figure 1-2) (1).

Type VI secretion system (T6SS) and Reactive oxygen species (ROS)

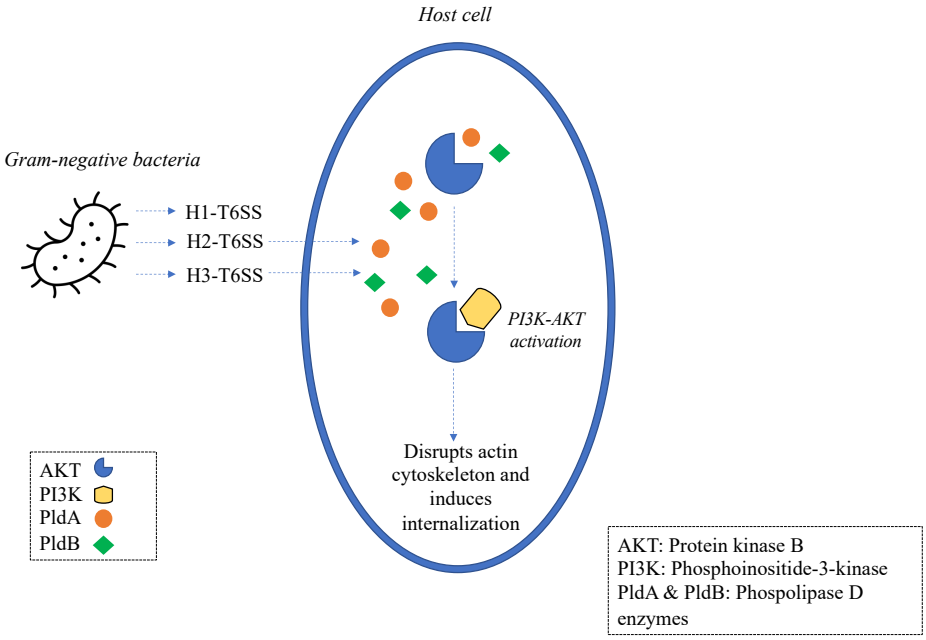

Figure 1-3: Internalization effect of virulence factors released from Type VI secretory system

H1, H2, and H3-T6SS are the three different gene clusters encoded by the T6SS of *P. aeruginosa* are involved in the specific activity of their survival over other bacteria and targeting epithelial cells (Figure 1-3) (1,13). Particularly, phospholipase D enzymes (PldA and PldB) released by H2 and H3-T6SS provide *P. aeruginosa* a competitive edge in the bacterial environment. Both PldA and PldB are reported to have interaction with protein kinase B (also known as AKT) that can eventually trigger the epithelial invasion (13,16). Furthermore, reactive oxygen species (ROS) corroborates host cell injury through various sources such as CYP450, xanthine oxidase, lipopolysaccharide, and pyocyanin. In this regard, pyocyanin oxidizes NADPH, which produces ROS and is suggested to have a connection with mitochondria where pyocyanin gets deposited, and ROS is generated. Such implications can lead to alveolar sac disruption (13).

Quorum sensing (QS) and biofilm formation

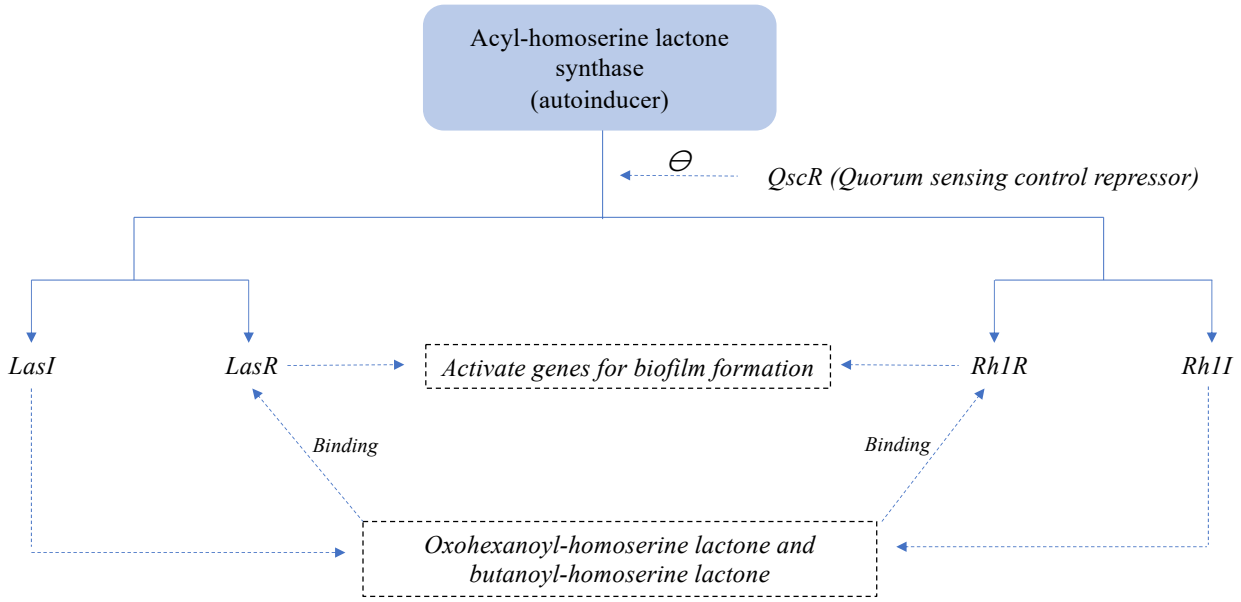

Figure 1-4: Quorum sensing signaling pathway leading to biofilm formation in *P. aeruginosa*

Quorum sensing is a communication system established among the *P. aeruginosa* bacteria for the regulation of gene transcription based on the transfer of chemical messengers produced by them. It is activated only in cases when the population density is higher and involves a complex mechanism between signals and receptors. Acyl-homoserine lactone (AHL), an autoinducer expresses LasR-LasI and RhlR-RhlI systems from which LasI/RhlI is involved in the production of N-oxo-dodecanoyl-homoserine lactone and N-butanoyl-homoserine lactone (Figure 1-4). These signaling molecules further get bound to LasR/RhlR respectively in the presence of significant population density leading to the transcription of genes (1,13). Most importantly, QscR (Quorum sensing control repressor) imparts a substantial role as an anti-activator in QS by subduing the expressions of LasR and RhlR, and hence it bolsters the fact that QscR-deprived strain is excessively virulent (Figure 1-4) (17). The biofilm matrix is developed when an optimal QS magnitude is attained which forms microcolonies within the extracellular matrix. This biofilm matrix forms an enormous network that sustains the bacteria by providing resistance from

antimicrobial agents. The matrix consists of phospholipids, alginate, extracellular DNA, and additionally, the CupA fimbriae provides biofilm formation on solid surfaces while, CupB and CupC fimbriae aids in the microcolony formation (13,18). Here, the alginate has a substantial role in the biofilm networking, and safeguards the bacteria from environmental traumas and host immune responses (1).

1.1.2 Mechanisms of antibiotic resistance

The mechanism of resistance for *P. aeruginosa* consists of three approaches, mainly; intrinsic resistance, adaptive resistance and acquired resistance. Specifically, intrinsic resistance involves lower outer membrane permeability, efflux pumps, and enzymes that inactivate the antibiotics. Adaptive resistance includes biofilm formation and persister cells, while the acquisition of resistance genes, target site alteration, and mutational resistance are classified under acquired mechanism (19,20). This resistance system of *P. aeruginosa* hinders the antibiotic action of drugs from the classes of tetracyclines, fluoroquinolones, cephalosporins, carbapenems, aminoglycosides, and β-lactamase inhibitors (20).

1.1.2.1 Intrinsic antibiotic resistance

Outer membrane permeability: A complex outer membrane layer of *P. aeruginosa* consists of lipopolysaccharide on its exterior face and phospholipid on the inner side. This layer provides a network of permeability barrier for invading substances like antibiotics (6). The outer membrane permeability of *P. aeruginosa* is reported to be 12 to 100 times lower than *Escherichia coli* (21). However, it carries several exchanging porins for the transfer of nutrients and antibiotics (6). The uptake mechanism for different antibiotics varies by either binding with the lipopolysaccharide or passing through the porin channels. For example, β-lactams and fluoroquinolones enter through the different types of porins. These porins are classified as non-specific (OprF), specific (OprB,

OprD, OprE, OprO, and OprP), and gated (OprC and OprH), from which the OprF is highly prevalent. This OprF accounts for the lower permeability of the outer membrane in *P. aeruginosa* due to its closed conformer, which is widespread. Generally, OprF consists of two conformers that form open channels and closed channels, but the conformer offering open channels is rare. They differ in their composition as the open channel conformer consists of only one transmembrane domain, while the closed channel conformer contains two distinctive domains (N-terminal transmembrane and C-terminal periplasm). Moreover, resistance to carbapenems is associated with the absence of OprD, which consists of favorable binding residues for its uptake (20). The impact created on the carbapenems' potency is noticeable in OprD-deficient strains of *P. aeruginosa*, and it was much significant on meropenem compared to other carbapenems. It reflected a major decline in the susceptibility by up to 4 to 32 times in meropenem and 4 to 16 times in imipenem (2).

Efflux-mediated resistance: The resistance-modulation-division (RND) pumps imparts a substantial role in the antibiotic resistance of *P. aeruginosa* as compared to other bacterial efflux pumps from the classes; multidrug and toxic compound extrusion (MATE), major facilitator superfamily (MFS), ATP-binding cassette (APC), and small multidrug resistance (SMR). MexAB-OprM, MexCD-OprJ, MexEF-OprN, and MexXY-OprM, are the sub-classified RND pumps, majorly responsible for the efflux of antibiotics (20). MexAB-OprM covers a wide range of antibiotics efflux, which include fluoroquinolones, β-lactams (cephalosporins like ceftazidime and cefotaxime, carbapenems like meropenem and panipenem), macrolides, and β-lactamase inhibitors. Overexpression of MexAB-OprM pumps due to mutation leads to multidrug-resistant *P. aeruginosa*, and it is mostly found in *nalB, nalC, and nalD* strains (2,20). A recent study revealed seven strains of *P. aeruginosa* contributing to the evasion of carbapenem by MexAB-

OprM pump (22). MexCD-OprJ efflux pump has a narrow coverage of antibiotic efflux, consisting of β-lactams like cefpirome and cefozopran (2,20). The strains expressing extensive MexCD-OprJ pumps contribute to the efflux of aminoglycosides also (2). Apart from these, MexEF-OprN and MexXY-OprM pumps are involved in evading fluoroquinolones and aminoglycosides, respectively. Other pumps from the RND family, which include MexJK-OprM/OprH, MexGHI-OpmD, MexPQ-OpmE, MexMN-OprM, and triABC, are responsible for the efflux of fluoroquinolones, tetracyclines, chloramphenicol, macrolides, and triclosan (2). To overcome the efflux-mediated resistance, phenylalanine-arginyl β-napthylamide (PAβN) has been extensively studied as it exhibits inhibitory activity against efflux pumps and majorly supports fluoroquinolones and β-lactam therapies (23).

Antibiotic-inactivating enzymes: P. aeruginosa releases enzymes that inactivate certain antibiotics as they target the pharmacophore groups. These enzymes include β-lactamases, which cleaves the amide bond in β-lactam antibiotics, and aminoglycoside-modifying enzymes that alter the structural features of amino and glycoside groups. The subclassified groups of β-lactamases differ in terms of the mechanism of action. i.e., the A, C, and D classes of β-lactamases will break the amide bond through the serine site, while class B will require divalent zinc ions. Class A β-lactamases targets carbenicillin, while the class C exhibits resistance activity against cephalosporins. Particularly, *ampC* is the gene involved in the expression of β-lactamases, and it is considered responsible for carbapenem resistance (20). It was also earlier reported that the strains deficient in *ampC* resulted in higher susceptibility of imipenem and panipenem, which validates the resistive role of *ampC* in *P. aeruginosa* (Figure 1-5) (2). Aminoglycoside-modifying enzymes conduct the transfer of phosphoryl group to 2'- and 3'-hydroxyl of kanamycin through aminoglycoside phosphotransferase (APH). The shifting of an acetyl group to the 1 and 6' position

in kanamycin is supported by aminoglycoside acetyltransferase (AAC), while the migration of adenylyl group to 2" and 4' is attributed to aminoglycoside nucleotidyltransferase (ANT) (Figure 1-6) (19,20).

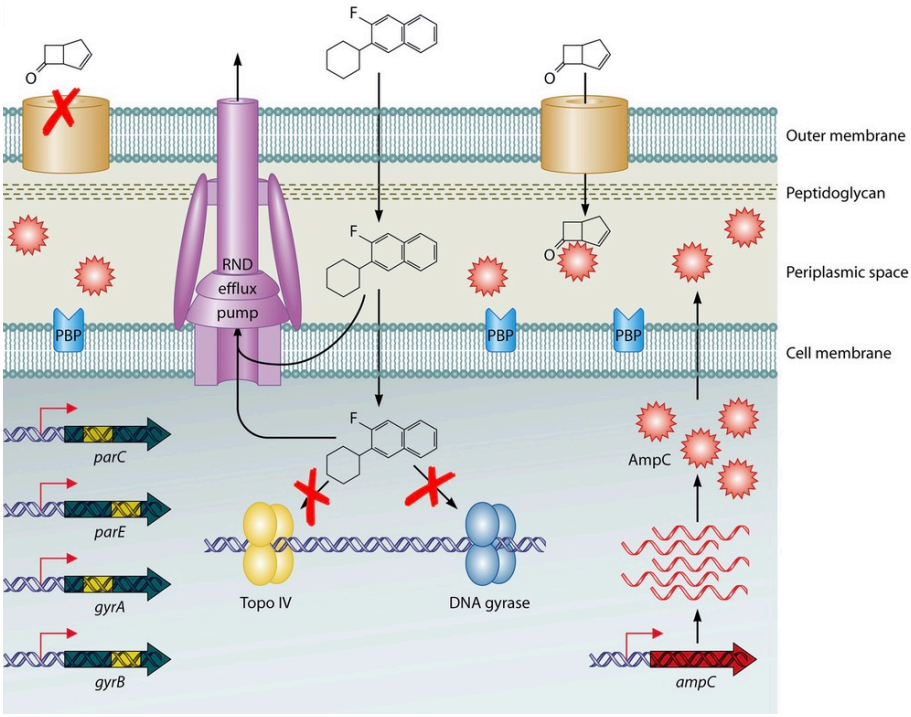

Figure 1-5: Intrinsic resistance in *P. aeruginosa* involving outer membrane permeability, efflux pumps, target-site modifications (topoisomerase IV and DNA gyrase), and antibiotic-inactivating enzymes from *ampC* (2).

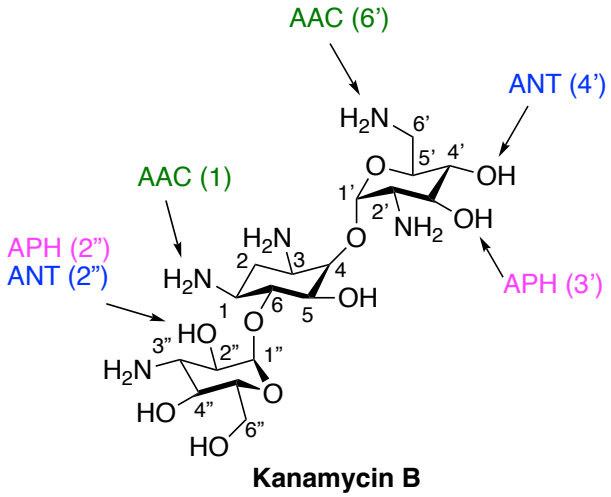

Figure 1-6: Aminoglycoside-modifying enzymes altering the functional groups of kanamycin B

1.1.2.2 Acquired antibiotic resistance

Horizontal gene transfer: The spreading of antibiotic resistance in *P. aeruginosa* is achieved by the horizontal gene transfer, including different mechanisms such as conjugation, transduction, and transformation. Conjugation involves the transfer of plasmid through a pilus structure from the donor cell to the recipient cell, and in this way, the antibiotic resistance genes are acquired by the recipient cells. Transduction and transformation differ from conjugation as there is no such pilus formation. Specifically, transduction occurs when the host DNA packaged into the bacteriophages are transferred to the recipient cell during cell lysis, while transformation occurs by the uptake of genetic materials (from the environment) containing antibiotic resistance features. Generally, these fragments are available from the dead bacterium (20,24). In *P. aeruginosa*, the gene encoding for aminoglycoside-modifying enzymes and β-lactamases is acquired by horizontal gene transfer mechanisms (20).

Mutational resistance: Resistance by mutation can result from overexpression of efflux pumps, enzymes that inactivate antibiotics, and alteration in the porins, resulting in permeability changes. AmpC overexpression is possible by the induction or derepression pathway, and from it, the latter is highly prevalent in *P. aeruginosa*. The induction mechanism (Figure 1-7) is activated under the stimulus of β-lactams and β-lactamase inhibitors, resulting in a significant increase in the the *ampC* gene expression by 100 to 1000 times (2,19). The overexpression of AmpC is coordinated by three proteins; AmpG, AmpD, and AmpR, which are associated with the plasma membrane, peptidoglycan recycling, and regulation of AmpC, respectively (25). In β-lactam induced overexpression of AmpC, the antibiotics strive to bind with the penicillin-binding proteins (PBPs), but the elevated levels of 1,6-anhydromuropeptides of the cell-wall which enters the cytoplasm

through the AmpG, activate sequential steps which resist this binding. Generally, the AmpD (present in the cytoplasm) is responsible for the conversion of 1,6-anhydromuropeptides to free tripeptides and finally to UDP-MurNAc-pentapeptides. In this case, the anhydro-MurNAc-peptides bind to the AmpR, which is attached to the DNA sequences between the *ampR* and *ampC* genes, leading to the overexpression of AmpC (2). Apart from this, derepression (Figure 1-8) is activated by defective *ampD* or during deprived expression of *ampD*. Schmidtke et al. findings identified that *ampDh2* is less important in the overexpression of *ampC* (25). Moreover, the subdued level and deletion of *ampD1, ampDh2,* and *ampDh3* are responsible for accumulating anhydro-MurNAc-peptides on the AmpR, which activates the overexpression of *ampC*, resulting into antibiotic resistance (2,25).

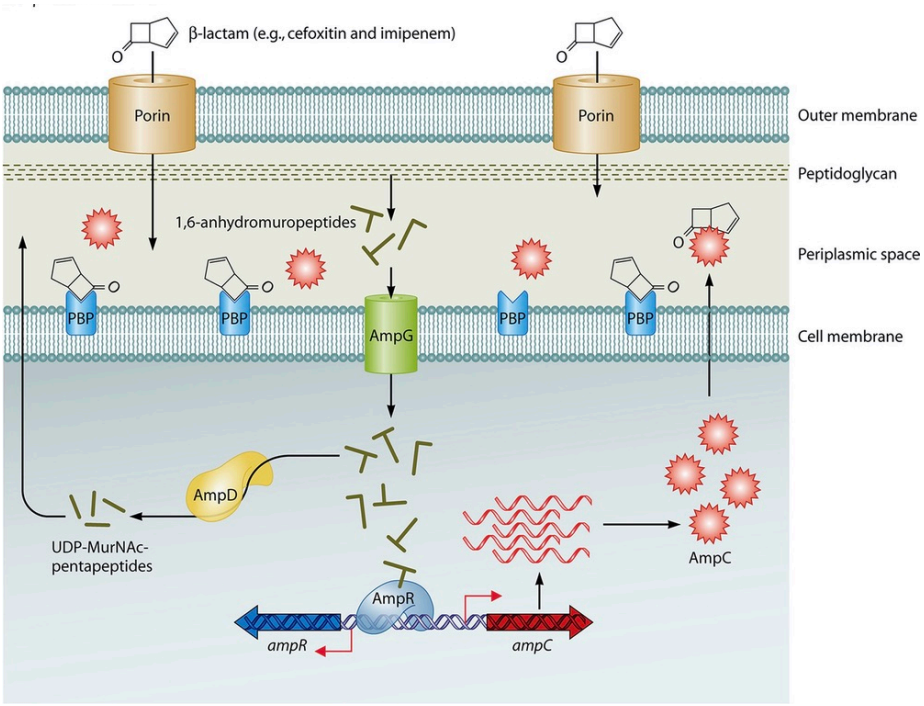

Figure 1-7. β-lactam-induced resistance in *P. aeruginosa* resulting in overexpression of *ampC* that eventually leads to overproduction of β-lactamases (2).

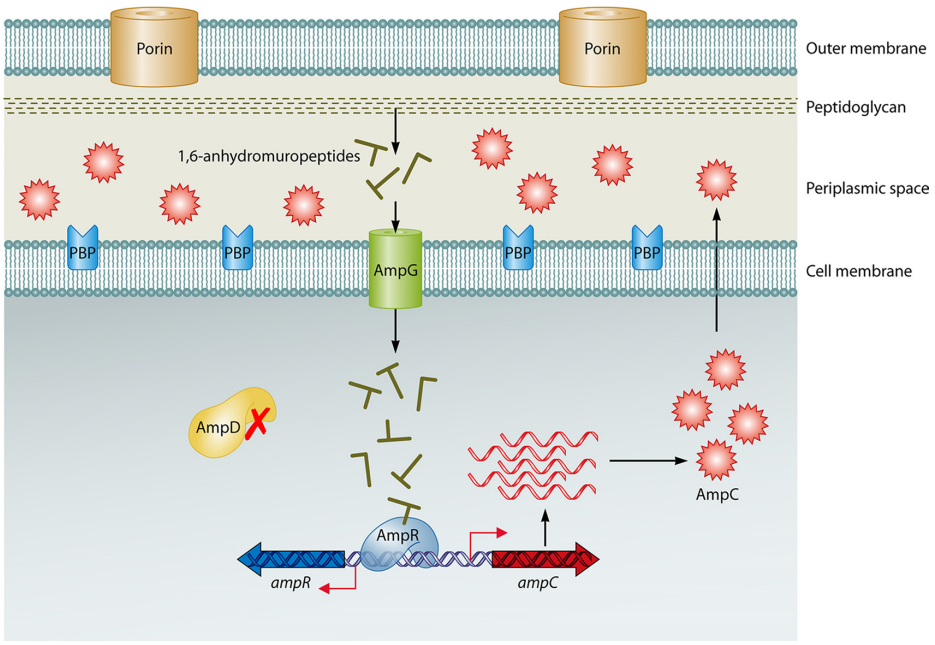

Figure 1-8. AmpD-associated derepression in *P. aeruginosa* resulting in overexpression of *ampC* that eventually leads to overproduction of β-lactamases (2).

1.1.2.3 Adaptive antibiotic resistance

Resistance due to biofilm formation: Biofilm network is an outcome of microcolony formation, which occurs due to the growth and accumulation of bacteria through the quorum sensing mechanism. It is executed only when a threshold population is available, and the matrix consists of phospholipids, alginate, extracellular DNA, and fimbriae, which are responsible for the formation and stability of the biofilm (20). The two regulatory systems involved in the coordination of biofilm formation include GacS/GacA and RetS/LadS, which are activated through phosphorylation by histidine protein kinase (HPK) (20,26). GacS/GacA is responsible for the positive regulation of biofilm formation, while the RetS/LadS deregulate it. A finding supported the role of GacS/GacA that the *P. aeruginosa* deprived of GacA resulted in ten times lower biofilm formation as compared to the wild strain (20). Apart from this, a nucleotide c-di-GMP governs the synthesis of alginate, Psl, and Pel that forms the biofilm and is accountable for its stability (26).

Additionally, the phenotype of *P. aeruginosa* is altered to mucoid in cystic fibrosis patients, which results in overexpression of alginate synthesis, leading to positive regulation of biofilm formation (26). Most importantly, antibiotic resistance to tobramycin, gentamicin, and ciprofloxacin is offered by the *tssC1* gene from the type VI secretory system because of its regulation in biofilm formation (20). Biofilm consists of persister cells that exhibit superior resistance against the antibiotics and these cells are formed under the influence of environmental disturbance. Although it accounts for only 1% of the biofilm, its presence can make the treatment much complicated. Specifically, these persister cells are an outcome of the toxin-antitoxin system, which is involved in the coordination of several cellular processes (20).

Swarming motility-induced adaptive resistance: P. aeruginosa induces rapid swarming motility in the lungs due to its viscous and nitrogen-limiting environment, and this type of motility resists the antibiotic treatment. The resistance caused by swarming motility is influenced by the *prtN* gene upregulation (27).

1.1.3 Tetracyclines and β-lactams

Tetracycline class of drugs are broad-spectrum antimicrobial agents used widely for respiratory infections caused by *Mycoplasma pneumoniae*, *Chlamydia pneumoniae*, and *Chlamydia psittaci*. Apart from these species, it covers several other infectious Gram-positive and Gram-negative pathogens along with its use in non-infectious condition like acne (28). The structure (Figure 1-9) consists of a fused tetracyclic ring possessing different functional groups. Drugs from this class harbor strong metal ion scavenging property due to the presence of keto-enol functional system. However; it lacks selectivity and can bind with Mg^{+2}, Zn^{+2} and Fe^{+3} (29). The entry of tetracyclines in Gram-negative bacteria is usually through the porin channels. Further, its transportation inside the cytoplasmic membrane takes place via δpH in the proton motive force (PMF). Successively,

the interaction of tetracycline with the 30S ribosomal unit of bacteria is favored by a magnesium bridge to inhibit the protein synthesis (28). Glycylcyclines (tigecycline) are the new derivatives under this class possessing less adverse effects as compared to other tetracyclines. Moreover, eravacycline is a recent FDA-approved (2018) fluorocycline drug clinically used in complicated intra-abdominal infections. It exhibited superior biological activity, microorganism coverage (*Klebsiella* spp., *Enterobacter* spp., and *E. coli*), and tolerability in comparison with conventional tetracyclines (30). Resistance to this class is mainly due to the presence of efflux pumps, binding-site mutations, and inactivation by enzymes. Alongside, several ribosomal protection proteins (RPPs) have been identified that are responsible for dissociating the interaction between the target site and ring D of tetracycline (Figure 1-9). However, the RPP resistance mechanism imparts inactivity to only minocycline and doxycycline, while tigecycline and eravacycline are able to retain the antimicrobial properties (31).

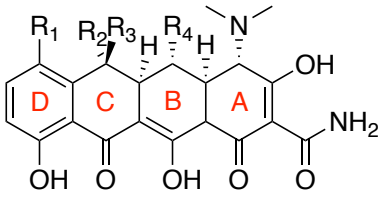

Tetracycline

Figure 1-9: Structure of tetracycline

Besides tetracyclines, β-lactams are considered as a prime choice for prescription as they target a broad-spectrum of Gram-negative bacteria like *P. aeruginosa*, *E. coli, A. baumannii*, *K. pneumoniae*, etc. These are the drugs comprising of a 4-membered β-lactam ring as the core scaffold, and enters the bacterial cell via different porin channels to ultimately interact with the penicillin-binding proteins (PBPs) (32). β-lactam antibiotics can be classified as penicillins (penicillinase-susceptible and -resistant), cephalosporins (narrow and broad spectrum),

carbapenems, and monobactams (Figure 1-10). Penicillins are bactericidal drugs possessing activity against *Streptococcal* and *Staphylococcal* infections, but are prone to enzymatic hydrolysis (penicillinases). Some adjuvants like clavulanic acid and sulbactam are able to overcome this hydrolytic effect on the β-lactam ring, and thus used as combination therapy. Advanced generation cephalosporins like ceftriaxone, cefotaxime, ceftolozane, and ceftazidime are used for conditions like pneumonia, meningitis, and gonorrhea but their effects are compromised due to β-lactamases (33). Specifically, a combination regimen of cephalosporin+β-lactamase inhibitors which include ceftolozane+tazobactam and ceftazidime+avibactam; are suggested in both bloodstream infection and ventilator-associated pneumonia. Loss of porin channels is another important reason for reduced accumulation of these antibiotics which results into loss of activity (34). To overcome the outer membrane issue, β-lactam antibiotics are linked to the catechol (Fe^{+3}-chelating) groups so that the uptake is favored by the siderophore-mediated system e.g; cefiderocol (35).

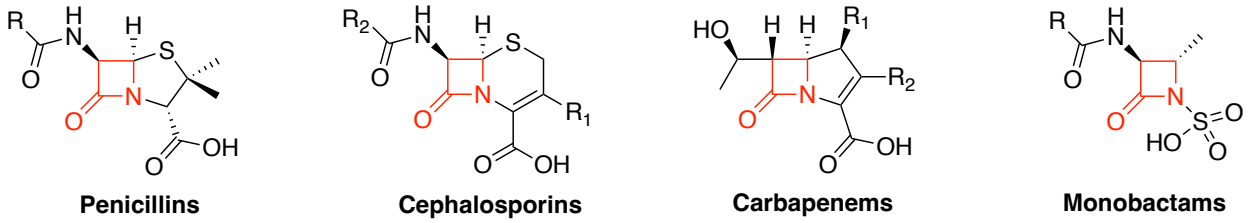

Figure 1-10: Structure of penicillins, cephalosporins, carbapenems, and monobactams

1.2 Contribution of iron-scavengers as antibacterial agents

Iron is important for sustaining various functions such as electron transport, metabolism and DNA synthesis (36). It is also involved in the "Fenton-type" reaction where hydroxyl or lipid radicals are generated in presence of hydrogen peroxide or lipid peroxides. These radicals lead to several disorders such as cancer, respiratory, neurodegenerative and digestive problems (37). To overcome the problem of reactive oxygen species (ROS) and iron overload, iron-chelators gained traction in medicinal chemistry. Iron scavenging molecules usually consists of nitrogen, oxygen, and sulfur

atoms (donors) in their structure which favors Fe^{+2} or Fe^{+3} binding. Most of the nitrogen and sulfur containing structures favor Fe^{+2} chelation over Fe^{+3}. Moreover, such chelators can also bind with other metal ions like Cu^{+2} and Zn^{+2}. Some of the iron chelators and their biological activities reported in the literature are mentioned in the table 1-1 (38).

Name	**Structure**	**Biological activity**
Deferoxamine	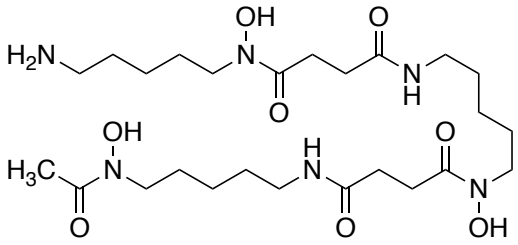	Treatment of thalassemia, sickle-cell anemia, and cancer chemotherapy *(human study)*
Desferrithiocin	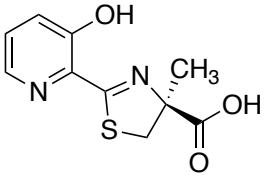	Reduces iron overload *(human study)*
Clioquinol	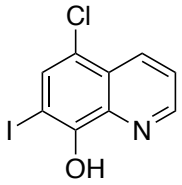	Used in neurodegenerative disorders like Alzheimer and Parkinson *(animal study)*
Deferiprone	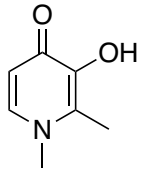	Treatment of thalassemia, sickle-cell anemia, and type-II diabetes *(human study)*

Deferasirox	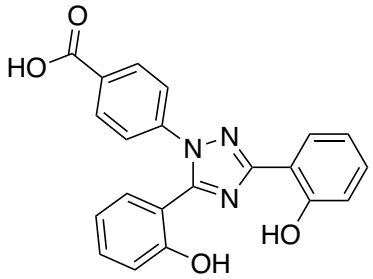	Used in Blackfan-Diamond and myelodysplastic syndrome *(human study)*
Tachpyr	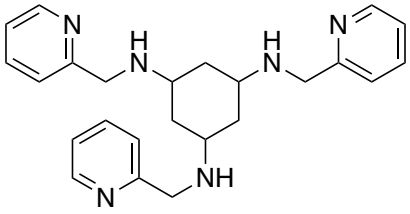	Anticancer properties *(cell-culture study)*
Dexrazoxane	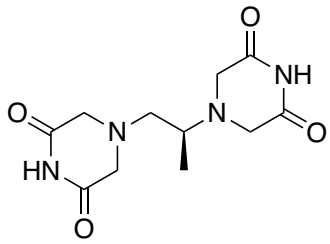	Alleviates cardiotoxicity which is induced by doxorubicin *(human study)*
Triapine	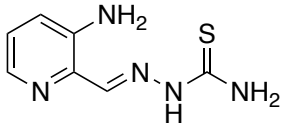	Anticancer properties *(human study)*
Floranol	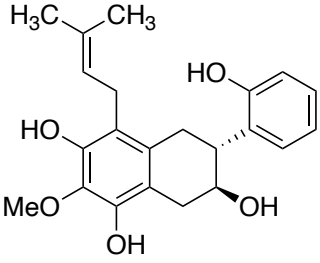	Atherosclerotic effect *(human study)*

Table 1-1. Different types of iron-chelator and their biological properties (38).

1.2.1 Siderophore-mediated uptake mechanism and antibiotics

Specifically, *P. aeruginosa* adopts multiple strategies for the iron uptake which is essential for its survival. One of the most pre-dominant approach is via the production of Fe^{+3}-scavenging

molecules like pyoverdine and pyochelin which are also known as siderophores. Alternatively, the pathogen also sustain its iron requirement through the ferrous iron transport system (Feo) which involves conversion of Fe^{+3} to Fe^{+2}. Fe^{+2} is abundantly available in anaerobic conditions at acidic pH (e.g. cystic fibrosis), and it is transported through the outer membrane of *P. aeruginosa* with the help of FeoA, FeoB, and FeoC proteins (39). Pyoverdines are constructed of 6-12 amino acid sequences eventually hybridized to a chromophore 2,3-diamino-6,7-dihydroxyquinoline. Different types of pyoverdines reported in the literature such as PVDI, PVDII, and PVDIII possesses varied peptide sequences. Apart from iron-chelation, these low-molecular weight molecules released by *P. aeruginosa* is also responsible for the upregulation of virulence factors like exotoxin A and endo-proteinase PrpL (40).

Based on this uptake mechanism, a novel trojan-horse approach has been adopted to design potent antibiotics e.g.; Cefiderocol (Figure 1-11). It has been recently approved for use against Gram-negative bacterial infections such as complicated urinary tract infections (cUTI) and ventilator-associated pneumonia. This hybrid consists of ceftazidime attached to the catechol 2-chloro-3,4-dihdroxybenzoic acid by a two-carbon chain length linker. Some of the distinct features of this molecule includes higher intracellular concentration in the periplasm and superior stability against serine- and metallo-β-lactamases (41). It also exhibited stand-alone antibacterial property against *Escherichia coli* and *K. pneumoniae* with 1 μg/mL and 0.125 μg/mL of MIC_{90} values (42). The catechol moiety in cefiderocol is responsible for the extracellular Fe^{+3}-complexation which mimics the siderophore released by *P. aeruginosa*. This eventually results into increased concentration of cefiderocol in the periplasm of *P. aeruginosa* as these catechol groups are recognized by the iron channels. In the periplasmic space, cefiderocol binds with its penicillin binding protein to illicit protein synthesis inhibitory response (41,43).

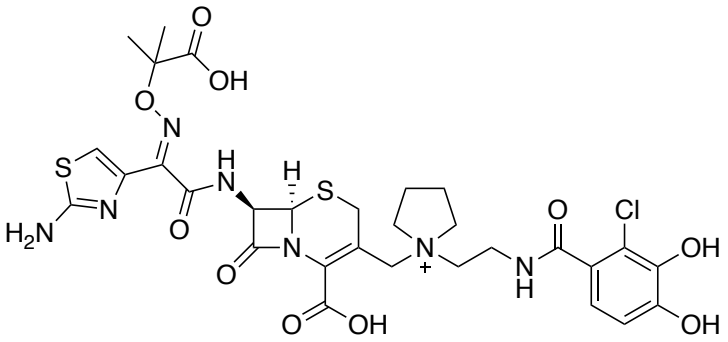

Figure 1-11: Structure of cefiderocol

Apart from cefiderocol, several other siderophore-based conjugates of antibiotics have been developed, and are currently under study for their biological effects and mechanistic approach. Albomycin (Figure 1-12), is one such example of natural siderophore-antibiotic hybrid synthesized by conjugating tri-hydroxamate iron-scavenger and thioribosyl pyrimidine scaffold possessing antimicrobial properties. The mechanism of albomycin uptake can be correlated with siderophore-mediated uptake system in *E. coli* via TonB-dependent transporters (TBDTs) (44,45). TBDTs are located on the outer membrane of *E. coli*, and this uptake process is energy-driven which is derived from the proton motive force. The energy is triggered due to the interaction of these transporters with TonB-ExbB-ExbD protein complex located in the inner membrane (46). Most importantly, the MIC values demonstrated 100-fold superior potency as compared to ampicillin against *E. coli*. Other examples include development of synthetic siderophore-based antibiotic conjugates such as compound **1** and **2** (Figure 1-13). **1** was synthesized by attaching a tripeptide to β-lactam antibiotic, carbacephalosporin and it demonstrated delayed growth of *E. coli* strains because of hindered uptake of iron. Another non-natural siderophore category includes the use of catechol groups. A ureidopenicillin was covalently linked to the catechol moiety (Compound **2**) to achieve 30-60- fold increase in the antibacterial activity when compared with piperacillin against *P. aeruginosa* (44).

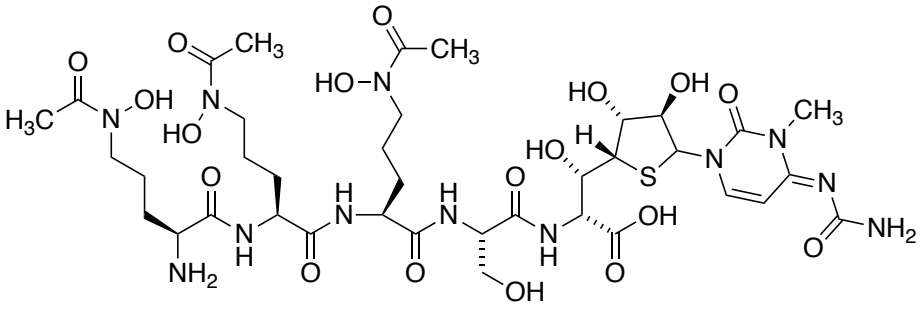

Figure 1-12: Structure of albomycin

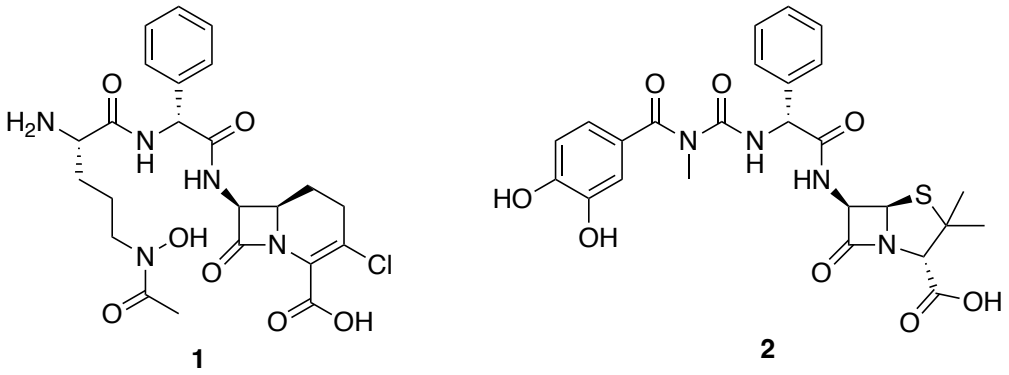

Figure 1-13: Examples of siderophore-based antibiotics

1.2.2 Significance of pyridone analogs in antimicrobial therapy

Pyridone analogs have been reported as Fe^{+3}-scavenging agents and one of its derivative-Deferiprone, is an FDA-approved drug used in thalassemia and sickle-cell anemia (38). Owing to the importance of iron uptake mechanism by Gram-negative bacteria, several pyridone-based iron-chelators are being used to conjugate with antibiotics. For instance, companies like Pfizer and Basilea have developed pyridone hybrids with monocarbams **3** (MC-1), monosulfactams **4** (BAL30072), and monobactams as isoxazole **5** (Figure 1-14). Compound **3** demonstrated very low MIC values against *K. pneumoniae* (0.5 μg/mL), *A. baumannii* (0.5 μg/mL), and *P. aeruginosa* (0.125 μg/mL) while **5** exhibited decent activity against penicillin- and β-lactam-resistant isolates of *P. aeruginosa* (4 μg/mL) (47,48). BAL30072 is a hybrid structure of tigemonam and

dihydropyridone derivative that enters the pathogen via siderophore-uptake route, and eventually binds with the penicillin binding protein to inhibit the protein synthesis. The MIC_{90} values for BAL30072 were reported as 4 μg/mL and 8 μg/mL against *A. baumannii* and *P. aeruginosa*. Moreover, it was found to be at least 8-16- fold potent as compared to aztreonam, imipenem, meropenem, cefepime, ceftazidime, piperacillin-tazobactam, and amoxicillin-clavulanic acid (>32 μg/mL) (49).

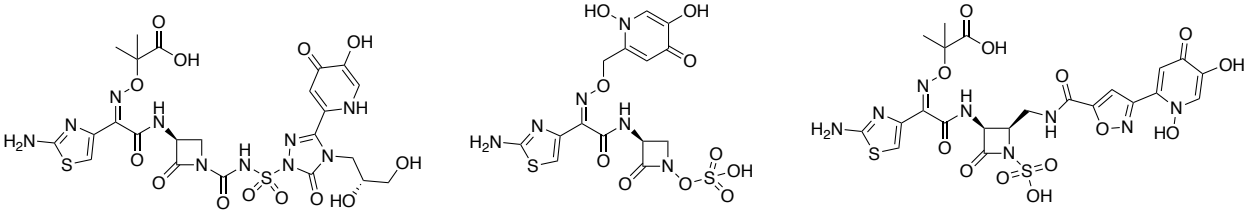

Figure 1-14: Examples of pyridone-based antibiotic conjugates

Apart from hybridization concept, the use of pyridone derivatives have been capitalized in adjuvant therapies as well. Some antibiotics like norfloxacin and doxycycline possesses non-selectivity for metal ion binding, and thus it chelates Fe^{+3} besides Ca^{+2}, Mg^{+2} and Zn^{+2}. This Fe^{+3}-complexation of norfloxacin and doxycycline has resulted into reduced affinity towards the target site (50,51). Zhou et al. synthesized a deferiprone-based iron-chelator **6** (Figure 1-15) for its use in combination with norfloxacin against *E. coli*. A drastic reduction in the bacterial count (7.72 to 2.0 Log_{10} CFU/mL) was observed with the combination therapy when compared with the use of norfloxacin alone (7.72 to 7.52 Log_{10} CFU/mL). It is assumed that the synergistic effect was witnessed by the use of **6** as it can bind with Fe^{+3} selectively, thereby; providing an enhanced binding of norfloxacin to DNA gyrase (target site) (52). Another iron-chelator molecule containing 3 scaffolds of hydroxypyridinone (CP762) **7** (Figure 1-15) was synthesized and studied for its Fe^{+3} binding selectivity (53). Faure et al. reported the use of CP762 along with doxycycline against

cystic fibrosis isolates of *P. aeruginosa*. The activity of doxycycline was potentiated by at least 2-16- fold along with its anti-biofilm property. Also, a significant increase in the bactericidal effect (P<0.01) was noted through the minimum biofilm eradication concentration (MBEC) assay using 2 mg/L doxycycline and 16 mg/L CP762 (51).

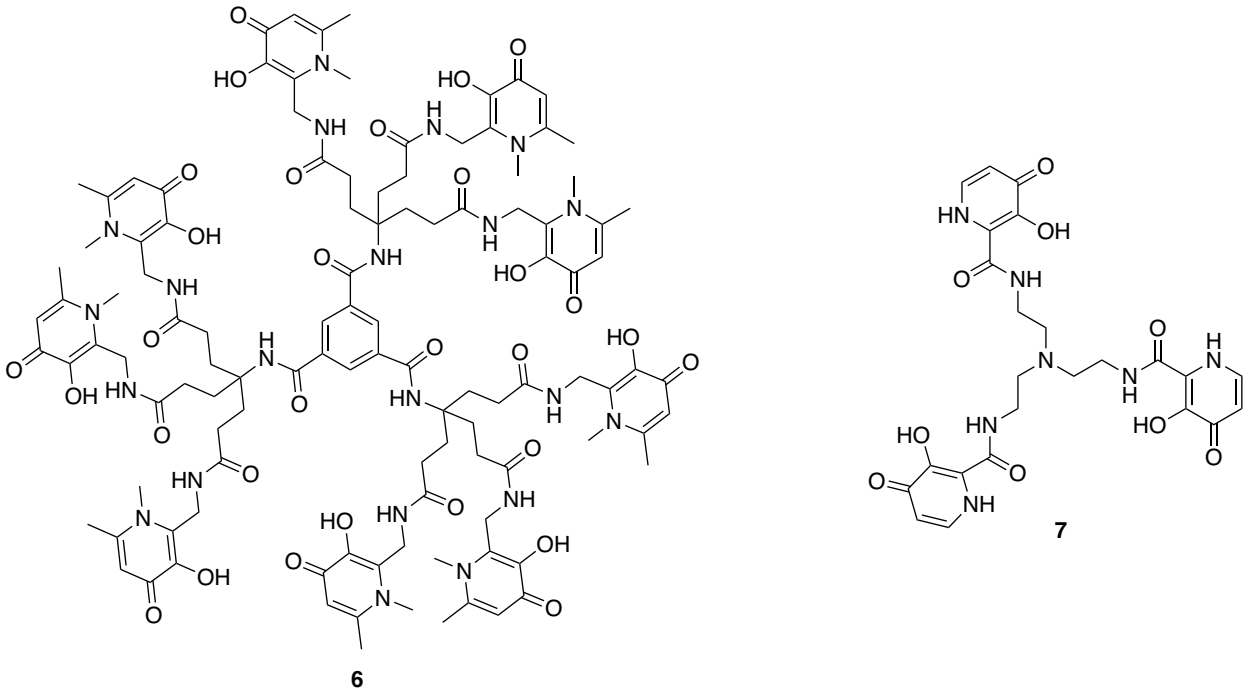

Figure 1-15: Examples of pyridone-based iron-chelators as adjuvants

1.3 Antibiotic Hybrids

The strategy of molecular hybridization links the pharmacophoric groups to form a single molecule that offers a superior pharmacological profile compared to the parent drug. One of the significant properties exhibited by the drug hybrids includes uniform pharmacokinetic, which can further avoid drug delivery and drug-drug interaction issues (54). These hybrid scaffolds are also referred to as multifunctional ligands, dual-acting compounds, and chimeric molecules as they possess a multimodal mechanism of interacting with different targets and eliciting a potential biological response (6).

1.3.1 Designing of antibiotic hybrids

The pharmacophore groups are attached covalently by the linker/tether that can be either stable or cleavable. Linkers that are cleaved by enzymatic reactions can separate pharmacophore entities and these molecules are termed as antibiotic hybrid prodrugs. On the contrary, linkers which remain intact and stable against enzymatic degradation are known as antibiotic hybrid drugs. Properties of the linker can be improved by substitution with aromatic groups or polyethylene glycol-based molecules (6). Specifically, hybrid drugs provide superiority by avoiding the issue of noncomplementary pharmacodynamics and pharmacokinetics, which are the drawbacks in combination therapy containing drugs with different physicochemical characteristics. Generally, an antibiotic hybrid consisting of two pharmacophores will have biological activities related to those active groups; however, the antibiotic action of the hybrid scaffold can be altered due to the covalent linking of these moieties. Additionally, the antibiotics discovered in the past may become susceptive again to the multidrug-resistant bacteria as an outcome of chemical modifications due to hybridization (42).

The challenges of designing antibiotic hybrids are associated with the molecular weight and attachment site of the pharmacophores (42). Out of various drug-likeness rules which include common properties in a drug candidate, the “Lipinski rule of 5” has gained much attention. Drugs like antibiotics usually violate these rules; specifically, the log P and molecular weight limits (55). As the antibiotic hybrids consists of more than one pharmacophoric group, the molecular weight strives to be at a higher-end, which obstructs the drugs’ porin-dependent uptake. Thus, an antibiotic hybrid can include a pharmacophore from the parent drug whose uptake mechanism is independent of the porin channels. For instance, aminoglycoside can be included as one of the active groups. It is taken up by the gram-negative bacteria through a self-promoted uptake mechanism that utilizes

the interaction between the cationic behavior of the aminoglycoside and the anionic nature of the lipopolysaccharide layer in the outer membrane of the bacteria. This uptake is further supported by the energy-dependent phase I (EDPI) and energy-dependent phase II (EDPII) (56). The attachment site is another critical factor while designing the antibiotic hybrids as they can obstruct the biological activity due to hindrance in the pharmacophoric region or by steric overlap due to the proximity of two groups. Such challenges can be avoided by attaching linkers at the auxophore sites, and the compound library should contain hybrid drugs with varying linker size to evaluate the steric effect on the antibiotic action. The term auxophore refers to the groups which are not involved in imparting any biological activity (42).

1.3.1.1 Antibiotic hybrid prodrugs

Designing of antibiotic hybrid prodrugs requires a rational approach for selecting the linker because it should be cleaved under the influence of bacterial enzymes at the site of action. If it is prone to degradation before that stage, then the antibiotic activity will be compromised (6).

Cephalosporin-based hybrids:

An extensive literature study revealed that most antibiotic hybrid prodrugs include β-lactams as one of the pharmacophore groups (42). Its hydrolytic reaction supports the rationale for selecting a β-lactam antibiotic. Specifically, electrons' delocalization occurs to form imine from amine (of β-lactam ring), leading to the displacement of a double bond at C2 and C3 carbon atoms followed by an exit of the leaving group which was previously adjacent to the C3 carbon (Figure 1-16) (57). Based on this study, the linking of two groups appear at the C3 carbon in most of the antibiotic hybrid prodrugs. Hybrid **8** (Figure 1-16) consists of an omadine molecule linked to the C3 carbon of cefamandole derivative. Omadine is a copper chelator that supports the activity of cefamandole derivative (containing β-lactam ring) by protecting it from degradation by β-lactamase.

Cefamandole acts by binding with the penicillin-binding protein and further inhibits the polymerization of disaccharide-peptide units for incorporating it in the growing chain of peptidoglycan (58,59). However, this hybrid **8** had minimal clinical significance owing to the toxic effects of the omadine. With further developments, hybrid **9** (Figure 1-16) was designed to have a desacetylcephalothin with a chloroalanyl dipeptide pharmacophore, which exhibits considerable antibiotic activity with minimal inhibitory concentration (MIC) ranging from 7.05 to 14.1 μg/mL against *E. coli* (42). Chloroalanyl dipeptide functions by downgrading the D-alanine levels through the inactivation of alanine racemase. This enzyme is involved in converting L-alanine to D-alanine to synthesize the peptidoglycan layer, but its inhibition by a dipeptide like chloroalanyl can provide antibiotic action (60). Its antibiotic effect has been supported by a β-lactam ring containing pharmacophore, desacetylcephalothin.

Similarly, NewBiotics Inc. utilized desacetylcephalothin as one pharmacophore and triclosan as another potent group linked to it (hybrid **10,** Figure 1-16). This hybrid was unable to demonstrate biological activity in *P. aeruginosa* due to its complex outer membrane layer and diversified collection of efflux pumps. However, it exhibited potent antibiotic activity against Gram-positive and other Gram-negative bacteria. The potency of this preclinical hybrid candidate (now discontinued) was majorly contributed by triclosan, which targets the enoyl-acyl carrier protein reductase FabI (42).

A cephalosporin-fluoroquinolone hybrid **11** (Figure 1-16), Ro 23-9424, was designed to demonstrate a bactericidal activity against Gram-positive and Gram-negative pathogens. However, this activity was compromised in *P. aeruginosa* due to less permeability through its outer membrane and several efflux pumps. It consisted of desacetylcephalothin connected to the fleroxacin molecule with the help of an ester linkage. This hybrid **11** was cleaved by the enzymatic

degradation of β-lactam ring of desacetylcephalothin followed by fleroxacin's exit. Specifically, fleroxacin targeted DNA gyrase and topoisomerase IV, which halted DNA synthesis (42,61). A broad-spectrum activity was witnessed for Ro 23-9424 against several pathogens resistant to cefotaxime and fleroxacin. Additionally, Beskid et al. conducted an *in-vivo* study of this hybrid **11** (Ro 23-9424) on *K. pneumoniae*, which revealed superior ED_{50} values (13 mg/kg) as compared to cefotaxime (100 mg/kg) and approximately similar to fleroxacin (9 mg/kg). Moreover, the hybrid molecule exhibited superior activity than cefotaxime against *Streptococcus pyogenes*, *E. coli*, and *K. pneumoniae* (62). Despite of this efficacy, the hybrid prodrug **11** (Ro 23-9424) was withdrawn from the clinical trials because of its ability to induce resistance in various bacteria, especially *E. coli*, due to a drastic decline in the uptake of this high molecular weight molecule (764.7 g/mol) and compromised activity of fleroxacin. Moreover, the linker was also cleaved by nonspecific enzymes in humans. Subsequently, this molecule supported the claim that an antibiotic hybrid should contain a pharmacophore with an uptake mechanism independent of porin channels to overcome drug resistance (42).

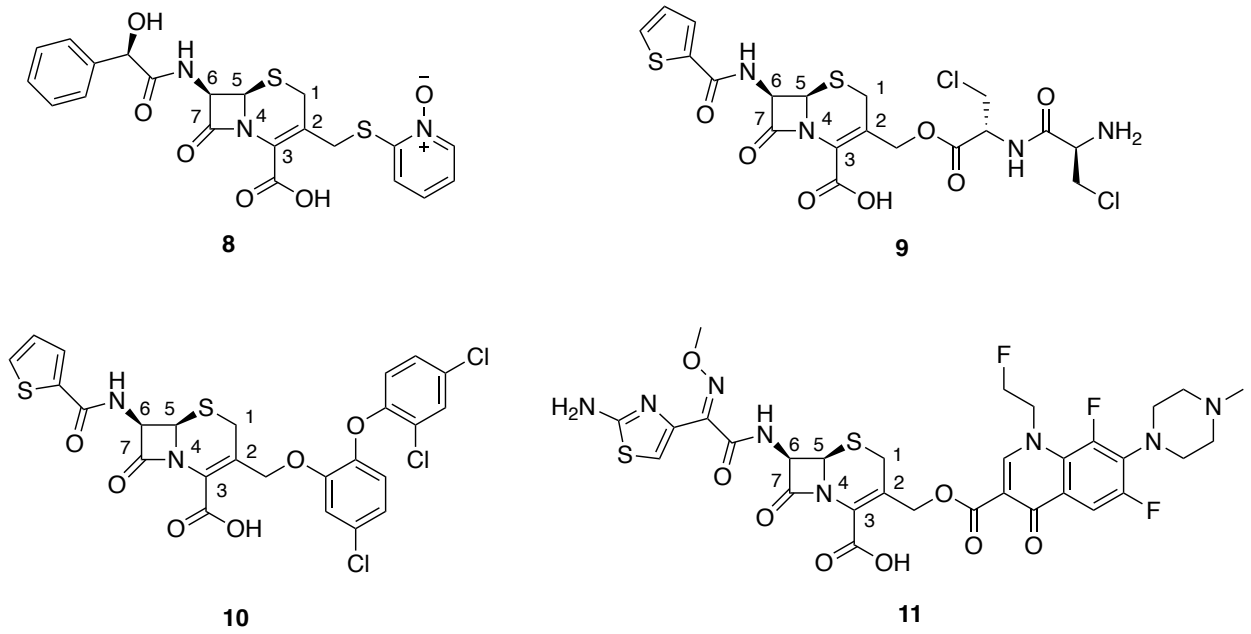

Figure 1-16: Examples of cephalosporin-based hybrids

1.3.2 Membrane permeabilizers as antibacterial agents

Membrane targeting agents act via several pathways like interacting with the lipophilic groups, interfering with the membrane proteins, and modifying the proton motive force (PMF). The target selectivity of these drugs is an important factor which sets them apart from the toxic effects. For instance, the presence of lipopolysaccharide is a distinctive feature for bacteria which is different from phosphatidylcholine of the mammalian cell. Aminoglycosides are the broad-spectrum bactericidal antibiotics widely used against Gram-negative bacteria such as *P. aeruginosa*, *A. baumannii*, and *Enterobacter* species (63). They can be classified as disubstituted 2-deoxystreptamine (amikacin, kanamycin A and B, tobramycin, and gentamicin C_1, C_{1a} and C_2, Figure 1-17 and 1-18) that acts by interacting with 16S and 50S ribosomal unit (64). Among this class, tobramycin has a wide range of clinical significance as it is used in respiratory, intra-abdominal, and complicated urinary tract infections. The ribosomal interaction is evident with

lower concentration (<4 mg/L) of tobramycin while a higher dose (⩾8 mg/L) is required for the disruption of outer membrane in *P. aeruginosa* (65). In the recent years, several multidrug-resistant Gram-negative bacteria have exhibited resistance against aminoglycosides by the modification of outer membrane and presence of aminoglycoside modifying enzymes. Owing to these hurdles, several amphiphilic aminoglycosides have been designed to improve the membrane disruption effect of conventional antibiotics. For example, attachment of hydrophobic moieties at the C-5" position of neomycin **14** and C-6" position of tobramycin **15** (Figure 1-19) favoured the membrane penetration effect over the ribosomal interaction mechanism (64). Other classes of membrane permeabilizers include lipopeptides and cyclopeptides. Lipopetide like daptomycin (Figure 1-20) which is clinically used against *Staphylococcus aureus*, acts by depolarizing the membrane by Ca^{+2}-dependant micelle-formation (63). Polymyxin B (from the cyclopeptide class, Figure 1-21) delocalizes the lipopolysaccharide layer by the displacement of Ca^{+2} and Mg^{+2} ions, and it is widely known as a self-promoted uptake mechanism. Its activity against Gram-negative pathogens is comparable with colistin and has clinical significance for the treatment of ventilator-associated pneumonia (66).

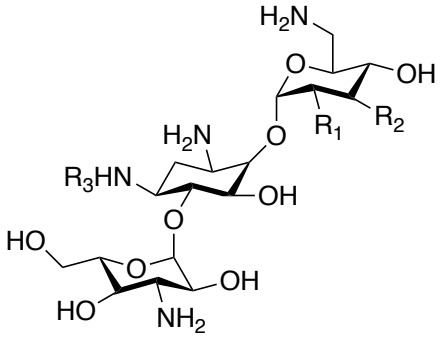

12

Compound	R_1	R_2	R_3
Amikacin	OH	OH	AHB
Kanamycin A	OH	OH	H
Kanamycin B	NH_2	OH	H
Tobramycin	NH_2	H	H

Figure 1-17: Structure of amikacin, kanamycin A and B, and tobramycin

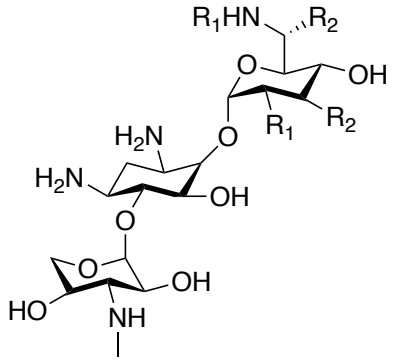

13

Compound	R_1	R_2
Gentamicin C_1	OH	OH
Gentamicin C_2	OH	OH
Gentamicin C_{1a}	NH_2	OH

Figure 1-18: Structure of gentamicin C_1, C_{1a} and C_2

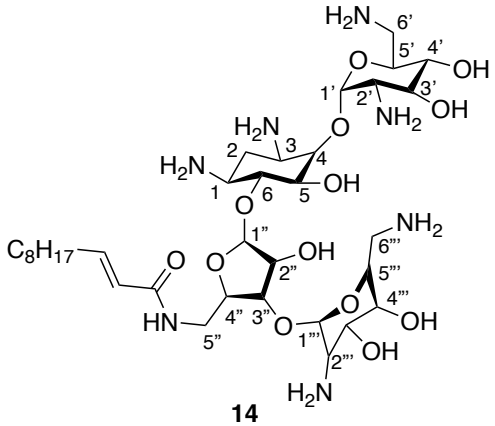

14

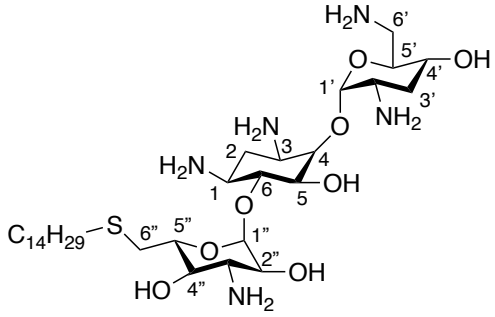

15

Figure 1-19: Examples of amphiphilic aminoglycoside derivatives

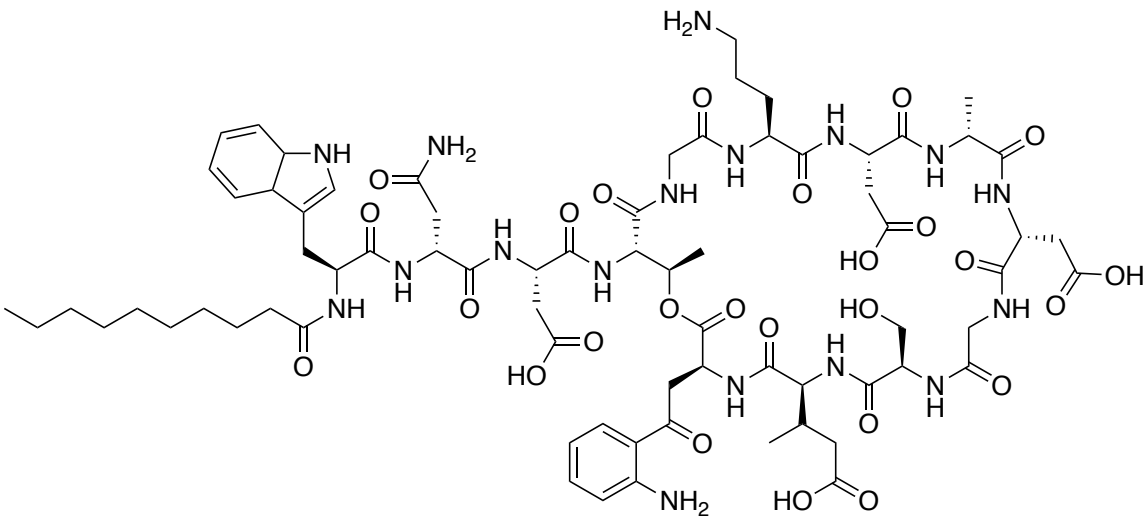

Figure 1-20: Structure of daptomycin

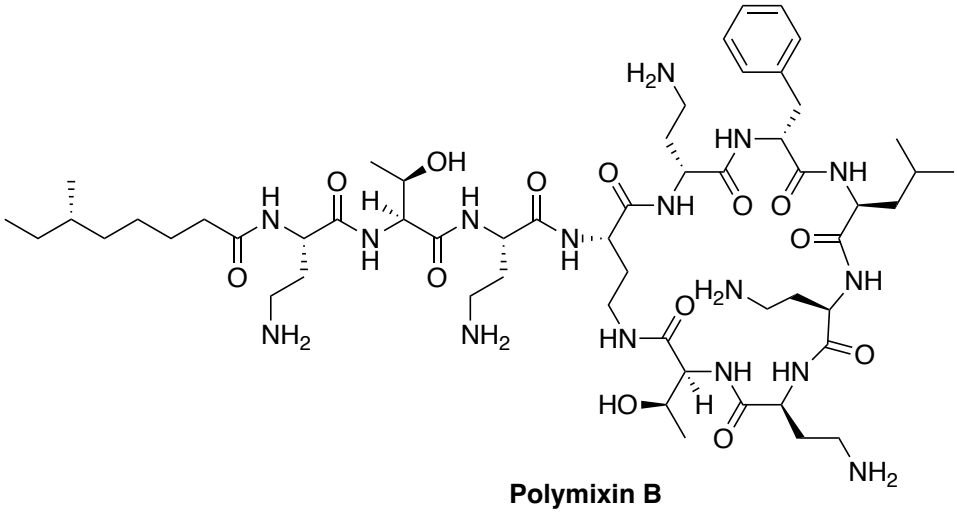

Figure 1-21: Structure of polymyxin B

1.3.3 Advantages of including membrane permeabilizer

Although both the hybrid drugs and prodrugs offer difficulty in the synthesis process, designing hybrid prodrugs is challenging due to its feature of bacterial enzyme-specific degradation. On the contrary, antibiotic hybrids may interact with only one target at a particular time, but it possesses bifunctional characteristics as these hybrids can subsequently interact with another target. For instance, a hybrid drug with the dual inhibitory function of DNA and protein synthesis can be

achieved sequentially, but the multimodal mechanism is still retained. In this regard, various antibiotic hybrids from the literature will be discussed in this section, highlighting their advantages in multidrug-resistant bacterial strains (6).

1.3.3.1 Aminoglycoside-fluoroquinolone hybrids

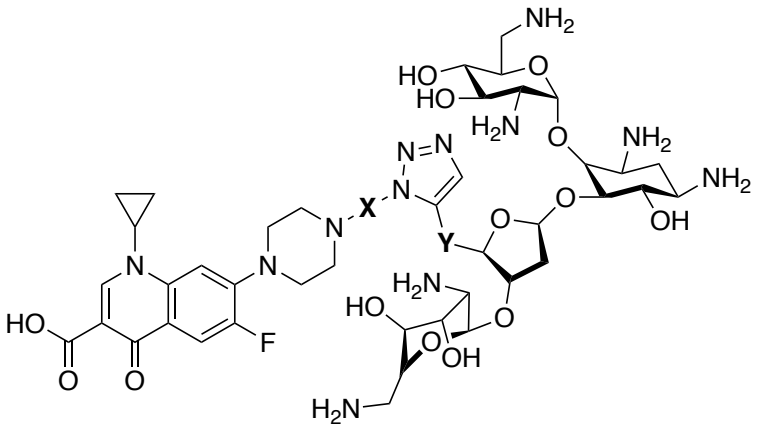

16a-q

Compound	X	Y
12a	-$(CH_2)_2$-	-C_6H_4-NHCO-
12b	-$(CH_2)_3$-	-C_6H_4-NHCO-
12c	-$(CH_2)_4$-	-C_6H_4-NHCO-
12d	-$(CH_2)_5$-	-C_6H_4-NHCO-
12e	-$(CH_2)_6$-	-C_6H_4-NHCO-
12f	-CH_2CH(OH)CH2-	-C_6H_4-NHCO-
12g	-$(CH_2)_2$-O-$(CH_2)_2$-	-C_6H_4-NHCO-
12h	-CH_2-*m*C_6H_4-CH_2-	-C_6H_4-NHCO-
12i	-CH_2-*p*C_6H_4-CH_2-	-C_6H_4-NHCO-
12j	-$(CH_2)_2$-	-CH_2-NHCO-
12k	-$(CH_2)_3$-	-CH_2-NHCO-
12l	-$(CH_2)_5$-	-CH_2-NHCO-
12m	-CH_2CH(OH)CH2-	-CH_2-NHCO-
12n	-$(CH_2)_2$-O-$(CH_2)_2$-	-CH_2-NHCO-
12o	-CH_2-*m*C_6H_4-CH_2-	-CH_2-NHCO-
12p	-CH_2-*p*C_6H_4-CH_2-	-CH_2-NHCO-
12q	-$(CH_2)_2$-	-CH_2-O-CH_2-

Figure 1-22: Example of neomycin B-ciprofloxacin hybrids with varying linkers

Several antibiotic hybrids containing pharmacophores from neomycin B and ciprofloxacin (**16a-q**, Figure 1-22) have been designed previously for potent antibiotic action against Gram-positive

and Gram-negative bacteria. Both the molecules were linked by a 1,2,3- triazole moiety with variable substitution at positions X and Y. These hybrid structures **16a-q** were subjected to *in-vitro* tests against the resistant strains of *E. coli* and methicillin-resistant *S. aureus* (MRSA), which revealed that the neomycin B was 2 to 16-folds less potent than the hybrids against *E. coli*. Similarly, a much higher potency (8 to 128-folds) was witnessed against MRSA by the hybrid structures (67). These hybrids consisted of Neomycin B (aminoglycoside) as one of the active groups, and this can be the reason for its self-promoted uptake mechanism (56). This similar concept was further observed in the development of tobramycin-moxifloxacin hybrids (**17, 18, 19**, Figure 1-23). The C5 position of tobramycin was used to link with the moxifloxacin molecule in hybrid **17**, while C2'' and C6'' positions were considered for hybrid **18** and **19,** respectively. Here, the linkers used in all the three hybrid structures were constant; i.e., C12 aliphatic chain. On further screening these compounds against several resistant strains of *P. aeruginosa*, it was revealed that hybrid **17** was 8-times more potent than the other two because of its linking position. This represents that C2'' and C6'' positions in tobramycin should remain free of any steric hindrance caused by either linking or proximity (16). Specifically, hybrid **17** possessed a MIC value of 1-8 µg/mL against extensively drug-resistant (XDR) and pandrug-resistant (PDR) strains of *P. aeruginosa*. XDR strains involved resistance from cephalosporins, carbapenems, fluoroquinolones, tetracyclines, and aminoglycosides, while the PDR strains were colistin-resistant. A synergistic effect was also observed for the hybrid **17** with ciprofloxacin, moxifloxacin, ceftazidime, and trimethoprim, except tobramycin and gentamicin. This superiority was exhibited due to its enhanced cellular uptake feature under the influence of tobramycin pharmacophore (68).

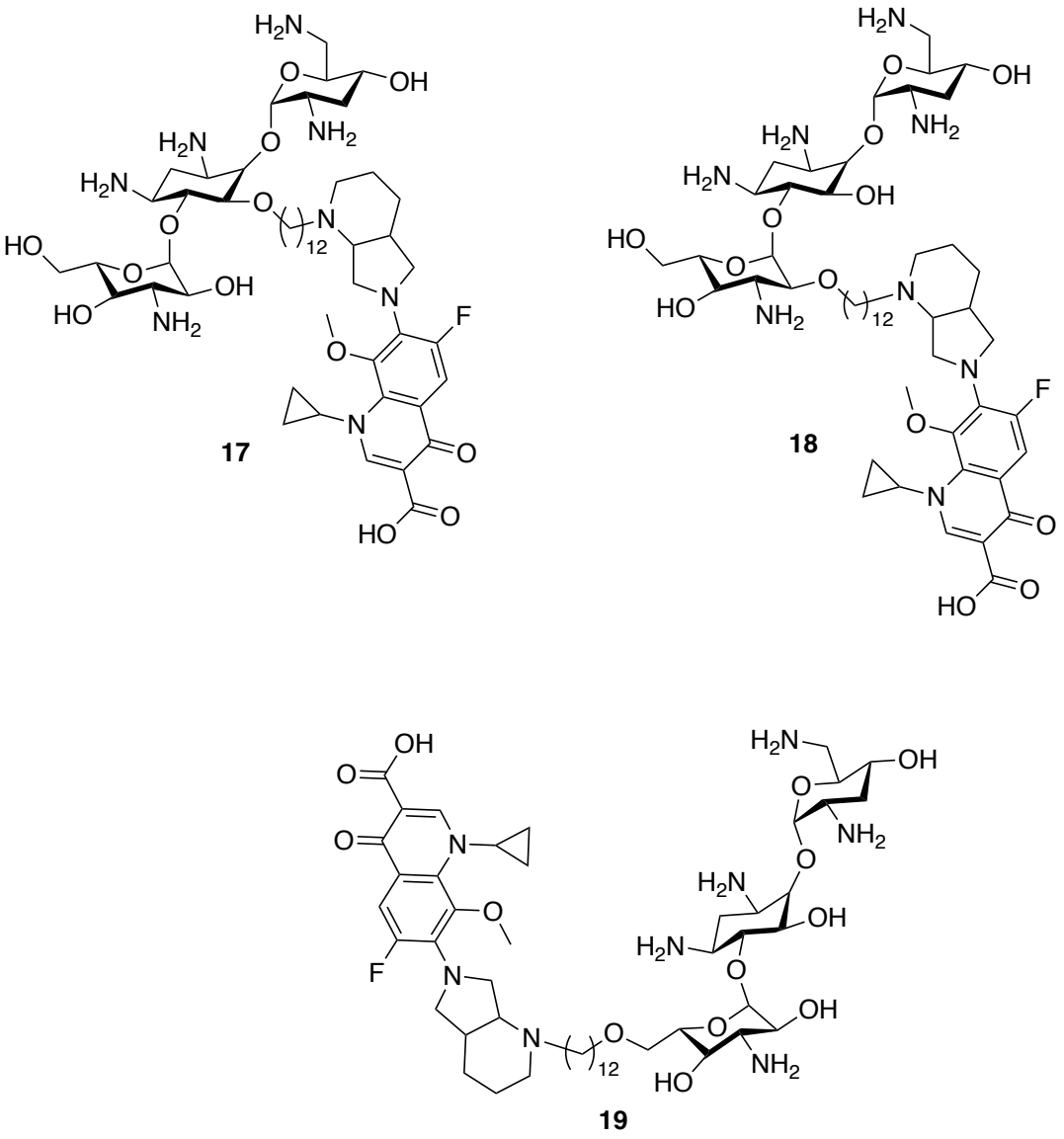

Figure 1-23: Example of tobramycin-moxifloxacin hybrids with different site of attachments

Similar to this hybrid, another bifunctional molecule containing tobramycin and ciprofloxacin (hybrid **20**, Figure 1-24) as pharmacophoric groups were designed recently. Also, its guanidinylated form *g*TOB-CIP hybrid candidate **21** (Figure 1-24) was developed for comparative study. Compound **20** was tested on the carbapenem-resistant *P. aeruginosa*, which deduced that an 8 μM concentration could restore the activity and support the potency of aztreonam, ceftazidime, and imipenem. *g*TOB-CIP also exhibited similar MIC, but the outer-membrane permeabilizing properties were significantly hindered (69).

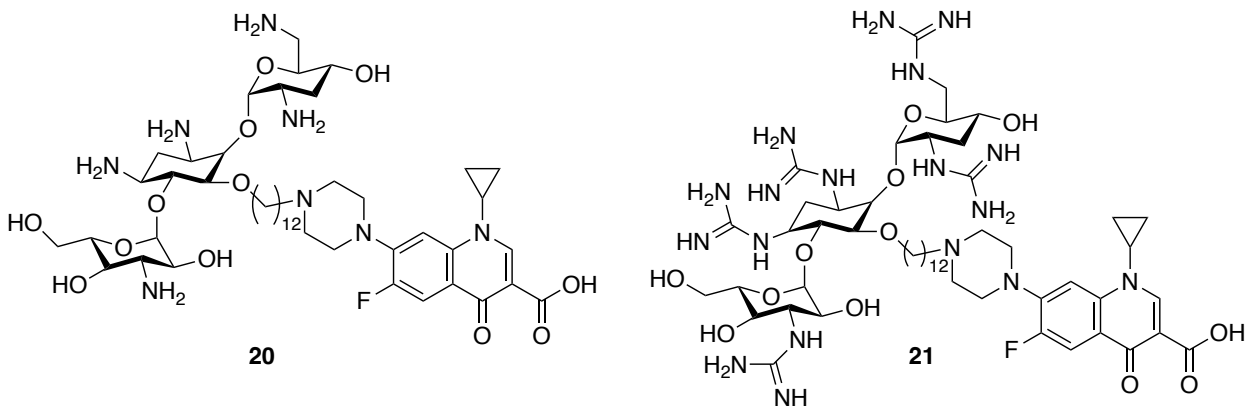

Figure 1-24: Structure of tobramycin-ciprofloxacin and guanidinylated tobramycin-ciprofloxacin hybrids

1.3.3.2 Peptide and peptoid-based antibiotic hybrids

Antimicrobial peptides (AMPs) are proven to be broad-spectrum agents useful in various multidrug-resistant bacterial strains. Deshayes et al. utilized this feature of AMPs to support the aminoglycoside molecules by conjugating penetratin (derived from a short peptide transporter) with tobramycin by an amide bond through a linker (1,2,3- triazole) at the N-terminus of tobramycin. The peptide-antibiotic hybrid **22** (Figure 1-25) exhibited notable MIC value of 6.3 μg/mL against *E. coli* and its membrane activity was considerably better than tobramycin alone. Subsequently, pentobra (hybrid **22**) augmented the drug delivery process in persister cells (70). Another essential hybrid of tobramycin-lysine peptoid (hybrid **23,** Figure 1-25) demonstrated a synergistic effect with other antibiotics against the resistant strains of *P. aeruginosa*, *A. baumannii, E. cloacae,* and *K. pneumoniae*. Most importantly, MICs declined by 32- and 256-times for minocycline and rifampin in the presence of 4 μg/mL of tobramycin-lysine peptoid when tested against wild-type *P. aeruginosa* PAO1 strain. However, no such effect was witnessed for β-lactams, colistin, and aminoglycosides. Mechanistically, both tobramycin and lysine peptoid can permeate through the outer membrane of *P. aeruginosa*, but most importantly; the lysine peptoid

carries out the depolarization of the inner membrane. The swimming motility of *P. aeruginosa*, usually found in cystic fibrosis patients, was also inhibited by this hybrid **23** along with considerably lower levels of ovine erythrocyte hemolysis (42).

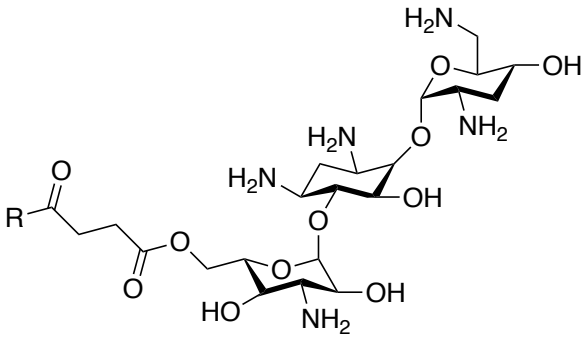

22

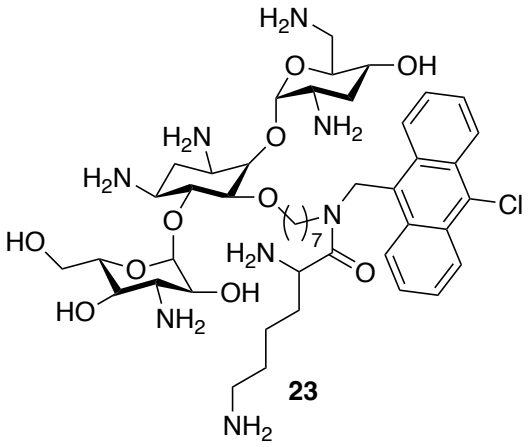

23

Figure 1-25: Examples of peptide- and peptoid-based antibiotic hybrids

1.4 Methods for evaluating biological activity

Several lead compounds are developed globally and require biological evaluation before reaching clinical trials. These techniques proposed in the past mainly include dilution and diffusion methods. With further developments for obtaining advanced data, methods such as time-kill curves, checkerboard assay, and larvae model have been established. This section particularly focuses on the use of laboratory techniques for the determination of MIC values and synergistic effect with other antibiotics (71). Additionally, these antibiotics offer toxic effects due to non-specific interactions, and thus, a critical screening is essential for finding a safe and potential drug candidate. The toxicity studies performed using methods such as larvae model and mammalian cell assay have been discussed below (72–74).

1.4.1 Dilution methods

It is considered one of the most reliable techniques for determining antibiotics' efficacy quantitatively in terms of minimum inhibitory concentration (MIC). MIC is the lowest

concentration of antibiotics that can elicit a biological response by inhibiting the bacterial growth, usually measured in μg/mL or mg/L. The protocols for testing and standards are published by the Clinical and Laboratory Standards Institute (CLSI) and the European Committee on Antimicrobial Susceptibility Testing (EUCAST). Moreover, the MIC values can be correlated for qualitative estimation with categories such as susceptible, intermediate, and resistant. If the MIC value is in a lower concentration than the recommended dose of the antibiotic, it is known as susceptible, while the term resistant is assigned when the MIC value is higher than the concentration required to achieve therapeutic effects. Additionally, the strategy of differentiating the susceptible and resistant bacterial species based on MIC is known as a breakpoint, and it is individualistic for the specific bacterial strain and the antibiotic candidate being tested. These breakpoints depend on several factors related to the antibiotics, bacterial species, and clinical outcomes (75). Dilution methods can be performed in agar and broth using petri dishes and test tubes/microplates, respectively, and the results are often used as a reference for comparing the performance of other methods for antibiotic assays (75,76).

1.4.1.1 Broth dilution method

This method utilizes a two-fold microdilution of antibiotic drug in a 96-well microtiter plate. The bacterial culture solution of 0.5 McFarland standard is made with saline and it is used for preparing the inoculum with the cation-adjusted mueller-hinton broth (CAMHB) in 1:50 dilution ratio. The adjuvants/antibiotics are tested with twice the desired concentration and incubated for 18 h at 37°C. The MIC is determined as the least concentration of drug required to inhibit the bacterial growth in a particular well. In this research, we have used EMax Plus microplate reader (Molecular Devices, Sunnyvale, CA, USA) to determine the growth/no growth of bacteria for estimating the MIC value (77).

1.4.2 Checkerboard assay

Determination of synergistic, additive, or antagonistic effects for a combination of antibiotics can be performed by the checkerboard method. This assay can be conducted using a 96-well microtiter plate and by preparing serial two-fold dilution antibiotic samples (to be evaluated). Bacterial culture is inoculated with a 0.5 McFarland turbidity standard and is diluted in 50µL of Muller-Hinton broth in the wells to achieve $5*10^5$ CFU/ml inocula. One of the antibiotics is diluted along the X-axis, while the other through the Y-axis of the plate, followed by incubation as per suitable conditions (Figure 1-26). Successively, fractional inhibitory concentration indices are calculated for the antibiotic combinations using the formula:

$$\Sigma\text{FIC} = \text{FIC of agent A} + \text{FIC of agent B}$$

$$\text{FIC of agent A} = \frac{\text{MIC of agent A in combination}}{\text{MIC of agent A alone}}$$

$$\text{FIC of agent B} = \frac{\text{MIC of agent B in combination}}{\text{MIC of agent B alone}}$$

A fractional inhibitory concentration index (FICI) of ≤0.5, 0.5 to ≤4, and >4 correlate with the synergistic, additive, and antagonistic effect of the antibiotic combination (78).

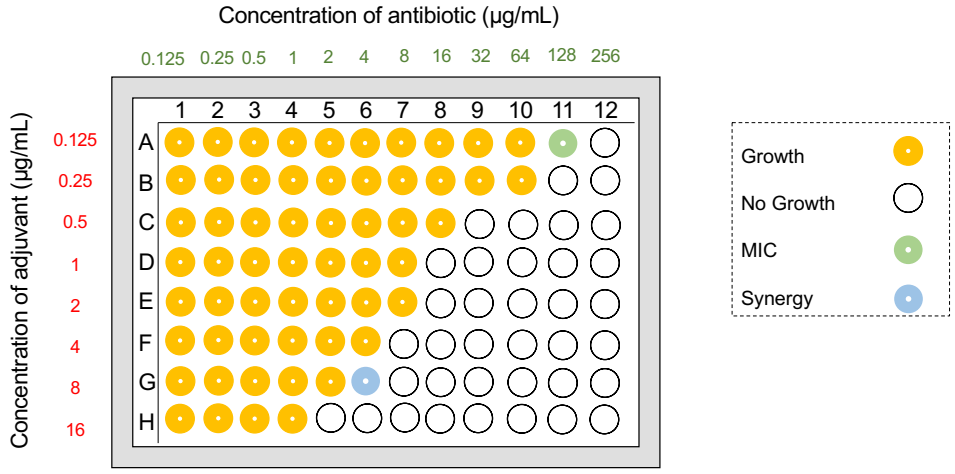

Figure 1-26. Example of checkerboard assay for determining synergy between adjuvant and antibiotic. Recreated with reference to Emery Pharma (79).

1.4.3 Toxicity study

The toxic effects of antibacterial agents range from CNS to cardiac tissues, and its evaluation is an extrapolation of antibiotic susceptibility testing. The larvae model has been widely used for determining the LD_{50} values, which signify the dose of antibiotics to kill 50% of larvae under study. The compounds are injected intraperitoneally at a specific concentration, and the mortality is observed for 5 days. If three or more (out of five) larvae is sacrificed, the dose is reassured by conducting the same test again. However, if three or more larvae survive the test, a higher dose of antibiotic is tested. Once a 60% mortality rate is observed, the test is performed again for the confirmation of a lethal dose of antibiotic (73).

Secondly, mammalian cell toxicity assay is a widely used approach for the assessment of antibiotics for toxicity profiles. Different cell-lines such as human hepatoma cell line (HepG2) and human embryonic kidney (HEK293) cell line are grown in Dulbecco's modified eagle's media (DMEM) along with 10% fetal bovine serum (FBS) in a humidified 5% atmospheric CO_2 incubator at 37°C. Further, a 96-well plate is filled with equal number of cancer cells (5000-HEK293 and 8000-HepG2) in media (50 μL). However, the two blank wells contain only media (50 μL) except the cancer cells for the fluorescent viability assay. Following the suitable incubation conditions, the antibiotics (50 μL) are added to each well with the desired concentration (0-200 μM) to assess the cell viability. 10% PrestoBlue reagent is used for treating the cells after the incubation period, and the absorbance reading is taken at suitable wavelengths (540/590 nm) using the plate reader. Based on this approach, cell viability can be estimated at particular concentration of antibiotic by subtracting the blank from each readings (80).

CHAPTER TWO

2. THESIS OBJECTIVE

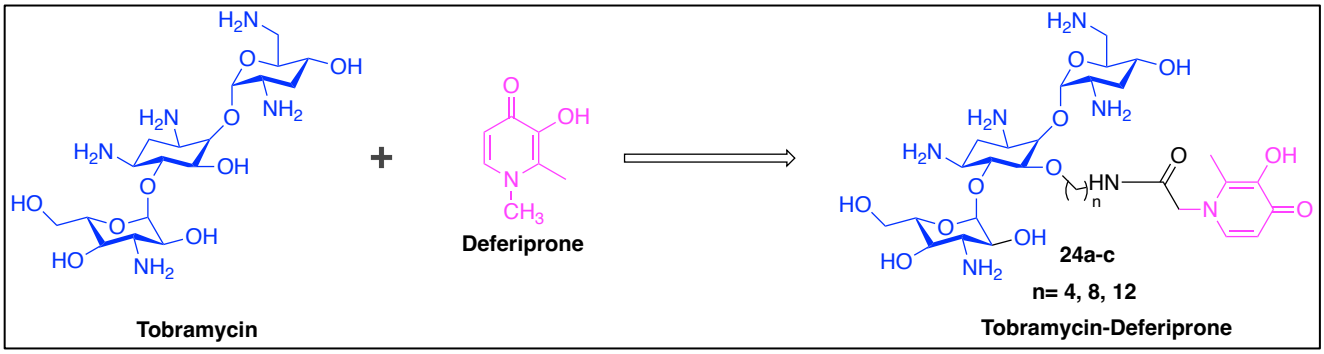

Figure 2-1: Designing of target structure; tobramycin-deferiprone

On the basis of evidences provided in chapter **1.2.2** and **1.3.2**, we were interested in studying the biological properties of tobramycin-deferiprone (TOB-C_n-DEF) hybrid molecules by linking them together.

The aim of this research is to examine the following:

1. Synthesis of TOB-C_n-DEF conjugates and investigating its antibacterial properties against wild-type and multidrug-resistant (MDR) Gram-negative bacteria.
2. Exploring the synergistic effect of these molecules in combination with FDA-approved antibiotics.
3. Analyzing cytotoxicity of TOB-C_n-DEF hybrids against HEK293 and HepG2 cell-lines.

Furthermore, to understand the significance of linking both the scaffolds; control compounds like TOB-C_n-linker and DEF-C_n-linker were inspected. To accomplish this, we pursued the following steps:

1. Synthesizing both the control compounds and evaluating their antibacterial/synergistic effect with a panel of antibiotics against wild-type and multidrug-resistant (MDR) Gram-negative bacteria.

2. Comparison of synergistic pattern of TOB-C_n-DEF vs control compounds.

All the molecules were characterized using NMR and mass spectrometry before conducting any microbiological testing such as antibacterial activity and checkerboard assay.

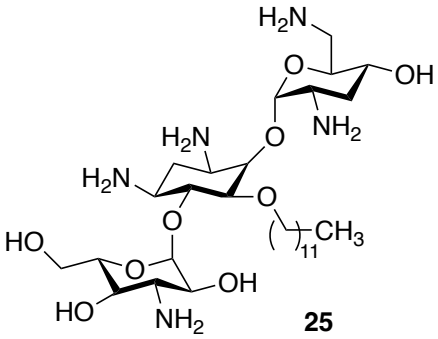

25

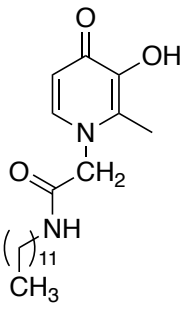

26

Figure 2-2: Structure of control compounds **25** (TOB-C_{12} linker) and **26** (DEF-C_{12} linker)

CHAPTER THREE: TOBRAMYCIN-DEFERIPRONE (N-LINKED) HYBRIDS

3. ABSTRACT

Several tetracycline antibiotics of clinical significance have gained resistance against clinical isolates of Gram-negative bacteria. Tobramycin-based hybrids (e.g. Tobramycin-Rifampicin and Tobramycin-NMP) have been reported to be beneficial adjuvants with doxycycline as it provides ease of entry/uptake. Tobramycin is widely used owing to its membrane permeabilizing mechanism of action against Gram-negative bacteria, especially; *P. aeruginosa*. Apart from this, literature suggests the potentiation of this class of antibiotics when the iron source is limited via chelating agents like hydroxypyridinone derivatives (e.g. Deferiprone). In this study, we were interested in linking deferiprone with tobramycin via an aliphatic tether of lengths 4, 8, and 12 respectively to achieve multi-modal action. Three TOB-C_n-N-DEF derivatives along with two control compounds were synthesized and tested for antibacterial activity and synergistic effect against clinical isolates of *P. aeruginosa*. The highest potentiating effect was observed by using hybrid **24c** with antibiotics such as novobiocin, rifampicin and all tetracycline class of drugs. Specifically, clinical breakpoints for minocycline, doxycycline and tigecycline were achieved in multidrug-resistant (MDR) *P. aeruginosa*. Based on these results, we extrapolated our hypothesis by synthesizing and testing two different control compounds; **25** and **26** to understand the importance of hybrid therapy as compared to single drug entities. Interestingly, control **25** potentiated the tetracycline antibiotics against *P. aeruginosa* while control **26** offered additive effect. But, it is noteworthy; that the synergistic effect of **24c** was at least 2-16- fold higher than combined **25** and **26** which validates our hypothesis of designing a hybrid drug. Mechanistic studies will be performed in future to understand the drug-iron complexation for the development of hybrid **24c**.

3.1 Introduction

The development of multiple resistance pathways in critical condition such as biofilm formation by Gram-negative bacteria has resulted into tetracycline resistance (81). These antibiotics enter the periplasm through the outer membrane porin channels such as OmpF and OmpC (31). Mutations or loss of the OmpF has led to the resistance of a broad range of antibiotics including tetracyclines (82,83). Upregulation of MexXY-OprM efflux pumps is another important factor contributing towards lowering the susceptibility of tigecycline- a glycylcycline antibiotic (84). Apart from this, recent studies have highlighted the presence of abundantly available iron to reduce the susceptibility of doxycycline as it competes with the drug-Mg^{+2} complex formation. This complex is essential for doxycycline to achieve its target site binding at 30S bacterial ribosomal unit (51). To overcome these multiple resistance barriers of tetracycline, an adjuvant therapy is empirical that can increase the drug accumulation in the bacteria and can facilitate the target-site interactions. Several tobramycin-based hybrids designed in the past display the importance of multi-modal mechanism of action required to treat multidrug-resistant (MDR) and extensively drug-resistant (XDR)- *P. aeruginosa*. For instance, when 1-(1-naphthylmethyl)-piperazine (NMP) was linked to tobramycin, there was a significant potentiation of minocycline. Here, tobramycin acts as an outer membrane permeabilizer while its counterpart moiety is responsible for efflux pump inhibition (85). Another hybrid, tobramycin-rifampicin was able to overcome the intrinsic resistance of doxycycline as the adjuvant facilitated higher drug accumulation (86). On its counterpart, a distinct strategy of using iron chelators was developed to synergize tetracycline antibiotics in a biofilm setting. CP762, a deferiprone-based iron chelating agent increased the bactericidal effect of doxycycline against *P. aeruginosa*. It utilized the concept of depriving iron such that the drug gets a free access to complex with magnesium ions and bind with the target site- 30S ribosome (51). In

this research, we intended to incorporate two features i.e., outer membrane disruption and iron-chelation into one molecule. To achieve this, we designed novel tobramycin-deferiprone hybrids as an adjuvant therapy against Gram-negative bacteria.

Conjugates of tobramycin synthesized with modifications at positions 5, 2", and 6" reveals the structure-activity-relationship for this molecule. For example, tobramycin-moxifloxacin conjugates linked via C-2" and C-6" displayed weaker antipseudomonal activity as compared to the C-5" hybrid. Several C-6" amphiphilic tobramycin displayed only membrane targeted action and no ribosomal interaction (68,87). The position 5 have been reported to be the most favorable site as it retained the ribosomal binding and inhibitory action of protein synthesis. The electrical potential (Ψ) of proton motive force (PMF) is also significantly affected with the use of tobramycin-based hybrids synthesized via position 5 (68). As a result, we utilized C-5 position of tobramycin to link with deferiprone, an FDA approved iron-chelator. Several literature studies indicate the diversity of deferiprone to synergize different antibiotics like gentamicin and vancomycin against coagulase-negative *Staphylococci epidermidis* (CNS) and *S. aureus* (88,89).

In this research, we designed a set of analogs; 1) TOB-C_n-N-DEF to explore the probable effect of membrane permeabilization and iron-chelation by a single molecule that could potentially overcome the resistance of tetracyclines, and 2) Control compounds like TOB-C_n linker and DEF-C_n linker that can provide us insights on the contribution by individual scaffold on the biological activity. These properties were evaluated on the basis of adjuvant effect with other antibiotics against clinical isolates of *P. aeruginosa*. Apart from this, cytotoxicity study have been conducted for these hybrids to understand its clinical significance.

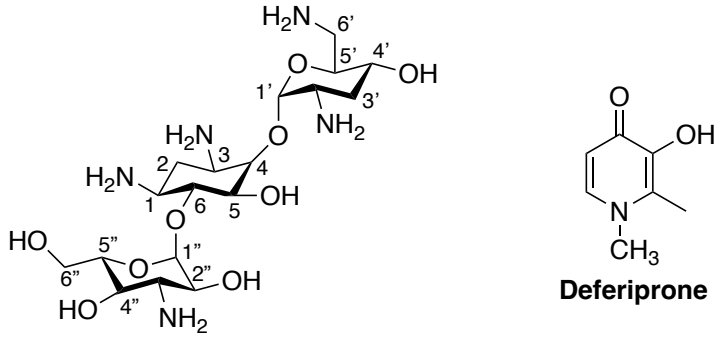

Tobramycin **Deferiprone**

Figure 3-1: Structure of tobramycin and deferiprone

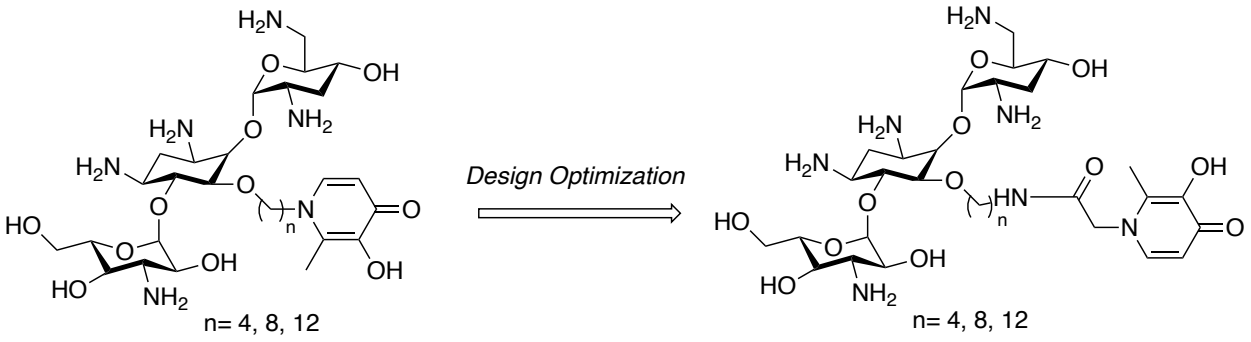

Figure 3-2: Design optimization of target structures by including an amide linkage

3.2 Results and Discussion

3.2.1 Chemistry

Previous literature reports signify the modifications of C-5 position in tobramycin to synthesize different hybrid molecules (68). Firstly, all the amine functional groups of the commercially available tobramycin were protected with Boc. Compound **28** (>90% yield) was synthesized by selectively protecting hydroxyl groups except C-5 position using TBDMS. This was achieved due to its bulky nature and steric hindrance resulting in freely accessible C-5 position for next steps. Further, it was reacted with different alkyl halides to yield compound **29a-c** with varying lengths of tether such as 4, 8, and 12 with 70-78% yield. On the other side, deferiprone ligand was prepared

by using maltol as a starting material. The hydroxyl group of maltol was protected with *p*-methoxybenzyl chloride which followed the substitution reaction mechanism to obtain compound **30** with 86% yield. Further, it was reacted with ammonium hydroxide which rendered compound **31** with 80% yield via aminolysis mechanism (90). We were aiming for a substitution reaction at the secondary amine group of **31** with **29a-c**. However, the desired pre-final compound was not synthesized and an O-linked product (**32a-c,** 65-72%) was obtained. This undesired product was formed due to the delocalization effect of **31** that causes the generation of nucleophile at the carbonyl group rather than the amine (Figure 3-3). Finally, the -NH_2 and -OH groups were deprotected in the presence of 3M methanolic HCl to get final molecules **27a-c** with 60-65% yield (Scheme 3-1).

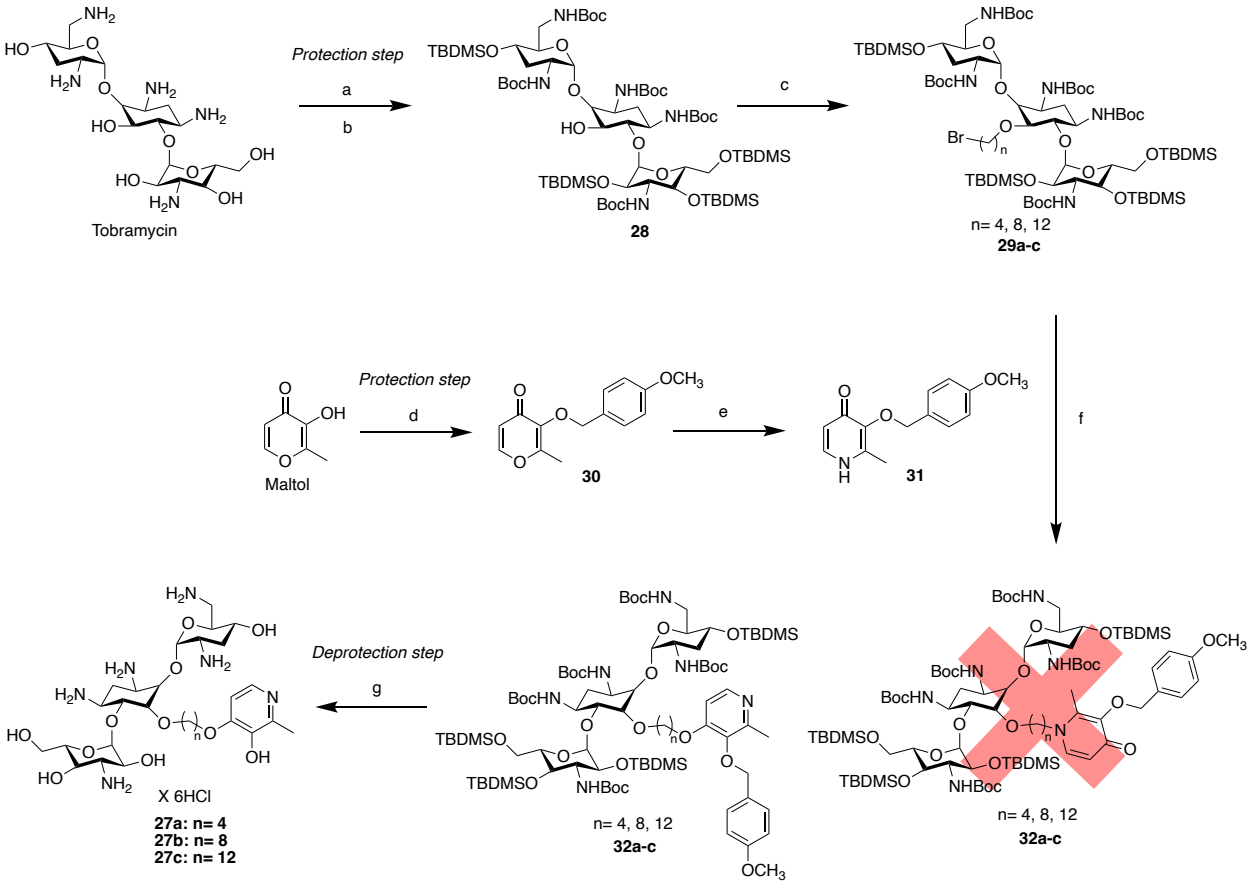

Scheme 3-1: Synthesis of compounds **27a-c**.

Reagents and conditions: (a) $(Boc)_2O$, Et_3N, $MeOH/H_2O$ (2:1), RT to 55 °C, overnight (95%). (b) TBDMSCl, 1-methylimidazole, DMF, RT, 4 days (92%). (c) Dibromoalkane, KOH, TBAHS, toluene, RT, overnight (70-78%). (d) *p*-methoxybenzyl chloride, K_2CO_3, DMF, 100 °C, 2 h (88%). (e) NH_4OH, 100 °C, overnight (80%). (f) K_2CO_3, DMF, 100 °C, 2 h (65-72%). (g) 3M HCl in MeOH, RT, 2 h (60-65%).

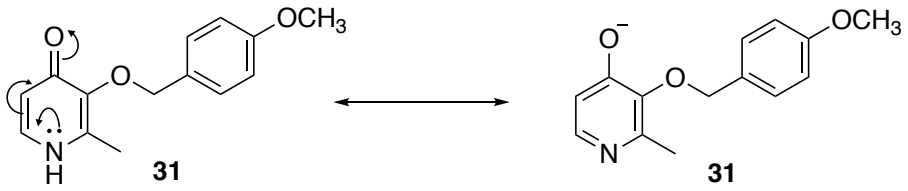

Figure 3-3. Delocalization effect of intermediate **31**.

To achieve the target molecules **27a-c**, several synthesis trials were conducted by adopting the reductive amination approach. However, the desired molecules **27a-c** were not obtained and thus, its design was optimized to simplify the synthetic strategy. New target molecules **24a-c** comprises of tobramycin-deferiprone conjugates linked via an amide bond through different lengths of linker like 4-, 8-, and 12-carbon tethers. As we now have access to the intermediate **29a-c**, azidation was carried out using sodium azide to yield compound **33a-c** with 86-90% yield. Subsequently, compound **34a-c** was obtained by catalytic hydrogenation reaction via $Pd(OH)_2$ on carbon with 55-60% yield (91). Alongside, maltol was subjected to an aminolysis reaction with glycine in basic condition. The intermediate **35**, 1-carboxymethyl-3-hydroxy-2-methylpyrid-4-one was retrieved (62% yield) from the reaction as precipitates in acidic medium (92). It was then coupled with the previously synthesized fully protected tobramycin-linker-amine **34a-c**. The coupling reagents used in this process includes HATU with triethylamine as a base. Fully protected tobramycin linked with deferiprone **36a-c** was obtained (50-60% yield) as a pre-final product which was then carried forward for the final deprotection step. Methanolic HCl (3M) was used to cleave off the protecting

groups such as Boc and TBDMS from compound **36a-c** to yield the desired product **24a-c** tobramycin-linker-deferiprone conjugates (55-68% yield) (Scheme 3-2). Also, we synthesized the control compound **26** (75% yield) by adopting amide coupling reaction using intermediate **35** and dodecylamine in presence of HATU and triethylamine (Scheme 3-3). Compound **25** was already synthesized previously as mentioned in the Scheme 3-3 and was used for microbiology assays.

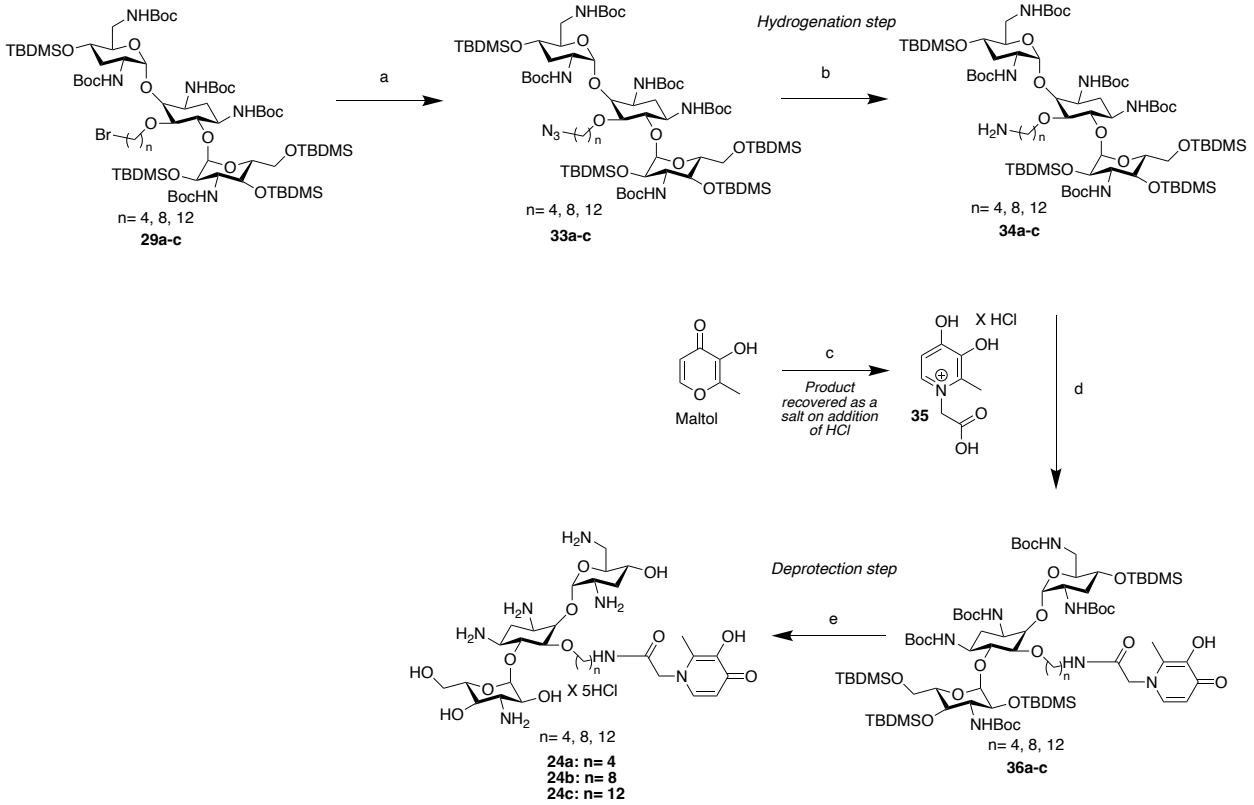

Scheme 3-2: Synthesis of compounds **24a-c**.

Reagents and conditions: (a) NaN_3, DMF, 75 °C, 4 h (86-90%). (b) $Pd(OH)_2/C$, H_2, RT, 5 h (55-60%). (c) Glycine, H_2O, NaOH (pH = 9), reflux, 20 h (62%). (d) HATU, Et_3N, DCM, RT, 1 h (50-60%). (e) 3M HCl in MeOH, RT, 2 h (55-68%).

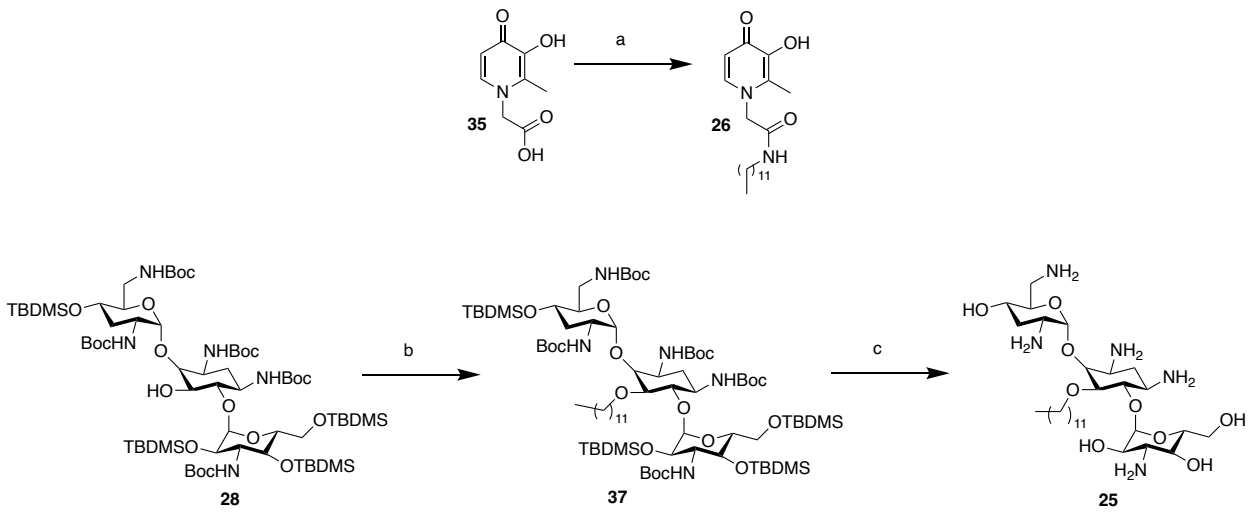

Scheme 3-3: Synthesis of control compounds **25** and **26**.

Reagents and conditions: (a) HATU, Et_3N, dodecylamine, DCM, RT, 1 h (75%). (b) 1-Bromododecane, KOH, TBAHS, toluene, RT, overnight (72%). (c) 3M HCl in MeOH, RT, 2 h (52%).

3.2.2 Microbiology

3.2.2.1 Antibacterial activity

All the six hybrids of TOB-C_n-N-DEF (**24a-c**) and TOB-C_n-O-DEF (**27a-c**) along with two control compounds **25** and **26** were tested against a panel of Gram-negative bacteria such as *P. aeruginosa*, *Escherichia coli*, and *Acinetobacter baumannii*. It was found that all the compounds under study had poor antimicrobial property which was estimated as minimal inhibitory concentration (MIC) >128 µg/mL (Table 3-1 and 4-1). This provided us an opportunity to test these compounds as an adjuvant which would possibly synergize existing antibiotics that are resistant to Gram-negative organisms. It can be particularly evaluated by fractional inhibitory concentration index (FICI) which indicates synergistic (≤0.5), additive (>0.5 to <4) and antagonistic action (≥4).

3.2.2.2 Adjuvant effect of TOB-C_n-N-DEF hybrids 24a, 24b and 24c

Antibiotic adjuvants started getting clinical relevance due to the lack of novel potent antimicrobials and also due to the persistent development of drug resistance mainly by ESKAPE pathogens which include *Enterococcus faecium*, *Staphylococcus aureus*, *Klebsiella pneumoniae*, *A. baumannii*, *P. aeruginosa*, and *Enterobacter* species (93,94). Adjuvants can be termed as a class of drugs which do not possess inherent antibacterial effect i.e. they do not kill or inhibit the growth of bacteria, however; it potentiates the effect of existing antibiotic either by hindering with the resistance pathway or by uplifting the host response (95). In the recent years, there have been development of several adjuvants such as avibactam, relebactam, and vaborbactam (96). Based on this motive, we performed checkerboard assays to evaluate the synergistic effect of our three hybrids. Synergy can be determined by a four-fold increase in the MIC value of an antibiotic with the help of an adjuvant at one-fourth of its MIC (97,98). In our case, all the three hybrids possessed MIC of >128 µg/mL when tested against wild-type *P. aeruginosa*. This allows us to use 32 µg/mL (one-fourth of MIC) as an effective concentration of adjuvant. However, we have been able to achieve promising results with the use of 8µg/mL concentration, giving an access to broad therapeutic window when correlated with cytotoxicity data. Initially, three hybrids of TOB-C_n-N-DEF were tested against a panel of 11 antibiotics against wild-type *P. aeruginosa*. The panel of antibiotics was selected critically to understand the synergism affecting different mechanistic pathway. For instance, novobiocin and rifampicin has gained resistance due to intact outer membrane permeability, while the β-lactams like ceftazidime and meropenem lost its activity through β-lactamases as well as loss of porin channels (7,8). The C_4, C_8, and C_{12} analogs were able to synergize novobiocin, rifampicin and all the tetracycline class of antibiotics (minocycline, doxycycline, tigecycline, and eravacycline) by at least 4-fold. However, none of the three hybrids potentiated β-lactam antibiotics such as meropenem, imipenem, and ceftazidime. It was noted that

the C_{12} analog was much superior in potentiating these antibiotics as compared to C_4 and C_8 (Table 3-2 and Figure 3-4). One of the major reasons corresponding to this effect is hydrophobicity that promotes membrane permeabilizing effect. Following these results, the C_{12} analog **24c** was selected for further study in clinical isolates of *P. aeruginosa* (Figure 3-5).

Three multidrug-resistant strains PA259, PA262, and PA264 were used along with same panel of antibiotics. Again, the antibacterial activity of TOB-C_{12}-N-DEF **24c** was determined as >128 μg/mL MIC (Table 3-1). The synergism trend remained consistent in clinical isolates as observed in the wild-type strain. Novobiocin and rifampicin were potentiated by hybrid **24c** in the range of 16-64-folds which indicates a glimpse of its mechanistic activity. Outer membrane layer in the Gram-negative bacteria acting as a barrier is a reason for their deprived activity as a stand-alone antibiotic. Here, we hypothesize that the hybrid **24c** was able to overcome this issue by disrupting the outer membrane, consequently providing an easy access for other antibiotics. Interestingly, the upliftment of activity in tetracycline class of antibiotics turned out to be crucial. Minocycline acts via the inhibition of protein synthesis as it binds with the 30S ribosomal subunit. It has been widely used clinically to treat infections caused by *Acinetobacter* spp. and Gram-positive bacteria (gastrointestinal disease, rickettsial infections, and many more) (99). Hybrid **24c** was able to attain the clinical breakpoint of minocycline (≤4 μg/mL, *Acinetobacter* spp.) in PA259 and PA262 isolates. Breakpoints by Clinical and Laboratory Standard Institute (CLSI) and European Committee on Antimicrobial Susceptibility Testing (EUCAST) suggest concentrations of antibiotic that can differentiate bacterial species as susceptible, intermediately-resistant, or resistant (86). Similarly, clinical breakpoints for doxycycline (≤4 μg/mL, *Acinetobacter* spp.) and tigecycline (≤1 μg/mL, *Staphylococcus* spp.) were achieved using hybrid **24c** in both PA259 and PA264 strains. Eravacycline, a recently FDA-approved fluorocycline used in intra-abdominal

infections, was synergized by 4-8-folds, however; the clinical breakpoint (≤0.5 µg/mL, *Enterobacter* spp.) was not achieved in the multidrug-resistant strains of *P. aeruginosa* (100) (Table 3-3 and Figure 3-5). To extrapolate this study in cystic fibrosis isolates of *P. aeruginosa*, PA095 non-mucoid strain was selected because tetracycline antibiotics exhibit resistance to it. It was observed that the C_{12} analog of N-linked TOB-DEF synergized minocycline (0.5 µg/mL), doxycycline (0.125 µg/mL), and eravacycline (0.5 µg/mL) by achieving the susceptible breakpoints. Also, it showed promising results with tigecycline by intensifying its activity to 8 folds (Absolute MIC: 2 µg/mL) (Table 3-3 and Figure 3-6).

To understand the importance of hybridization of two drugs, control compounds **25** (TOB-C_{12} linker) and **26** (TOB-C_{12} linker) were tested with tetracycline antibiotics against PAO1 and PA259. The tobramycin-C_{12} linker control synergized the antibiotics up to some extent, but the deferiprone-C_{12} linker demonstrated only additive effect. When the results were compared with the hybrid molecule **24c**, there was a drastic increase in the activity (Table 3-4, Figure 3-7 and 3-8). These results validate our goal to achieve desired biological activity through the linkage of tobramycin and deferiprone.

			Tobramycin–deferiprone (N-linked) hybrids		
Test organism	Tobramycin	Deferiprone	**24a**	**24b**	**24c**
P. aeruginosa ATCC 15692	0.5	>128	>128	>128	>128
PA259	512	>128	>128	>128	>128
PA262	512	>128	>128	>128	>128
PA264	128	>128	>128	>128	>128
PA095	ND	>128	>128	>128	>128
E. coli ATCC25922	2	>128	>128	>128	>128

A. Baumannii ATCC 17978	0.5	>128	>128	>128	>128

Table 3-1. Minimum inhibitory concentrations (MICs, μg/mL) of tobramycin, deferiprone and compounds **24a-c** against a panel of Gram-negative bacteria in CAMHB.

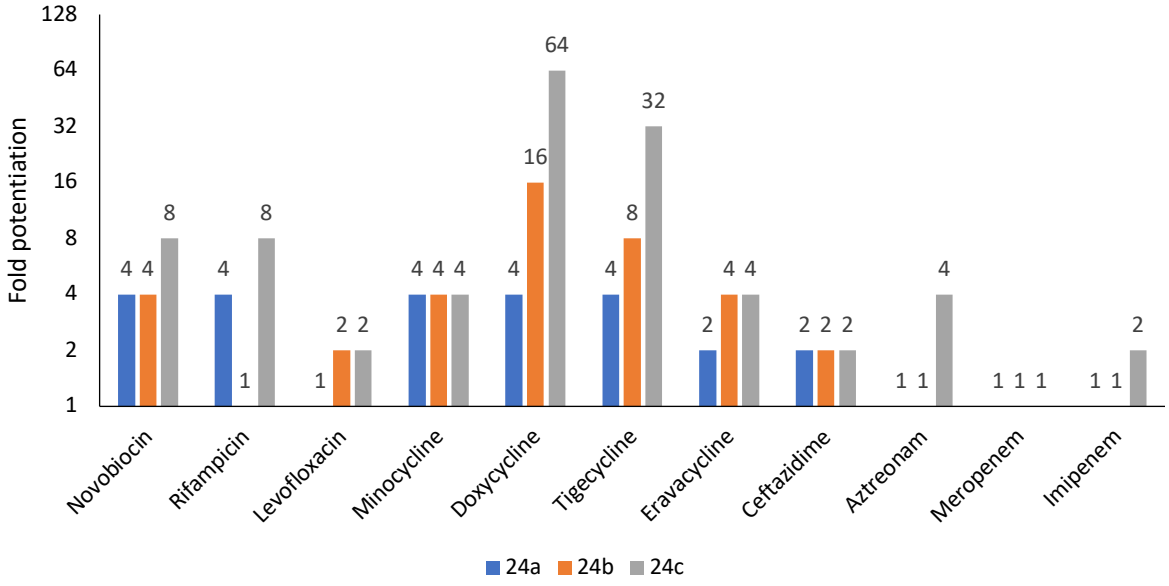

Figure 3-4. Fold potentiation of select antibiotics against wild-type *P. aeruginosa* (PA) in the presence of 8.0 μM of compound **24a-c** in CAMHB.

Antibiotics (MIC alone)	MIC of Antibiotics (FICI) in the presence of (maximum concentration = 8 μM) of		
	24a	**24b**	**24c**
Novobiocin (1024)	256 (0.25-0.31)	256 (0.25-0.31)	128 (0.12-0.18)
Rifampicin (32)	8 (0.25-0.31)	32 (1-1.002)	4 (0.12-0.14)
Levofloxacin (0.5)	0.5 (1-1.002)	0.25 (0.5-0.508)	0.25 (0.5-0.503)
Minocycline (32)	8 (0.25-0.28)	8 (0.25-0.31)	8 (0.25-0.26)
Doxycycline (16)	4 (0.25-0.31)	1 (0.06-0.08)	0.25 (0.01-0.04)
Tigecycline (64)	16 (0.25-0.31)	8 (0.125-0.13)	2 (0.03-0.06)

Eravacycline (8)	4 (0.5-0.56)	2 (0.25-0.31)	2 (0.25-0.28)
Ceftazidime (2)	1 (0.5-0.53)	1 (0.5-0.53)	1 (0.5-0.501)
Aztreonam (4)	4 (1-1.004)	4 (1-1.1)	1 (0.25-0.28)
Meropenem (1)	1 (1-1.002)	1 (1-1.002)	1 (1-1.002)
Imipenem (2)	2 (1-1.002)	2 (1-1.002)	1 (0.5-0.53)

Table 3-2. Combination studies of compounds **24a-c** with different antibiotics against WT *P. aeruginosa* PAO1 in CAMHB. MICs are reported in µg/mL. FICI = Fractional inhibitory concentration index. FICI of ≤ 0.5, > 0.5 – 4, and > 4 indicate synergy, additive or no interaction, and antagonism, respectively. Synergistic combinations are highlighted in green.

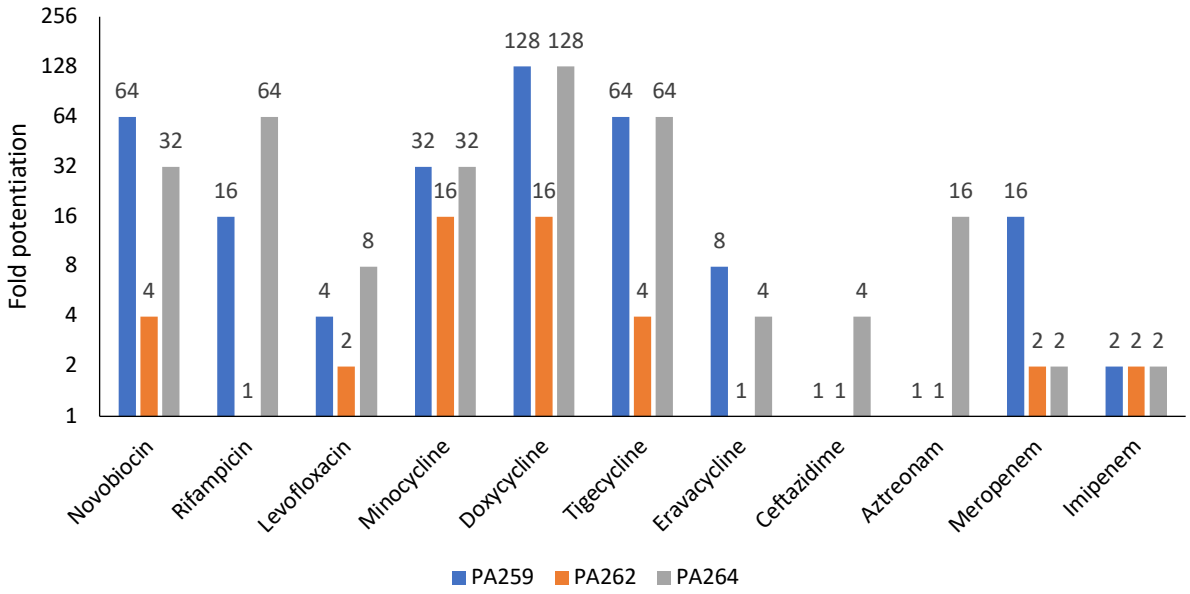

Figure 3-5. Fold potentiation of select antibiotics against multidrug- and extensively drug-resistant clinical isolates of *P. aeruginosa* (PA259, PA262, and PA264) in the presence of 8.0 µM of compound **24c** in CAMHB.

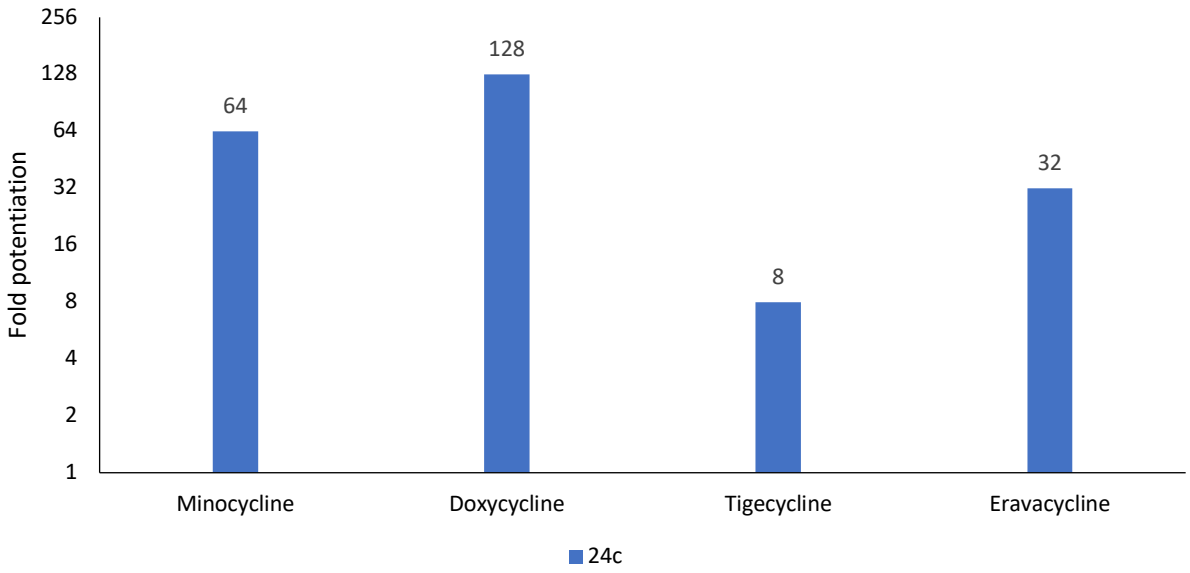

Figure 3-6. Fold potentiation of select antibiotics against cystic fibrosis isolates of *P. aeruginosa* (PA095) in the presence of 8.0 μM of compound **24c** in CAMHB.

Strain	Antibiotic	MIC (mg/L) of Antibiotic		Fold Potentiation	FICI
		Alone	+ Compound **24c**		
PA259	MIN	32	1	32	0.03-0.06
	DOX	64	0.5	128	0.01-0.03
	TIG	64	1	64	0.02-0.04
	ERV	16	2	8	0.13-0.16
PA262	MIN	128	8	16	0.06-0.09
	DOX	256	16	16	0.06-0.08
	TIG	64	16	4	0.25-0.27
	ERV	16	16	1	0.5-0.501
PA264	MIN	64	2	32	0.03-0.06
	DOX	32	0.25	128	0.01-0.04
	TIG	64	1	64	0.02-0.08
	ERV	16	4	4	0.25-0.28
	MIN	32	0.5	64	0.02-0.03
	DOX	16	0.125	128	0.01-0.04

PA095	TIG	16	2	8	0.13-0.14
	ERV	16	0.5	32	0.03-0.05

Table 3-3. Interactions of compound **24c** (8.0 μM) with minocycline (MIN), doxycycline (DOX), tigecycline (TIG), and eravacycline (ERV) against clinical isolates of *P. aeruginosa* in CAMHB. MICs are reported in μg/mL. FICI of ≤ 0.5, > 0.5 – 4, and > 4 indicate synergy, additive or no interaction, and antagonism, respectively. PA = *Pseudomonas aeruginosa*; ND = not determined. Synergistic combinations are highlighted in green.

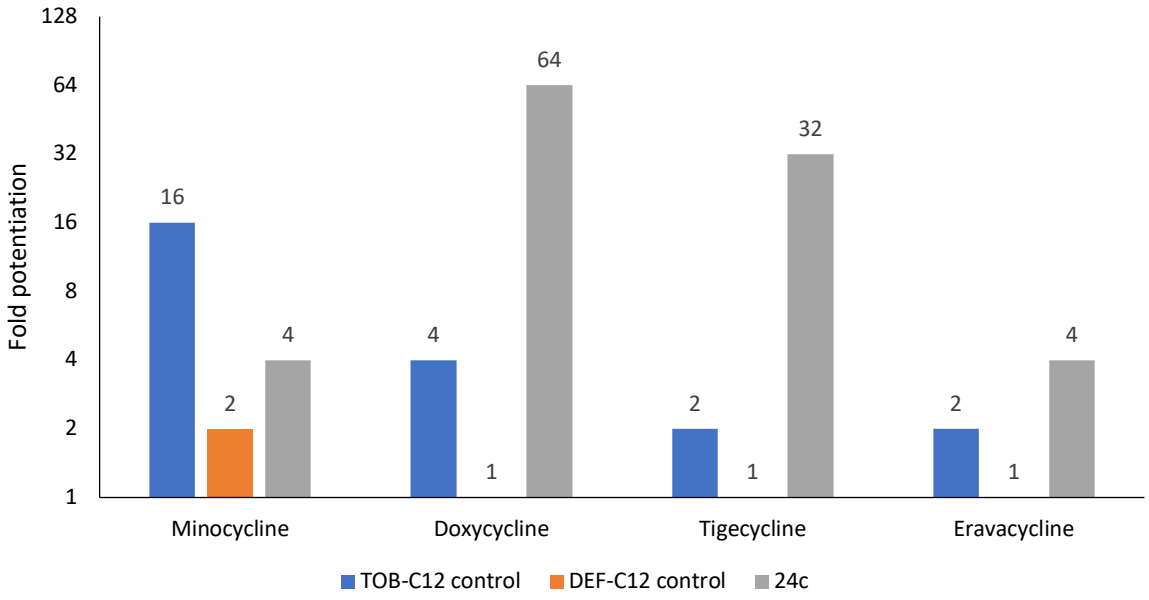

Figure 3-7. Comparison of fold potentiation of select antibiotics against wild-type *P. aeruginosa* PAO1 in the presence of 8.0 μM of compound TOB-C_{12} control **25**, DEF-C_{12} control **26**, and **24c** in CAMHB.

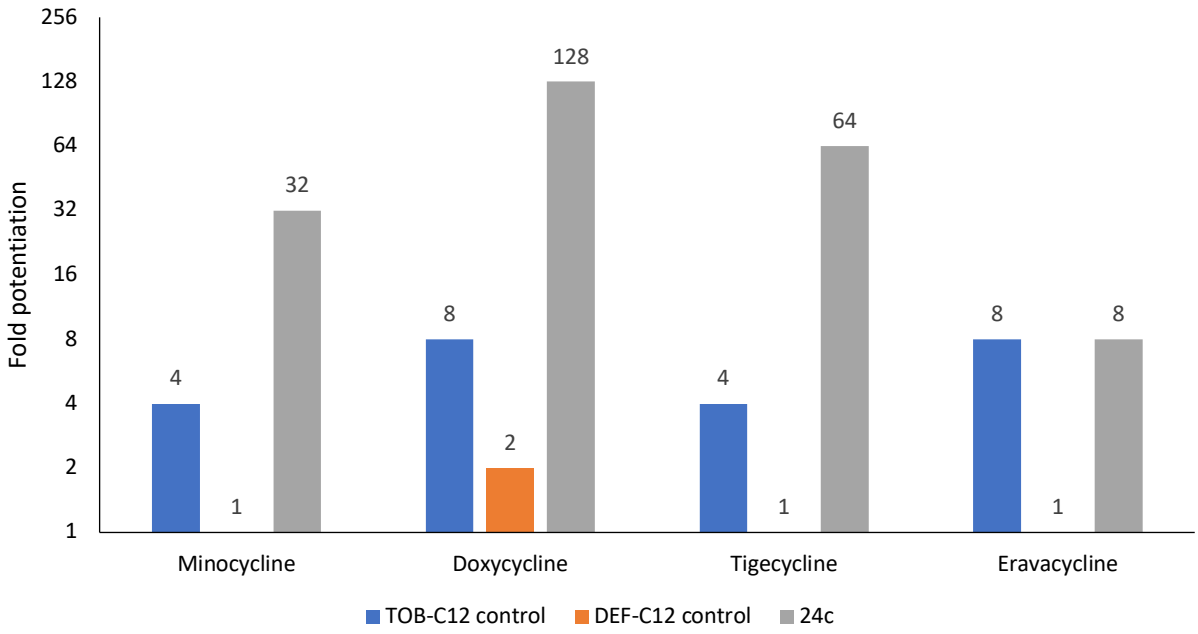

Figure 3-8. Comparison of fold potentiation of select antibiotics against clinical isolates of *P. aeruginosa* (PA259) in the presence of 8.0 μM of compound TOB-C_{12} control **25**, DEF-C_{12} control **26**, and **24c** in CAMHB.

Strain	Antibiotic (MIC alone)	MIC of Antibiotics (FICI) in the presence of (maximum concentration=8 μg/mL) of		
		TOB-C_{12} (**25**)	DEF-C_{12} (**26**)	**24c**
PAO1	MIN (32)	2 (0.06-0.08)	16 (0.5-0.53)	8 (0.25-0.26)
	DOX (16)	4 (0.25-0.26)	16 (1-1.002)	0.25 (0.01-0.04)
	TIG (64)	32 (0.5-0.504)	64 (1-1.01)	2 (0.03-0.06)
	ERV (8)	4 (0.5-0.53)	8 (1-1.003)	2 (0.25-0.28)
PA259	MIN (32)	8 (0.25-0.28)	32 (1-1.002)	1 (0.03-0.06)
	DOX (64)	8 (0.13-0.14)	32 (0.5-0.53)	0.5 (0.01-0.03)
	TIG (64)	16 (0.25-0.28)	64 (1-1.002)	1 (0.02-0.04)
	ERV (16)	2 (0.13-0.19)	16 (1-1.002)	2 (0.13-0.16)

Table 3-4. Interactions of compound TOB-C_{12} control **25**, DEF-C_{12} control **26**, and **24c** (8.5 μM) with minocycline (MIN), doxycycline (DOX), tigecycline (TIG), and eravacycline (ERV) against

wild-type and clinical isolates of *P. aeruginosa* in CAMHB. MICs are reported in μg/mL. FICI of ≤ 0.5, > 0.5 – 4, and > 4 indicate synergy, additive or no interaction, and antagonism, respectively. PA = *Pseudomonas aeruginosa*; ND = not determined. Synergistic combinations are highlighted in green.

3.3 Conclusions

All the three hybrids of TOB-C_n-N-DEF (**24a-c**) along with two control compounds were synthesized with decent yields. It was achieved by optimizing the target design, adopting different synthetic routes, and strategies for purification like normal- & reverse-phase chromatography and recrystallization. Based on the microbiology assays, it can be concluded that the C_{12} analog proved to be a potent adjuvant due to the hydrophobicity as compared to C_4 and C_8 conjugates. Also, the hybrid **24c** was observed as the most superior molecule in aspects of biological activity as it potentiated tetracycline antibiotics by 4- to 128-fold against multidrug-resistant strains PA259, PA262, and PA264. Susceptible clinical breakpoints were also achieved for minocycline, doxycycline and tigecycline against clinical isolates of *P. aeruginosa*. Most importantly, the concept of designing a hybrid drug proved advantageous because the control compounds failed to render comparative results like TOB-C_{12}-N-DEF **24c**. It is hypothesized that the hybrid **24c** possesses outer membrane permeabilizing effect as it potentiated novobiocin and rifampicin against clinical isolates of *P. aeruginosa*. However, mechanistic studies are required to understand the effect of iron-chelation.

CHAPTER FOUR: TOBRAMYCIN-DEFERIPRONE (O-LINKED) HYBRIDS

4.1 Results and Discussion

4.1.1 Microbiology

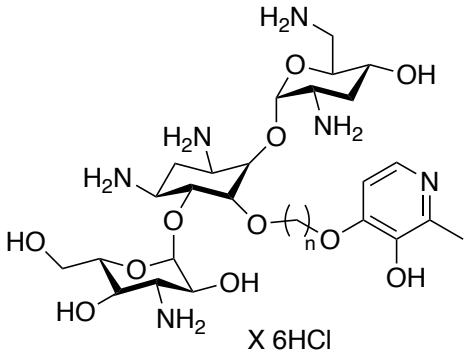

Figure 4-1: Structure of O-linked tobramycin-deferiprone

4.1.1.1 Adjuvant effect of TOB-C_n-O-DEF hybrids 27a, 27b and 27c

All the three conjugates **27a-c** were used for checkerboard assay with 16 antibiotics against wild-type *P. aeruginosa*. The C_4 and C_8 analogs did not exhibit potential results but the C_{12} analog synergized novobiocin (4-fold), rifampicin (32-fold), ceftazidime (8-fold), ceftolozane (4-fold), meropenem (4 fold), aztreonam (8 fold), minocycline (4-fold), and doxycycline (16-fold). However, it just reflected additive action with tigecycline and eravacycline (Table 4-2, Figure 4-2). Subsequently, MDR clinical isolates PA259, PA262, and PA264 were selected to investigate the synergistic pattern by TOB-C_{12}-O-DEF **27c**. The membrane permeabilizing effect was retained with the C_{12} analog which was confirmed by the synergism of novobiocin and rifampicin by 8-16-folds and 32-512-folds respectively in MDR strains. Apart from this, ceftazidime and aztreonam were potentiated remarkably such that their breakpoints (≤8 μg/ml) were achieved in PA259 and PA264. Biological activity of carbapenems like meropenem and imipenem were notably enhanced

using **27c** by 4-16-folds in the same clinical isolates. Tetracycline class of antibiotics were also tested with hybrid **27c** to compare the activity with the previously N-linked conjugate **24c** (Figure 4-6). Clinical breakpoints were achieved with minocycline (4µg/mL), doxycycline (4µg/mL), tigecycline (2µg/mL), and eravacycline (0.5µg/mL) against PA259. In PA262 isolates, minocycline, tigecycline, and eravacycline were potentiated by 8-, 16- and 4- folds respectively, while in PA264 strain, only minocycline and eravacycline were synergized and 8- and 4-folds respectively (Table 4-3, Figure 4-3). Later, these tetracycline antibiotics were included for further study against cystic fibrosis isolates PA095, where hybrid **27c** was able to uplift the activity of minocycline and doxycycline by attaining clinical breakpoints. Despite of potentiation of tigecycline and eravacycline by 4-folds, breakpoint was not achieved in both the cases (Table 4-3, Figure 4-5).

The β-lactamase harboring isolates (PA86052, PA88949 and PA108590) were included in the study as the adjuvant **27c** potentiated β-lactam antibiotics in the initial screening against PAO1 and MDR isolates of *P. aeruginosa*. Susceptible breakpoints were achieved for ceftazidime (4 µg/ml), cefepime (1 µg/ml), ceftolozane (0.25 µg/ml), meropenem (0.25 µg/ml), imipenem (0.25 µg/ml) and aztreonam (4 µg/ml) against PA86052 (Table 4-3, Figure 4-4). Moreover, similar results were observed when some of these β-lactam antibiotics were tested against cystic fibrosis isolates PA083 and PA095 as shown in table 4-3.

Triple combination using TOB-C_{12}-O-DEF **27c** *supports FDA-approved dual combination therapy:*

Ceftazidime-avibactam combination therapy is being currently used in complicated urinary tract infections and hospital-acquired pneumonia, especially; against *P. aeruginosa*. Ceftazidime is a β-lactam antibiotic which gets inactivated by the release of β-lactamases from *P. aeruginosa*.

Avibactam, a non- β-lactam β-lactamase inhibitor prevents the degradation of ceftazidime, thereby; uplifting its activity (101). Inclusion of **27c** (Figure 4-7) as an adjuvant in this combination lowered the MIC value to 0.125 µg/ml, where the concentration of avibactam was kept constant (8 µg/ml). Significantly lower MIC value (0.0625 µg/ml) was achieved when **27c** (Figure 4-8) was tested along with imipenem-relebactam; a recently approved combination therapy used against carbapenem-resistant *P. aeruginosa* and extended-spectrum β-lactamase (ESBL) Enterobacterales (102). Ceftolozane-tazobactam is an advanced combination therapy currently used for intra-abdominal infections caused by *P. aeruginosa* (103). On addition of **27c** as a third component (Figure 4-9), MIC of ceftolozane was reduced to 0.125 µg/mL with 8 µM concentration of tazobactam (Figure 4-6).

From all of these triple combinations, it can be comprehended that the TOB-C_{12}-O-DEF (**27c**) hybrid acted as an outer membrane permeabilizer that eventually increased the accumulation of β-lactam/β-lactamase inhibitor against PA86052, thereby; achieving the clinical breakpoints in all the cases.

	Tobramycin–deferiprone (O-linked) hybrids		
Test organism	**27a**	**27b**	**27c**
P. aeruginosa ATCC 15692	>128	>128	>128
PA259	>128	>128	>128
PA262	>128	>128	>128
PA264	>128	>128	>128
PA86052	ND	ND	>128
PA88949	ND	ND	>128
PA108590	ND	ND	>128

PA083	ND	ND	64
PA095	ND	ND	>128
E. coli ATCC25922	>128	>128	>128
A. Baumannii ATCC 17978	>128	>128	>128

Table 4-1. Minimum inhibitory concentrations (MICs, μg/mL) of compounds **27a-c** against a panel of Gram-negative bacteria in CAMHB.

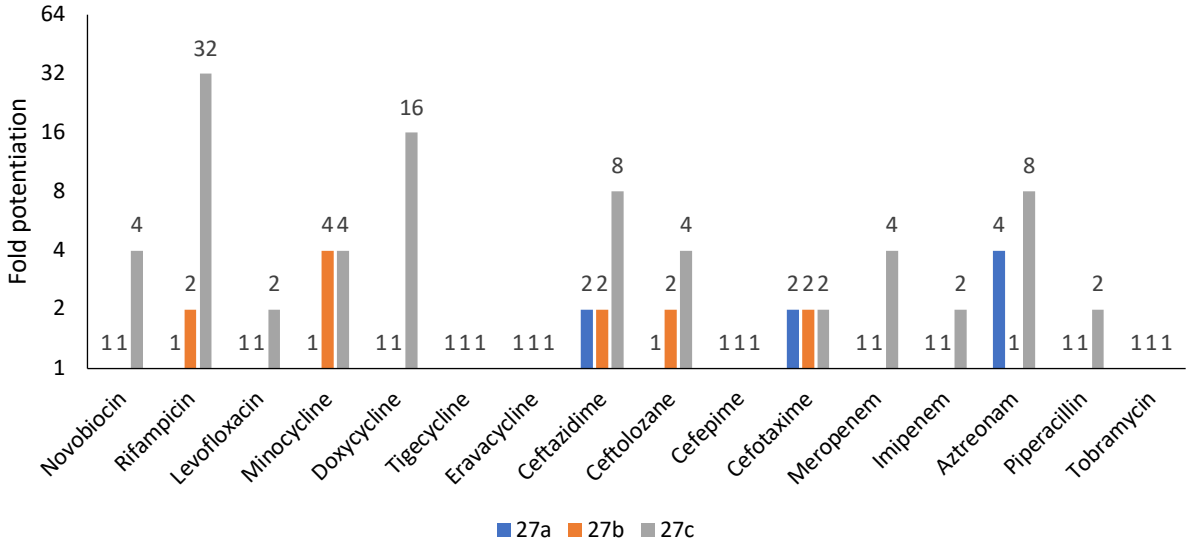

Figure 4-2. Fold potentiation of select antibiotics against wild-type *P. aeruginosa* PAO1in the presence of 8.5 μM of compound **27a-c** in CAMHB.

Antibiotics (MIC alone)	MIC of Antibiotics (FICI) in the presence of (maximum concentration=8.5 μM) of		
	27a	**27b**	**27c**
Novobiocin (1024)	1024 (1.00-1.06)	1024 (1.00-1.06)	256 (0.25-0.28)
Rifampicin (16)	16 (1.00-1.002)	8 (0.5-0.51)	0.5 (0.03-0.09)
Levofloxacin (0.25)	0.25 (1.00-1.004)	0.25 (1.00-1.002)	0.125 (0.5-0.56)

Minocycline (16)	16 (1.00-1.002)	4 (0.25-0.31)	4 (0.25-0.26)
Doxycycline (16)	16 (1.00-1.002)	16 (1.00-1.002)	1 (0.06-0.09)
Tigecycline (64)	64 (1.00-1.002)	64 (1.00-1.002)	64 (1.00-1.002)
Eravacycline (8)	8 (1.00-1.002)	8 (1.00-1.002)	8 (1.00-1.002)
Ceftazidime (2)	1 (0.5-0.56)	1 (0.5-0.56)	0.25 (0.12-0.19)
Ceftolozane (1)	1 (1.00-1.002)	0.5 (0.5-0.56)	0.25 (0.25-0.27)
Cefepime (1)	1 (1.00-1.002)	1 (1.00-1.002)	1 (1.00-1.002)
Cefotaxime (16)	8 (0.50-0.56)	8 (0.50-0.502)	8 (0.50-0.56)
Meropenem (1)	1 (1.00-1.002)	1 (1.00-1.002)	0.125 (0.25-0.28)
Imipenem (2)	2 (1.00-1.002)	2 (1.00-1.002)	1 (0.50-0.53)
Aztreonam (4)	1 (0.25-0.31)	4 (1.00-1.002)	0.5 (0.13-0.16)
Piperacillin (4)	4 (1.00-1.02)	4 (1.00-1.002)	2 (0.5-0.53)
Tobramycin (1)	1 (1.00-1.002)	1 (1.00-1.002)	1 (1.00-1.002)

Table 4-2. Combination studies of compounds **27a-c** with different antibiotics against WT *P. aeruginosa* PAO1 in CAMHB. MICs are reported in μg/mL. FICI = Fractional inhibitory concentration index. FICI of ≤ 0.5, > 0.5 – 4, and > 4 indicate synergy, additive or no interaction, and antagonism, respectively. Synergistic combinations are highlighted in green.

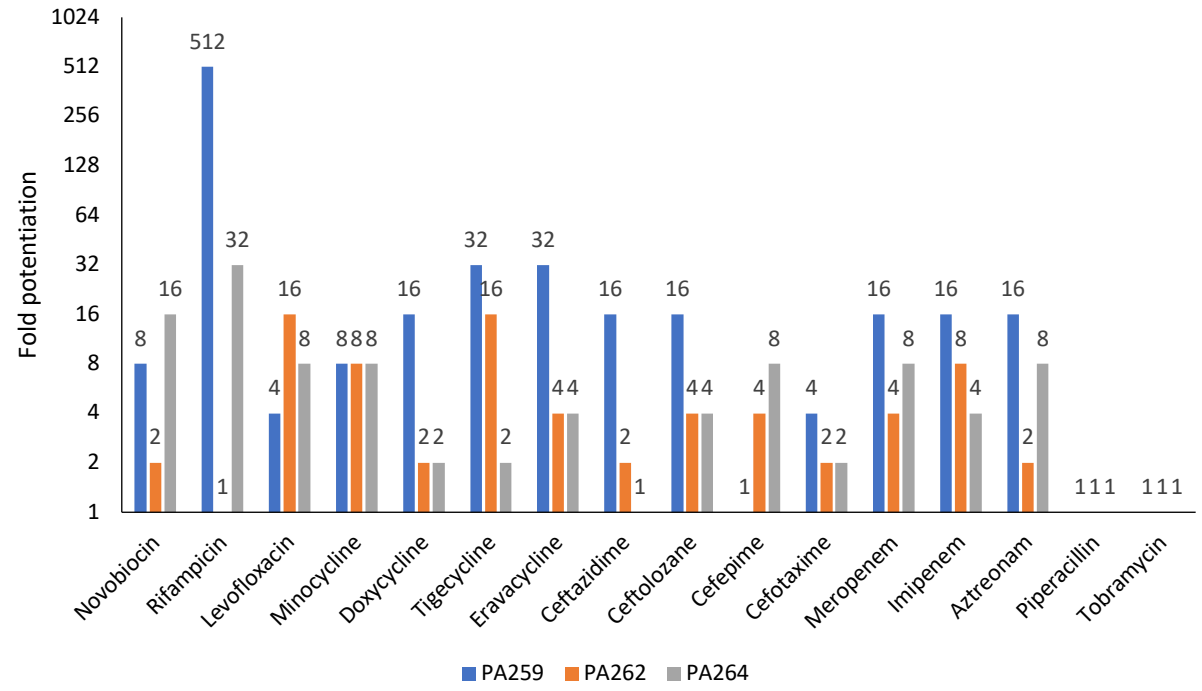

Figure 4-3. Fold potentiation of select antibiotics against multidrug- and extensively drug-resistant clinical isolates of *P. aeruginosa* (PA259, PA262, and PA264) in the presence of 8.5 μM of compound **27c** in CAMHB.

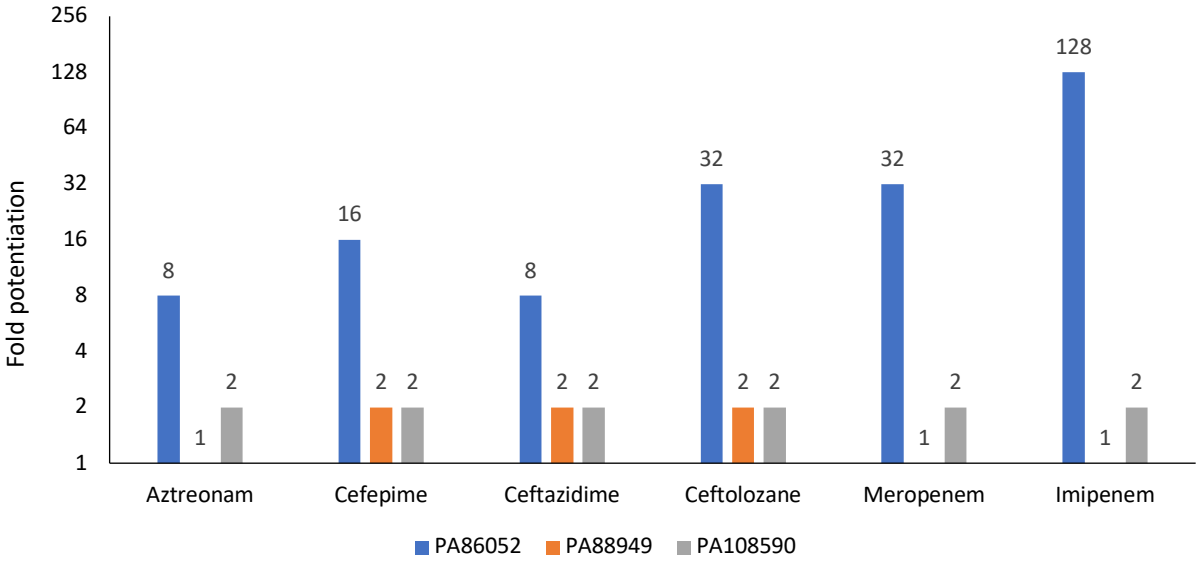

Figure 4-4. Fold potentiation of select antibiotics against β-lactamase harboring clinical isolates of *P. aeruginosa* (PA86052, PA88949, and PA108590) in the presence of 8.5 μM of compound **27c** in CAMHB.

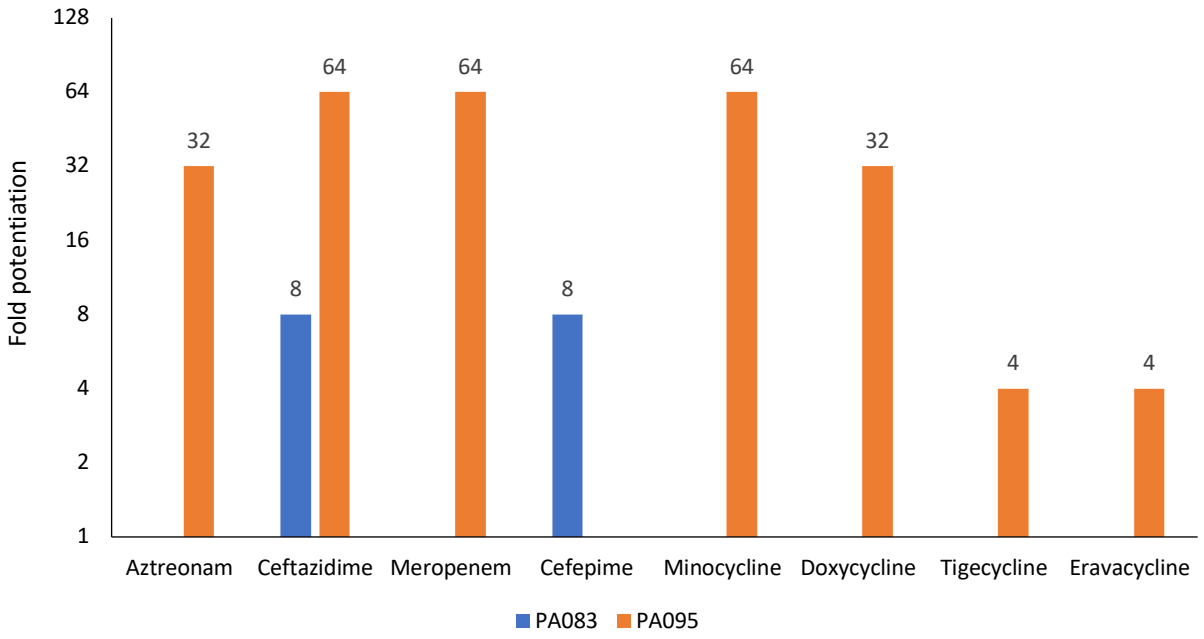

Figure 4-5. Fold potentiation of select antibiotics against cystic fibrosis isolates of *P. aeruginosa* (PA083 and PA095) in the presence of 8.5 μM of compound **27c** in CAMHB *(Note: Some antibiotics are not selected for either of the strains due to susceptibility)*.

Strain	Antibiotic	MIC (μg/mL) of Antibiotic		Fold Potentiation	FICI
		Alone	+ Compound **27c**		
PA259	MIN	32	4	8	0.12-0.19
	DOX	64	4	16	0.06-0.13
	TIG	64	2	32	0.03-0.09
	ERV	16	0.5	32	0.03-0.1
	AZT	32	2	16	0.06-0.09
	CAZ	512	32	16	0.06-0.13
	MER	512	32	16	0.06-0.13

	IMI	64	4	16	0.13-0.19
	CPM	>128	ND	ND	ND
PA262	MIN	128	16	8	0.13-0.16
	DOX	256	128	2	0.5-0.53
	TIG	64	4	16	0.06-0.13
	ERV	16	4	4	0.25-0.31
	AZT	32	16	2	0.50-0.53
	CAZ	16	8	2	0.50-0.52
	MER	16	4	4	0.25-0.31
	IMI	32	4	8	0.13-0.19
	CPM	16	4	4	0.25-0.31
	CTZ	4	1	4	0.25-0.31
PA264	MIN	64	8	8	0.13-0.14
	DOX	64	32	2	0.5-0.53
	TIG	64	32	2	0.5-0.504
	ERV	16	4	4	0.25-0.28
	AZT	32	4	8	0.13-0.19
	CAZ	128	128	1	1.00-1.002
	MER	64	8	8	0.13-0.16
	IMI	32	8	4	0.25-0.28
	CPM	64	8	8	0.13-0.19
	CTZ	4	1	4	0.25-0.31
PA86052	AZT	32	4	8	0.12-0.13
	CAZ	32	4	8	0.12-0.13
	MER	8	0.25	32	0.03-0.06
	IMI	32	0.25	128	0.008-0.07
	CPM	16	1	16	0.06-0.09
	CTZ	8	0.25	32	0.03-0.06
PA88949	AZT	32	32	1	1.00-1.002
	CAZ	64	32	2	0.50-0.56
	MER	16	16	1	1.00-1.002
	IMI	32	32	1	1.00-1.002
	CPM	32	16	2	0.50-0.502
PA108590	AZT	32	16	2	0.50-0.56

	CAZ	64	32	2	0.50-0.56
	MER	8	4	2	0.50-0.53
	IMI	32	16	2	0.50-0.53
	CPM	ND	ND	ND	ND
PA083	CAZ	8	1	8	0.25
	CPM	8	1	8	0.14
PA095	MIN	32	0.5	64	0.02-0.08
	DOX	16	0.5	32	0.03-0.1
	TIG	16	4	4	0.2-0.3
	ERV	32	8	4	0.2-0.3

Table 4-3. Interactions of compound **27c** (8.5 μM) with aztreonam (AZT), ceftazidime (CAZ), meropenem (MER), imipenem (IMI), cefepime (CPM), ceftolozane (CTZ), minocycline (MIN), doxycycline (DOX), tigecycline (TIG), and eravacycline (ERV) against clinical isolates of *P. aeruginosa* (PA259, PA262, PA264, PA86052, PA88949, PA108590, PA083 and PA095) in CAMHB. MICs are reported in μg/mL. FICI of ≤ 0.5, > 0.5 – 4, and > 4 indicate synergy, additive or no interaction, and antagonism, respectively. PA = *Pseudomonas aeruginosa*; ND = not determined. Synergistic combinations are highlighted in green.

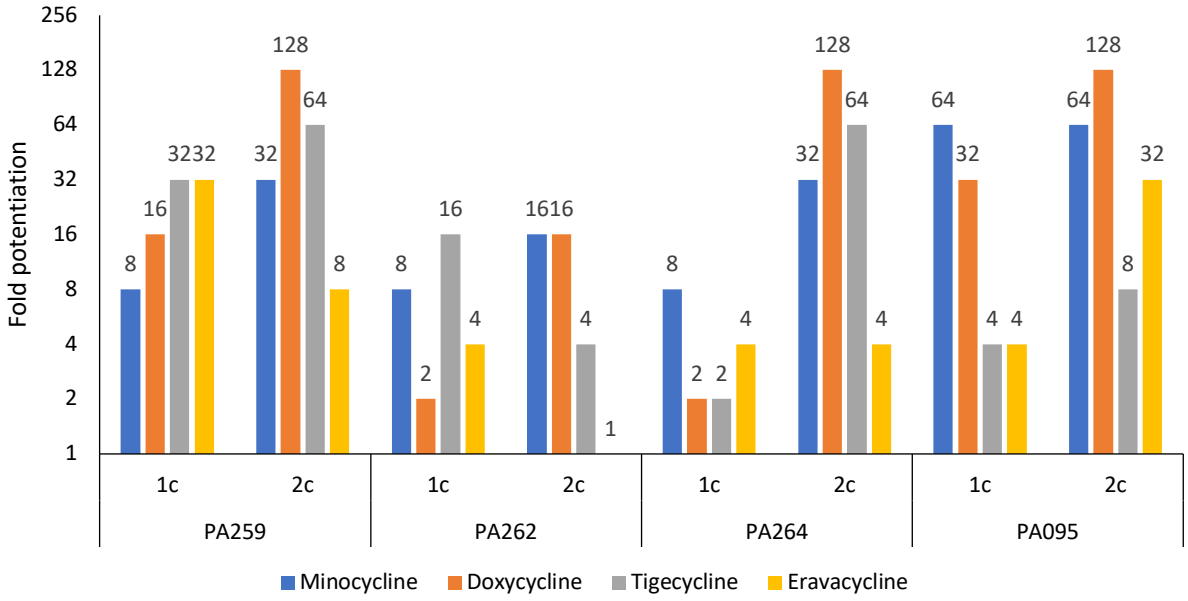

Figure 4-6. Comparison study of fold potentiation of select antibiotics against multidrug-, extensively drug-resistant and cystic fibrosis isolates of *P. aeruginosa* (PA259, PA262, PA264, and PA095) in the presence of compound **24c** (8 µg/mL) and **27c** (8 µg/mL) in CAMHB.

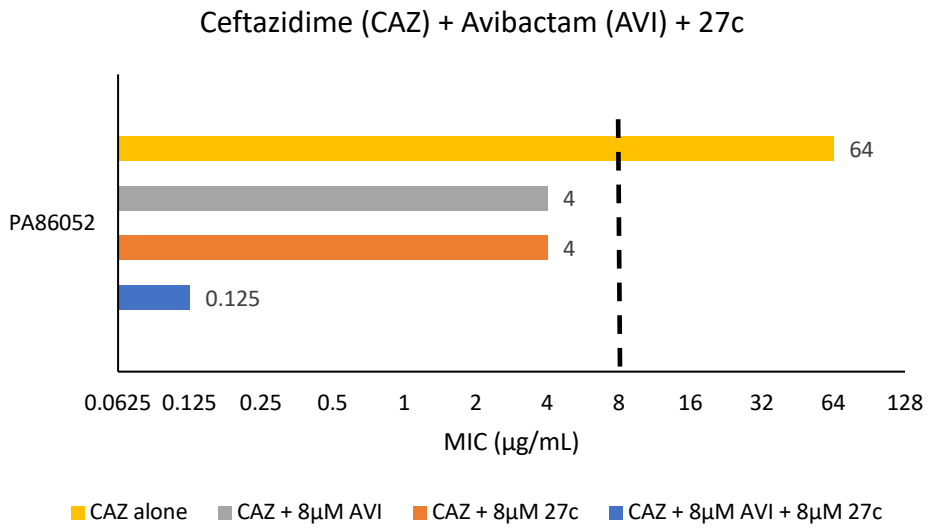

Figure 4-7. Triple combination study using **27c** (8.5 µM) and ceftazidime/avibactam (CAZ/AVI) against β-lactamase harboring clinical isolates of *P. aeruginosa* (PA86052) in CAMHB. Dashed-line indicates breakpoint.

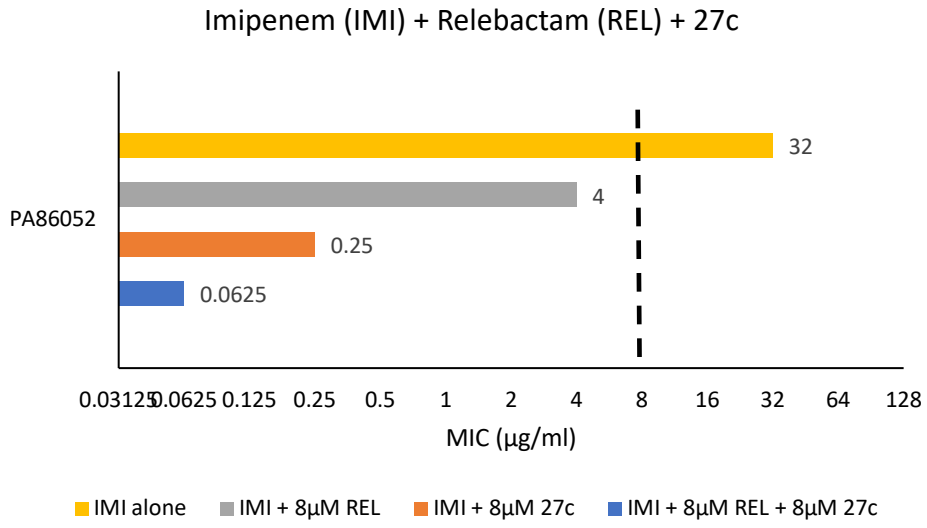

Figure 4-8. Triple combination study using **27c** (8.5 µM) and imipenem/relebactam (IMI/REL) against β-lactamase harboring clinical isolates of *P. aeruginosa* (PA86052) in CAMHB. Dashed-line indicates breakpoint.

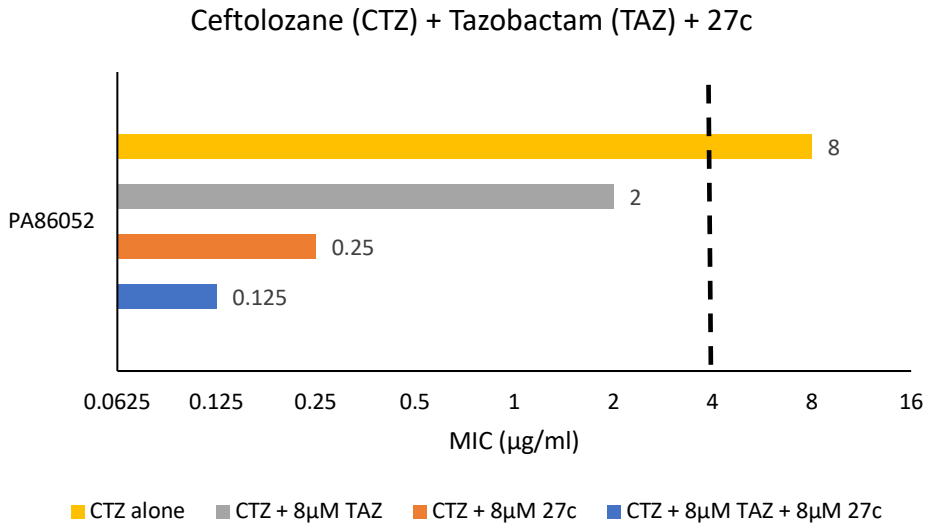

Figure 4-9. Triple combination study using **27c** (8.5 µM) ceftolozane/tazobactam (CTZ/TAZ) against β-lactamase harboring clinical isolates of *P. aeruginosa* (PA86052) in CAMHB. Dashed-line indicates breakpoint.

4.2 Conclusions

The O-linked derivatives of tobramycin-deferiprone (**27a-c**) were obtained due to an over-looked delocalization effect in the hydroxypyridinone scaffold. Microbiology testing revealed some interesting results as the hybrid **27c** was able to synergize β-lactam antibiotics which are considered to be the first-line drugs clinically. Moreover, triple combination with ceftazidime/avibactam, imipenem/relebactam, and ceftolozane/tazobactam lowered the MICs significantly below the clinical breakpoints. Also, the tetracycline antibiotics were potentiated by **27c**, however; it was calculated to be 2-4-fold less effective than the N-linked molecule **24c**. It is hypothesized that an increased accumulation of β-lactam antibiotics by hybrid **27c** can be due to the outer membrane permeabilization. The synergism of novobiocin and rifampicin can be an indication for the internalization effect but it needs to be confirmed through the membrane polarization assays.

CHAPTER FIVE: CONCLUSIONS

5. CONCLUSIONS AND FUTURE WORK

5.1 Conclusions

Despite of the use of advanced antimicrobial agents, drug resistance still remain as a prevailing factor that hinders the management of several nosocomial infections caused by Gram-negative bacteria. The FDA-approval of avibactam, relebactam, and tazobactam has significantly impacted the development of novel antibiotic adjuvants in the recent years. However, the current situation reveals that the clinical use of these adjuvants are limited as β-lactamase inhibitors only, and there is no FDA-approved adjuvant that can rescue old generation tetracyclines. Efforts are being made to develop outer membrane permeabilizer as an adjuvant and some of its examples are polymyxin B nonapeptide, oligo-acyl-lysyls, and tobramycin-based hybrids (85,104,105). Recently, catechol groups have also gained importance due to its unique siderophore-mediated uptake mechanism e.g. cefiderocol, which possesses stand-alone antibiotic effect. Literature review indicates the use of similar groups (e.g. Deferiprone- a pyridone derivative) in the development of adjuvants for resuscitating tetracyclines (51).

Tobramycin have been explored widely to develop as an adjuvant; owing to its magnesium- and calcium-chelating properties that destabilize the outer membrane. One of the major reasons responsible for this effect is the presence of polycationic charges across the molecule (106). In this study, the hybridization of tobramycin with deferiprone (TOB-C_{12}-N-DEF, **24c**) proved to be beneficial in potentiating tetracycline antibiotics as they achieved clinical breakpoints. Additionally, the susceptible MICs were reduced by at least 2-16-fold when tetracyclines were used with N-linked hybrid **1c** rather than the control compounds **25** and **26**. Mechanistic assays are yet to be explored to support the hypothesis that such encouraging results were due to the

exposure of iron-chelating group with the internalization action of tobramycin. Such strategies can be adopted to develop novel tobramycin-based hybrids as a potential adjuvant against extensively drug-resistant Gram-negative bacteria.

5.2 Future Work

Two different sets of tobramycin linked with deferiprone were synthesized and tested for antibacterial activity and synergistic properties. From our findings, both TOB-C_{12}-N-DEF **24c** and TOB-C_{12}-O-DEF **27c** displayed synergistic effect with multiple tetracycline antibiotics.

Future scope of this work include animal studies to explore whether the observed *in vitro* effects translates into measurable *in vivo* effects and mechanistic assays with the lead molecule that can help to develop adjuvants with improved biological activity and less cytotoxic effect. Also, the hybrid **24c** was observed to potentiate all the tetracycline antibiotics in the cystic fibrosis isolates of *P. aeruginosa*. The introduction of biofilm assay in this study can provide us a better understanding of this molecule's adjuvant effect in critical conditions where the infection is difficult to treat. Time-kill curves can also be advantageous to gain insights on the type of effect-bacteriostatic or bactericidal. In addition to this, hemolytic studies will demonstrate the tolerance of red blood cells when subjected to the lead molecule.

Optimization of these conjugates can be done by incorporating multiple deferiprone moieties with tobramycin to enhance the probable iron-chelating effect. Moreover, it would be interesting to witness the effect when deferiprone is hybridized to β-lactam antibiotics whose uptake is mainly porin- dependent (This approach has been adopted by Pfizer with monobactams which provided noteworthy findings e.g, MC-1 (47)). Comparison of these hybrids can also be studied extensively by replacing deferiprone with other iron-chelators like deferasirox and deferoxamine.

The use of tobramycin-deferiprone hybrids have proved advantageous from this research findings, and it will be interesting to explore more on this work to develop an adjuvant which acts as a membrane permeabilizer.

CHAPTER SIX: EXPERIMENTAL SECTION

6. EXPERIMENTAL PROCEDURES

6.1 Chemistry

General: All the reagents were purchased from Sigma Aldrich (Canada) except 4-methoxybenzyl chloride which was obtained from TCI chemicals (USA). The intermediates and final molecules were characterized using Bruker 300, 400 and 500 MHz nuclear magnetic resonance (NMR) spectra with chemical shifts (δ) being reported in parts per million (ppm). Different types of NMR experiments used in this study includes ^{1}H, ^{13}C, COSY, HSQC, HMBC, and NOESY. All the intermediates and final compounds were purified using flash chromatography with silica gel P60 purchased from Merck, Ontario, Canada. Purification of certain intermediates were carried out using Biotage Selekt, an automated-chromatography system. For purity analysis of final compounds **24a-c** and **27a-c**, high-performance liquid chromatography (HPLC) was adopted using Thermo Scientific Vanquish Ultra-HPLC (Waltham, MA, USA) system connected to Synergi 2.5 μM Polar-RP 100 Å LC column (50 mm × 2 mm, Phenomenex). For inert condition reactions, nitrogen atmosphere was supplemented. A detailed procedure along with the spectroscopy data for the intermediates and final molecules are given below.

General Procedure A: 5-*O*-alkylation of *Boc* and TBDMS protected Tobramycin for the preparation of 5-O-(4-bromoalkane)-1,3,2',6',3"-penta-N-(tert-butoxycarbonyl)-4',2",4",6"-tetra-OTBDMS-tobramycin 29a-c. Tobramycin protected with Boc and TBDMS groups bearing a selectively free site C5-OH (**28**) was dissolved in toluene to react with 1,*n*-dibromoalkane (3.0 equivalents) in presence of KOH (3.0 equivalents) and tetrabutylammonium hydrogen sulphate TBAHS (0.1 equivalents). The mixture was stirred for 16 hours at RT and further, extracted with ethyl acetate and water (×3). Moreover, the ethyl acetate fraction was

washed with brine and dried with anhydrous Na_2SO_4 and concentrated using high vacuum. Pure white solids of **29a-c** were obtained after purification of crude compound using column chromatography (12% ethyl acetate/hexane).

General Procedure B: Azidation of 29a-c for the preparation of 5-O-(azido-alkylated)-1,3,2',6',3"-penta-N-(tert-butoxycarbonyl)-4',2",4",6"-tetra-OTBDMS-tobramycin 33a-c. Compounds **29a-c** (0.820 - 1.320 g, 1.0 equivalent) were reacted with NaN_3 (0.545 - 0.700 g, 20.0 equivalents) in DMF under N_2 atmosphere at 80 °C for 6 h. The workup was performed by using ethyl acetate and water (×3) followed by washing the organic layer with brine and drying it over anhydrous Na_2SO_4. The organic layer was concentrated using high vacuum and dried overnight to yield compounds **33a-c** (0.500 - 0.820 g). This intermediate was not purified by column chromatography due to same retention factor (rf) as starting materials. It was carried forward for the next step reaction.

General Procedure C: Hydrogenation of 33a-c for the preparation of 5-O-(amino-alkylated)-1,3,2',6',3"-penta-N-(tert-butoxycarbonyl)-4',2",4",6"- tetra-OTBDMS-tobramycin 34a-c. Compounds **33a-c** (1.0 equivalent) were reacted in methanol under hydrogen gas conditions with a catalytic amount of $Pd(OH)_2/C$ (0.1 equivalent) at RT. The reaction mixture was stirred for 5 h followed by filtration using celite and the organic layer was concentrated under high vacuum. The crude mixture was purified by column chromatography at 10% methanol/dichloromethane which yielded **34a-c** as white solids.

General Procedure D: Amide coupling reaction for the preparation of compounds 36a-c: Compound **35** was dissolved in dichloromethane followed by the addition of triethylamine (1.5 equivalents) and HATU coupling reagent (1.5 equivalents). Reaction mixture was stirred for 5 mins and compounds **34a-c** were added to it. The mixture was reacted under N_2 atmosphere for 1

h at RT. The organic layer was washed with dichloromethane with water (×3), brine and $NaHCO_3$ and dried with Na_2SO_4. The dichloromethane layer was concentrated using high vacuum and the crude was purified by column chromatography using 5% methanol/dichloromethane to afford pure products **36a-c**.

General Procedure E: Substitution of 29a-c with 3-[(4-methoxyphenyl)methyl]-2-methyl-1,4-dihydropyridin-4-one for the preparation of compounds 32a-c. Protected tobramycin with varying lengths of linker **29a-c** was reacted with **31** (2.0 equivalents) in DMF along with K_2CO_3 (2.0 equivalents) under N_2 gas conditions. The reaction mixture was stirred for 2 hours at 100 °C and the workup was carried out with ethyl acetate and water (×3). The ethyl acetate fraction was washed with brine and dried with anhydrous Na_2SO_4 and concentrated using high vacuum. The crude compound was purified with column chromatography using 35% ethyl acetate/hexane to yield white solids **32a-c**.

General Procedure F: Removal of all the protecting groups for the preparation of compounds 24a-c and **27a-c.** A 3M Hydrogen chloride solution in methanol was stirred with **32a-c** or **36a-c** under N_2 gas condition at RT for 2 hours and further concentrated with high vacuum. The crude product was washed with diethyl ether (×2) and dried to remove non-polar impurities. Pure solids (HCl salt) **24a-c** or **27a-c** were obtained after purification with reverse-phase column chromatography (deionized water).

Compound 24a: Synthesized as per the general procedure F using compound **36a** (0.042 g, 0.0253 mmol) and 3M HCl in MeOH (5 mL). The residual was purified by C-18 reverse-phase column chromatography to yield pure dark orange HCl salts of **24a** (0.012 g, 68%). ^{1}H NMR (500 MHz, D_2O) δ 8.06 (d, J = 6.5 Hz, 1H, H-5$_{def}$), 7.21 (d, J = 6.6 Hz, 1H, H-6$_{def}$), 5.40 (s, 1H, H-1'), 5.22 (s, 3H, H-1", H-2'$_{def}$), 4.28 – 4.21 (m, 2H), 3.95 (m, 5H), 3.89 – 3.77 (m, 6H), 3.73 (s, 1H), 3.61

(q, *J* = 9.4 Hz, 4H), 3.43 (m, 2H, H-6'), 3.32 (d, *J* = 9.9 Hz, 2H, *N*-CH_2 linker), 2.51 (s, 4H), 2.30 – 2.20 (m, 2H), 2.07 – 1.99 (m, 1H), 1.70 – 1.55 (m, 4H). ^{13}C NMR (126 MHz, D_2O) δ 166.89, 159.74, 142.97, 142.73, 140.19, 111.10, 101.15 (anomeric), 92.67 (anomeric), 92.05, 82.12, 81.67, 76.54, 75.56, 73.18, 72.90, 68.61, 64.87, 63.30, 59.35, 58.06, 54.82, 49.66, 48.48, 47.36, 39.84, 38.61, 28.11, 27.73, 26.91, 25.00, 12.50. MALDI TOF-MS *m/e* calcd for $C_{31}H_{54}N_6O_{12}Na^+$, 725.79; measured *m/e*, 726.250 $[M+Na]^+$

Compound 24b: Synthesized as per the general procedure F using compound **36b** (0.209 g, 0.122 mmol) and 3M HCl in MeOH (5 mL). The residual was purified by C-18 reverse-phase column chromatography to yield pure dark orange HCl salts of **24b** (0.058 g, 62%). ^{1}H NMR (500 MHz, D_2O) δ 7.67 (s, 1H, H-5$_{def}$), 6.61 (s, 1H, H-6$_{def}$), 5.39 (d, *J* = 5.0 Hz, 1H, H-1'), 5.18 (d, *J* = 5.2 Hz, 1H, H-1"), 4.91 (s, 2H, H-2'$_{def}$), 4.29 (m, 1H), 4.19 (t, *J* = 9.8 Hz, 1H, *O*-CH_2 linker), 3.97 – 3.93 (m, 3H), 3.92 – 3.80 (m, 6H), 3.78 – 3.70 (m, 3H), 3.65 – 3.55 (m, 3H), 3.42 (m, 1H, H-6'), 3.34 (m, 1H, H-6'), 3.28 (t, *J* = 6.8 Hz, 2H, *N*-CH_2 linker), 2.55 (m, 1H), 2.36 (s, 3H, H-1$_{def}$), 2.26 (m, 2H), 1.99 (q, *J* = 12.7 Hz, 1H), 1.65 (s, 2H), 1.55 (m, 2H), 1.36 – 1.26 (m, 8H, CH_2 linker). ^{13}C NMR (126 MHz, D_2O) δ 169.46, 168.31, 144.64, 140.06, 135.23, 112.53, 101.38 (anomeric), 92.77 (anomeric), 81.87, 76.78, 75.76, 73.77, 73.19, 68.55, 64.77, 63.19, 59.24, 56.53, 54.79, 49.78, 48.45, 47.33, 39.47, 38.52, 29.43, 28.83, 28.20, 28.10, 27.81, 25.84, 25.17, 11.73. MALDI TOF-MS *m/e* calcd for $C_{35}H_{62}N_6O_{12}Na^+$, 781.90; measured *m/e*, 782.416 $[M+Na]^+$

Compound 24c: Synthesized as per the general procedure F using compound **36c** (0.450 g, 0.251 mmol) and 3M HCl in MeOH (5 mL). The residual was purified by C-18 reverse-phase column chromatography to yield pure dark orange HCl salts of **24c** (0.112 g, 55%). ^{1}H NMR (500 MHz, D_2O) δ 7.65 (d, *J* = 7.2 Hz, 1H, H-5$_{def}$), 6.58 (d, *J* = 7.1 Hz, 1H, H-6$_{def}$), 5.40 (d, *J* = 2.6 Hz, 1H, H-1'), 5.18 (d, *J* = 3.5 Hz, 1H, H-1"), 4.89 (s, 2H, H-2'$_{def}$), 4.29 – 4.26 (m, 1H), 4.16 (t, *J* = 9.8

Hz, 1H, *O*-CH_2 linker), 3.97 – 3.89 (m, 5H), 3.86 – 3.78 (m, 4H), 3.74 – 3.69 (m, 2H), 3.64 – 3.54 (m, 4H), 3.42 – 3.33 (m, 2H, H-6'), 3.28 (t, *J* = 6.8 Hz, 2H, *N*-CH_2 linker), 2.56 – 2.52 (m, 1H), 2.36 (s, 3H, H-1_{def}), 2.28 – 2.21 (m, 2H), 2.01 – 1.90 (m, 1H), 1.64 (s, 2H), 1.54 (d, *J* = 6.6 Hz, 2H), 1.36 – 1.26 (m, 15H, CH_2 linker). ^{13}C NMR (126 MHz, D_2O) δ 169.73, 169.65, 168.31, 144.70, 140.05, 134.75, 112.54, 101.37 (anomeric), 92.75 (anomeric), 81.87, 76.84, 73.20, 68.54, 64.78, 63.23, 59.25, 56.45, 54.79, 49.83, 48.45, 47.33, 39.53, 38.56, 29.46, 28.96, 28.82, 28.70, 28.61, 28.58, 28.17, 28.12, 25.84, 25.31, 11.71. MALDI TOF-MS *m/e* calcd for $C_{39}H_{70}N_6O_{12}Na^+$, 838.01; measured *m/e*, 838.482 $[M+Na]^+$

Compound 27a: Synthesized as per the general procedure F using compound **32a** (0.185 g, 0.107 mmol) and 3M HCl in MeOH (5 mL). The residual was purified by C-18 reverse-phase column chromatography to yield pure white HCl salts of **27a** (0.045 g, 65%). ^{1}H NMR (500 MHz, D_2O) δ 8.10 (d, *J* = 6.9 Hz, 1H, H-5_{def}), 7.36 (d, *J* = 6.9 Hz, 1H, H-6_{def}), 5.41 (d, *J* = 2.5 Hz, 1H, H-1'), 5.21 (d, *J* = 3.4 Hz, 1H, H-1"), 4.40 (m, 2H, *O*-CH_2 linker), 4.31 – 4.26 (m, 1H), 4.26 – 4.21 (m, 1H), 4.00 – 3.92 (m, 4H), 3.88 – 3.72 (m, 8H), 3.66 – 3.55 (m, 3H), 3.46 – 3.42 (m, 1H, H-6'), 3.35 – 3.29 (m, 1H, H-6'), 2.57 – 2.52 (m, 4H), 2.32 – 2.18 (m, 2H), 2.05 – 1.91 (m, 3H), 1.88 – 1.82 (m, 2H); ^{13}C NMR (126 MHz, D_2O) δ 159.57, 142.33, 140.36, 134.46, 107.96, 101.16 (anomeric), 92.76 (anomeric), 82.05, 81.70, 76.81, 75.85, 73.18, 72.86, 70.68, 68.55, 64.85, 63.18, 59.32, 54.79, 49.67, 48.44, 47.30, 38.52, 28.04, 27.71, 25.87, 24.52, 13.68. MALDI TOF-MS *m/e* calcd for $C_{28}H_{50}N_6O_{11}Na^+$, 669.34; measured *m/e*, 669.2 $[M+Na]^+$

Compound 27b: Synthesized as per the general procedure F using compound **32b** (0.180 g, 0.101 mmol) and 3M HCl in MeOH (5 mL). The residual was purified by C-18 reverse-phase column chromatography to yield pure white HCl salts of **27b** (0.045 g, 63%). ^{1}H NMR (500 MHz, D_2O) δ 8.10 (d, *J* = 6.8 Hz, 1H, H-5_{def}), 7.36 (d, *J* = 6.8 Hz, 1H, H-6_{def}), 5.40 (d, *J* = 2.5 Hz, 1H H-1'),

5.20 (d, *J* = 3.4 Hz, 1H, H-1”), 4.38 (t, *J* = 6.7 Hz, 2H, *O*-CH_2 linker), 4.33 – 4.28 (m, 1H), 4.23 (t, *J* = 9.8 Hz, 1H), 3.99 – 3.94 (m, 3H), 3.92 – 3.73 (m, 8H), 3.68 – 3.58 (m, 3H), 3.46 – 3.41 (m, 1H, H-6’), 3.33 (dd, *J* = 14.0, 3.8 Hz, 1H H-6’), 2.58 – 2.56 (m, 4H), 2.32 – 2.22 (m, 2H), 2.07 – 1.98 (m, 1H), 1.90 (m, 2H), 1.69 – 1.60 (m, 2H), 1.48 (m, 2H), 1.41 – 1.29 (m, 6H, CH_2 linker); ^{13}C NMR (126 MHz, D_2O) δ 159.71 (CO), 142.36, 140.04, 134.38, 107.95, 101.35 (anomeric), 92.72 (anomeric), 81.86, 81.81, 76.64, 75.74, 73.78, 73.15, 71.19, 68.58, 64.83, 63.28, 59.28, 54.80, 49.80, 48.50, 47.36, 38.59, 29.49, 28.93, 28.49, 28.12, 27.79, 27.73, 25.25, 24.93, 13.67. MALDI TOF-MS *m/e* calcd for $C_{28}H_{50}N_6O_{11}$, 702.85; measured *m/e*, 703.3 $[M+H]^+$

Compound 27c: Synthesized as per the general procedure F using compound **32c** (0.252 g, 0.137 mmol) and 3M HCl in MeOH (5 mL). The residual was purified by C-18 reverse-phase column chromatography to yield pure white HCl salts of **27c** (0.062 g, 60%). ^{1}H NMR (500 MHz, D_2O) δ 8.12 (d, *J* = 6.5 Hz, 1H, H-5$_{def}$), 7.38 (d, *J* = 6.5 Hz, 1H, H-6$_{def}$), 5.42 (d, *J* = 2.6 Hz, 1H H-1’), 5.21 (d, *J* = 3.4 Hz, 1H, H-1”), 4.39 (t, *J* = 6.7 Hz, 2H, *O*-CH_2 linker), 4.35 – 4.30 (m, 1H), 4.26 (t, *J* = 9.8 Hz, 1H), 4.02 – 3.96 (m, 3H), 3.95 – 3.87 (m, 4H), 3.86 – 3.81 (m, 2H), 3.79 – 3.74 (m, 2H), 3.70 – 3.61 (m, 3H), 3.47 – 3.42 (m, 1H, H-6’), 3.35 (m, 1H, H-6’), 2.60 – 2.56 (m, 4H), 2.34 – 2.24 (m, 2H), 2.10 – 2.03 (m, 1H), 1.89 (p, *J* = 6.9 Hz, 2H), 1.71 – 1.61 (m, 2H), 1.50 – 1.43 (m, 2H), 1.40 – 1.25 (m, 14H, CH_2 linker); ^{13}C NMR (126 MHz, D_2O) δ 159.68, 142.45, 139.95, 134.39, 108.00, 101.39 (anomeric), 92.71 (anomeric), 81.87, 81.85, 76.67, 75.79, 73.88, 73.19, 71.26, 68.60, 64.88, 63.33, 59.34, 54.82, 49.84, 48.53, 47.38, 38.63, 29.52, 29.05, 28.96, 28.86, 28.82, 28.78, 28.44, 28.16, 27.78, 27.75, 25.36, 24.94, 13.72. MALDI TOF-MS *m/e* calcd for $C_{36}H_{66}N_6O_{11}Na^+$, 781.47; measured *m/e*, 781.4 $[M+Na]^+$

1,3,2´,6´,3˝-penta-*N*-Boc- 4´, 2˝, 4˝,6˝-tetra-*O*-TBDMS-tobramycin (28): Boc-anhydride (23.34 g, 107 mmol) was added dropwise to the solution of tobramycin (5.0 g, 10.691 mmol) dissolved

in a mixture of water (70 mL) and methanol (140 mL). The mixture was reacted with triethylamine (32.821 g, 235 mmol) at 55 °C for 18 h. Boc-protected tobramycin was obtained as a crude product after concentrating the reaction mixture using rotavapor. The product was dried overnight under high vacuum to yield white solids (9.42 g, 91%). This intermediate was used without purification for the next step. TBDMS-Cl (14.01 g, 92.97 mmol) was added to a solution containing Boc-protected tobramycin (9.0 g, 9.29 mmol) dissolved in dry DMF. To this mixture, 1-methylimidazole (11.43 mL, 139.461 mmol) was added and reacted for 4 days at RT. The workup was performed by evaporating DMF using rotavapor followed by washing with ethyl acetate and water (×3). The organic layer was then washed with brine and dried over anhydrous Na_2SO_4. Ethyl acetate layer was concentrated using rotavapor and dried overnight to obtain crude product. The crude was purified using flash chromatography at 15% ethyl acetate/hexane mobile phase to obtain **28** as white solids (10.64 g, 80.36%). ^{1}H NMR (500 MHz, $CDCl_3$) δ 5.40 (s, 1H), 5.26 (s, 1H), 4.99 – 4.90 (m, 2H), 4.51 (s, 1H), 4.32 (s, 1H), 3.88 – 3.83 (m, 2H), 3.70 – 3.14 (m, 13H), 2.74 – 2..72 (m, 1H), 2.04– 2.02 (m, 1H), 1.45 – 1.42 (m, 45H), 0.92 – 0.87 (m, 36H), 0.13 – -0.05 (m, 24H). MALDI TOF-MS *m/e* calcd for $C_{67}H_{133}N_5O_{19}Si_4Na^+$, 1446.86; measured *m/e*, 1446.80

5-O-(4-bromobutyl)-1,3,2',6',3"-penta-N-(tert-butoxycarbonyl)-4',2",4",6"-tetra-OTBDMS-tobramycin 29a: Synthesized as per the general procedure A using compound **28** (1.00 g, 0.701 mmol), 1,4-dibromobutane (0.25 mL, 2.105 mmol), TBAHS (0.023 g, 0.0701 mmol), KOH (0.117 g, 2.105 mmol), and toluene (7 mL). The crude was purified by flash chromatography with 10% ethyl acetate/hexane to yield **29a** (0.821 g, 75%) as white solids. ^{1}H NMR (500 MHz, $CDCl_3$) δ 5.19 (s, 1H, H-1'), 5.13 (s, 1H, H-1"), 5.04 – 4.97 (m, 1H), 4.76 (s, 1H), 4.51 (s, 1H), 4.14 – 4.08 (m, 2H), 3.84 – 3.53 (m, 9H), 3.45 – 3.42 (m, 2H), 3.39 – 3.36 (m, 3H), 3.25 – 3.24 (m, 2H, H-6'), 2.49 – 2.46 (m, 1H), 2.03 – 2.00 (m, 2H), 1.92 – 1.87 (m, 2H), 1.68 (s, 1H), 1.66 –

1.63 (m, 1H), 1.45 – 1.29 (m, 45H, Boc), 0.95 – 0.86 (m, 36H, TBDMS-^{t}Bu), 0.16 – 0.03 (m, 24H, TBDMS-SiMe$_2$). MALDI TOF-MS *m/e* calcd for $C_{71}H_{140}BrN_5O_{19}Si_4Na^+$, 1583.2; measured *m/e*, 1582.906 $[M+Na]^+$

5-O-(4-bromooctane)-1,3,2',6',3"-penta-N-(tert-butoxycarbonyl)-4',2",4",6"-tetra-OTBDMS-tobramycin 29b: Synthesized as per the general procedure A using compound **28** (1.5 g, 1.052 mmol), 1,8-dibromooctane (0.6 mL, 3.157 mmol), TBAHS (0.035 g, 0.105 mmol), KOH (0.176 g, 3.157 mmol), and toluene (7 mL). The crude was purified by flash chromatography with 10% ethyl acetate/hexane to yield **29b** (1.32 g, 78%) as white solids. ^{1}H NMR (500 MHz, $CDCl_3$) δ 5.22 (s, 1H), 5.14 (s, 1H, H-1'), 5.03 – 5.01 (m, 1H), 4.76 (s, 1H, H-1"), 4.50 (s, 1H), 4.24 – 4.07 (m, 3H), 3.82 – 3.53 (m, 10H), 3.40 (t, *J* = 6.9 Hz, 3H), 3.36 – 3.34 (m, 1H), 3.27 – 3.20 (m, 3H), 2.48 – 2.45 (m, 1H), 2.04 – 1.98 (m, 1H), 1.85 (p, *J* = 7.2 Hz, 2H), 1.73 (s, 1H), 1.44 – 1.42 (m, 45H, Boc), 1.31 – 1.26 (m, 8H, CH_2 linker), 0.94 – 0.86 (m, 36H, TBDMS-^{t}Bu), 0.15 – 0.02 (m, 24H, TBDMS-SiMe$_2$). MALDI TOF-MS *m/e* calcd for $C_{75}H_{148}BrN_5O_{19}Si_4Na^+$, 1639.26; measured *m/e*, 1639.047 $[M+Na]^+$

5-O-(4-bromododecane)-1,3,2',6',3"-penta-N-(tert-butoxycarbonyl)-4',2",4",6"-tetra-OTBDMS-tobramycin 29c: Synthesized as per the general procedure A using compound **28** (1.00 g, 0.701 mmol), 1,12-dibromododecane (0.690 g, 2.103 mmol), TBAHS (0.023 g, 0.070 mmol), KOH (0.118 g, 2.103 mmol), and toluene (7 mL). The crude was purified by flash chromatography with 10% ethyl acetate/hexane to yield **29c** (0.820 g, 70%) as white solids. ^{1}H NMR (500 MHz, $CDCl_3$) δ 5.21 (s, 1H, H-1'), 5.15 (s, 1H, H-1"), 5.06 – 5.04 (m, 2H), 4.77 (s, 1H), 4.50 (s, 1H), 4.26 – 4.06 (m, 3H), 3.81 – 3.48 (m, 9H), 3.41 (t, *J* = 6.9 Hz, 3H), 3.35 – 3.34 (m, 1H), 3.25 – 3.17 (m, 2H), 2.48 – 2.45 (m, 1H), 2.02 – 1.96 (m, 1H), 1.85 (p, *J* = 7.2 Hz, 2H), 1.72 (s, 1H), 1.59 – 1.53 (m, 1H), 1.45 – 1.41 (m, 45H, Boc), 1.31 – 1.32 (m, 17H, CH_2 linker), 0.94 – 0.86 (m, 36H,

TBDMS-^{t}Bu), 0.15 – 0.02 (m, 24H, TBDMS-SiMe$_2$). MALDI TOF-MS *m/e* calcd for $C_{79}H_{156}BrN_5O_{19}Si_4Na^+$, 1692.95; measured *m/e*, 1692.978 $[M+Na]^+$

5-O-(aminobutyl)-1,3,2',6',3"-penta-N-(tert-butoxycarbonyl)-4',2",4",6"- tetra-OTBDMS-tobramycin (34a): Synthesized as per the general procedure C using compound **33a** (0.820 g, 0.538 mmol), $Pd(OH)_2/C$ (0.007 g, 0.053 mmol) and MeOH (9 mL). The crude was purified using column chromatography and pure product **34a** (0.483 g, 60%) was eluted with 10% methanol/dichloromethane. ^{1}H NMR (500 MHz, $CDCl_3$) δ 5.24 (s, 1H, H-1'), 5.16 (s, 1H, H-1"), 5.05 (s, 1H), 4.83 (s, 1H), 4.52 (s, 1H), 4.31 – 4.06 (m, 3H), 3.81 – 3.70 (m, 4H), 3.62 – 3.30 (m, 10H), 3.24 – 3.18 (m, 2H, H-6'), 2.66 (s, 2H), 2.52 – 2.46 (m, 1H), 2.01 – 1.99 (m, 1H), 1.57 – 1.50 (m, 3H), 1.45 – 1.42 (m, 45H), 1.32 – 1.26 (m, 1H), 0.95 – 0.87 (m, 36H, TBDMS-^{t}Bu), 0.15 – 0.04 (m, 24H, TBDMS-SiMe$_2$). MALDI TOF-MS *m/e* calcd for $C_{79}H_{142}N_6O_{19}Si_4Na^+$, 1517.93; measured *m/e*, 1518.868 $[M+Na]^+$

5-O-(aminooctyl)-1,3,2',6',3"-penta-N-(tert-butoxycarbonyl)-4',2",4",6"- tetra-OTBDMS-tobramycin (34b): Synthesized as per the general procedure C using compound **33b** (0.500 g, 0.317 mmol), $Pd(OH)_2/C$ (0.005 g, 0.031 mmol) and MeOH (8 mL). The crude was purified using column chromatography and pure product **34b** (0.285 g, 58%) was eluted with 10% methanol/dichloromethane. ^{1}H NMR (500 MHz, $CDCl_3$) δ 5.23 (s, 1H, H-1'), 5.14 (s, 1H, H-1"), 5.05 – 5.00 (m, 1H), 4.79 (s, 1H), 4.54 (s, 1H), 4.30 – 4.06 (m, 4H), 3.79 – 3.63 (m, 7H), 3.54 – 3.47 (m, 5H), 3.38 – 3.33 (m, 1H), 3.29 – 3.23 (m, 3H), 2.76 (s, 2H), 2.51 – 2.44 (m, 1H), 2.03 – 1.97 (m, 2H), 1.45 – 1.42 (m, 45H, Boc), 1.28 – 1.24 (m, 10H, CH_2 linker), 0.95 – 0.86 (m, 36H, TBDMS-^{t}Bu), 0.16 – 0.03 (m, 24H, TBDMS-SiMe$_2$). MALDI TOF-MS *m/e* calcd for $C_{75}H_{150}N_6O_{19}Si_4Na^+$, 1573.99; measured *m/e*, 1574.943 $[M+Na]^+$

5-O-(aminododecyl)-1,3,2',6',3"-penta-N-(tert-butoxycarbonyl)-4',2",4",6"- tetra-OTBDMS-tobramycin (34c): Synthesized as per the general procedure C using compound **33c** (0.780 g, 0.473 mmol), $Pd(OH)_2/C$ (0.007 g, 0.047 mmol) and MeOH (9 mL). The crude was purified using column chromatography and pure product **34c** (0.418 g, 55%) was eluted with 10% methanol/dichloromethane. ^1H NMR (500 MHz, $CDCl_3$) δ 5.22 (s, 1H, H-1'), 5.15 (s, 1H, H-1"), 5.09 – 5.03 (m, 1H), 4.78 (s, 1H), 4.53 (s, 1H), 4.27 – 4.08 (m, 4H), 3.79 – 3.71 (m, 4H), 3.63 – 3.34 (m, 9H), 3.25 – 3.23 (m, 3H), 2.80 (s, 2H), 2.50 – 2.45 (m, 1H), 2.02 – 2.00 (m, 1H), 1.57 – 1.55 (m, 2H), 1.45 – 1.42 (m, 45H, Boc), 1.27 – 1.24 (m, 16H, CH_2 linker), 0.95 – 0.76 (m, 36H), 0.16 – 0.03 (m, 24H, TBDMS-$SiMe_2$). MALDI TOF-MS *m/e* calcd for $C_{79}H_{158}N_6O_{19}Si_4Na^+$, 1630.06; measured *m/e*, 1630.102 $[M+Na]^+$

2-(3-hydroxy-4-oxo-1,4-dihydropyridin-1-yl) acetic acid (35): Commercially available maltol (1.20 g, 9.523 mmol) was dissolved in hot water (80 ml) with glycine (0.357 g, 4.761 mmol). The mixture was stirred at 85 °C and the pH was adjusted to 9 using 6 M NaOH. The reaction mixture was reacted for 15 h under reflux conditions. Later, the mixture was cooled and about 30 mL of water was removed using high vacuum. To the remaining mixture, pH was adjusted to 3 using 6 M HCl to afford light brown precipitates which were obtained by filtration. The precipitates were then crystallized using hot water and dried overnight to afford light brown crystals of **35** (1.18 g, 62%). ^1H NMR (500 MHz, D_2O) δ 7.95 (d, J = 7.0 Hz, 1H), 7.06 (d, J = 7.0 Hz, 1H), 4.92 (s, 2H), 2.48 (s, 3H). ^{13}C NMR (126 MHz, D_2O) δ 172.27, 161.07, 142.89, 141.60, 139.51, 111.23, 59.04, 12.20. ESI-MS *m/e* calcd for $C_8H_9NO_4Na^+$, 206.04; measured *m/e*, 206.0393 $[M+Na]^+$

Compound 36a: Synthesis was conducted by following the general procedure D using compound **34a** (0.070 g, 0.046 mmol), **35** (0.020 g, 0.093 mmol), triethylamine (0.013 mL, 0.0935 mmol),

HATU (0.035 g, 0.093 mmol), and dichloromethane (5 mL). The crude was purified by column chromatography with 6% methanol/dichloromethane to afford pure light brown solids **36a** (0.042 g, 60%). ^{1}H NMR (500 MHz, $CDCl_3$) δ 7.28 (d, *J* = 7.2 Hz, 1H, H-5$_{def}$), 6.40 (d, *J* = 7.2 Hz, 1H, H-6$_{def}$), 5.25 (s, 1H, H-1'), 5.15 (s, 1H, H-1"), 5.04 (s, 1H), 4.51 (s, 2H, H-2'$_{def}$), 4.15 – 4.09 (m, 1H), 3.80 – 3.20 (m, 18H), 3.12 – 3.04 (m, 1H), 2.41 (s, 1H), 2.33 (s, 3H, H-1$_{def}$), 1.95 – 1.92 (m, 1H), 1.52 (s, 5H), 1.45 – 1.39 (m, 45H, Boc), 0.93 – 0.86 (m, 36H, TBDMS-^{t}Bu), 0.13 – 0.04 (m, 24H, TBDMS-$SiMe_2$). ^{13}C NMR (126 MHz, $CDCl_3$) δ 170.02, 165.65, 155.42, 154.85, 138.18, 128.09, 111.35, 96.06, 79.92, 79.49, 79.34, 72.48, 68.00, 63.15, 57.08, 56.15, 50.68, 48.40, 41.67, 39.85, 35.99, 28.62, 28.49, 28.48, 28.44, 27.43, 26.09, 26.03, 25.98, 25.92, 25.78, 18.47, 18.21, 18.04, 17.93, 12.09, 0.99, -3.79, -4.20, -4.84, -4.99, -5.15. MALDI TOF-MS *m/e* calcd for $C_{79}H_{149}N_7O_{22}Si_4Na^+$, 1682.97; measured *m/e*, 1682.936 $[M+Na]^+$.

Compound 36b: Synthesis was conducted by following the general procedure D using compound **34b** (0.380 g, 0.244 mmol), **35** (0.107 g, 0.489 mmol), triethylamine (0.07 mL, 0.489 mmol), HATU (0.186 g, 0.489 mmol), and dichloromethane (6 mL). The crude was purified by column chromatography with 6% methanol/dichloromethane to afford pure light brown solids **36b** (0.209 g, 55%). ^{1}H NMR (500 MHz, MeOD) δ 7.53 (d, J = 7.2 Hz, 1H, H-5$_{def}$), 6.37 (d, J = 7.1 Hz, 1H, H-6$_{def}$), 5.44 – 5.40 (m, 2H, H-1', H-1"), 4.73 (s, 2H, H-2'$_{def}$), 4.21 – 4.17 (m, 1H), 3.97 – 3.95 (m, 1H), 3.89 (s, 1H), 3.75 – 3.51 (m, 11H), 3.46 – 3.42 (m, 1H), 3.37 – 3.32 (m, 3H), 3.23 – 3.19 (m, 2H, *N*-CH_2 linker), 2.31 (s, 3H, H-1$_{def}$), 2.05 – 2.01 (m, 1H), 1.90 – 1.88 (m, 1H), 1.63 – 1.58 (m, 2H), 1.56 – 1.49 (m, 3H), 1.48 – 1.40 (m, 45H, Boc), 1.37 – 1.21 (m, 10H, CH_2 linker), 0.96 – 0.86 (m, 36H, TBDMS-^{t}Bu), 0.15 – 0.06 (m, 24H, TBDMS-$SiMe_2$). ^{13}C NMR (126 MHz, MeOD) δ 169.86, 166.85, 156.86, 156.67, 156.10, 155.61, 145.52, 139.01, 131.72, 111.03, 95.37, 85.21, 79.29, 79.19, 78.98, 78.78, 78.13, 76.76, 73.39, 71.16, 67.39, 63.74, 56.19, 55.50, 51.57, 48.49,

40.71, 39.42, 35.30, 30.48, 29.84, 29.21, 29.04, 27.85, 27.79, 27.69, 27.52, 27.46, 26.78, 26.31, 25.52, 25.45, 25.27, 25.19, 25.09, 18.14, 18.10, 17.66, 17.53, 17.50, 10.71, -4.72, -5.28, -5.40, -5.53, -5.61, -5.66, -5.86, -6.09, -6.35. MALDI TOF-MS *m/e* calcd for $C_{83}H_{157}N_7O_{22}Si_4Na^+$, 1740.53; measured *m/e*, 1740.001 $[M+Na]^+$.

Compound 36c: Synthesis was conducted by following the general procedure D using compound **34c** (0.450 g, 0.279 mmol), **35** (0.092 g, 0.419 mmol), triethylamine (0.06 mL, 0.419 mmol), HATU (0.159 g, 0.419 mmol), and dichloromethane (6 mL). The crude was purified by column chromatography with 6% methanol/dichloromethane to afford pure light brown solids **36c** (0.225 g, 50%). ^{1}H NMR (500 MHz, MeOD) δ 7.53 (d, *J* = 7.1 Hz, 1H, H-5$_{def}$), 6.38 (d, *J* = 7.1 Hz, 1H, H-6$_{def}$), 5.44 (s, 1H, H-1'), 5.40 (s, 1H, H-1"), 4.73 (s, 2H, H-2'$_{def}$), 4.18 – 4.15 (m, 1H), 4.02 – 3.89 (m, 2H), 3.75 – 3.41 (m, 13H), 3.36 – 3.33 (m, 2H, H-6'), 3.21 (t, *J* = 7.1 Hz, 2H, *N*-CH_2 linker), 2.31 (s, 3H, H-1$_{def}$), 2.05 – 2.00 (m, 1H), 1.92 – 1.87 (m, 1H), 1.60 – 1.51 (m, 5H), 1.45 – 1.42 (m, 45H, Boc), 1.33 – 1.28 (m, 17H, CH_2 linker), 0.95 – 0.89 (m, 36H, TBDMS-^{t}Bu), 0.15 – 0.09 (m, 24H, TBDMS-$SiMe_2$). ^{13}C NMR (126 MHz, MeOD) δ 169.87, 166.95, 156.84, 156.65, 156.09, 155.62, 145.55, 138.99, 131.71, 111.03, 95.38, 85.18, 79.27, 79.18, 78.98, 78.78, 78.14, 76.83, 73.85, 73.40, 72.49, 71.20, 67.39, 63.73, 60.10, 56.21, 55.49, 51.56, 40.72, 39.31, 35.28, 30.84, 30.50, 29.92, 29.50, 29.43, 29.37, 29.33, 29.06, 28.97, 27.86, 27.81, 27.70, 27.53, 27.48, 26.64, 26.32, 25.57, 25.49, 25.29, 25.26, 25.22, 25.11, 19.46, 18.15, 18.10, 17.69, 17.67, 17.55, 17.51, 13.06, 10.65, -4.60, -4.69, -5.26, -5.37, -5.50, -5.60, -5.64, -5.76, -5.84, -6.07, -6.32. MALDI TOF-MS *m/e* calcd for $C_{87}H_{165}N_7O_{22}Si_4Na^+$, 1796.63; measured *m/e*, 1796.047 $[M+Na]^+$

N-dodecyl-2-(3-hydroxy-4-oxo-1,4-dihydropyridin-1-yl) acetamide (26): Compound **35** (0.105 g, 0.522 mmol) was dissolved in dichloromethane followed by the addition of triethylamine (0.073

mL, 0.522 mmol) and HATU coupling reagent (0.198 g, 0.522 mmol). After reacting for 5 mins, dodecylamine (0.048 g, 0.261 mmol) was added to the mixture and the reaction was stirred for 1 h at RT. The workup was carried out using dichloromethane and water (×3) followed by washing of organic layer with brine and $NaHCO_3$. The organic layer was dried over Na_2SO_4 and concentrated using high vacuum. The crude mixture was purified using column chromatography with 5% methanol/dichloromethane to afford **35** (0.137 g, 75%) as white solids. ^{1}H NMR (500 MHz, MeOD) δ 7.53 (d, *J* = 7.5 Hz, 1H, H-5$_{def}$), 6.38 (d, *J* = 6.7 Hz, 1H, H-6$_{def}$), 4.74 (s, 2H, H-2'$_{def}$), 3.22 (t, *J* = 7.0 Hz, 2H, *N*-CH_2 linker), 2.30 (s, 3H, H-1$_{def}$), 1.55 – 1.49 (m, 2H, CH_2 linker), 1.33 – 1.28 (m, 18H, CH_2 linker), 0.89 (t, *J* = 6.8 Hz, 3H). ^{13}C NMR (126 MHz, MeOD) δ 169.87, 167.00, 145.53, 138.99, 131.79, 111.04, 55.48, 39.26, 31.64, 29.34, 29.31, 29.27, 29.25, 29.04, 28.95, 28.90, 26.54, 22.30, 13.00, 10.59. MALDI TOF-MS *m/e* calcd for $C_8H_9NO_4$, 183.16; measured *m/e*, 184.207 $[M+Na]^+$

3-[(4-methoxyphenyl)methyl]-2-methyl-4H-pyran-4-one (30). Commercially available maltol (0.200g, 1.587 mmol) was dissolved in DMF to react with *p*-methoxybenzyl chloride (0.320 mL, 2.380 mmol) in the presence of K_2CO_3 (0.323 g, 2.380 mmol) at 100 °C for 2 hours. The extraction was carried out by ethyl acetate and water (×3) followed by the wash of organic layer with brine. It was further dried with anhydrous Na_2SO_4 and concentrated using high vacuum. The crude mixture was purified with 30% ethyl acetate/hexane to yield **30** (0.175 g, 88%) as viscous orange liquid. ^{1}H NMR (300 MHz, $CDCl_3$) δ 7.50 (d, *J* = 5.7 Hz, 1H, H-5$_{def}$), 7.22 – 7.16 (m, 2H), 6.77 – 6.72 (m, 2H), 6.22 (d, *J* = 5.7 Hz, 1H, H-6$_{def}$), 4.98 (s, 2H), 3.66 (s, 3H, *O*-CH_3), 1.95 (s, 3H, H-1$_{def}$). ESI-MS *m/e* calcd for $C_{14}H_{14}O_4Na^+$, 269.08; measured *m/e*, 269.07 $[M+Na]^+$

3-[(4-methoxyphenyl)methyl]-2-methyl-1,4-dihydropyridin-4-one (31). Synthesis of **31** was carried out by reacting **30** (0.175 g, 0.711 mmol) with ammonium hydroxide (3 ml) in a sealed

tube. The reaction mixture was stirred overnight at 100 °C to yield white solids. The crude mixture was extracted with dichloromethane and water (×3), and the organic layer was dried over anhydrous Na_2SO_4 and concentrated in *vacuo*. Pure white solids **31** (0.140 g, 80%) were obtained after purification of crude product with column chromatography (10% methanol/dichloromethane). ^{1}H NMR (500 MHz, $CDCl_3$) δ 7.41 (d, *J* = 7.0 Hz, 1H, H-5$_{def}$), 7.26 – 7.19 (m, 2H), 6.84 – 6.77 (m, 2H), 6.36 (d, *J* = 6.9 Hz, 1H, H-6$_{def}$), 5.00 (s, 2H), 3.76 (s, 3H, *O*-CH_3), 2.13 (s, 3H, H-1$_{def}$). ESI-MS *m/e* calcd for $C_{13}H_{13}NO_3Na^+$, 268.09; measured *m/e*, 268.091 $[M+Na]^+$

Compound 32a: Synthesis was performed by following general procedure E using compound **29a** (0.223 g, 0.142 mmol), **31** (0.070 g, 0.285 mmol), K_2CO_3 (0.039 g, 0.285 mmol), and DMF (4 mL). The crude was purified by column chromatography with 35% ethyl acetate/hexane to afford pure white solids **32a** (0.185 g, 72%). ^{1}H NMR (500 MHz, $CDCl_3$) δ 8.07 (d, *J* = 5.7 Hz, 1H, H-5$_{def}$), 7.30 (d, *J* = 8.1 Hz, 2H), 6.86 (d, *J* = 8.1 Hz, 2H), 6.69 (d, *J* = 5.6 Hz, 1H, H-6$_{def}$), 5.22 (s, 1H, H-1'), 5.13 (s, 1H, H-1"), 4.98 – 4.88 (m, 3H), 4.70 (s, 1H), 4.53 (s, 1H), 4.19 (s, 1H), 4.04 – 4.02 (m, 3H), 3.78 – 3.71 (m, 5H), 3.62 – 3.53 (m, 5H), 3.41 – 3.32 (m, 3H), 3.26 (d, 2H), 3.16 (s, 1H), 2.45 (s, 1H), 2.29 (s, 3H, H-1$_{def}$), 1.97 – 1.92 (m, 3H), 1.70 (s, 2H), 1.43 – 1.24 (m, 45H, Boc), 1.24 (s, 2H), 0.91 – 0.84 (m, 36H, TBDMS-^{t}Bu), 0.18 – -0.11 (m, 24H, TBDMS-$SiMe_2$); ^{13}C NMR (125 MHz, $CDCl_3$) *δ* 159.85, 158.06, 155.78, 155.07, 154.92, 153.47, 145.39, 142.34, 130.49, 129.99, 114.10, 106.90, 96.67, 86.35, 80.28, 79.77, 79.67, 79.56, 75.68, 74.47, 73.00, 72.04, 68.97, 68.36, 67.59, 63.56, 57.42, 55.52, 50.87, 49.13, 48.61, 42.02, 36.30, 36.02, 29.98, 28.92, 28.81, 28.71, 27.30, 26.41, 26.27, 26.08, 26.03, 19.63, 18.76, 18.58, 18.36, 18.22, 14.41, -3.19, -3.45, -3.92, -4.56, -4.59, -4.74, -4.85, -4.91. MALDI TOF-MS *m/e* calcd for $C_{85}H_{154}N_6O_{22}Si_4$, 1724.53; measured *m/e*, 1725.0 $[M+H]^+$

Compound 32b: Synthesis was performed by following general procedure E using compound **29b** (0.230 g, 0.142 mmol), **31** (0.070 g, 0.285 mmol), K_2CO_3 (0.039 g, 0.285 mmol), and DMF (4 mL). The crude was purified by column chromatography with 35% ethyl acetate/hexane to afford pure white solids **32b** (0.180 g, 68%). ^{1}H NMR (500 MHz, $CDCl^3$) δ 8.08 (d, *J* = 5.6 Hz, 1H, H-5_{def}), 7.32 (d, *J* = 8.2 Hz, 2H), 6.87 (d, *J* = 8.8 Hz, 2H), 6.69 (d, *J* = 5.5 Hz, 1H, H-6_{def}), 5.22 (s, 1H, H-1'), 5.13 (s, 1H, H-1"), 5.06 – 5.00 (m, 2H), 4.91 (s, 2H), 4.75 (s, 1H), 4.52 (s, 1H), 4.23 – 4.07 (m, 3H), 4.03 (t, *J* = 6.7 Hz, 2H), 3.80 – 3.75 (m, 5H), 3.70 – 3.66 (m, 2H), 3.61 (s, 2H), 3.53 – 3.52 (m, 3H), 3.42 – 3.34 (m, 3H), 3.26 – 3.20 (m, 3H), 2.47 – 2.44 (m, 1H), 2.35 (s, 3H, H-1_{def}), 2.02 – 1.97 (m, 1H), 1.88 – 1.83 (m, 2H), 1.43 – 1.39 (m, 45H, Boc), 1.35 – 1.24 (m, 8H, CH_2 linker), 0.93 – 0.84 (m, 36H, TBDMS-^{t}Bu), 0.13 – 0.00 (m, 24H, TBDMS-$SiMe_2$); ^{13}C NMR (126 MHz, $CDCl_3$) δ 159.90, 158.17, 155.84, 155.03, 154.90, 153.50, 145.52, 142.33, 130.39, 130.00, 129.86, 123.48, 119.16, 114.10, 106.75, 98.20, 96.78, 86.11, 80.24, 79.69, 79.56, 79.51, 75.61, 74.47, 73.59, 73.02, 71.91, 68.70, 68.36, 67.20, 63.46, 57.56, 55.54, 50.82, 49.19, 48.65, 41.99, 36.26, 36.00, 30.95, 30.25, 29.98, 29.63, 29.31, 29.05, 28.94, 28.81, 28.70, 26.46, 26.43, 26.32, 26.29, 26.08, 19.56, 18.78, 18.62, 18.40, 18.22, -3.10, -3.47, -3.89, -4.57, -4.64, -4.78, -4.87, -4.91. MALDI TOF-MS *m/e* calcd for $C_{89}H_{162}N_6O_{22}Si_4$, 1780.64; measured *m/e*, 1780.9 $[M+H]^+$

Compound 32c: Synthesis was performed by following general procedure E using compound **29a** (0.340 g, 0.203 mmol), **31** (0.100 g, 0.407 mmol), K_2CO_3 (0.056 g, 0.407 mmol), and DMF (4 mL). The crude was purified by column chromatography with 35% ethyl acetate/hexane to afford pure white solids **32c** (0.252 g, 65%). ^{1}H NMR (500 MHz, $CDCl_3$) δ 8.06 (s, 1H, H-5_{def}), 7.30 (d, *J* = 8.4 Hz, 2H), 6.84 (s, 2H), 6.66 (s, 1H, H-6_{def}), 5.19 (s, 1H, H-1'), 5.12 (s, 1H, H-1"), 5.03 (m, 1H), 4.88 (s, 2H), 4.75 (s, 1H), 4.54 (s, 1H), 4.23 – 4.13 (m, 2H), 4.09 – 3.97 (m, 3H), 3.76 – 3.67 (m, 7H), 3.59 – 3.32 (m, 8H), 3.26 – 3.05 (m, 3H), 2.43 (s, 1H), 2.33 (s, 3H, H-1_{def}), 1.98 – 1.96

(m, 1H), 1.83 (s, 2H), 1.40 – 1.38 (m, 45H, Boc), 1.25 – 1.21 (m, 16H), 0.91 – 0.71 (m, 36H, TBDMS-^{t}Bu), 0.11 – 0.01 (m, 24H, TBDMS-SiMe$_2$); ^{13}C NMR (126 MHz, $CDCl_3$) δ 171.26, 159.84, 158.12, 155.77, 154.99, 154.82, 153.43, 145.46, 142.30, 130.26, 129.79, 119.09, 114.02, 106.66, 98.09, 96.77, 85.98, 80.12, 79.61, 79.44, 75.53, 74.39, 73.64, 72.96, 71.81, 68.66, 68.29, 67.08, 63.35, 60.56, 57.51, 55.45, 50.77, 49.21, 48.63, 41.93, 36.16, 35.90, 30.88, 30.29, 29.95, 29.93, 29.88, 29.83, 29.63, 29.31, 29.14, 28.88, 28.75, 28.64, 26.43, 26.38, 26.32, 26.26, 26.23, 26.03, 21.24, 19.48, 18.84, 18.72, 18.68, 18.57, 18.44, 18.34, 18.15, 14.43, -3.19, -3.55, -3.96, -4.63, -4.70, -4.83, -4.93, -4.99. MALDI TOF-MS *m/e* calcd for $C_{93}H_{170}N_6O_{22}Si_4$, 1836.74; measured *m/e*, 1836.9 $[M+H]^+$

Compound 25: Control compound was previously synthesized in the research group and directly used for microbiology testing. ^{1}H NMR (500 MHz, D_2O) δ 5.18 (d, J = 2.6 Hz, 1H, H-1'), 4.97 (d, J = 3.5 Hz, 1H, H-1"), 4.09 – 4.06 (m, 1H), 4.01 – 3.97 (m, 1H), 3.75 – 3.66 (m, 5H), 3.64 – 3.56 (m, 4H), 3.51 (m, 2H), 3.45 – 3.41 (m, 1H), 3.40 – 3.35 (m, 2H), 3.22 – 3.16 (m, 1H, H-6'), 3.11 (m, 1H, H-6'), 2.33 (m, 1H), 2.07 – 2.02 (m, 2H), 1.79 (m, 1H), 1.43 (m, 2H), 1.08 (m, 18H, CH_2 linker), 0.67 – 0.63 (m, 3H). MALDI TOF-MS *m/e* calcd for $C_{30}H_{61}N_5O_9Na$, 658.44; measured *m/e*, 658.473 $[M+Na]^+$

6.2 Microbiology

Antibacterial susceptibility assay: This study was performed using all the six hybrids (**24a-c** and **27a-c**) and control compounds **25** and **26** against Gram-negative bacteria as per the guidelines of Clinical and Laboratory Standards Institute (CLSI). A 0.5 McFarland turbidity standard solution was prepared by using saline and bacterial culture. Later, this solution was used with the cation-adjusted mueller-hinton broth (CAMHB) as a 1:50 dilution factor. The testing was conducted in a 96-well plate by diluting (2-fold) the hybrids in CAMHB and incubating with equal volumes of

inoculum at 37 °C for 18 h. MIC was determined as the least concentration of hybrid required to inhibit the growth of bacteria. A no growth 'well' was noted visibly as well as with the use of EMax Plus microplate reader (Molecular Devices, Sunnyvale, CA, USA) (91).

Checkerboard assay: The adjuvants under study were diluted along the ordinate while the antibiotics were through the abscissa in a 10 × 7 matrix. The bacterial solution (0.5 McFarland turbidity standard) and inoculum was made similarly as discussed above. Later, it was incubated with equal volumes of inoculum at 37 °C for 18 h and the growth pattern was observed using the EMax Plus microplate reader. MICs were determined as the least concentration of drugs responsible for no growth (91). Successively, fractional inhibitory concentration indices (FICI) were calculated for the antibiotic combinations using the formula:

$$\Sigma\text{FIC} = \text{FIC of agent A} + \text{FIC of agent B}$$

$$\text{FIC of agent A} = \frac{\text{MIC of agent A in combination}}{\text{MIC of agent A alone}}$$

$$\text{FIC of agent B} = \frac{\text{MIC of agent B in combination}}{\text{MIC of agent B alone}}$$

A fractional inhibitory concentration index (FICI) of ≤0.5, 0.5 to ≤4, and >4 correlate with the synergistic, additive, and antagonistic effect of the antibiotic combination (78).

6.3 Cytotoxicity

Human hepatoma cell line (HepG2) and human embryonic kidney (HEK293) cell line were grown in Dulbecco's modified eagle's media (DMEM) along with 10% fetal bovine serum (FBS) in a humidified 5% atmospheric CO_2 incubator at 37°C. A 96-well plate was filled with equal number of cancer cells (5000-HEK293 and 8000-HepG2) in media (50 μL). However, the two blank wells consisted only media (50 μL) except the cancer cells for the fluorescent viability assay. Following the suitable incubation conditions, the antibiotics (50 μL) are added to each well with the desired

concentration (0-200 μM) to assess the cell viability. For the fluorescence treatment of these cells, 10% PrestoBlue reagent was used, and the absorbance was taken at suitable wavelengths (540/590 nm) using the plate reader (80).

REFERENCES

1. Wu W, Jin Y, Bai F, Jin S. *Pseudomonas aeruginosa*. In: Molecular medical microbiology. Elsevier; 2015, 753-767.

2. Lister P, Wolter D, Hanson N. Antibacterial-resistant *Pseudomonas aeruginosa*: clinical impact and complex regulation of chromosomally encoded resistance mechanisms. Clinical microbiology reviews. 2009; 22(4):582-610.

3. Antibiotic resistance threats in the United States, 2019. Centers for disease control and prevention (U.S.); 2019 [cited 2022 Oct 9]. Available from: https://stacks.cdc.gov/view/cdc/82532

4. Planet P. *Pseudomonas aeruginosa*. In: Principles and practice of pediatric infectious diseases. Elsevier; 2018. 866-870.

5. Regulation and function of versatile aerobic and anaerobic respiratory metabolism in *Pseudomonas aeruginosa*. Frontiers in microbiology. 2011;2(103):1-13.

6. Chevalier S, Bouffartigues E, Bodilis J, Maillot O, Lesouhaitier O, Feuilloley M, Orange N, Dufour A, Cornelis P. Structure, function and regulation of *Pseudomonas aeruginosa* porins. FEMS microbiology reviews. 2017;41(5):698-722.

7. Klockgether J, Cramer N, Wiehlmann L, Davenport C, Tummler B. *Pseudomonas aeruginosa* genomic structure and diversity. Frontiers in microbiology. 2011;2(150):1-18.

8. When antibiotics fail: the expert panel on the potential socio-economic impacts of antimicrobial resistance in Canada. 2019 [cited 2020 Oct 2]. Available from: http://www.deslibris.ca/ID/10102747

9. Aloush V, Navon-Venezia S, Seigman-Igra Y, Cabili S, Carmeli Y. Multidrug-resistant *Pseudomonas aeruginosa*: risk Factors and clinical impact. Antimicrobial Agents and Chemotherapy. 2006;50(1):43-48.

10. Raman G, Avendano E, Chan J, Merchant S, Puzniak L. Risk factors for hospitalized patients with resistant or multidrug-resistant *Pseudomonas aeruginosa* infections: a systematic review and meta-analysis. Antimicrobial resistance & infection control. 2018;7(1):1-14.

11. Bucior I, Pielage J, Enjel J. *Pseudomonas aeruginosa* pili and flagella mediate distinct binding and signaling events at the apical and basolateral surface of airway epithelium. PLOS pathogens. 2012, 8(4):e1002616,1-18.

12. Cendra M del M, Christodoulides M, Hossain P. Signaling mediated by toll-like receptor 5 sensing of *Pseudomonas aeruginosa* flagellin influences IL-1β and IL-18 production by primary fibroblasts derived from the human cornea. Frontiers in cellular and infection microbiology. 2017;7(130):1-13.

13. Alhazmi A. *Pseudomonas aeruginosa*- pathogenesis and pathogenic mechanisms. International journal of biology. 2015;7(2):44-67.

14. Foulkes D, McLean K, Haneef A, Fernig D, Winstanley , Berry N, Kaye S. *Pseudomonas aeruginosa* toxin ExoU as a therapeutic target in the treatment of bacterial infections. Microorganisms. 2019;7(707):1-17.

15. Kuang Z, Hao Y, Walling B, Jeffries J, Ohman D, Lau G. *Pseudomonas aeruginosa* elastase provides an escape from phagocytosis by degrading the pulmonary surfactant protein-A. PLOS one. 2011;6(11);e27091,1-14.

16. Jiang F, Waterfield N, Yang J, Yang G, Jin Q. A *Pseudomonas aeruginosa* type VI secretion phospholipase D effector targets both prokaryotic and eukaryotic cells. Cell host microbe. 2014;15(5):600-610.

17. Ding F, Oinuma K, Smalley N, Schaefer A, Hamwy O, Greenberg E, Dandekar A. The *Pseudomonas aeruginosa* orphan quorum sensing signal receptor QscR regulates global quorum sensing gene expression by activating a single linked operon. MBio. 2018;9(4),e01274-18,1-10.

18. Ruer S, Stender S, Filloux A, de Bentzmann S. Assembly of fimbrial structures in *Pseudomonas aeruginosa*: functionality and specificity of chaperone-usher machineries. Journal of bacteriology. 2007;189(9):3547-55.

19. Pachori P, Gothalwal R, Gandhi P. Emergence of antibiotic resistance *Pseudomonas aeruginosa* in intensive care unit; a critical review. Genes & diseases. 2019;6(2):109-119.

20. Pang Z, Raudonis R, Glick B, Lin T, Cheng Z. Antibiotic resistance in *Pseudomonas aeruginosa*: mechanisms and alternative therapeutic strategies. Biotechnology Advances. 2019;37(1):177-192.

21. Botelho J, Grosso F, Peixe L. Antibiotic resistance in *Pseudomonas aeruginosa*- mechanisms, epidemiology and evolution. Drug resistance updates. 2019;44(100640): 26-47.

22. Pan Y, Xu Y, Wang Z, Fang Y, Shen J. Overexpression of MexAB-OprM efflux pump in carbapenem-resistant *Pseudomonas aeruginosa*. Archives of microbiology. 2016;198(6):565-571.

23. Lamers R, Cavallari J, Burrows L. The efflux inhibitor phenylalanine-arginine beta-naphthylamide (PAβN) permeabilizes the outer membrane of Gram-negative bacteria. PLOS one. 2013;8(3),e60666, 1-7.

24. Bello-Lopez J, Cabrero-Martinez O, Ibanez-Cervantes G, Hernandez-Cortez C, Pelcastre-Rodriguez L, Gonzalez-Avila L, Castro-Escarpulli G. Horizontal gene transfer and its association with antibiotic resistance in the genus *Aeromonas* spp. Microorganisms. 2019;7(363):1-11.

25. Schmidtke A, Hanson N. Role of ampD homologs in overproduction of AmpC in clinical isolates of *Pseudomonas aeruginosa*. Antimicrobial agents and chemotherapy. 2008;52(11):3922-3927.

26. Yi L, Li J, Liu B, Wang Y. Advances in research on signal molecules regulating biofilms. World journal of microbiology and biotechnology. 2019;35(8):1-8.

27. Coleman S, Blimkie T, Falsafi R, Hancock R. Multidrug adaptive resistance of *Pseudomonas aeruginosa* swarming cells. Antimicrobial agents and chemotherapy. 2020;64(3):e01999-19, 1-17.

28. Eliopoulos G, Roberts M. Tetracycline therapy: update. Clinical infectious diseases. 2003;36(4):462-467.

29. Chopra I, Roberts M. Tetracycline antibiotics: mode of action, applications, molecular biology, and epidemiology of bacterial resistance. Microbiology and molecular biology reviews. 2001;65(2):232-260.

30. Scott L. Eravacycline: a review in complicated intra-abdominal infections. Drugs. 2019;79(3):315-324.

31. Grossman T. Tetracycline antibiotics and resistance. Colds spring harbor perspectives in medicine. 2016;6(4):a025387,1-24.

32. Arslan I. Trends in antimicrobial resistance in healthcare-associated infections: a global concern. In: Encyclopedia of Infection and Immunity. Elsevier; 2022, 652-661.

33. Trevor A, Katzung B, Masters S. Basic & Clinical Pharmacology, 15th edition. McGraw Hill Medical. 2021; 43:1-11.

34. Bassetti M, Vena A, Croxatto A, Righi E, Guery B. How to manage *Pseudomonas aeruginosa* infections? Drugs in context. 2018;7(212527):1-18.

35. Minandri F, Imperi F, Frangipani E, Bonchi C, Visaggio D, Facchini M, Pasquali P, Bragonzi A, Visca P. Role of iron uptake systems in *Pseudomonas aeruginosa* virulence and airway infection. Infection and immunity. 2016;84(8):2324-2335.

36. Lieu P, Heiskala M, Peterson P, Yang Y. The roles of iron in health and disease. Molecular aspects of medicine. 2001;22(2):1-87.

37. Liu Z, Ren Z, Zhang J, Chuang C, Kandaswamy E, Zhou T, Zuo L. Role of ROS and nutritional antioxidants in human diseases. Frontiers in physiology. 2018;9(477):1-14.

38. Hatcher H, Singh R, Torti F, Torti S. Synthetic and natural iron chelators: therapeutic potential and clinical use. Future medicinal chemistry. 2009;1(9):1-35.

39. Cornelis P, Dingemans J. *Pseudomonas aeruginosa* adapts its iron uptake strategies in function of the type of infections. Frontiers in cellular and infection microbiology. 2013;3(75):1-7.

40. Bonneau A, Roche B, Schalk I. Iron acquisition in *Pseudomonas aeruginosa* by the siderophore pyoverdine: an intricate interacting network including periplasmic and membrane proteins. Scientific reports. 2020;10(120)-1-11.

41. Wu J, Srinivas P, Pogue J. Cefiderocol: a novel agent for the management of multidrug-resistant Gram-negative organisms. Infectious diseases and therapy. 2020;9(1):17-40.

42. Domalaon R, Idowu T, Zhanel G, Schweizer F. Antibiotic Hybrids: the next generation of agents and adjuvants against Gram-negative pathogens? Clinical microbiology reviews. 2018;31(2):e00077-17, 1-45.

43. Ito A, Nishikawa T, Matsumoto S, Yoshizawa H, Sato T, Nakamura R, Tsuji M, Yamano Y. Siderophore Cephalosporin Cefiderocol Utilizes Ferric Iron Transporter Systems for Antibacterial Activity against Pseudomonas aeruginosa. Antimicrob Agents Chemother. 2016;60(12):7396-7401.

44. Negash K, Norris J, Hodgkinson J. Siderophore-antibiotic conjugate design: new drugs for bad bugs? Molecules. 2019;24(18):1-16.

45. Braun V, Braun M. Iron transport and signaling in *Escherichia coli*. FEBS letters. 2002;529(1):78-85.

46. Noinaj N, Guillier M, Barnard T, Buchanan S. TonB-dependent transporters: regulation, structure, and function. Annual review of microbiology. 2010;64(1):43-60.

47. Brown M, Mitton-Fry M, Arcari J, Barham R, Casavant J, Gerstenberger B, Han S, Hardink J, Harris T, Hoang T, Huband M. Pyridone-conjugated monobactam antibiotics with Gram-negative activity. Journal of medicinal chemistry. 2013;56(13):5541-5552.

48. Mitton-Fry M, Arcari J, Brown M, Casavant J, Finegan S, Flanagan M, Gao H, George D, Gerstenberger B, Han S, Hardink J. Novel monobactams utilizing a siderophore uptake mechanism for the treatment of Gram-negative infections. Bioorganic & medicinal chemistry letters. 2012;22(18):5989-5994.

49. Page M, Dantier C, Desarbre E. *In vitro* properties of BAL30072, a novel siderophore Sulfactam with activity against multiresistant Gram-negative bacilli. Antimicrobial agents and chemotherapy. 2010;54(6):2291-2302.

50. Uivarosi V. Metal complexes of quinolone antibiotics and their applications: an update. Molecules. 2013;18(9):11153-11197.

51. Faure M, Cilibrizzi A, Abbate V, Bruce K, Hider R. Effect of iron chelation on anti-pseudomonal activity of doxycycline. International journal of antimicrobial agents. 2021;58(6):106438,1-8.

52. Zhou Y, Zhang M, Hider R, Zhou T. *In vitro* antimicrobial activity of hydroxypyridinone hexadentate-based dendrimeric chelators alone and in combination with norfloxacin. FEMS microbiology letters. 2014;355(2):124-130.

53. Piyamongkol S, Zhou T, Liu Z, Khodr H, Hider R. Design and characterisation of novel hexadentate 3-hydroxypyridin-4-one ligands. Tetrahedron letters. 2005;46(8):1333-1336.

54. Viegas-Junior C, Barreiro E, Fraga C. Molecular hybridization: a useful tool in the design of new drug prototypes. Current medicinal chemistry. 2007;14(17):1829-1852.

55. Machado D, Girardini M, Viveiros M, Pieroni M. Challenging the drug-likeness dogma for new drug discovery in tuberculosis. Frontiers in microbiology. 2018, 9(1367):1-23.

56. Becker B, Cooper M. Aminoglycoside antibiotics in the 21st century. ACS chemical biology. 2013;8(1):105-115.

57. Melia C, Ferrer S, Moliner V, Bertran J. Theoretical studies of the hydrolysis of antibiotics catalyzed by a metallo-β-lactamase. Archives of biochemistry and biophysics. 2015;582(1):116-126.

58. Cefamandole. Pubchem; 2022 [cited 2022 Oct 9]. Available from: https://pubchem.ncbi.nlm.nih.gov/compound/456255

59. Scheffers D, Pinho M. Bacterial cell wall synthesis: New insights from localization studies. Microbiology and molecular biology reviews. 2005;69(4):585-607.

60. Milligan D, Tran S, Strych U, Cook G, Krause K. The alanine racemase of *Mycobacterium smegmatis* is essential for growth in the absence of d-alanine. Journal of bacteriology. 2007;189(22):8381-8386.

61. Christenson J, Chan K, Cleeland R, Dix-Holzknecht B, Farrish H, Patel I, Specian A. Pharmacokinetics of Ro 23-9424, a dual-action cephalosporin, in animals. Antimicrobial agents and chemotherapy. 1990;34(10):1895-1900.

62. Beskid G, Siebelist J, McGarry C, Cleeland R, Chan K, Keith D. *In vivo* evaluation of a dual-action antibacterial, Ro 23-9424, compared to cefotaxime and fleroxacin. Chemotherapy. 1990;36(2):109-116.

63. Mingeot-Leclercq M, Decout J. Bacterial lipid membranes as promising targets to fight antimicrobial resistance, molecular foundations and illustration through the renewal of aminoglycoside antibiotics and emergence of amphiphilic aminoglycosides. Medicinal chemistry communications. 2016;7(4):586-611.

64. Fosso M, Li Y, Garneau-Tsodikova S. New trends in the use of aminoglycosides. Medicinal chem communications. 2014;5(8):1075-1091.

65. Bulitta J, Ly N, Landersdorfer C, Wanigaratne N, Velkov T, Yadav R, Oliver A, Martin L, Shin B, Forrest A, Tsuji B. Two mechanisms of killing of *Pseudomonas aeruginosa* by tobramycin assessed at multiple inocula via mechanism-based modeling. Antimicrobial agents and chemotherapy. 2015;59(4):2315-2327.

66. Zavascki A, Goldani L, Li J, Nation R. Polymyxin B for the treatment of multidrug-resistant pathogens: a critical review. Journal of antimicrobial chemotherapy. 2007;60(6):1206-1215.

67. Pokrovskaya V, Belakhov V, Hainrichson M, Yaron S, Baasov T. Design, synthesis, and evaluation of novel fluoroquinolone−aminoglycoside hybrid antibiotics. Journal of medicinal chemistry. 2009;52(8):2243-2254.

68. Gorityala B, Guchhait G, Goswami S, Fernando D, Kumar A, Zhanel G, Schweizer F. Hybrid antibiotic overcomes resistance in *P. aeruginosa* by enhancing outer membrane penetration and reducing efflux. Journal of medicinal chemistry. 2016;59(18):8441-8455.

69. Idowu T, Ammeter D, Brizuela M, Jackson G, Alam S, Schweizer F. Overcoming β-lactam resistance in *Pseudomonas aeruginosa* using non-canonical tobramycin-based antibiotic adjuvants. Bioorganic & medicinal chemistry letters. 2020;30(21):127575,1-9.

70. Deshayes S, Xian W, Schmidt N, Kordbacheh S, Lieng J, Wang J, Zarmer S, Germain S, Voyen L, Thulin J, Wong G. Designing hybrid antibiotic peptide conjugates to cross bacterial membranes. Bioconjugate Chemistry. 2017;28(3):793-804.

71. Balouiri M, Sadiki M, Ibnsouda S. Methods for *in vitro* evaluating antimicrobial activity: a review. Journal of pharmaceutical analysis. 2016;6(2):71-79.

72. Rolain J, Baquero F. The refusal of the society to accept antibiotic toxicity: missing opportunities for therapy of severe infections. Clinical microbiology and infection. 2016;22(5):423-427.

73. Ignasiak K. Galleria mellonella (greater wax moth) larvae as a model for antibiotic susceptibility testing and acute toxicity trials. BMC research notes. 2017;10(1):1-8.

74. Sarver J, Trendel J, Bearss N, Wang L, Luniwal A, Erhardt P, Viola R. Early stage efficacy and toxicology screening for antibiotics and enzyme inhibitors. Journal of biomolecular screening. 2012;17(5):673-682.

75. Wiegand I, Hilpert K, Hancock R. Agar and broth dilution methods to determine the minimal inhibitory concentration (MIC) of antimicrobial substances. Nature protocols. 2008;3(2):163-175.

76. Murray P. The clinician and the microbiology laboratory. In: Mandell, Douglas, and Bennett's Principles and practice of infectious diseases. Elsevier; 2015, 191-223.

77. Lopez-Carballo G, Gomez-Estaca J, Catala R, Hernandez-Munoz P, Gavara R. Active antimicrobial food and beverage packaging. In: Emerging food packaging technologies. Elsevier; 2012,27-54.

78. Ramirez D, Berry L, Domalaon R, Brizuela M, Schweizer F. Dilipid ultrashort tetrabasic peptidomimetics potentiate novobiocin and rifampicin against multidrug-resistant Gram-negative bacteria. ACS infectious diseases. 2020;6(6)1413-1426.

79. Antimicrobial synergy study- checkerboard assay. 2022; [cited 2022 Oct 9]. Available from: https://emerypharma.com/biology/antimicrobial-synergy-study-checkerboard-assay/

80. Idowu T, Samadder P, Arthur G, Schweizer F. Design, synthesis and antitumor properties of glycosylated antitumor ether lipid (GAEL)- chlorambucil-hybrids. Chemistry and physics of lipids. 2016;194(1):139-148.

81. Cho H, Kwon K, Kim S, Park Y, Koo S. Association between biofilm formation and antimicrobial resistance in carbapenem-resistant *Pseudomonas aeruginosa*. Annals of clinical and laboratory sciences. 2018;48(3):363-368.

82. Fernandez L, Hancock R. Adaptive and mutational resistance: role of porins and efflux pumps in drug resistance. Clinical microbiology reviews. 2012;25(4):661-681.

83. Choi U, Lee C. Distinct roles of outer membrane porins in antibiotic resistance and membrane integrity in *Escherichia coli*. Frontiers in microbiology. 2019;10(953):1-9.

84. Dean C, Visalli M, Projan S, Sum P, Bradford P. Efflux-mediated resistance to tigecycline (GAR-936) in *Pseudomonas aeruginosa* PAO1. Antimicrobial agents and chemotherapy. 2003;47(3):972-978.

85. Yang X, Goswami S, Gorityala B, Domalaon R, Lyu Y, Kumar A, Zhanel G, Schweizer F. A tobramycin vector enhances synergy and efficacy of efflux pump inhibitors against multidrug-resistant Gram-negative bacteria. Journal of medicinal chemistry. 2017;60(9):3913-3932.

86. Idowu T, Arthur G, Zhanel G, Schweizer F. Heterodimeric rifampicin-tobramycin conjugates break intrinsic resistance of *Pseudomonas aeruginosa* to doxycycline and chloramphenicol in

vitro and in a *Galleria mellonella in vivo* model. European journal of medicinal chemistry. 2019;174(1):16-32.

87. Herzog I, Green K, Berkov-Zrihen Y, Feldman M, Vidavski R, Eldar-Boock A, Satchi-Fainaro R, Garneau-Tsodikova S, Fridman M, . 6″-thioether tobramycin analogues: towards selective targeting of bacterial membranes. Angewandte chemie international edition. 2012;51(23):5652-5656.

88. Coraca-Huber D, Dichtl S, Steixner S, Nogler M, Weiss G. Iron chelation destabilizes bacterial biofilms and potentiates the antimicrobial activity of antibiotics against coagulase-negative *Staphylococci*. Pathogens and disease. 2018;76(5):52, 1-8.

89. Richter K, Thomas N, Zhang G, Prestidge C, Coenye T, Wormald P, Vreugde S. Deferiprone and gallium-protoporphyrin have the capacity to potentiate the activity of antibiotics in *Staphylococcus aureus* small colony variants. Frontiers in cellular and infection microbiology. 2017;7(280):1-10.

90. Yu X, Zhu X, Zhou Y, Li Q, Hu Z, Li T, Tao J, Dou M, Zhang M, Shao Y, Sun R. Discovery of N-aryl-pyridine-4-ones as novel potential agrochemical fungicides and bactericides. Journal of agricultural and food Chemistry. 2019;67(50):13904-13913.

91. Lyu Y, Yang X, Goswami S, Gorityala B, Idowu T, Domalaon R, Zhanel G, Shan A, Schweizer F. Amphiphilic tobramycin–Lysine conjugates sensitize multidrug resistant Gram-negative bacteria to rifampicin and minocycline. Journal of medicinal chemistry. 2017;60(9):3684-3702.

92. Mawani Y, Cawthray J, Chang S, Sachs-Barrable K, Weekes D, Wasan K, Orvig C. *In vitro* studies of lanthanide complexes for the treatment of osteoporosis. Dalton transactions. 2013;42(17):5999-6011.

93. Wright G. Antibiotic adjuvants: rescuing antibiotics from resistance. Trends in microbiology. 2016;24(11):862-871.

94. Mulani M, Kamble E, Kumkar S, Tawre M, Pardesi K. Emerging strategies to combat ESKAPE pathogens in the era of antimicrobial resistance: a review. Frontiers in microbiology. 2019;10(539):1-24.

95. Bernal P, Molina-Santiago C, Daddaoua A, Llamas M. Antibiotic adjuvants: identification and clinical use. Microbial biotechnology. 2013;6(5):445-449.

96. Liu Y, Li R, Xiao X, Wang Z. Antibiotic adjuvants: an alternative approach to overcome multi-drug resistant Gram-negative bacteria. Critical reviews in microbiology. 2019;45(3):301-314.

97. Idowu T, Ammeter D, Arthur G, Zhanel G, Schweizer F. Potentiation of β-lactam antibiotics and β-lactam/β-lactamase inhibitor combinations against MDR and XDR *Pseudomonas aeruginosa* using non-ribosomal tobramycin-cyclam conjugates. Journal of antimicrobiology and chemotherapy. 2019;74(9):2640-2648.

98. Tyers M, Wright G. Drug combinations: a strategy to extend the life of antibiotics in the 21st century. Nature reviews microbiology. 2019;17(3):141-155.

99. Asadi A, Abdi M, Kouhsari E, Panahi P, Sholeh M, Sadeghifard N, Amiriani T, Ahmadi A, Maleki A, Gholami M. Minocycline, focus on mechanisms of resistance, antibacterial activity,

and clinical effectiveness: back to the future. Journal of global antimicrobial resistance. 2020;22(1):161-174.

100. Lee Y, Burton C. Eravacycline, a newly approved fluorocycline. European journal of clinical and microbiology infectious diseases. 2019;38(10):1787-1794.

101. Fiore M, Alfieri A, Di Franco S, Pace M, Simeon V, Ingoglia G, Cortegiani A. Ceftazidime-avibactam combination therapy compared to ceftazidime-avibactam monotherapy for the treatment of severe infections due to carbapenem-resistant pathogens: a systematic review and network meta-analysis. Antibiotics. 2020;9(388):1-12.

102. Campanella T, Gallagher J. A clinical review and critical evaluation of imipenem-relebactam: evidence to date. Infection and drug resistance. 2020;13(1):4297-4308.

103. Fiore M, Corrente A, Pace M, Alfieri A, Simeon V, Ippolito M, Giarratano A, Cortegiani A. Ceftolozane-tazobactam combination therapy compared to ceftolozane-tazobactam monotherapy for the treatment of severe infections: a systematic review and meta-analysis. Antibiotics. 2021;10(79):1-11.

104. Vaara M, Vaara T. Sensitization of Gram-negative bacteria to antibiotics and complement by a nontoxic oligopeptide. Nature. 1983;303(5917):526-528.

105. Radzishevsky I, Rotem S, Bourdetsky D, Navon-Venezia S, Carmeli Y, Mor A. Improved antimicrobial peptides based on acyl-lysine oligomers. Nature biotechnology. 2007;25(6):657-659.

106. Dhondikubeer R, Bera S, Zhanel G, Schweizer F. Antibacterial activity of amphiphilic tobramycin. The journal of antibiotics. 2012;65(10):495-498.

SUPPORTING INFORMATION

Cytotoxicity data for hybrids **24a-c**

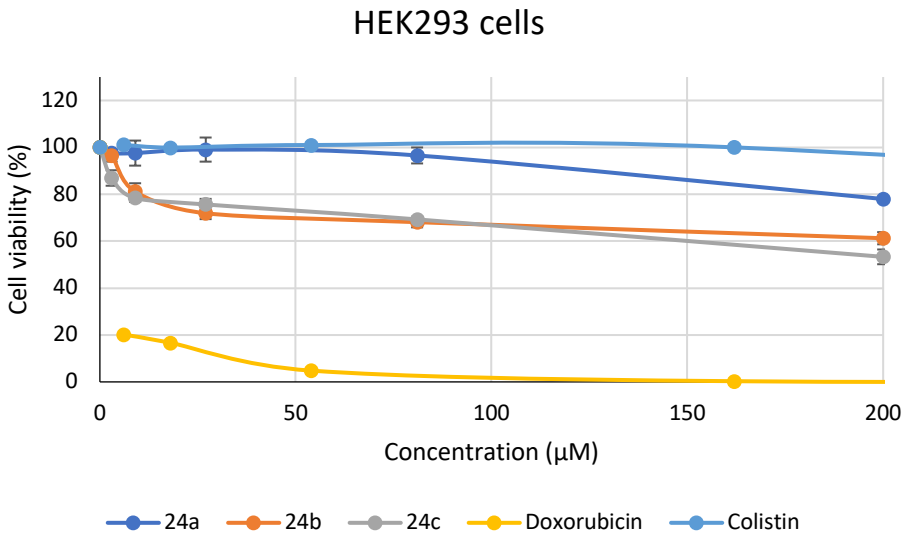

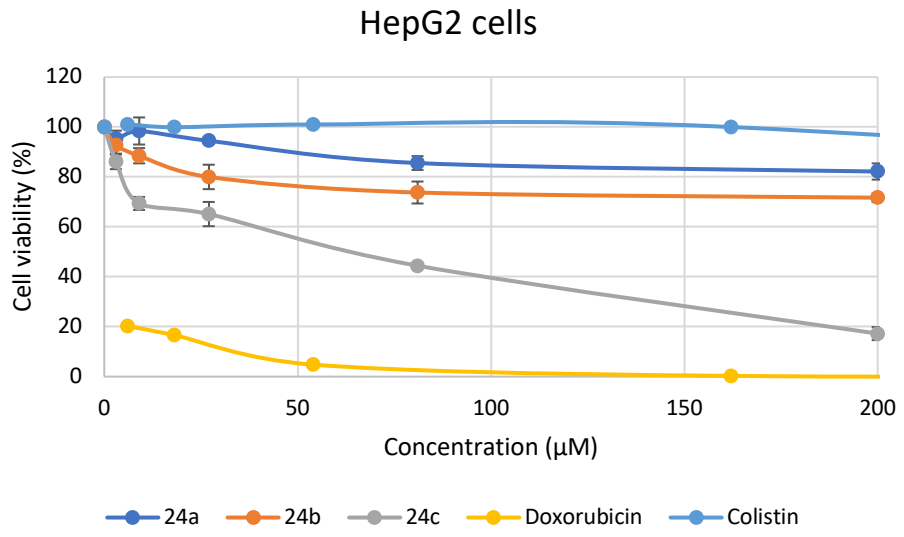

Cytotoxicity data for compounds **27a-c**

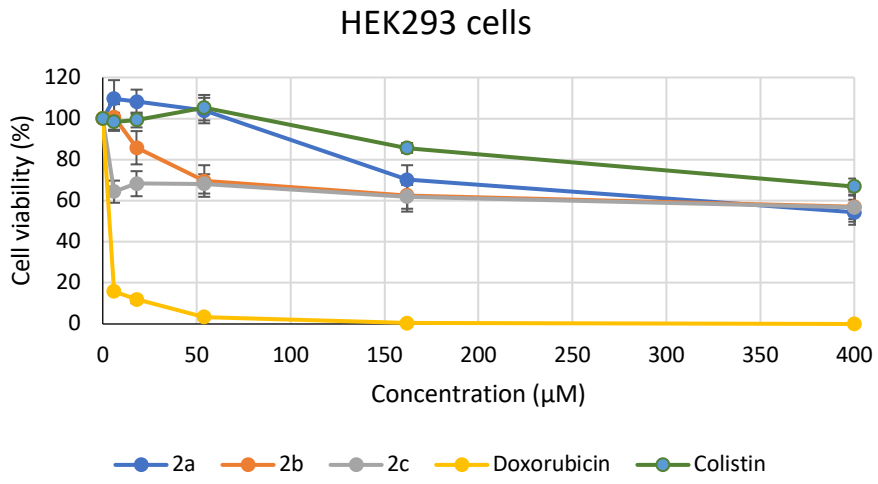

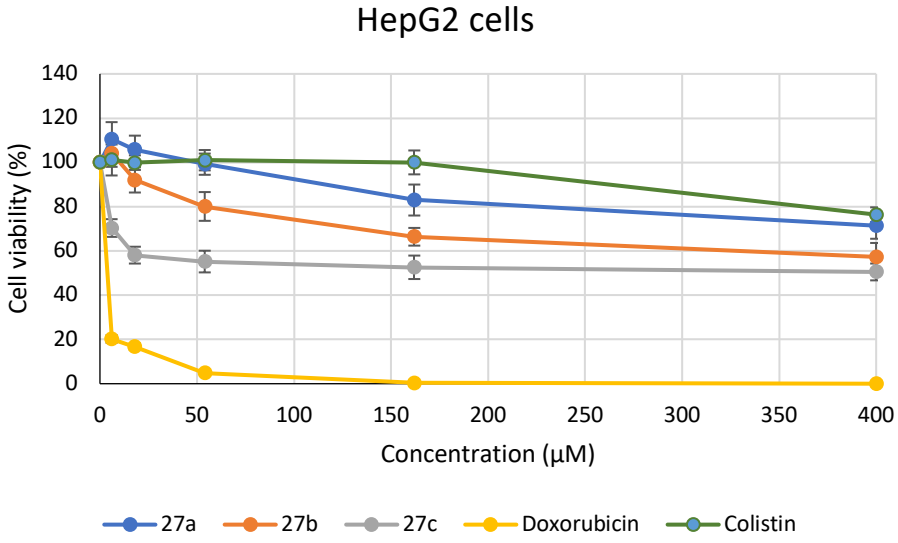

NMR data for final and intermediate molecules

Compound 24a

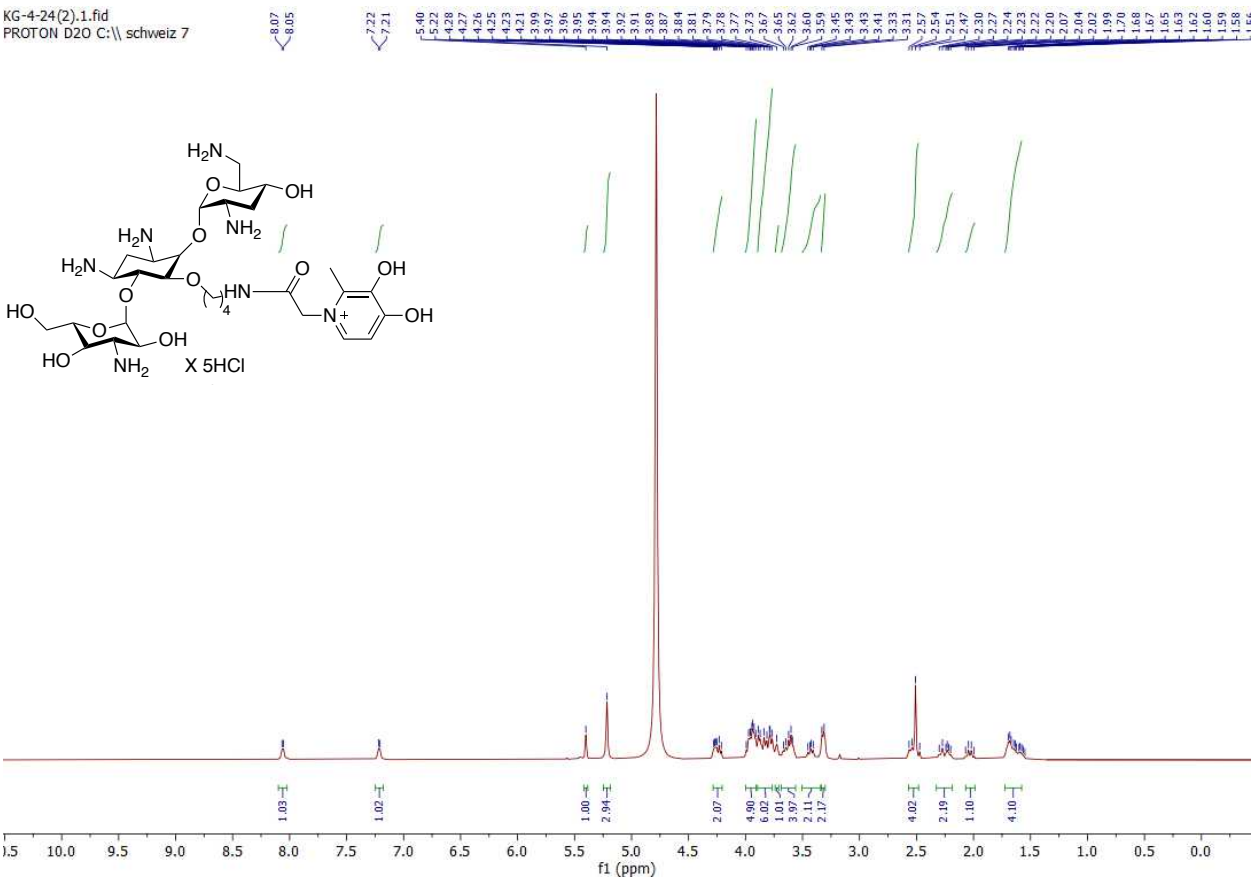

KG-4-24(2).3.fid
C13CPD D2O C:\\ schweiz 1

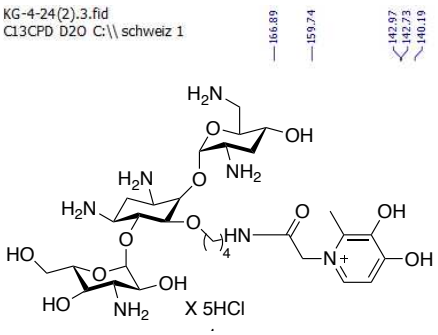

166.89 159.74 142.97 142.73 140.19 111.10 101.15 92.67 92.05 82.12 81.67 76.54 75.56 73.18 72.90 68.61 64.87 63.30 59.35 58.06 54.82 49.66 48.48 47.36 39.84 38.61 28.11 27.73 26.91 25.00 12.50

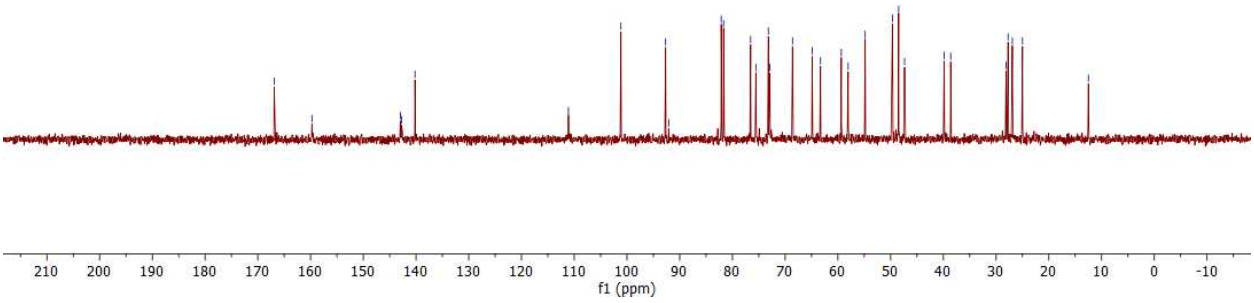

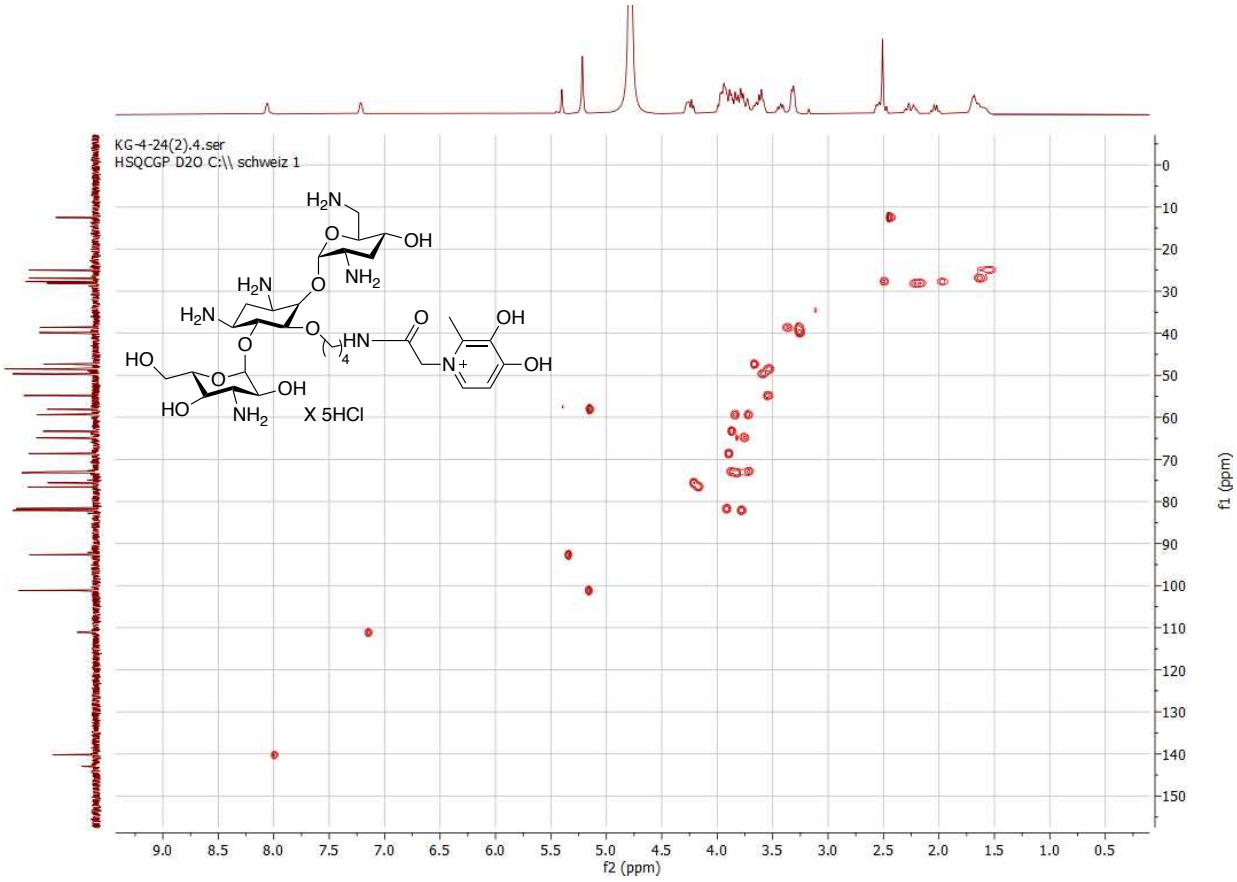
KG-4-24(2).4.ser
HSQCGP D2O C:\\ schweiz 1
X 5HCl
f2 (ppm)
f1 (ppm)

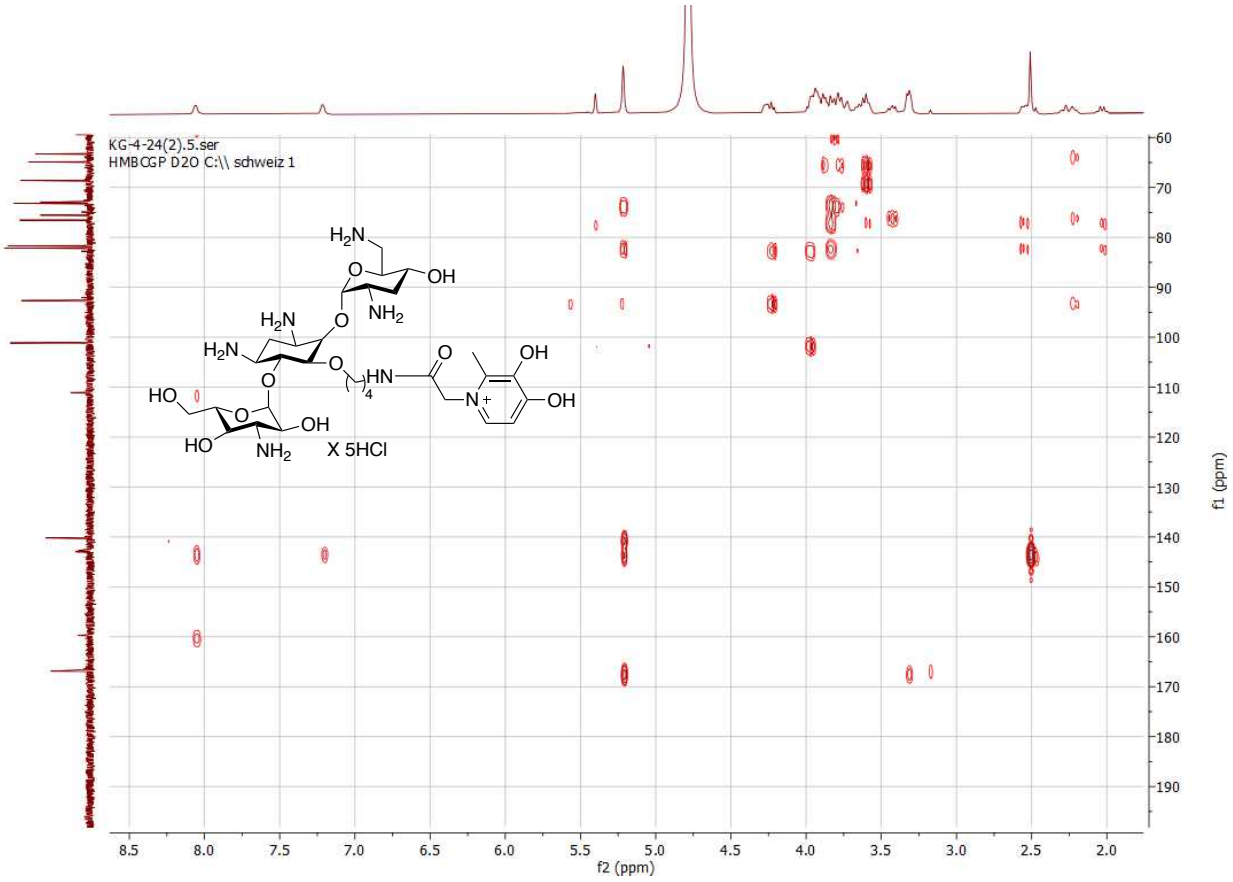
KG-4-24(2).5.ser
HMBCGP D2O C:\\ schweiz 1
X 5HCl
f2 (ppm)
f1 (ppm)

Compound 24b

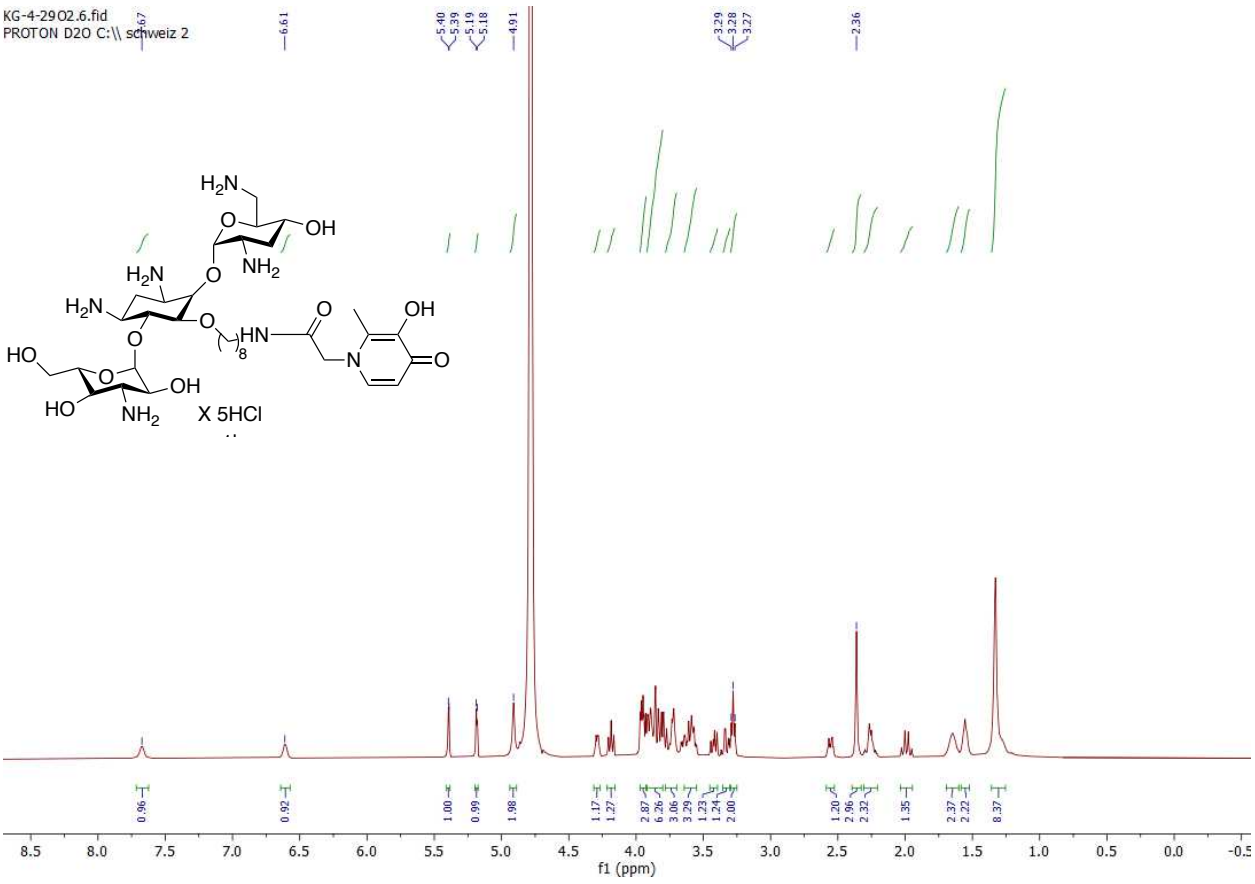

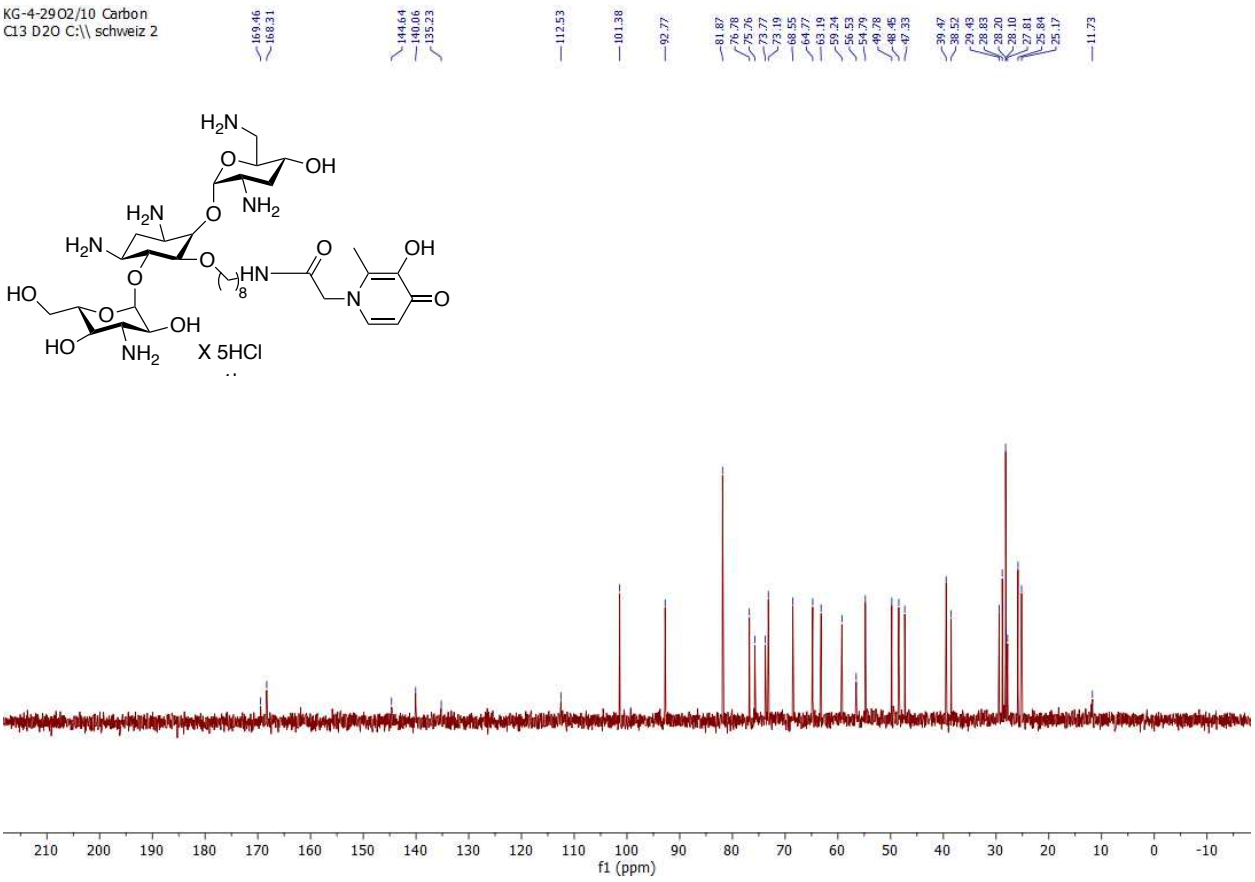
KG-4-2902/10 Carbon
C13 D2O C:\\ schweiz 2
169.46
168.31
144.64
140.06
135.23
112.53
101.38
92.77
81.87
76.78
75.76
73.77
73.19
68.55
64.77
63.19
59.24
56.53
54.79
49.78
48.45
47.33
39.47
38.52
29.43
28.83
28.20
28.10
27.81
25.84
25.17
11.73
X 5HCl
210
200
190
180
170
160
150
140
130
120
110
100
90
80
70
60
50
40
30
20
10
0
-10
f1 (ppm)

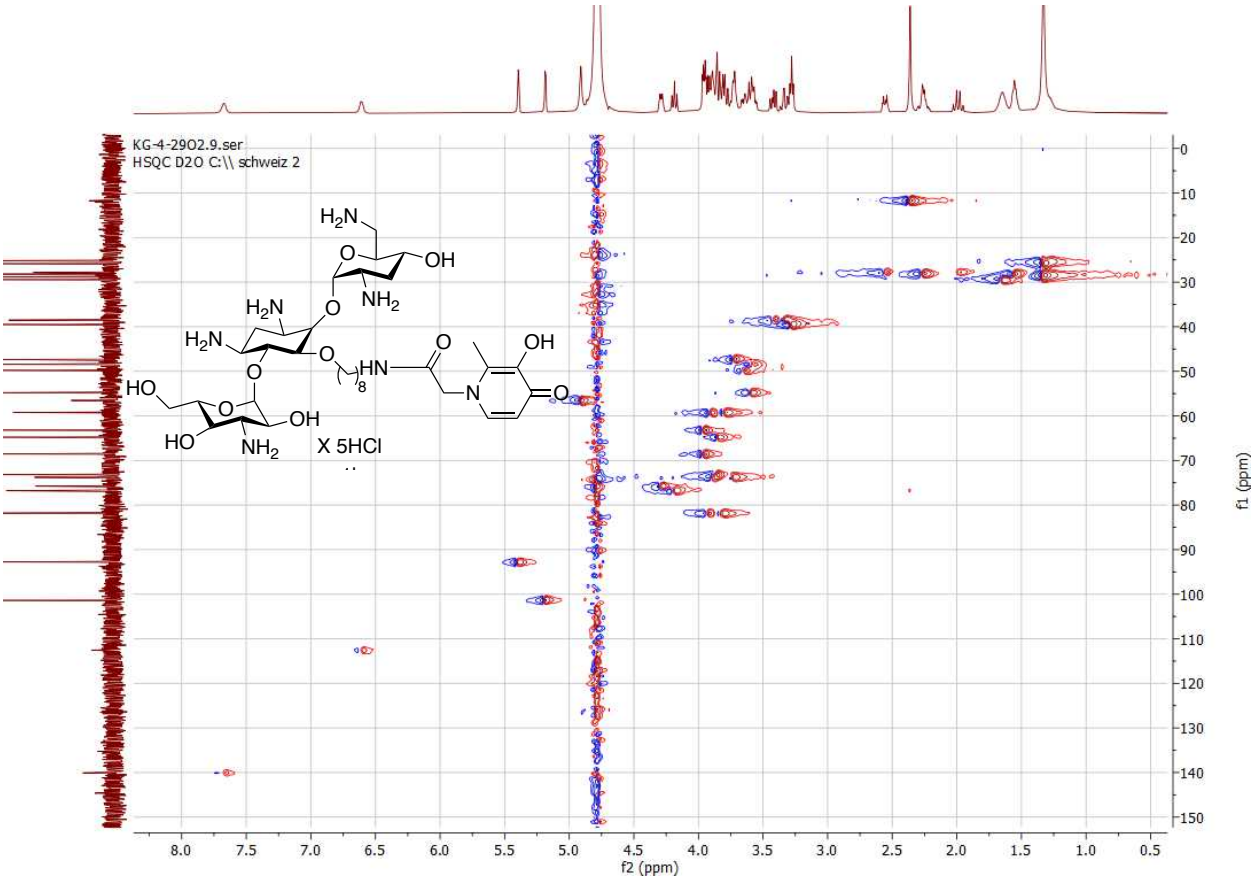
KG-4-2902.9.ser
HSQC D2O C:\\ schweiz 2
X 5HCl
f2 (ppm)
f1 (ppm)

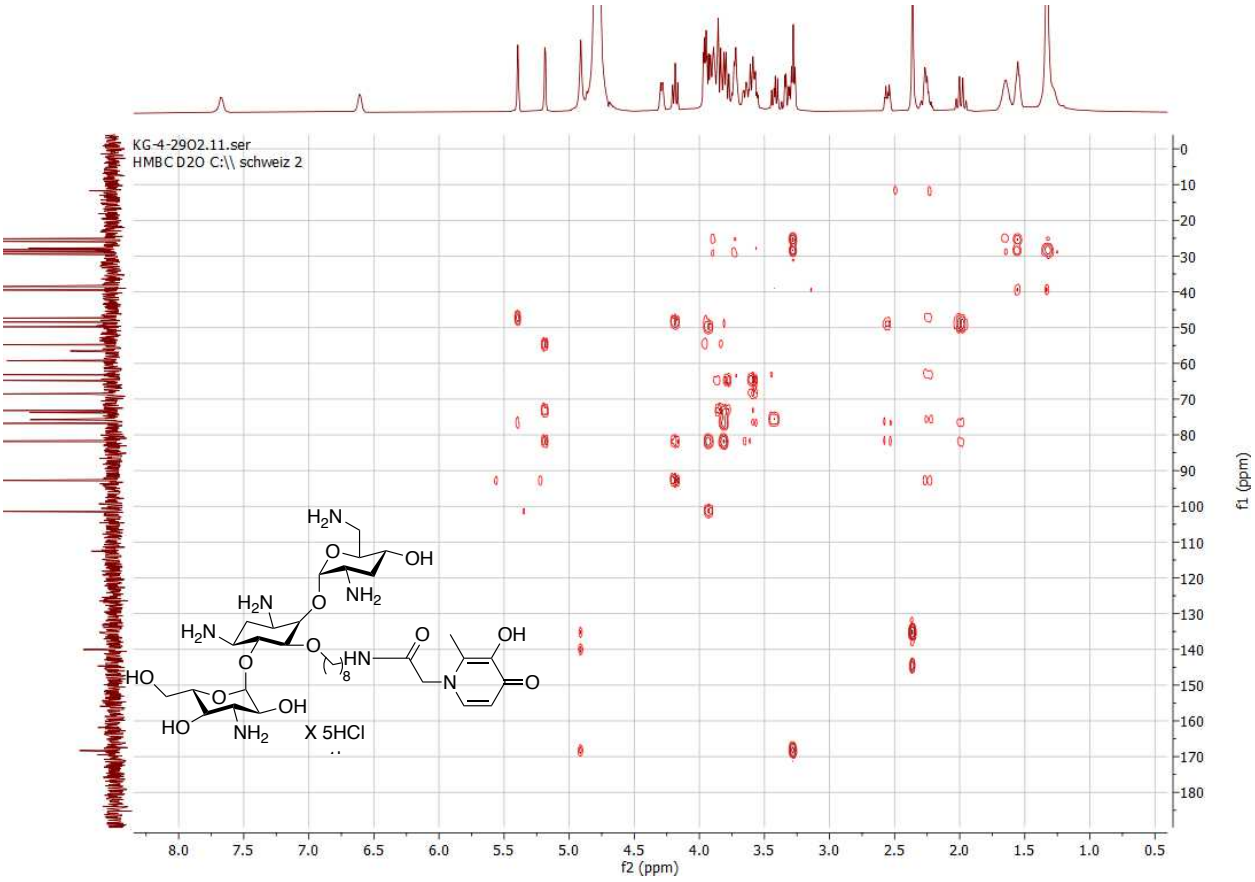
KG-4-2902.11.ser
HMBC D2O C:\\ schweiz 2
f2 (ppm)
f1 (ppm)
X 5HCl

Compound 24c

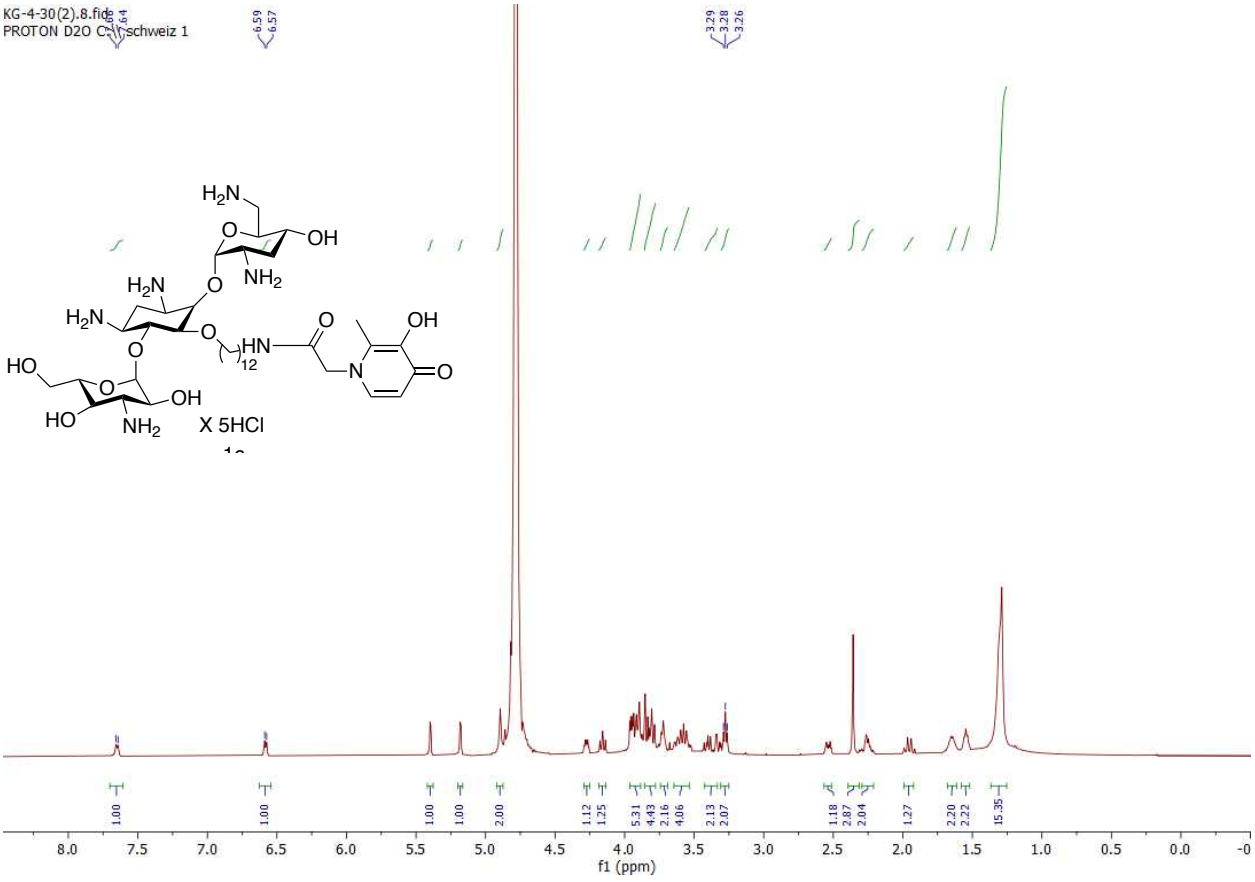

KG-4-30(2).6.fid
C13 D2O C:\\ schweiz 1

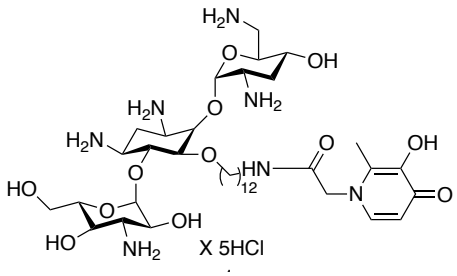

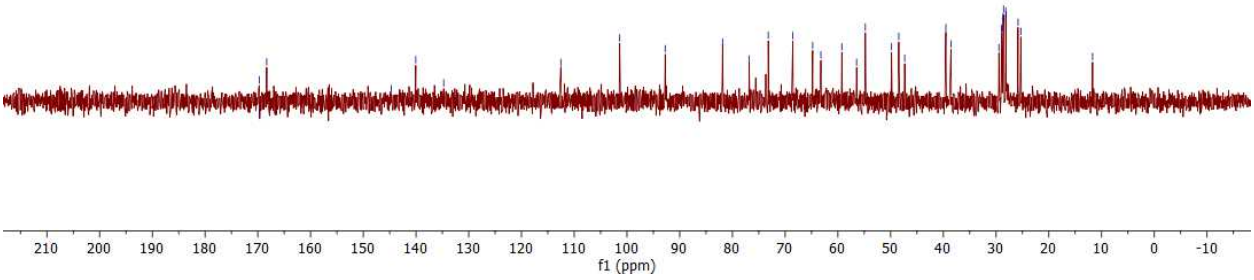

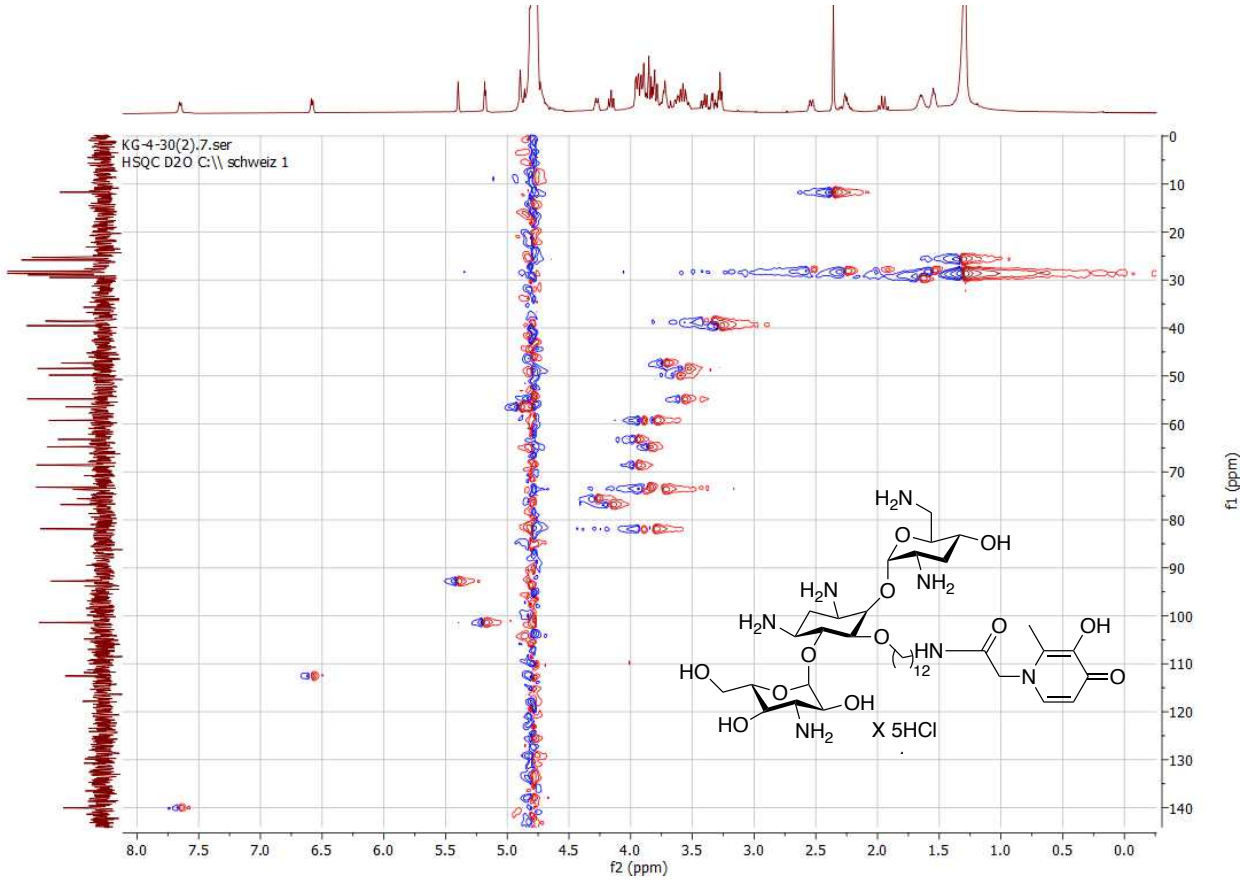
KG-4-30(2).7.ser
HSQC D2O C:\\ schweiz 1
f2 (ppm)
f1 (ppm)
X 5HCl

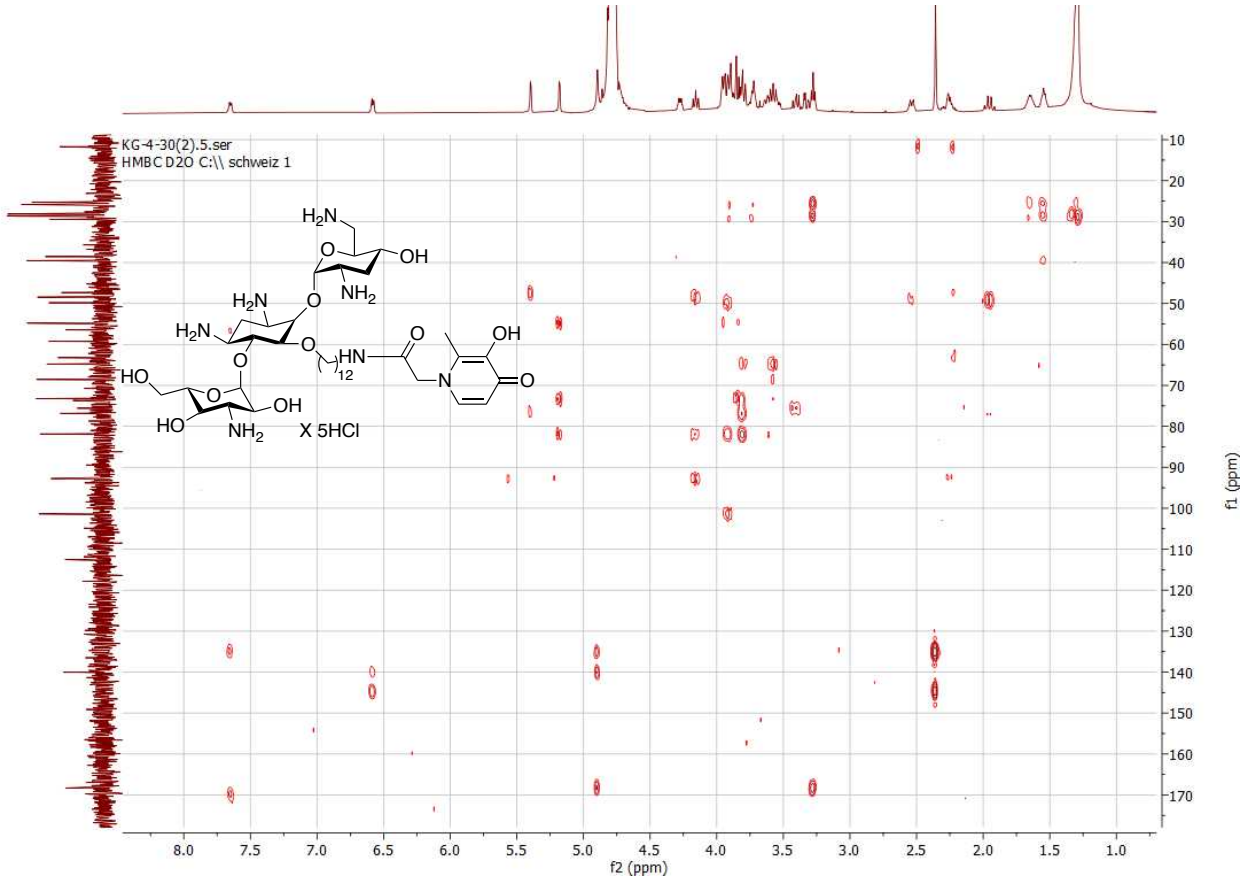
KG-4-30(2).5.ser
HMBC D2O C:\\ schweiz 1
X 5HCl
f2 (ppm)
f1 (ppm)

Compound 27a

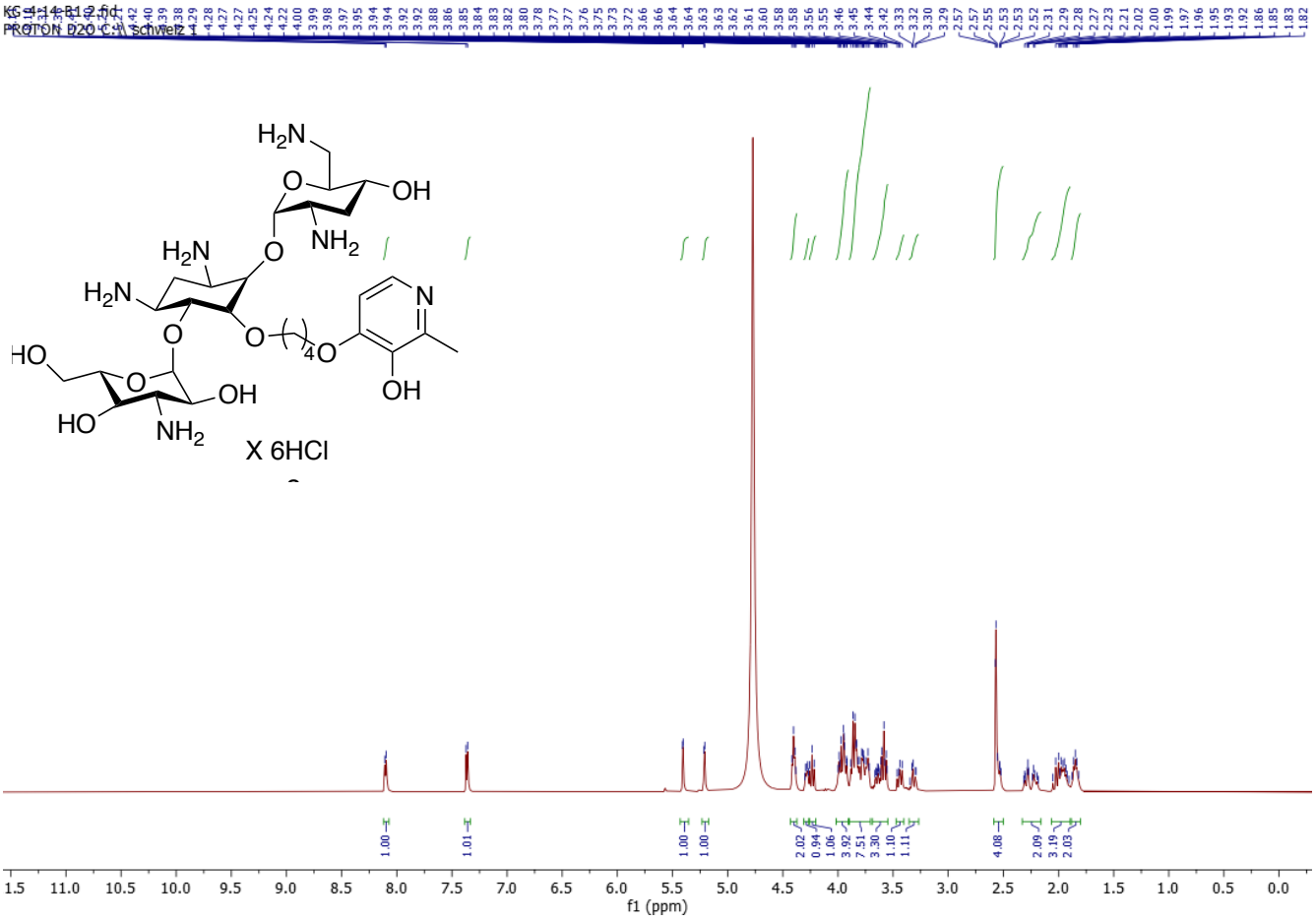

KG-4-14-B1.3.fid
C13CPD D2O C:\\ schweiz 1

159.57
142.33
140.36
134.46
107.96
101.16
92.76
82.05
81.70
76.81
75.85
73.18
72.86
70.68
68.55
64.85
63.18
59.32
54.79
49.67
48.44
47.30
38.52
28.04
27.71
25.87
24.52
13.68

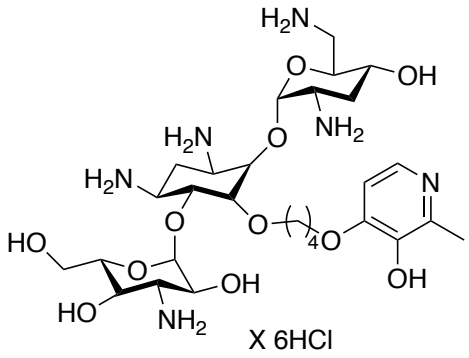

X 6HCl

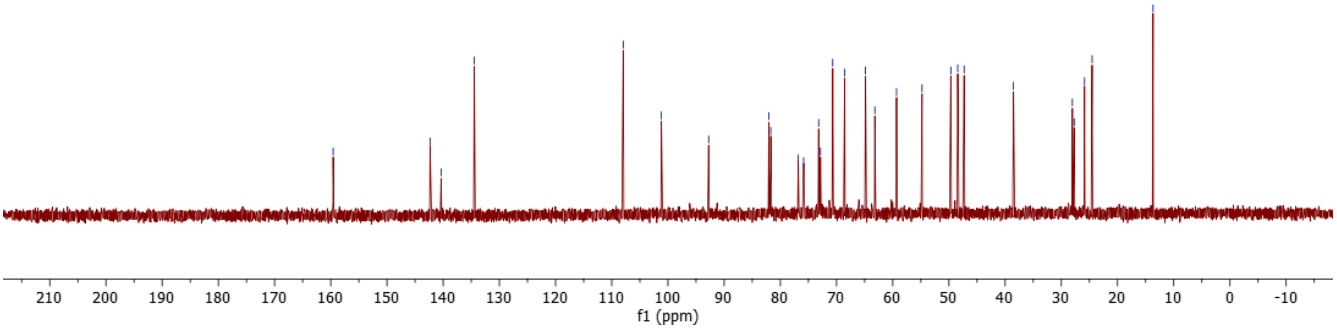

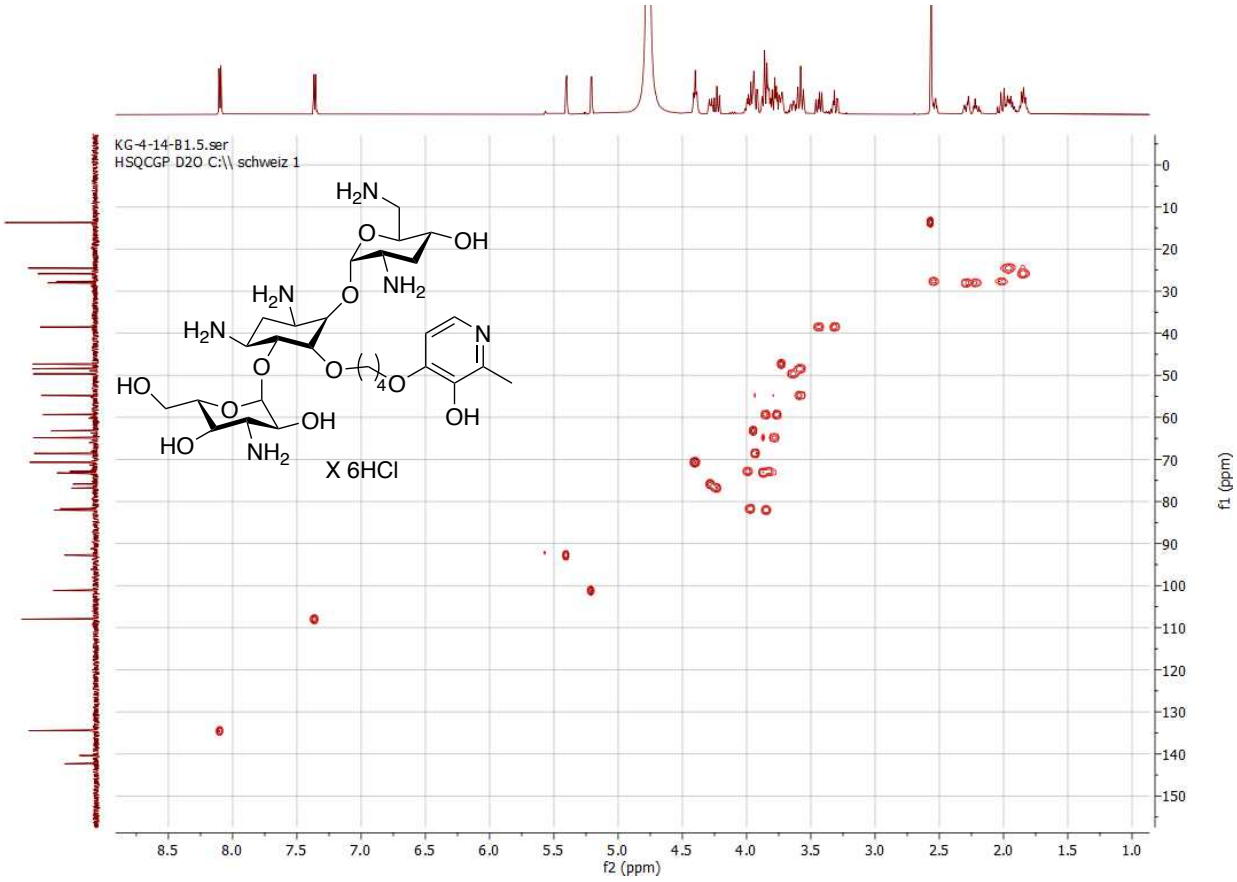
KG-4-14-B1.5.ser
HSQCGP D2O C:\\ schweiz 1
X 6HCl
f2 (ppm)
f1 (ppm)

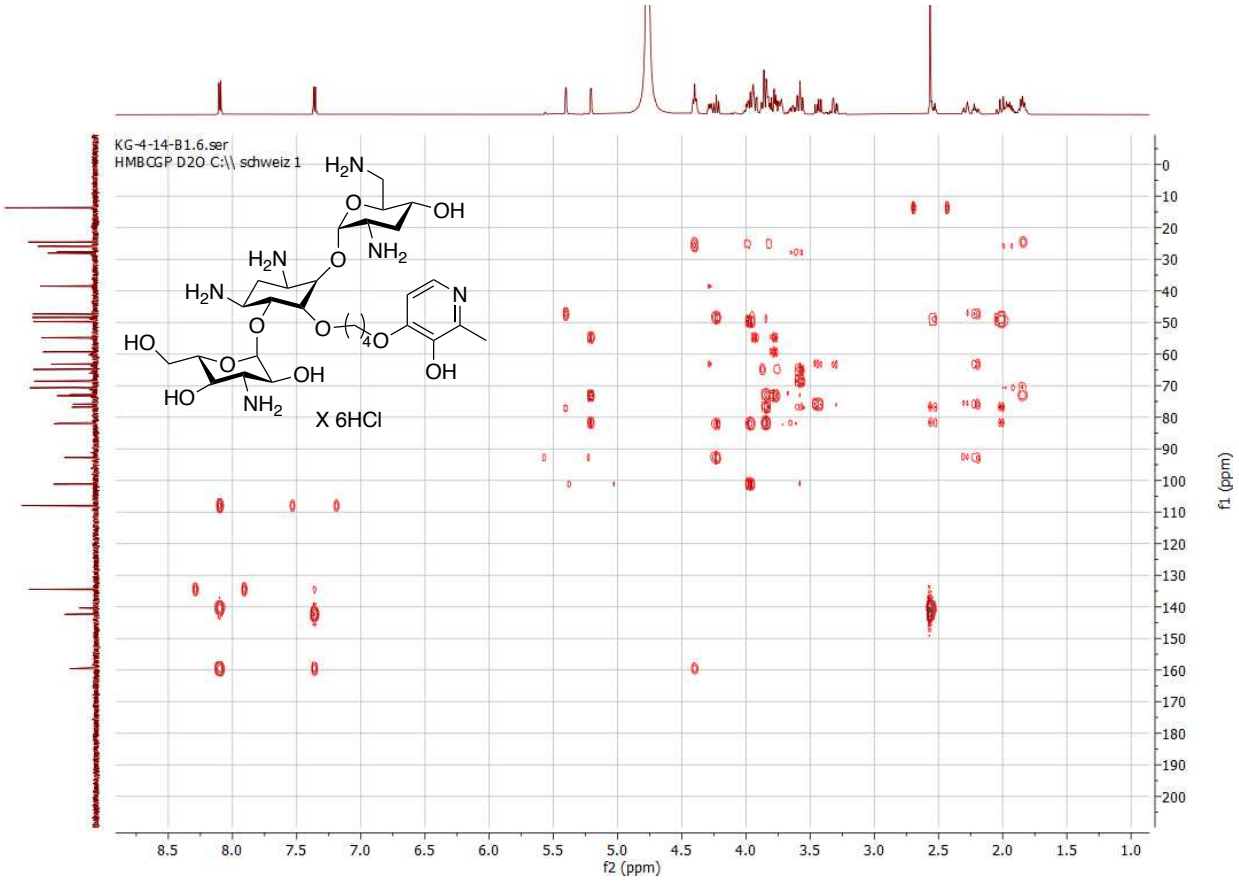
KG-4-14-B1.6.ser
HMBCGP D2O C:\\ schweiz 1
X 6HCl
f2 (ppm)
f1 (ppm)

Compound 27b

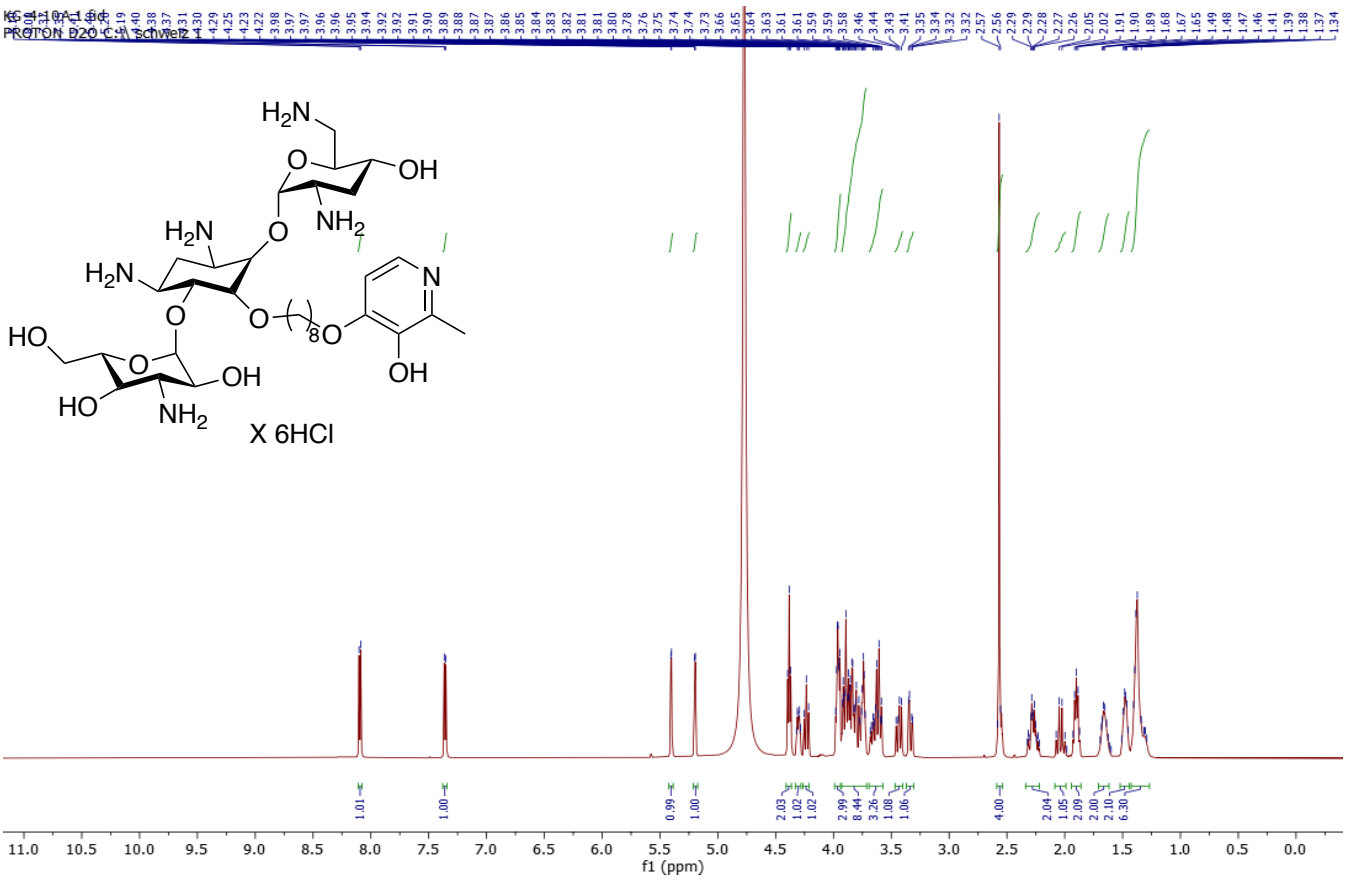

KG-4-10A.4.fid
C13CPD D2O C:\\ schweiz 1

159.71 142.36 140.04 134.38 107.95 101.35 92.72 81.86 81.81 76.64 75.74 73.78 73.15 71.19 68.58 64.83 63.28 59.28 54.80 49.80 48.50 47.36 38.59 29.49 28.93 28.49 28.12 27.79 27.73 25.25 24.93 13.67

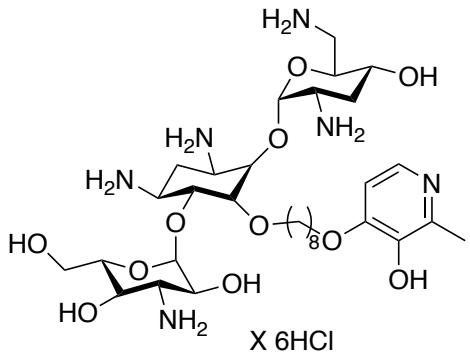

X 6HCl

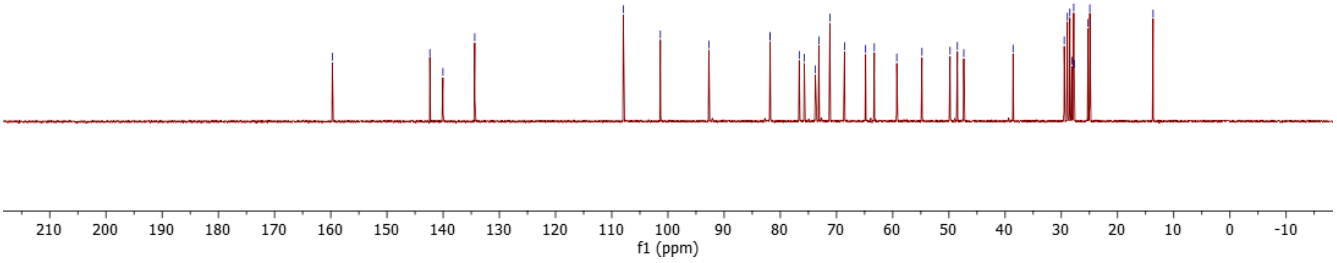

Compound 27c

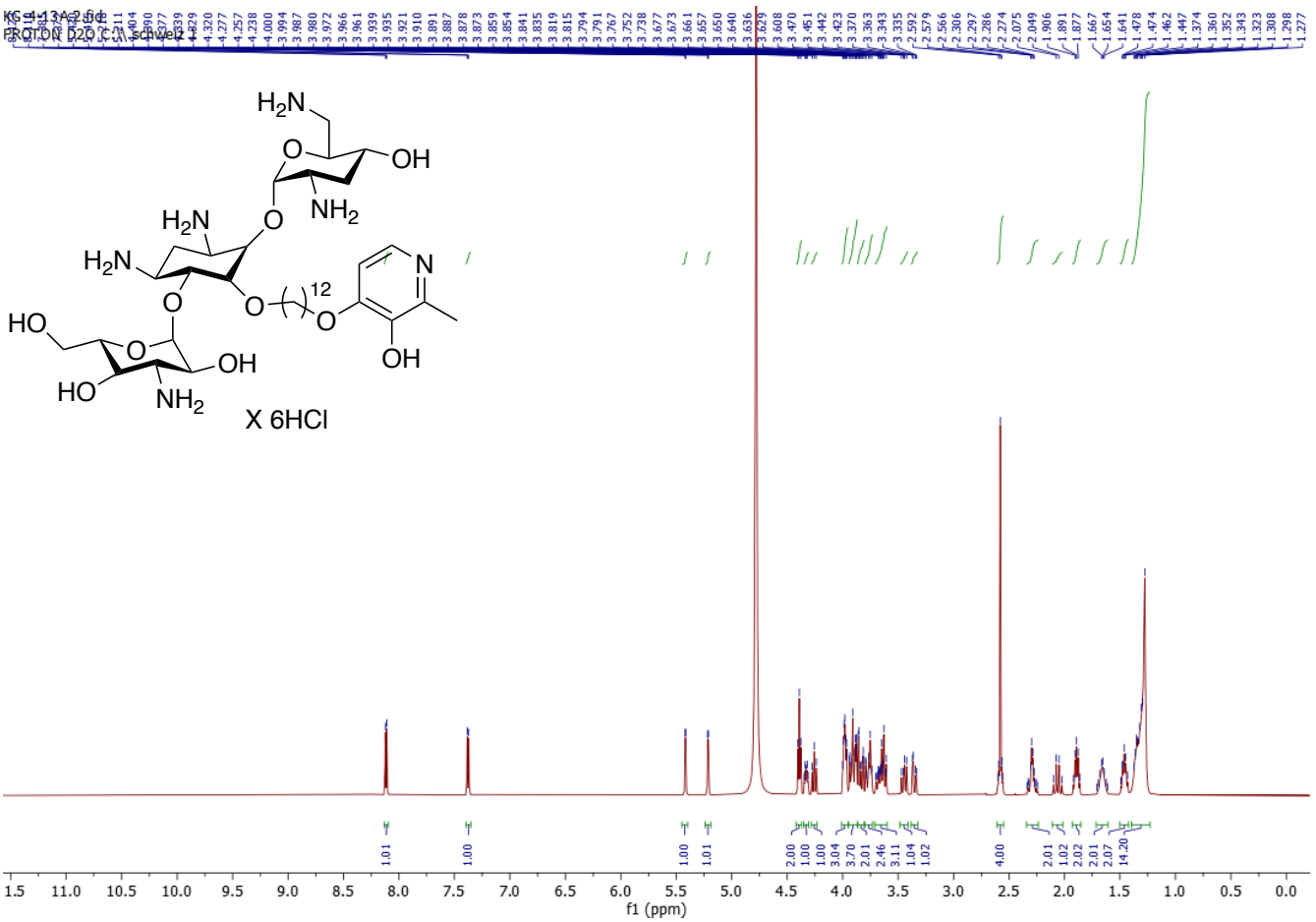

KG-4-13A.3.fid
C13CPD D2O C:\\ schweiz 1

159.68
142.45
139.95
134.39
108.00
101.39
92.71
81.87
81.85
76.67
75.79
73.88
73.19
71.26
68.60
64.88
63.33
59.34
54.82
49.84
48.53
47.38
38.63
29.52
29.05
28.96
28.86
28.82
28.78
28.44
28.16
27.78
27.75
25.36
24.94
13.72

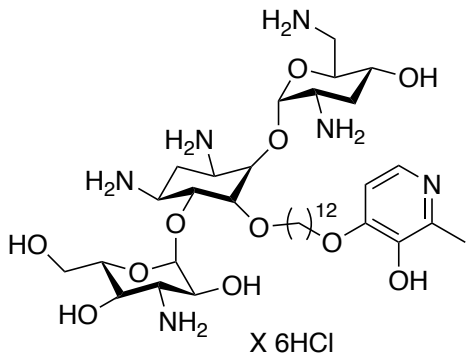

X 6HCl

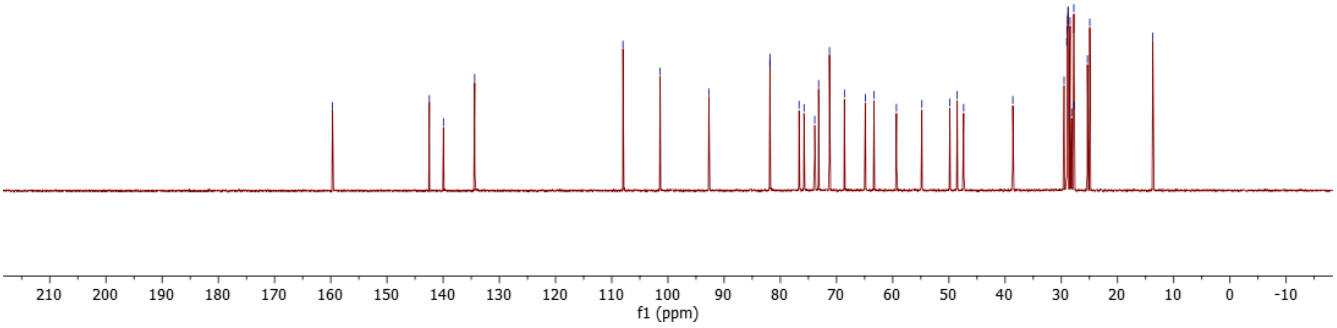

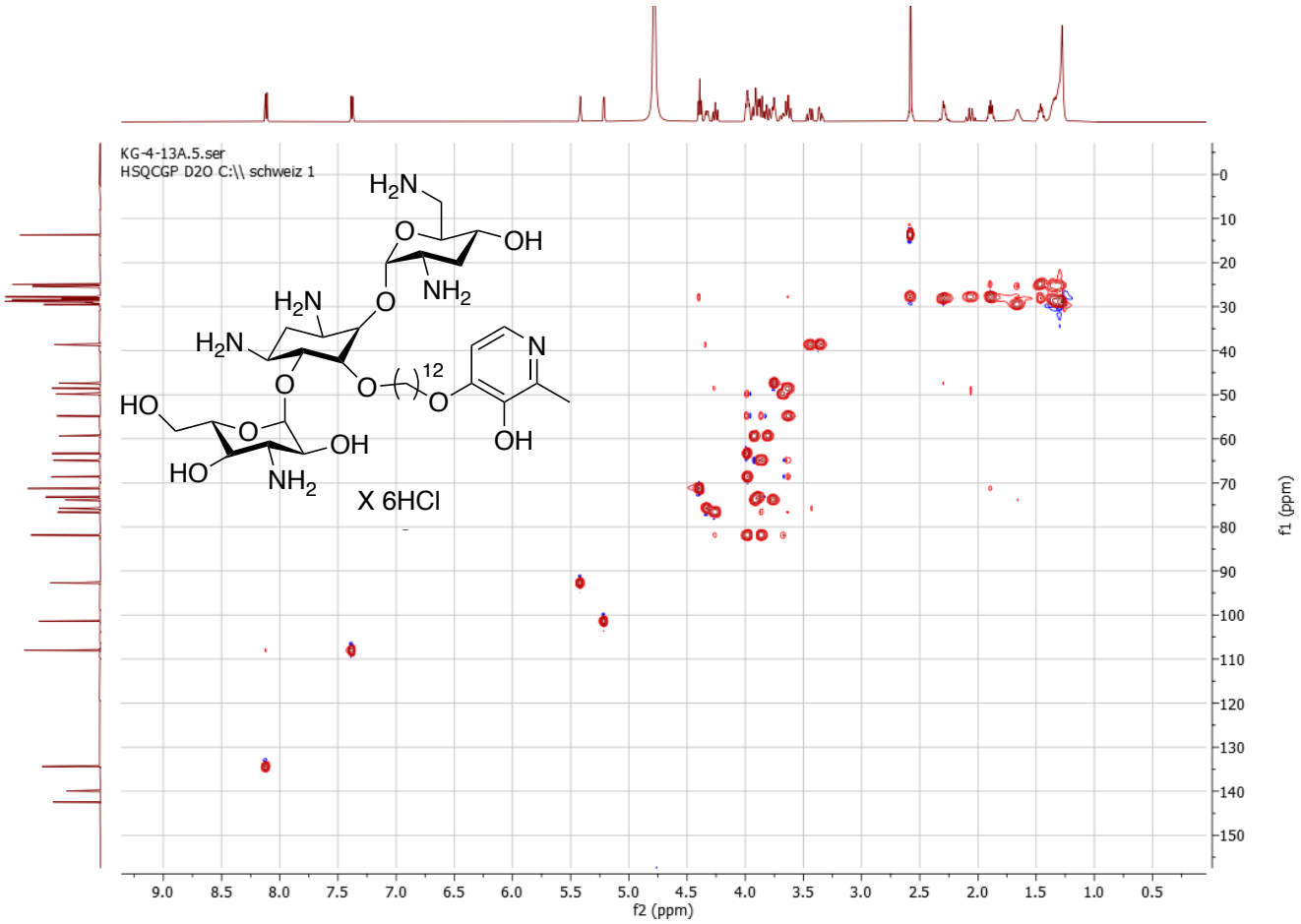
KG-4-13A.5.ser
HSQCGP D2O C:\\ schweiz 1
X 6HCl
f2 (ppm)
f1 (ppm)

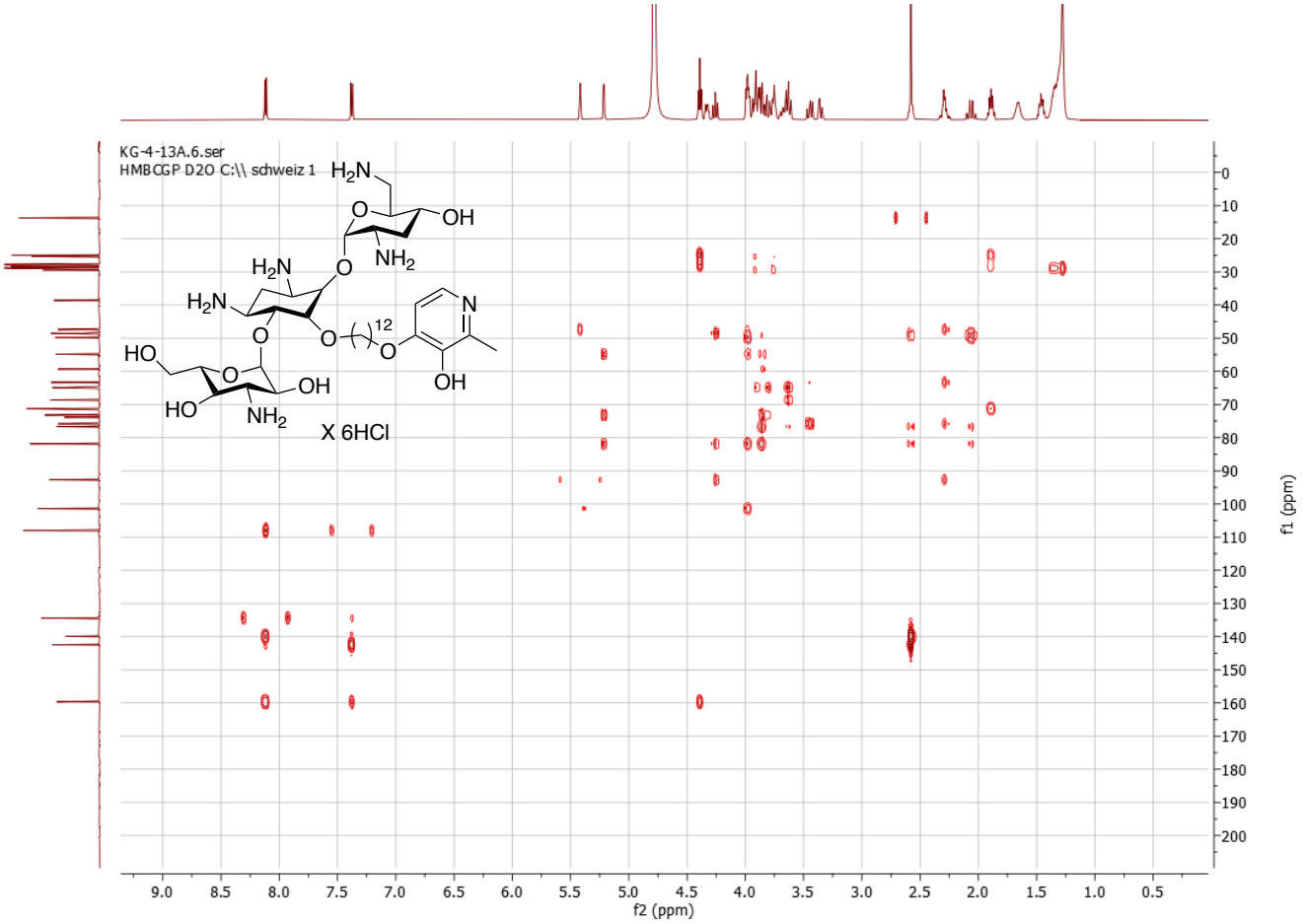
KG-4-13A.6.ser
HMBCGP D2O C:\\ schweiz 1
X 6HCl
f2 (ppm)
f1 (ppm)

Compound 30

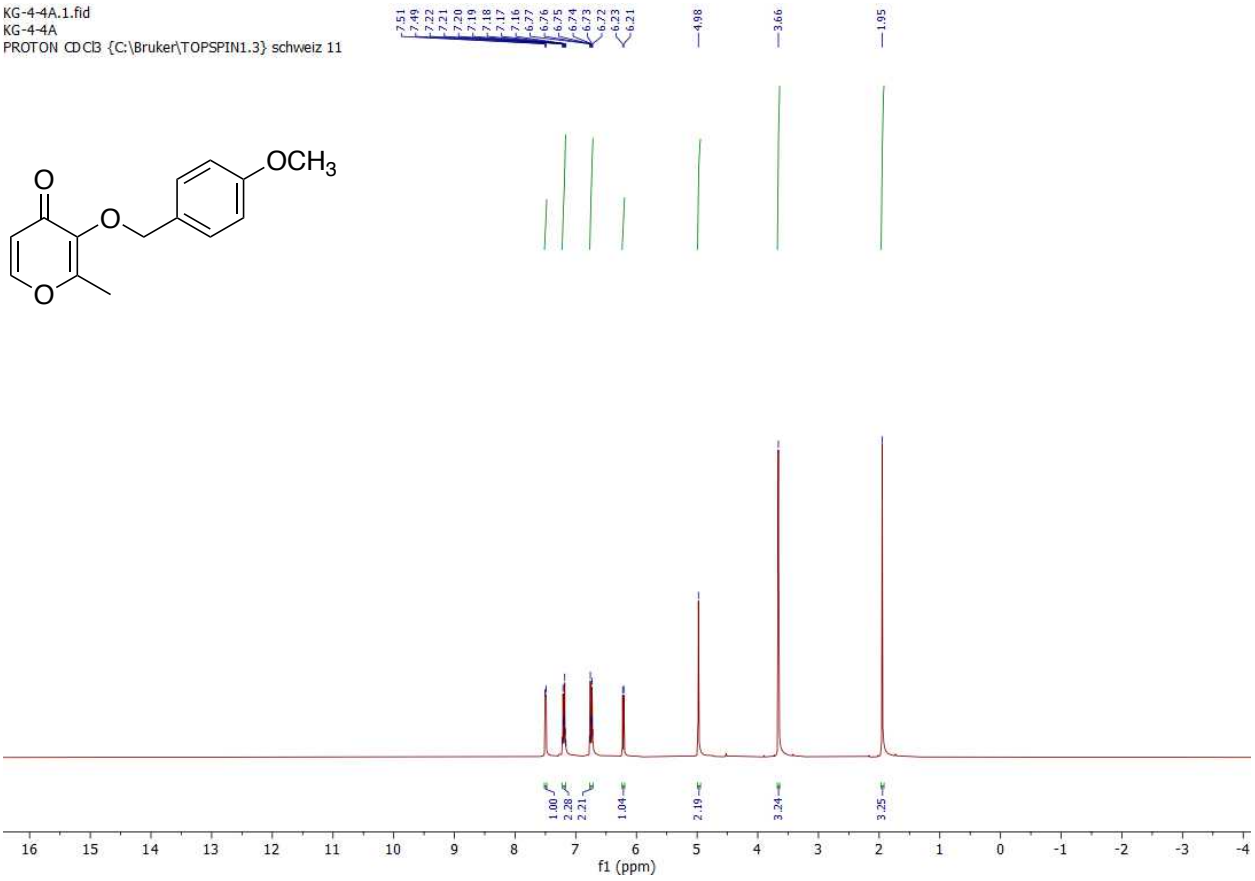
KG-4-4A.1.fid
KG-4-4A
PROTON CDCl3 {C:\Bruker\TOPSPIN1.3} schweiz 11
7.51
7.49
7.22
7.21
7.20
7.19
7.18
7.17
7.16
6.77
6.76
6.75
6.74
6.73
6.72
6.23
6.21
4.98
3.66
1.95
O
O
O
OCH3
1.00
2.28
2.21
1.04
2.19
3.24
3.25
16
15
14
13
12
11
10
9
8
7
6
5
4
3
2
1
0
-1
-2
-3
-4
f1 (ppm)

KG-4-4A.2.fid
KG-4-4A
C13CPD CDCl3 {C:\Bruker\TOPSPIN1.3} schwarz 11

175.01
159.70
159.65
153.58
143.52
130.59
128.97
116.93
113.69
113.65
72.97
55.11
14.67

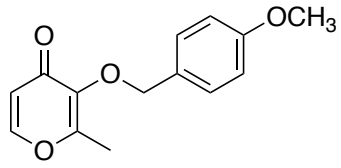

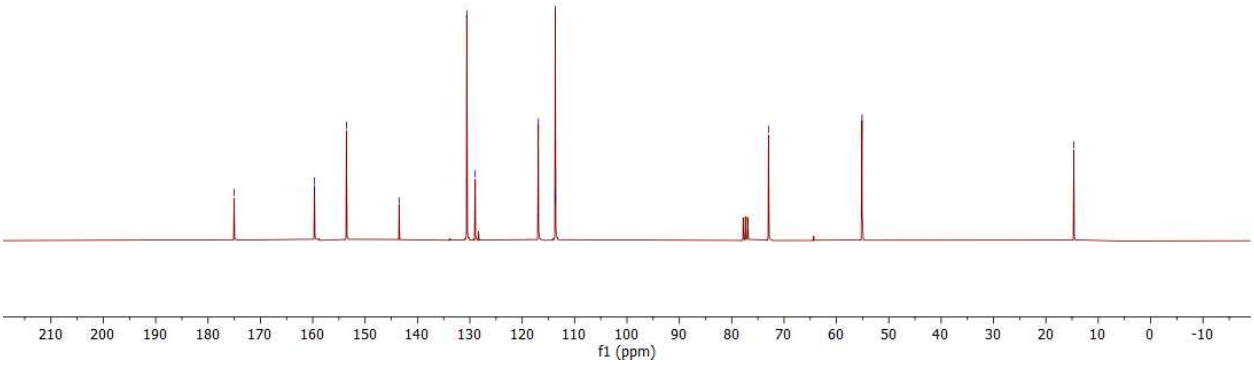

Compound 31

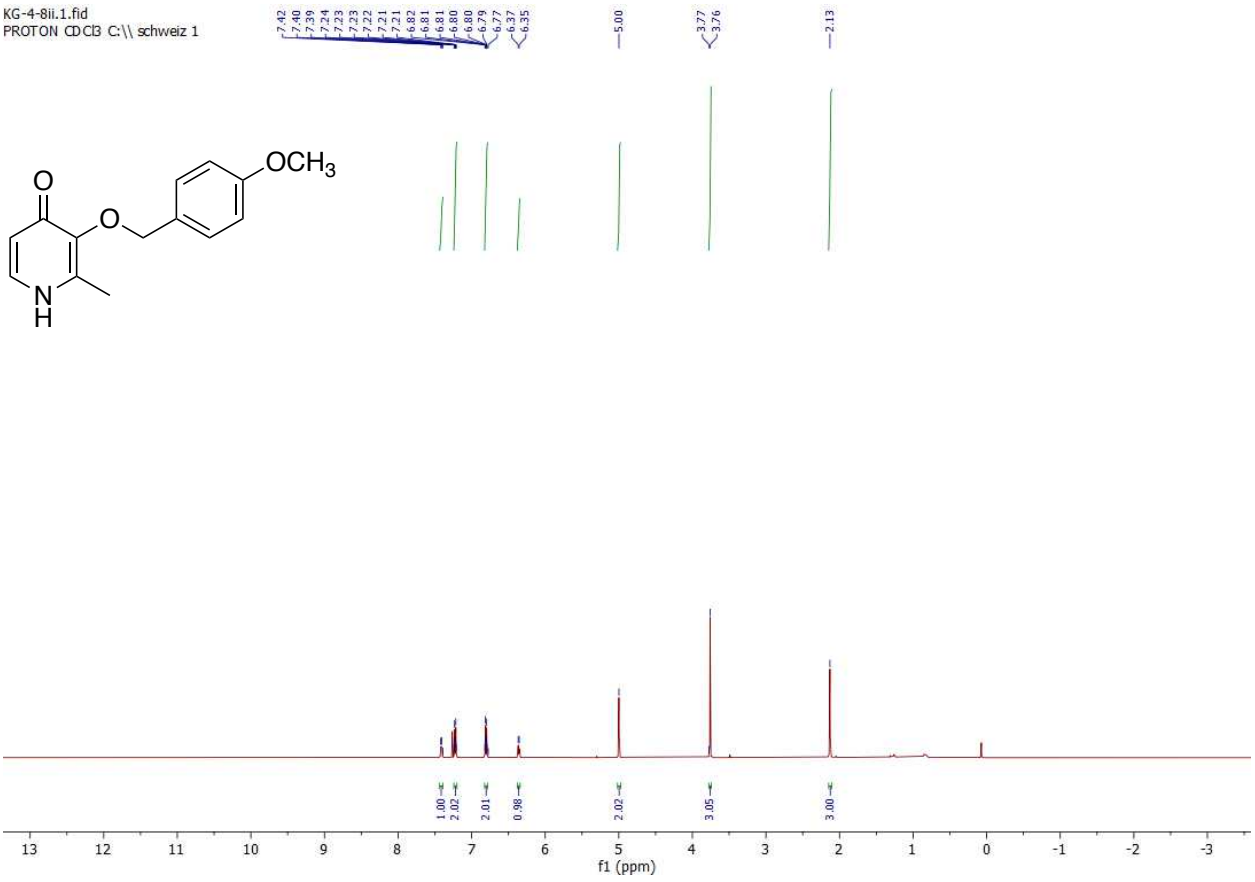
KG-4-8ii.1.fid
PROTON CDCl3 C:\\ schweiz 1
7.42
7.40
7.39
7.24
7.23
7.23
7.22
7.21
7.21
6.82
6.81
6.81
6.80
6.79
6.77
6.37
6.35
5.00
3.77
3.76
2.13
O
O
OCH3
N
H
1.00
2.02
2.01
0.98
2.02
3.05
3.00
13
12
11
10
9
8
7
6
5
4
3
2
1
0
-1
-2
-3
f1 (ppm)

Compound 32a

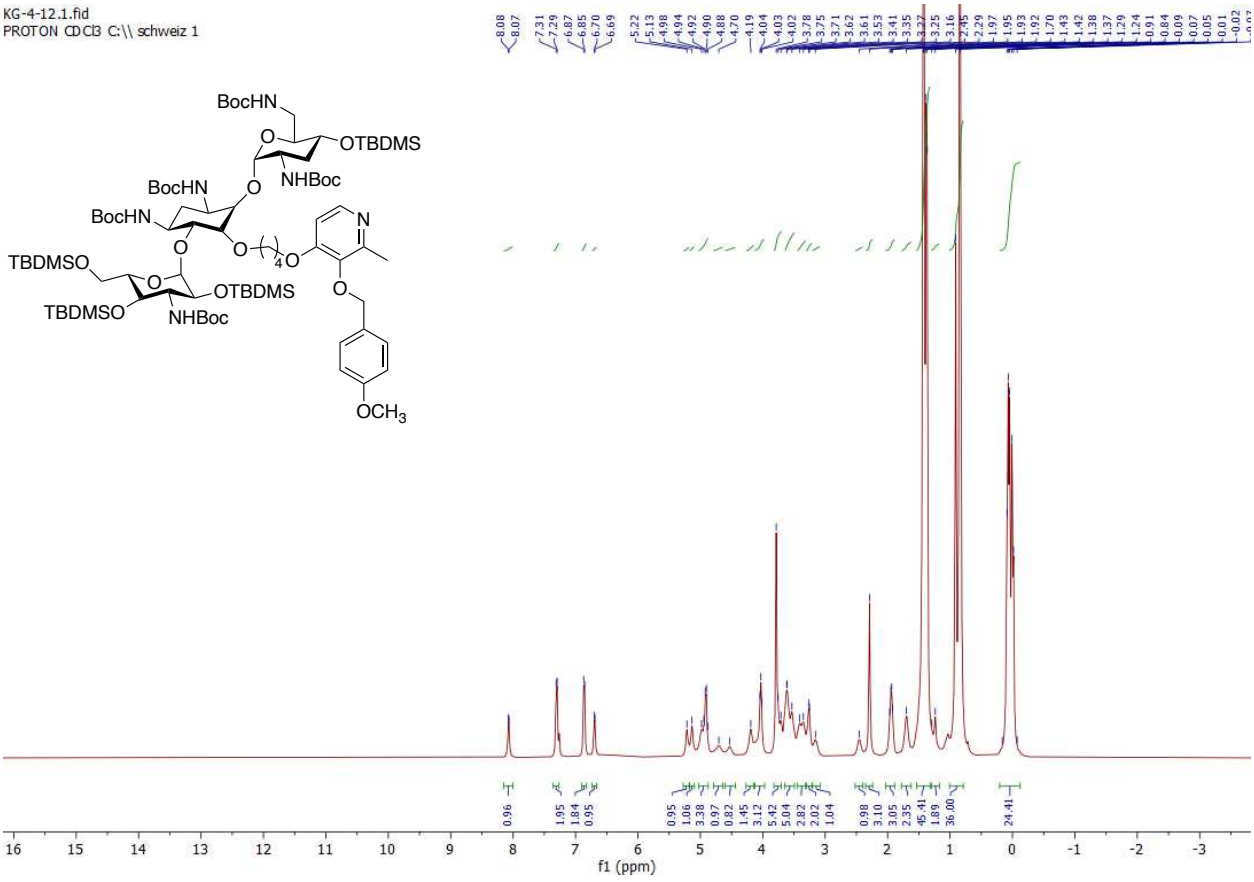

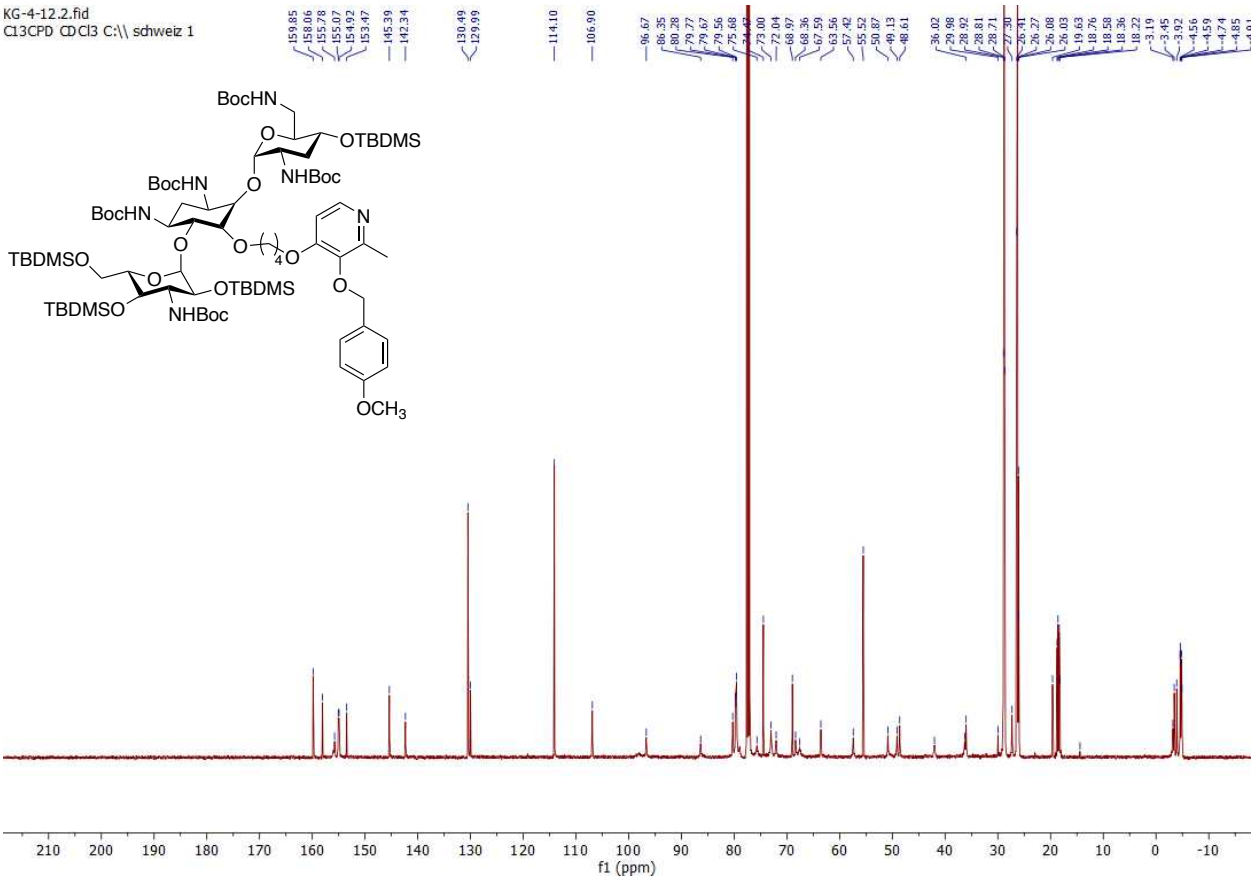
KG-4-12.2.fid
C13CPD CDCl3 C:\\ schweiz 1
BocHN
OTBDMS
NHBoc
BocHN
BocHN
TBDMSO
OTBDMS
TBDMSO
NHBoc
N
O
4
OCH3
f1 (ppm)

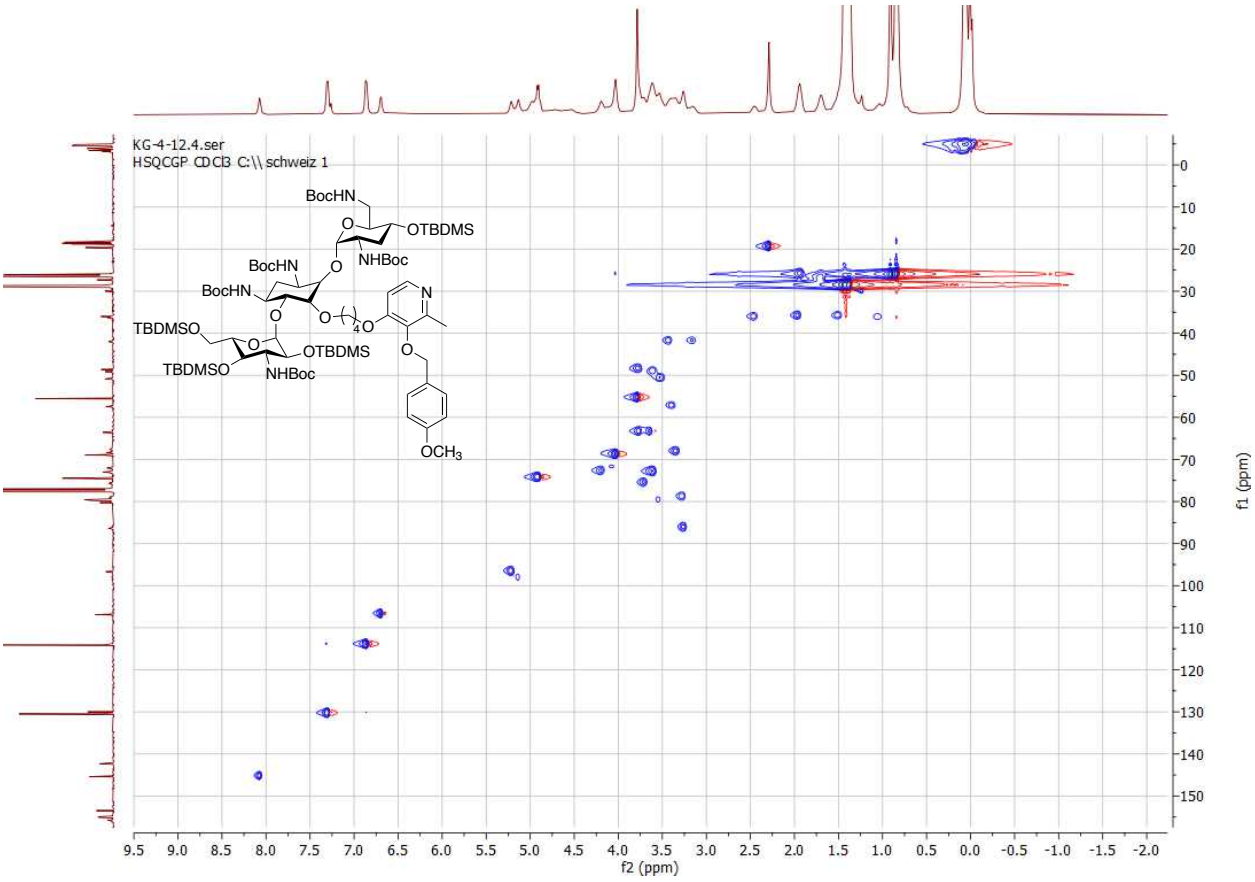
KG-4-12.4.ser
HSQCGP CDCl3 C:\\ schweiz 1
BocHN
OTBDMS
NHBoc
BocHN
BocHN
N
TBDMSO
OTBDMS
TBDMSO
NHBoc
OCH3
f2 (ppm)
f1 (ppm)

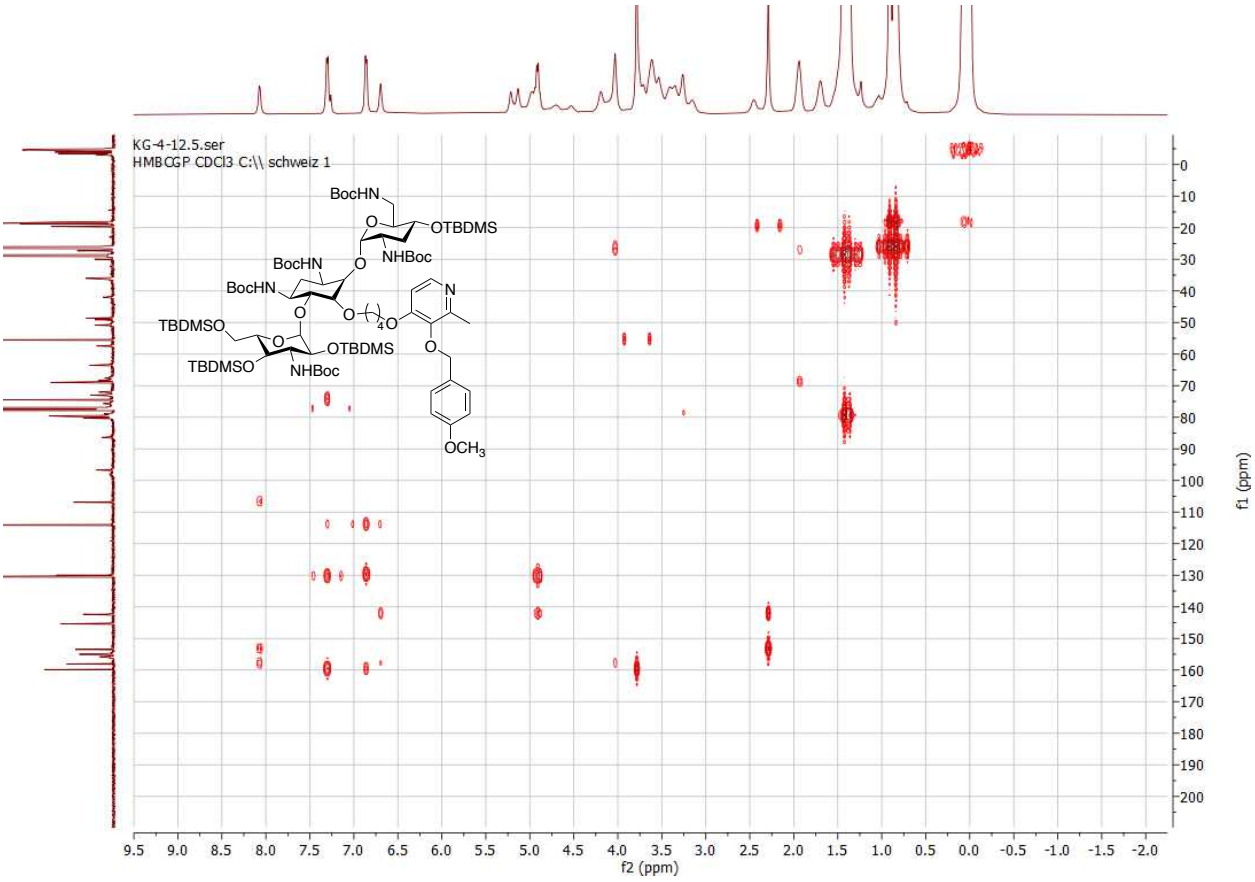
KG-4-12.5.ser
HMBCGP CDCl3 C:\\ schweiz 1
BocHN
OTBDMS
NHBoc
BocHN
BocHN
TBDMSO
TBDMSO
OTBDMS
NHBoc
N
OCH3
f2 (ppm)
f1 (ppm)

Compound 32b

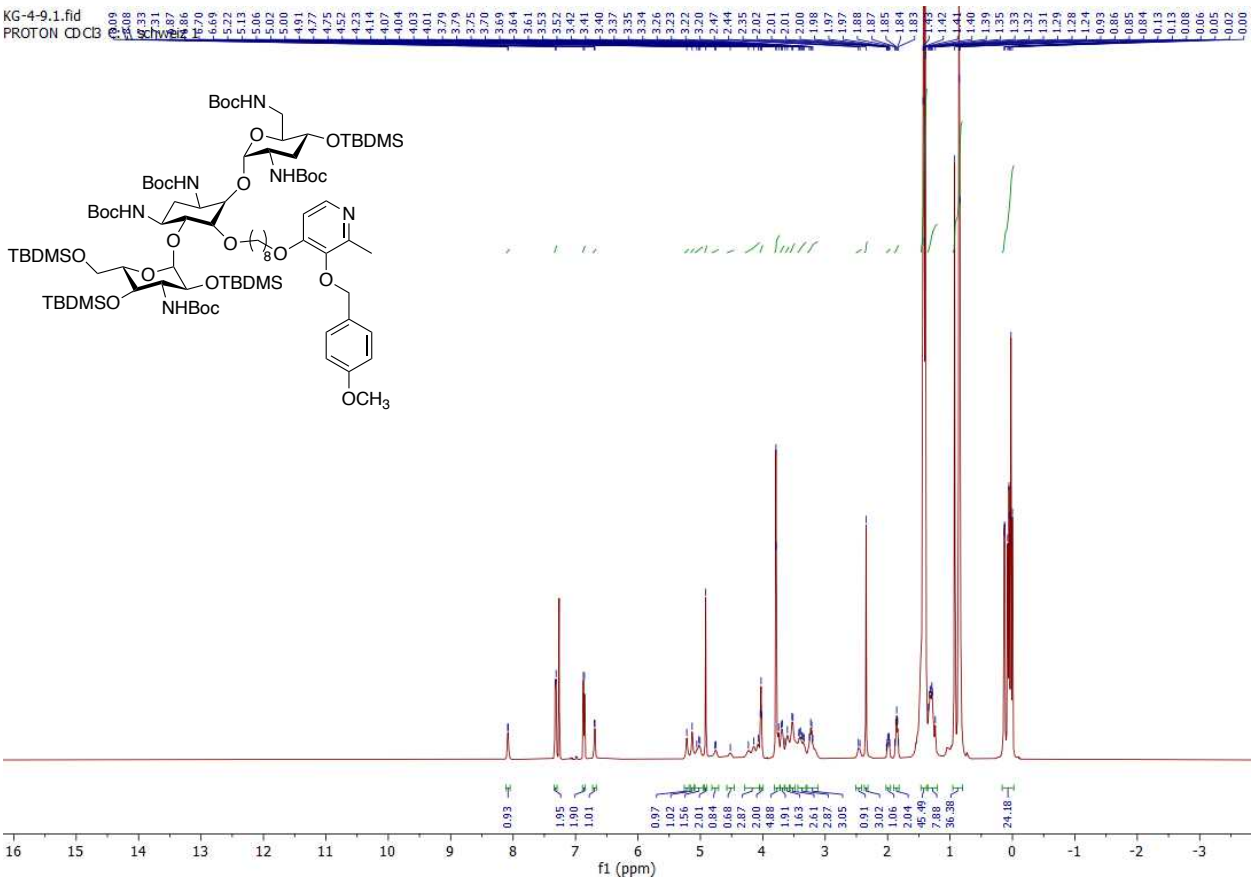

KG-4-9.2.fid
C13CPD CDCl3 C:\\ schweiz 1

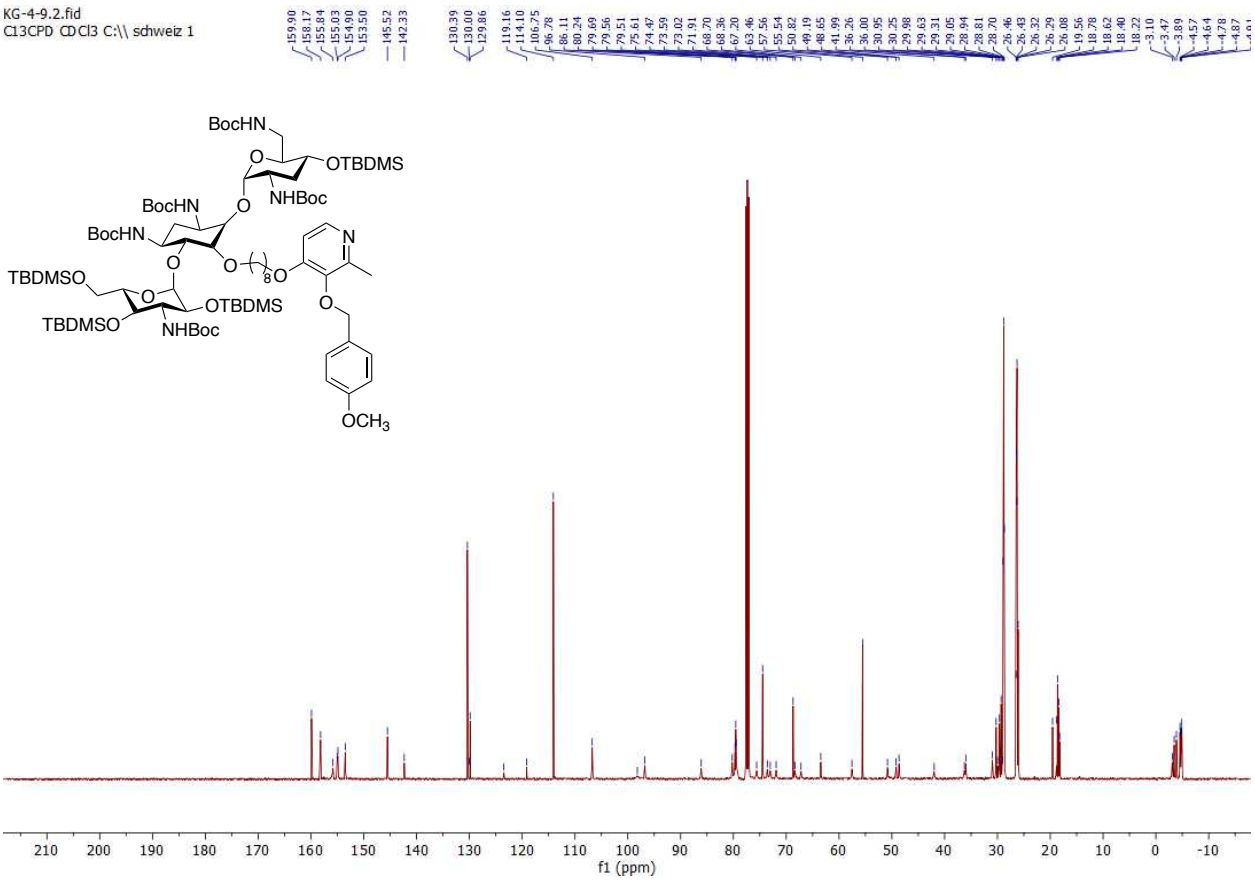

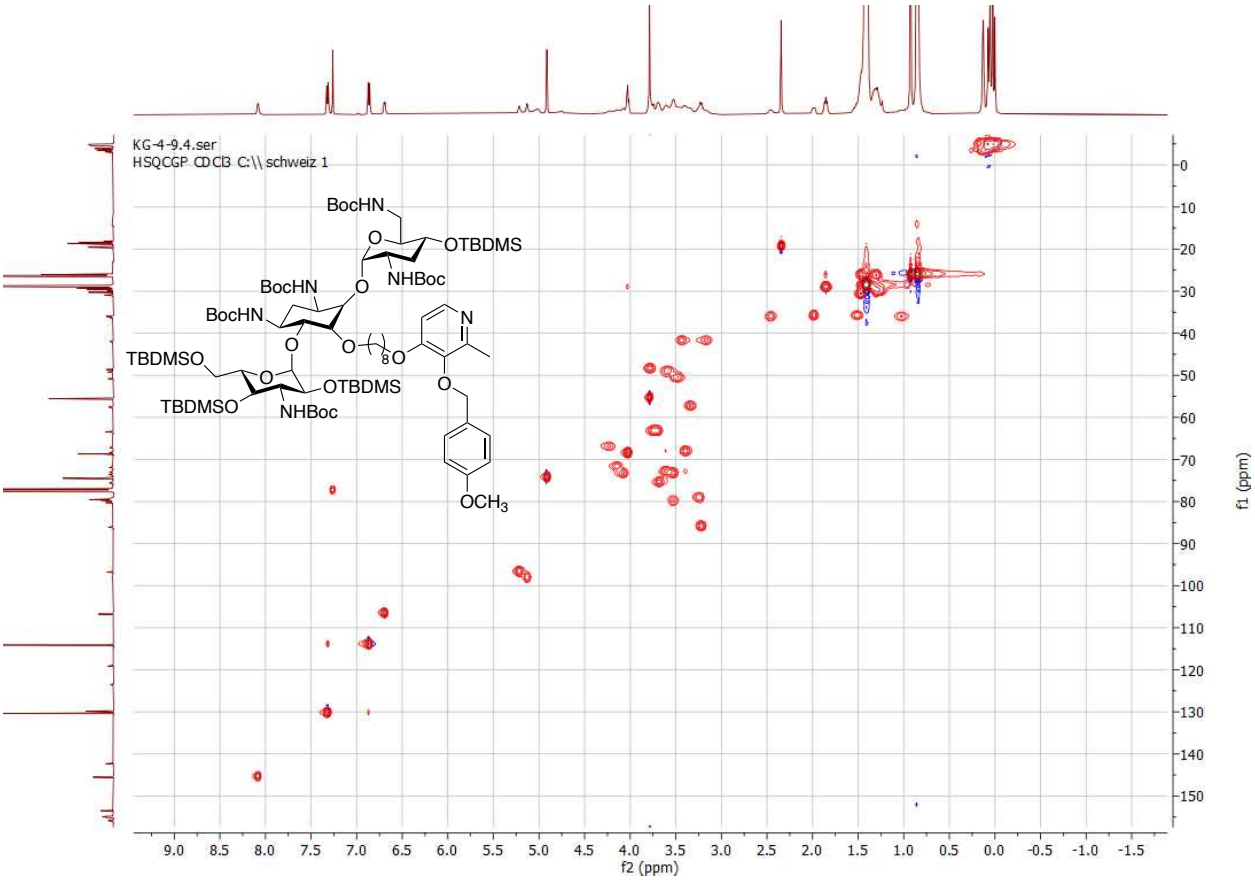
KG-4-9.4.ser
HSQCGP CDCl3 C:\\ schweiz 1
BocHN
OTBDMS
NHBoc
BocHN
BocHN
TBDMSO
TBDMSO
OTBDMS
NHBoc
N
8
OCH3
f2 (ppm)
f1 (ppm)

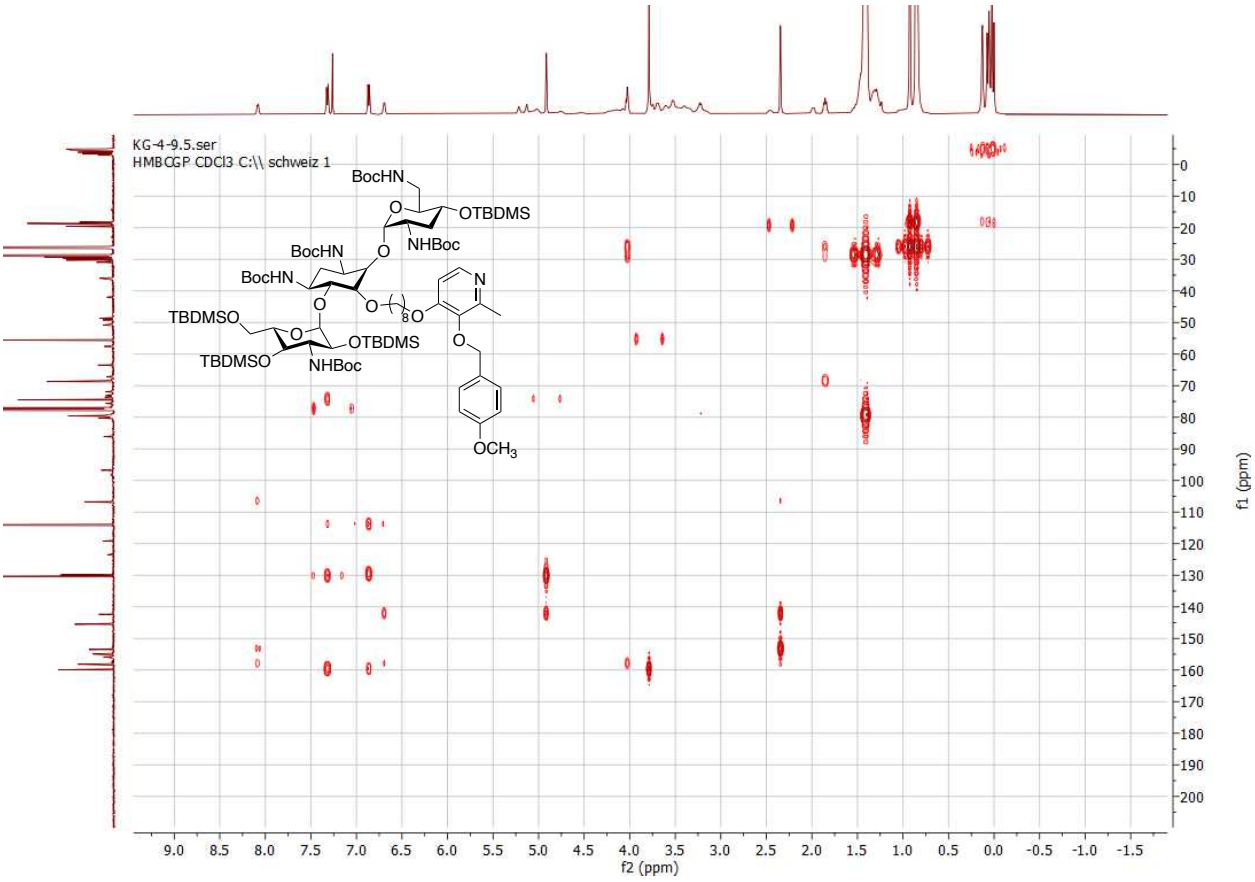
KG-4-9.5.ser
HMBCGP CDCl3 C:\\ schweiz 1
BocHN
OTBDMS
NHBoc
BocHN
BocHN
TBDMSO
TBDMSO
OTBDMS
NHBoc
N
8
OCH3
f2 (ppm)
f1 (ppm)

Compound 32c

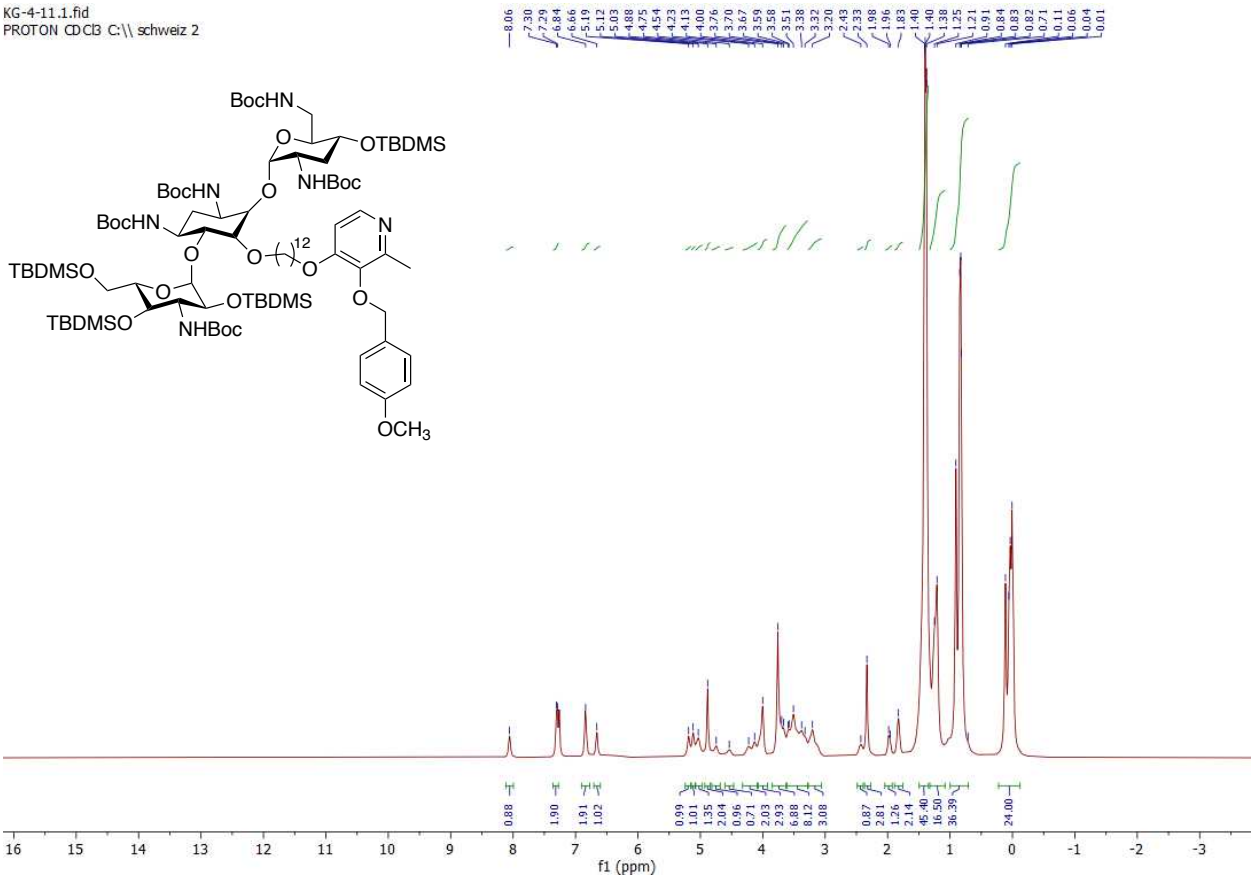

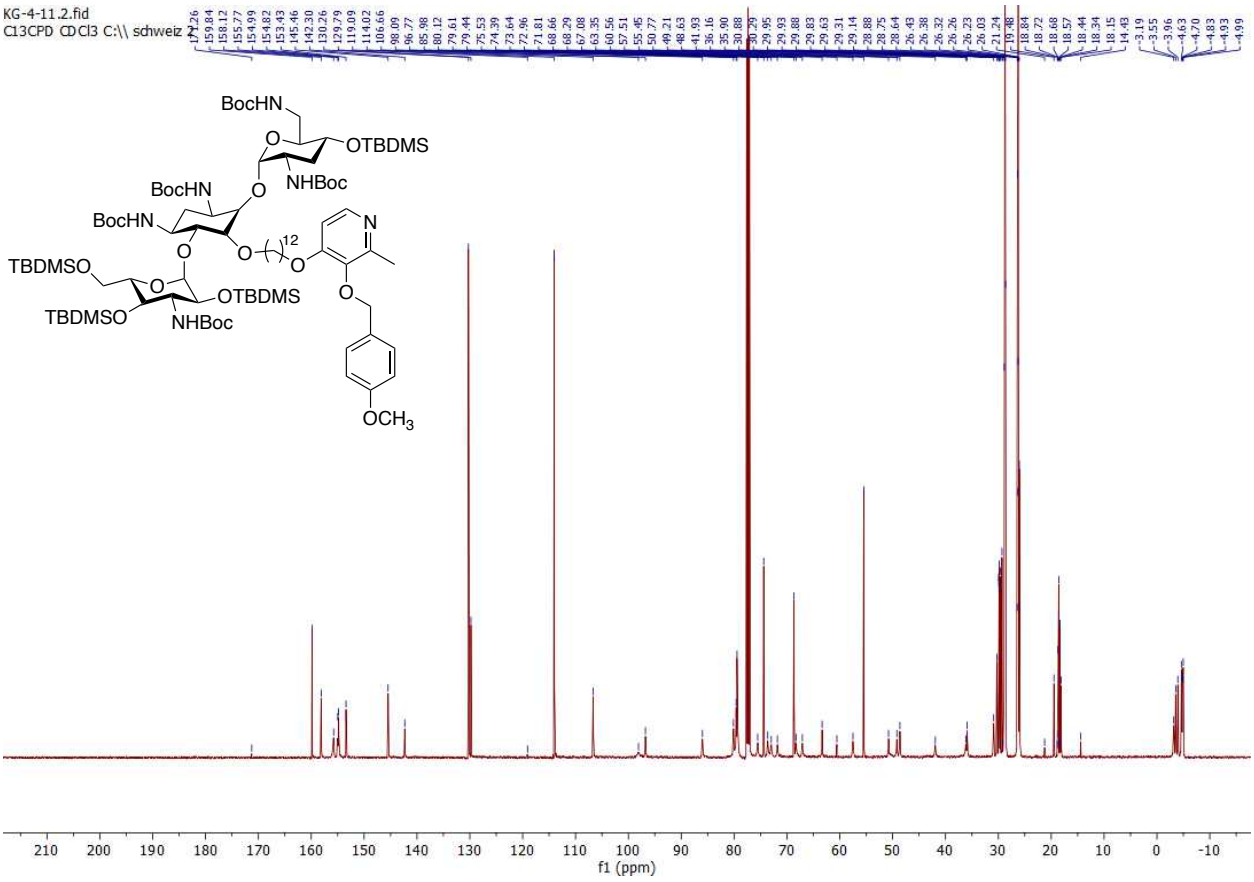
KG-4-11.2.fid
C13CPD CDCl3 C:\\ schweiz
BocHN
O
OTBDMS
NHBoc
BocHN
O
BocHN
N
O
O
12
O
TBDMSO
O
O
OTBDMS
TBDMSO
NHBoc
O
OCH3
210 200 190 180 170 160 150 140 130 120 110 100 90 80 70 60 50 40 30 20 10 0 -10
f1 (ppm)

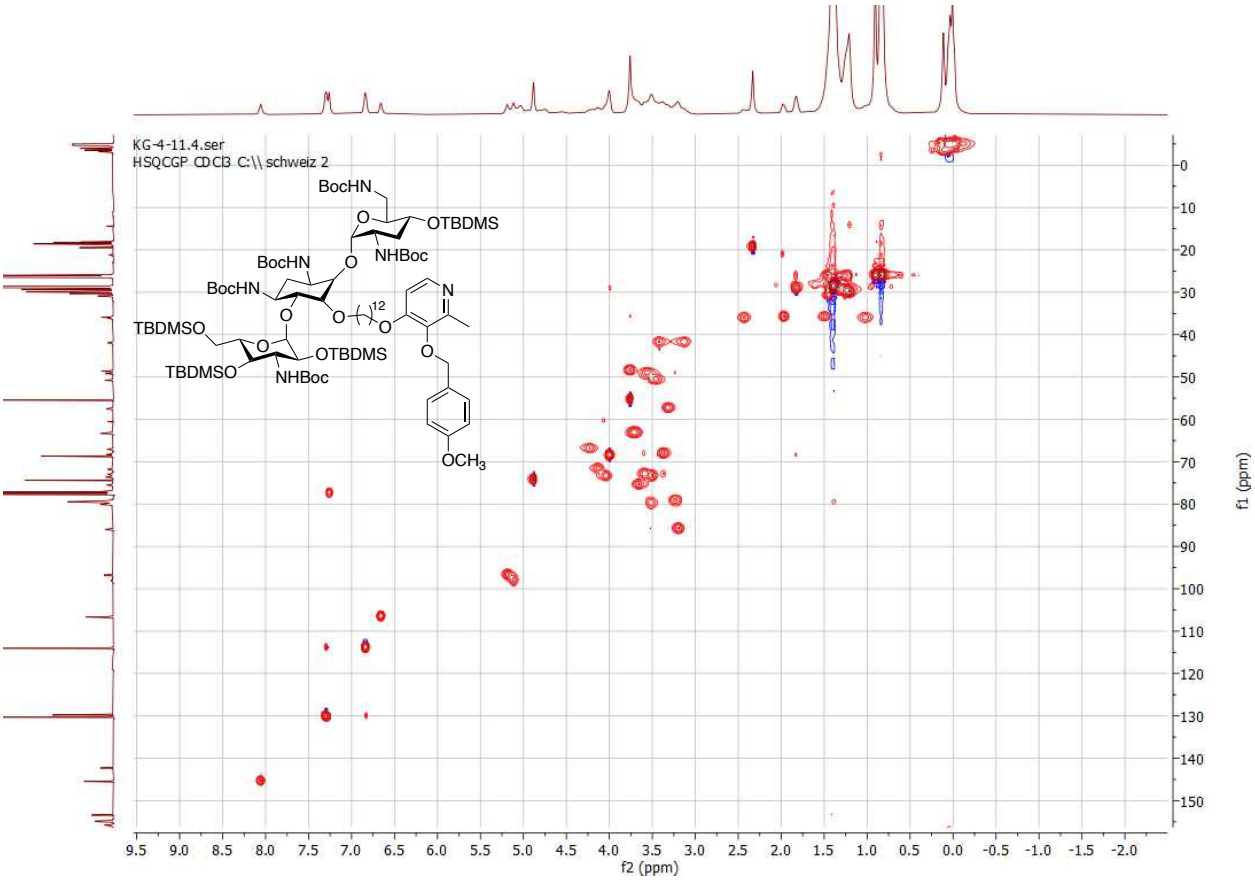
KG-4-11.4.ser
HSQCGP CDCl3 C:\\ schweiz 2
BocHN
OTBDMS
NHBoc
BocHN
BocHN
12
TBDMSO
OTBDMS
TBDMSO
NHBoc
N
O
OCH3
f2 (ppm)
f1 (ppm)

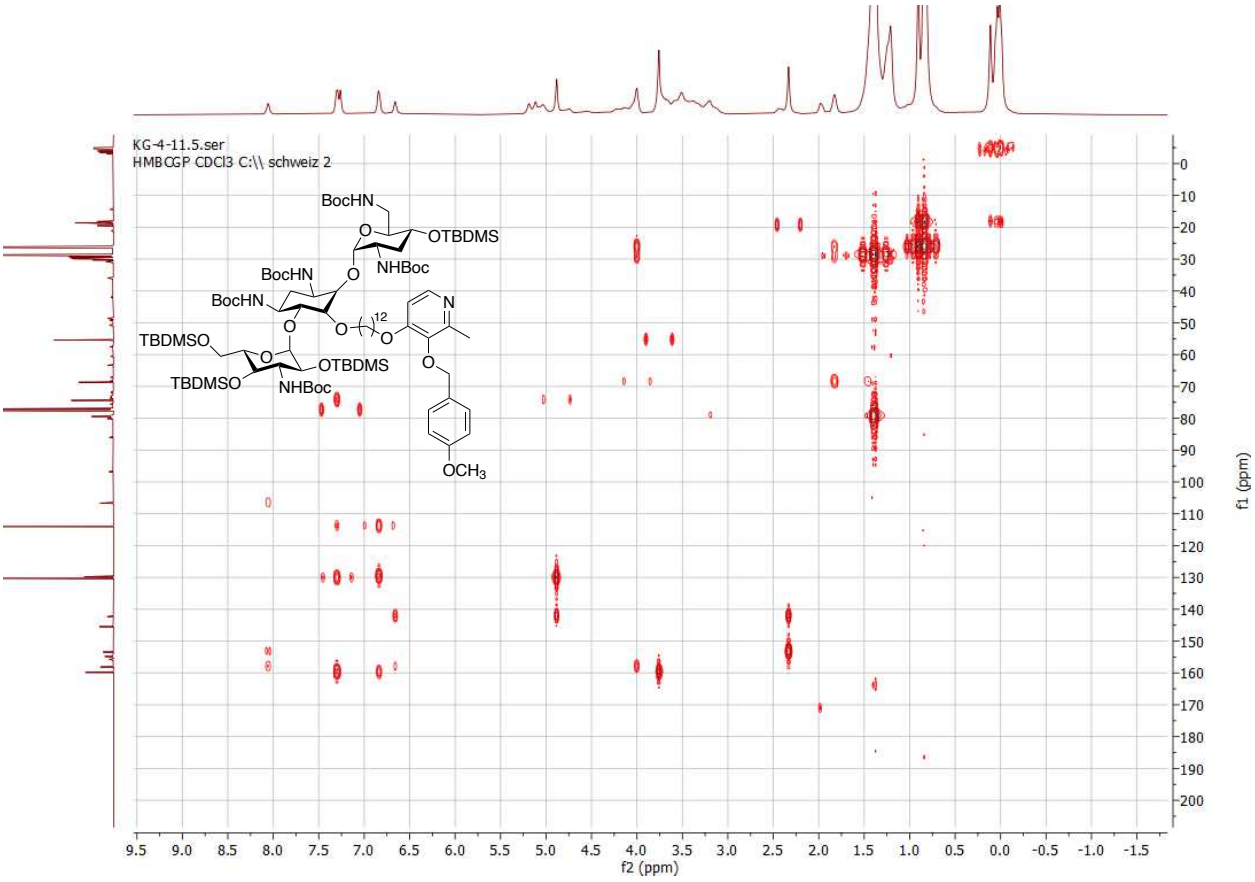
KG-4-11.5.ser
HMBCGP CDCl3 C:\\ schweiz 2
BocHN
OTBDMS
NHBoc
BocHN
BocHN
TBDMSO
OTBDMS
TBDMSO
NHBoc
12
N
O
OCH3
f2 (ppm)
f1 (ppm)

Compound 28

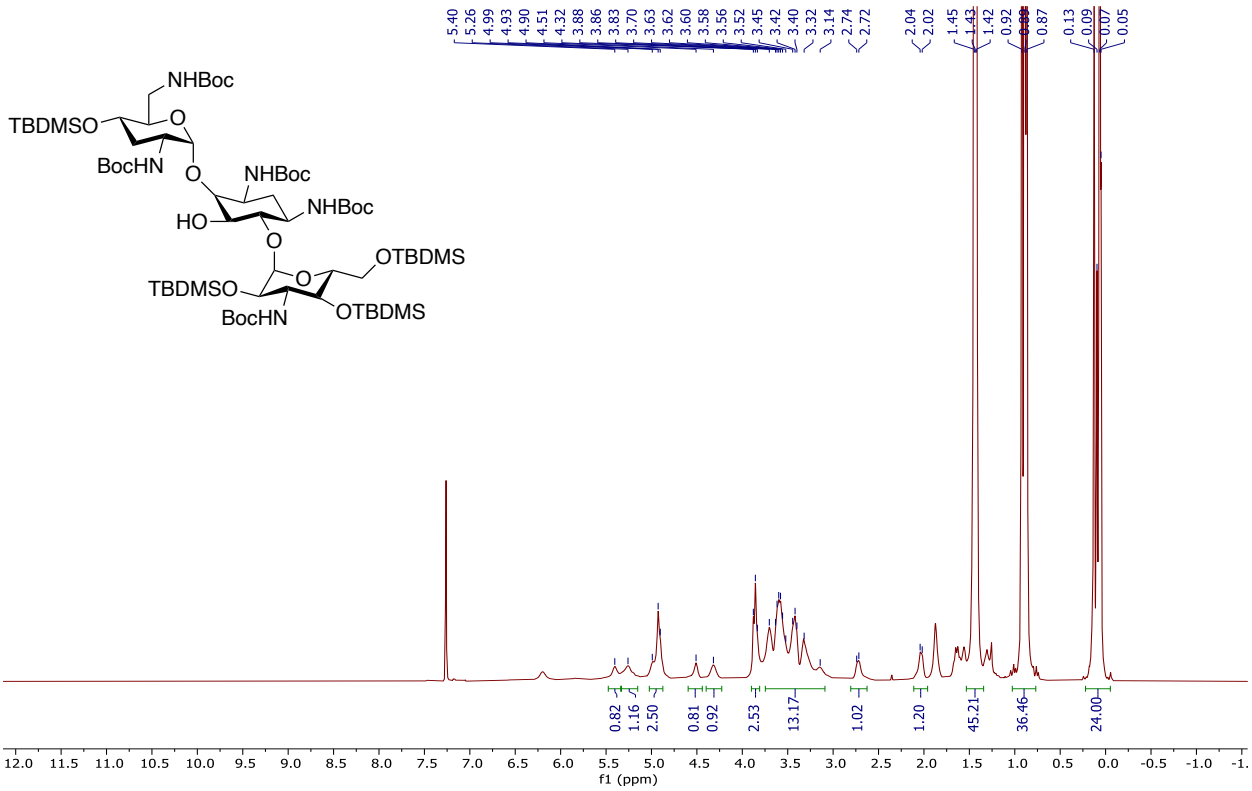
NHBoc
TBDMSO
O
BocHN
O
NHBoc
NHBoc
HO
O
OTBDMS
O
TBDMSO
BocHN
OTBDMS
5.40
5.26
4.99
4.93
4.90
4.51
4.32
3.88
3.86
3.83
3.70
3.63
3.62
3.60
3.58
3.56
3.52
3.45
3.42
3.40
3.32
3.14
2.74
2.72
2.04
2.02
1.45
1.43
1.42
0.92
0.87
0.13
0.09
0.07
0.05
0.82
1.16
2.50
0.81
0.92
2.53
13.17
1.02
1.20
45.21
36.46
24.00
12.0 11.5 11.0 10.5 10.0 9.5 9.0 8.5 8.0 7.5 7.0 6.5 6.0 5.5 5.0 4.5 4.0 3.5 3.0 2.5 2.0 1.5 1.0 0.5 0.0 -0.5 -1.0 -1.
f1 (ppm)

Compound 29a

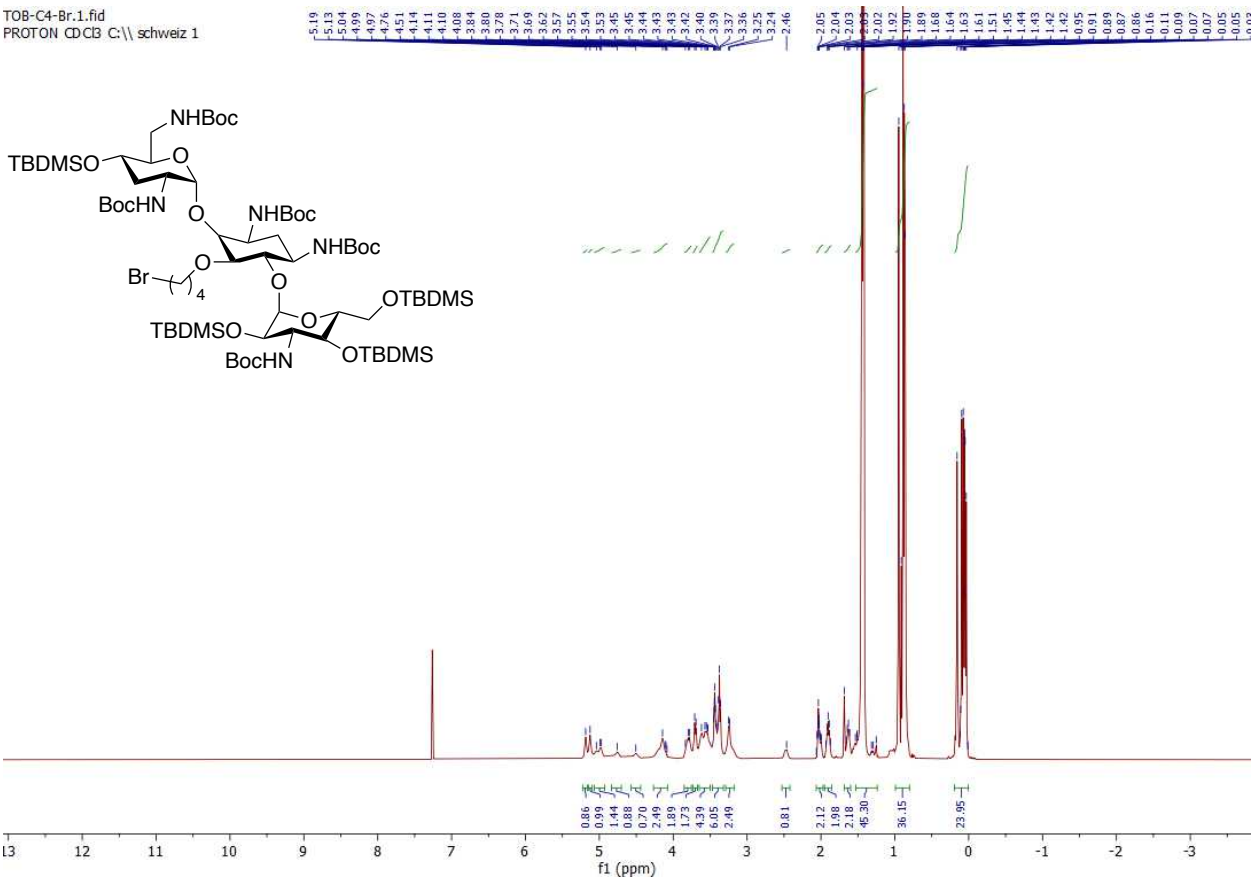

Compound 29b

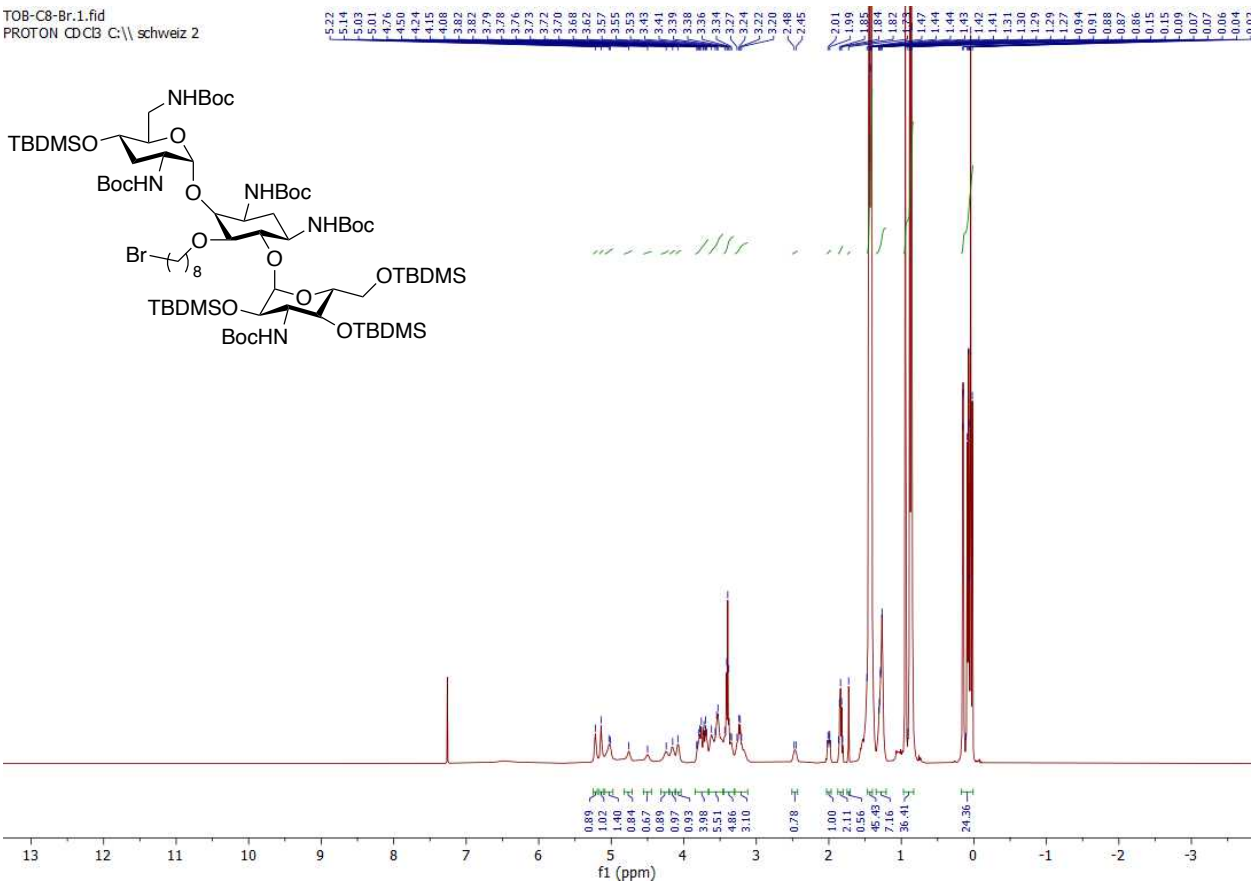

Compound 29c

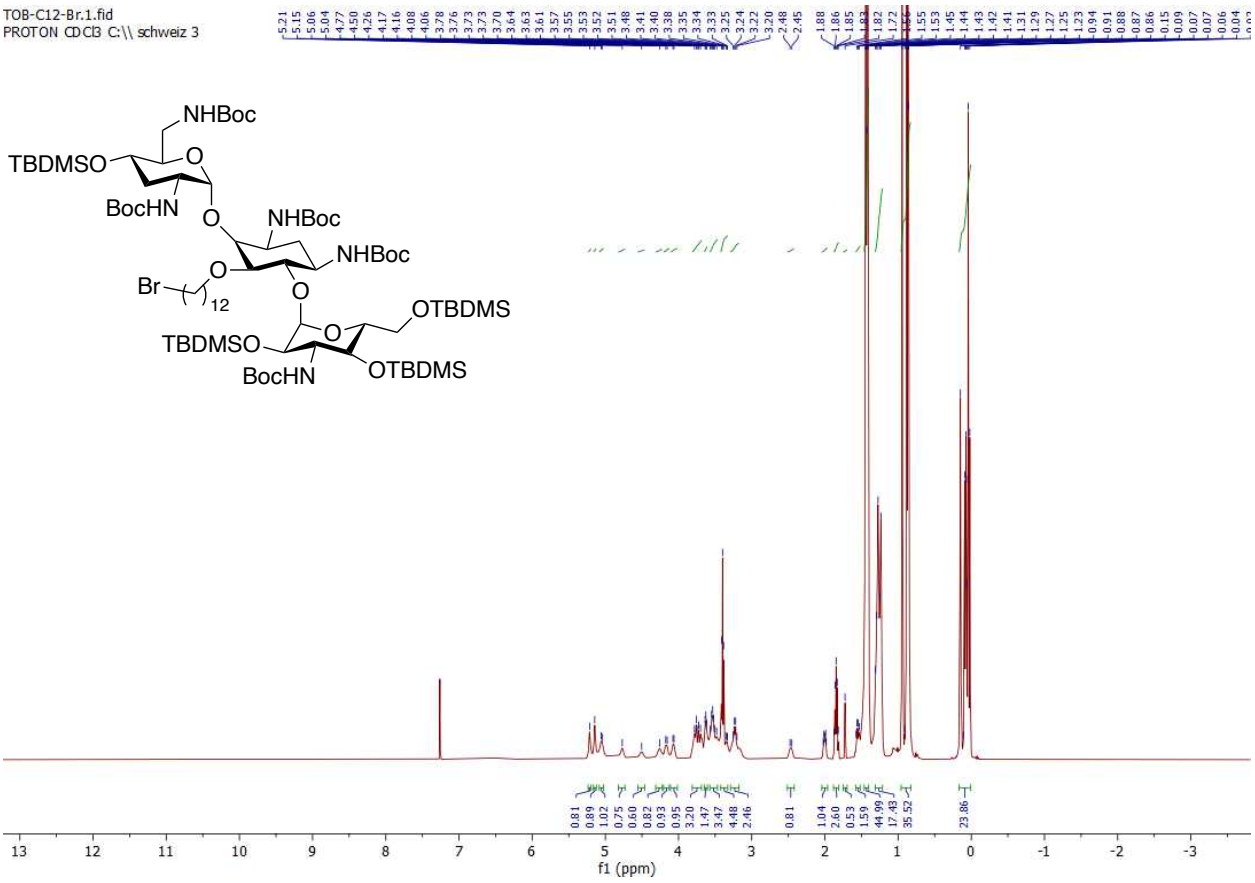

Compound 34a

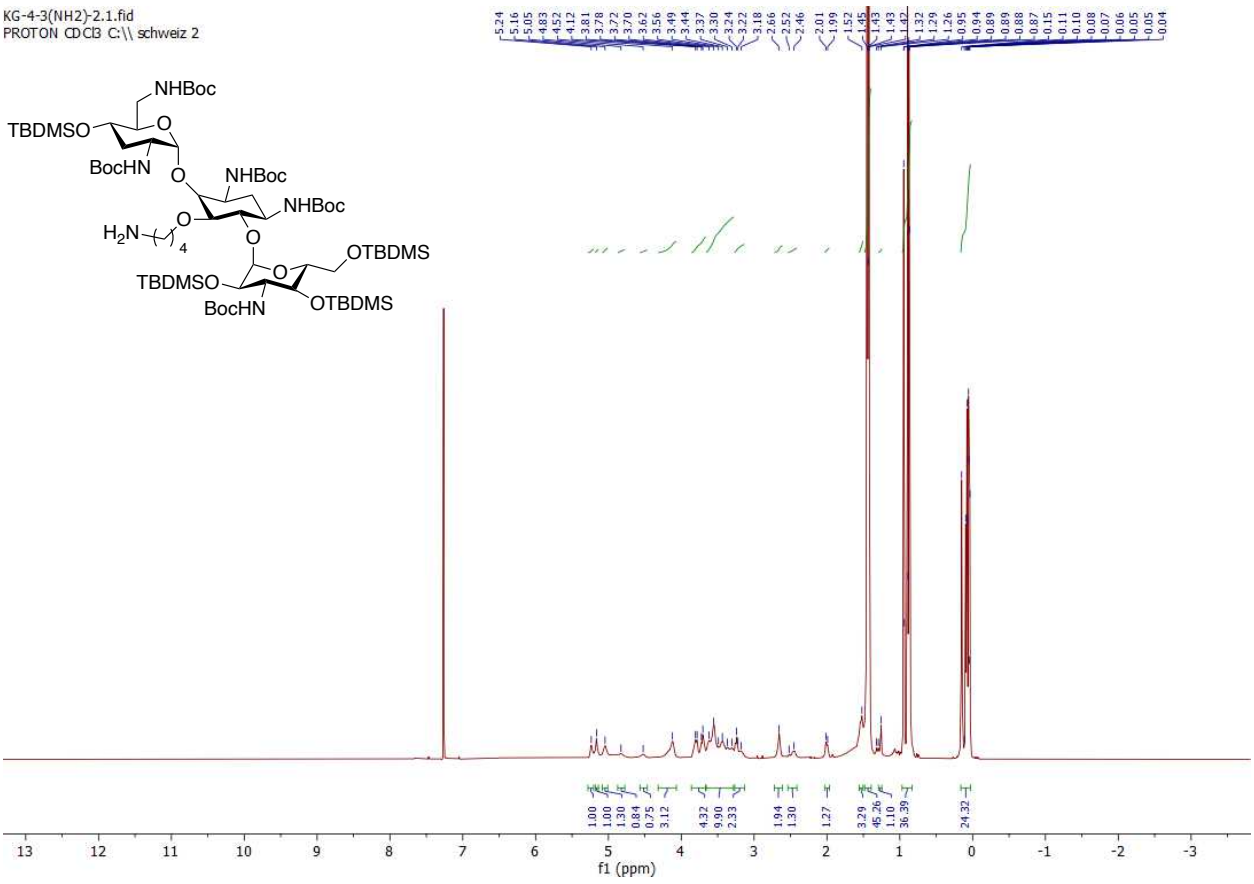

Compound 34b

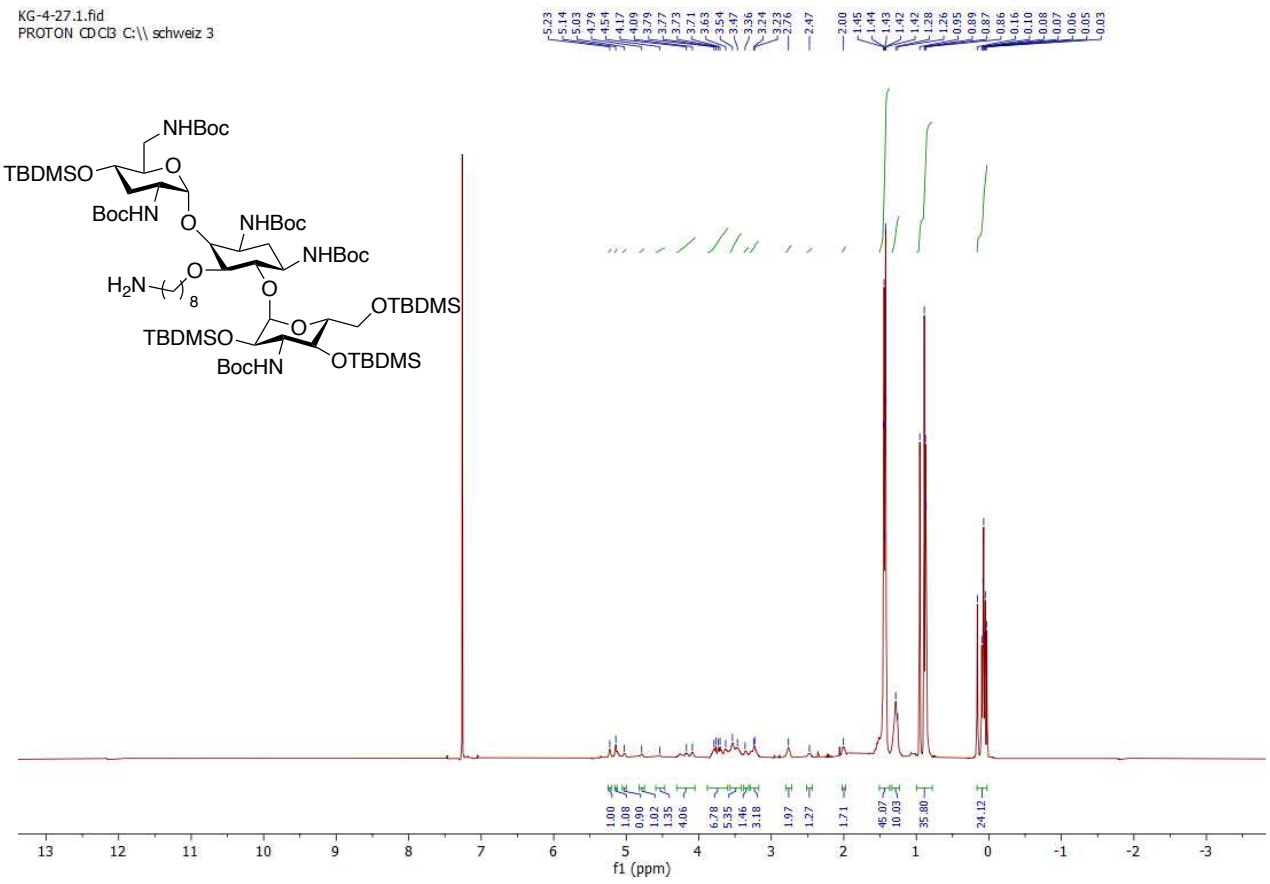

Compound 34c

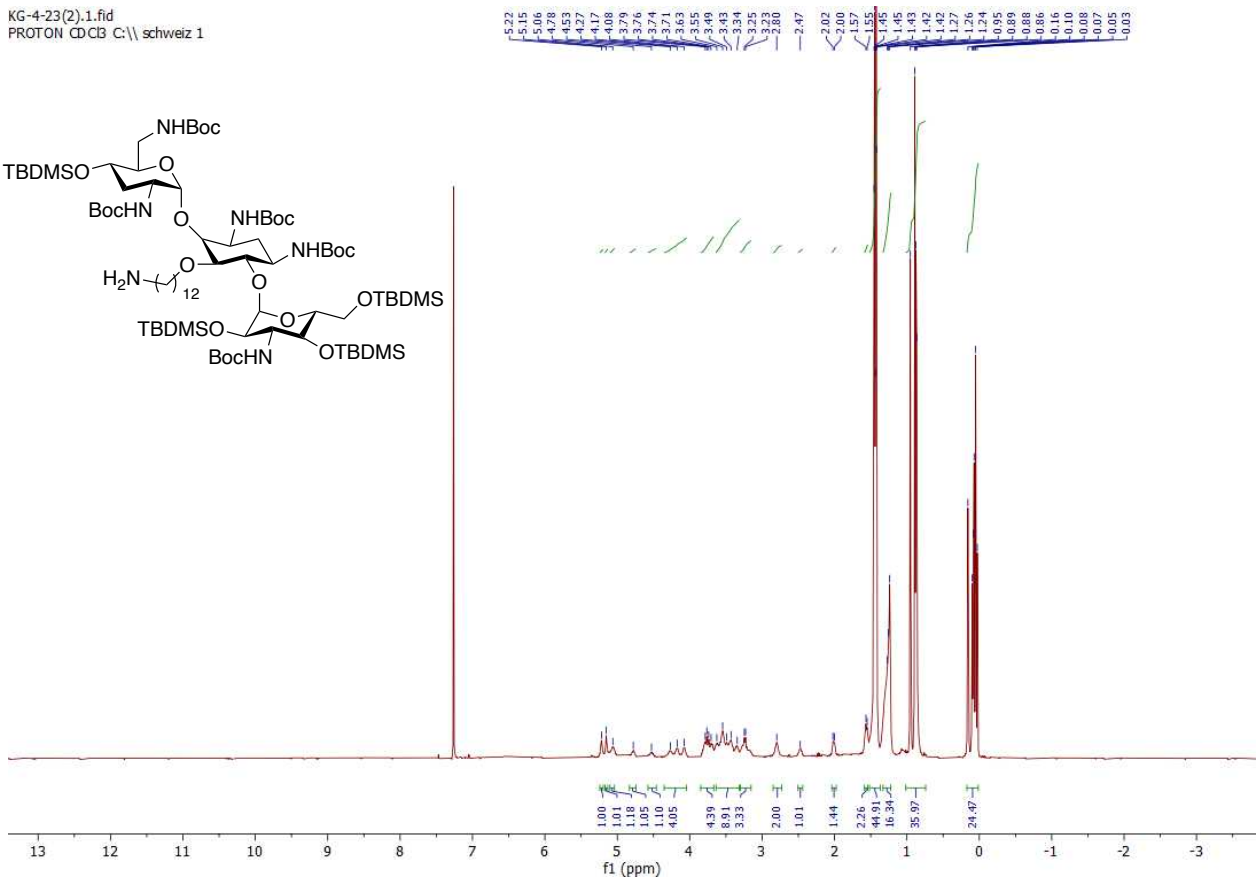

Compound 35

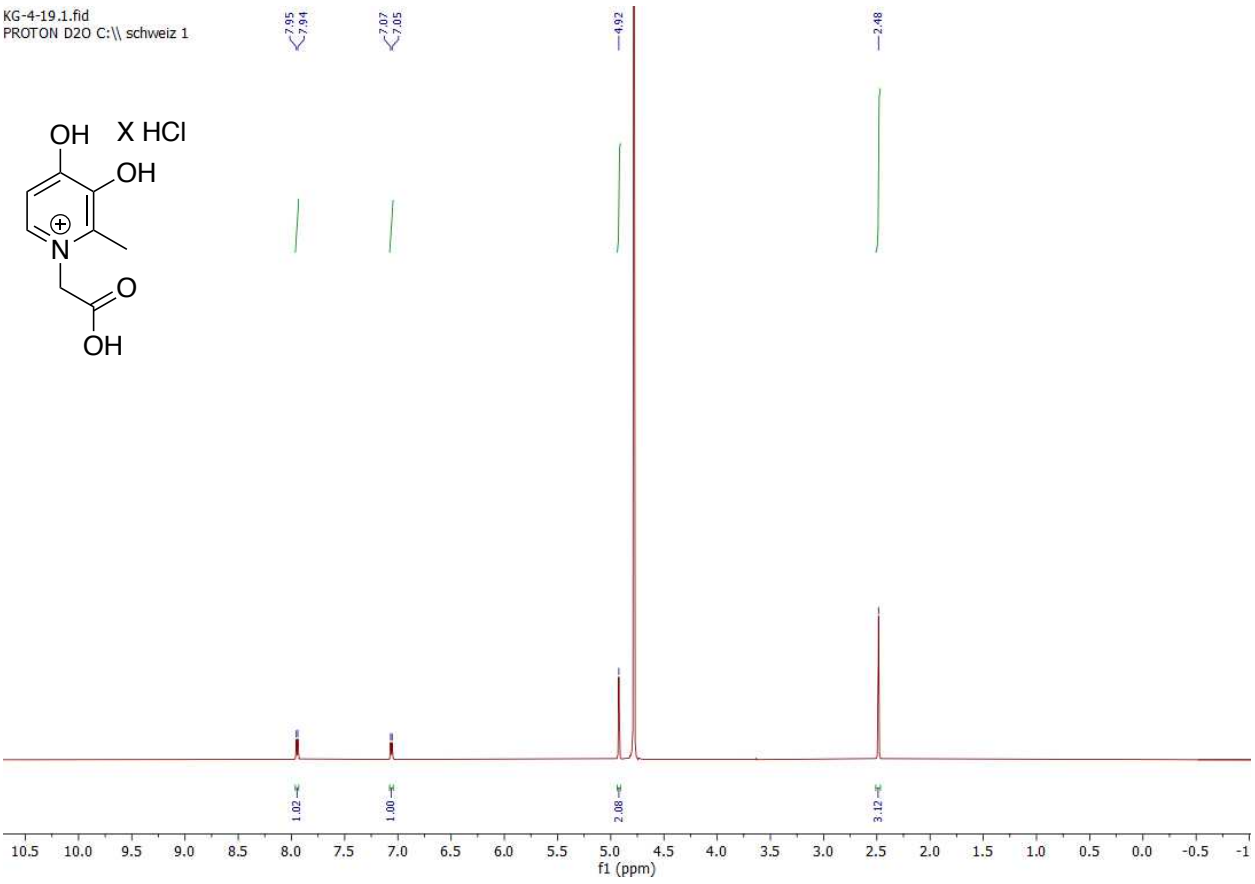
KG-4-19.1.fid
PROTON D2O C:\\ schweiz 1
7.95
7.94
7.07
7.05
4.92
2.48
OH
X HCl
OH
N
O
OH
1.02
1.00
2.08
3.12
10.5 10.0 9.5 9.0 8.5 8.0 7.5 7.0 6.5 6.0 5.5 5.0 4.5 4.0 3.5 3.0 2.5 2.0 1.5 1.0 0.5 0.0 -0.5 -1
f1 (ppm)

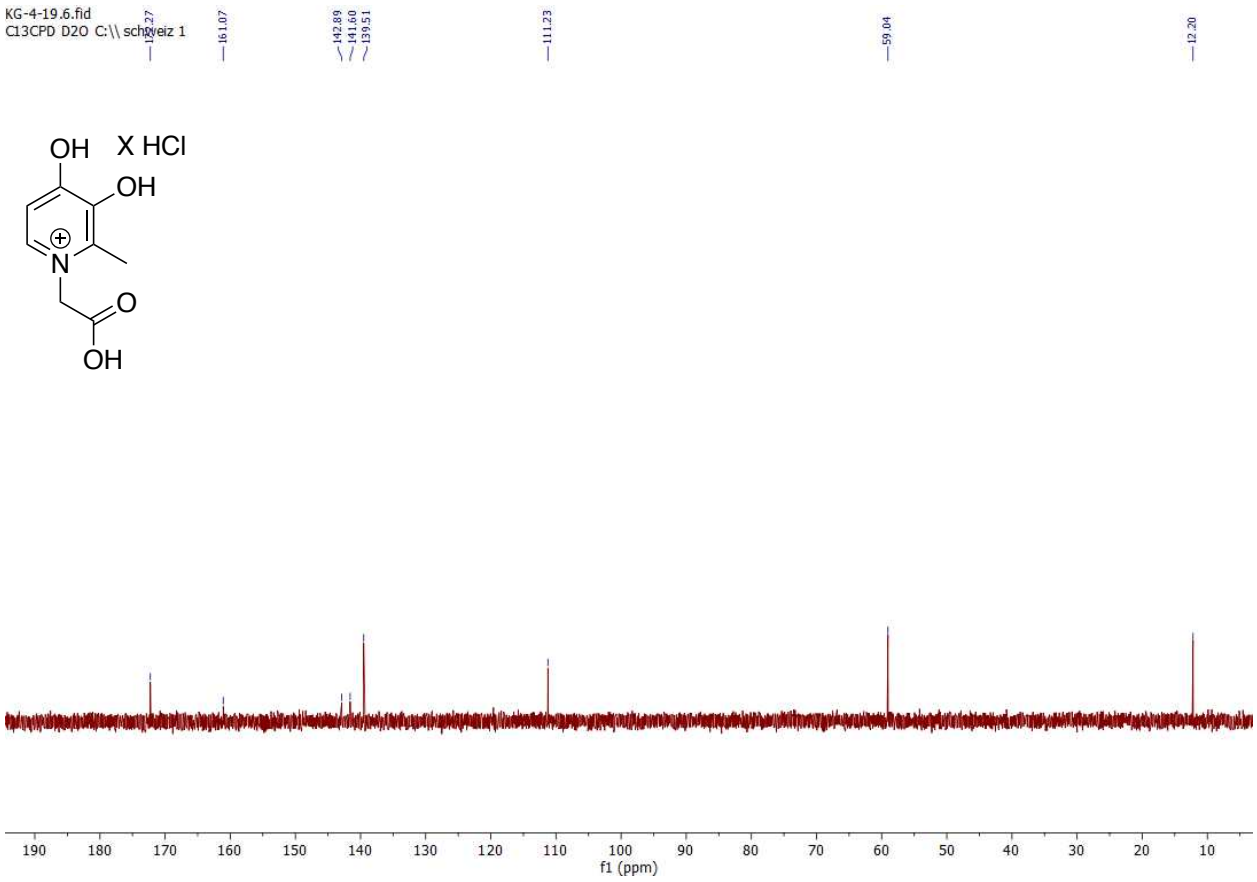
KG-4-19.6.fid
C13CPD D2O C:\\ schweiz 1
172.27
161.07
142.89
141.60
139.51
111.23
59.04
12.20
OH
X HCl
OH
N
O
OH
190
180
170
160
150
140
130
120
110
100
90
80
70
60
50
40
30
20
10
f1 (ppm)

Compound 36a

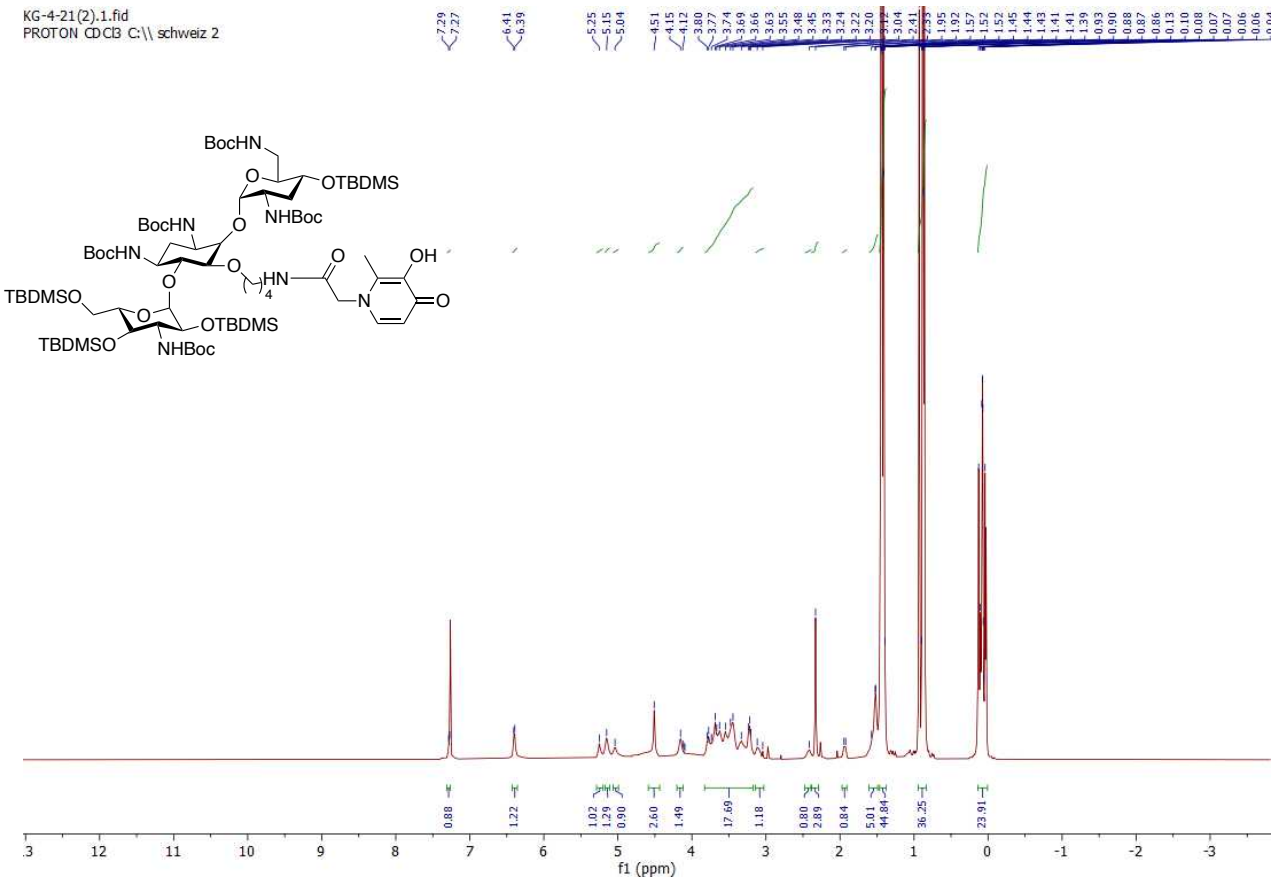

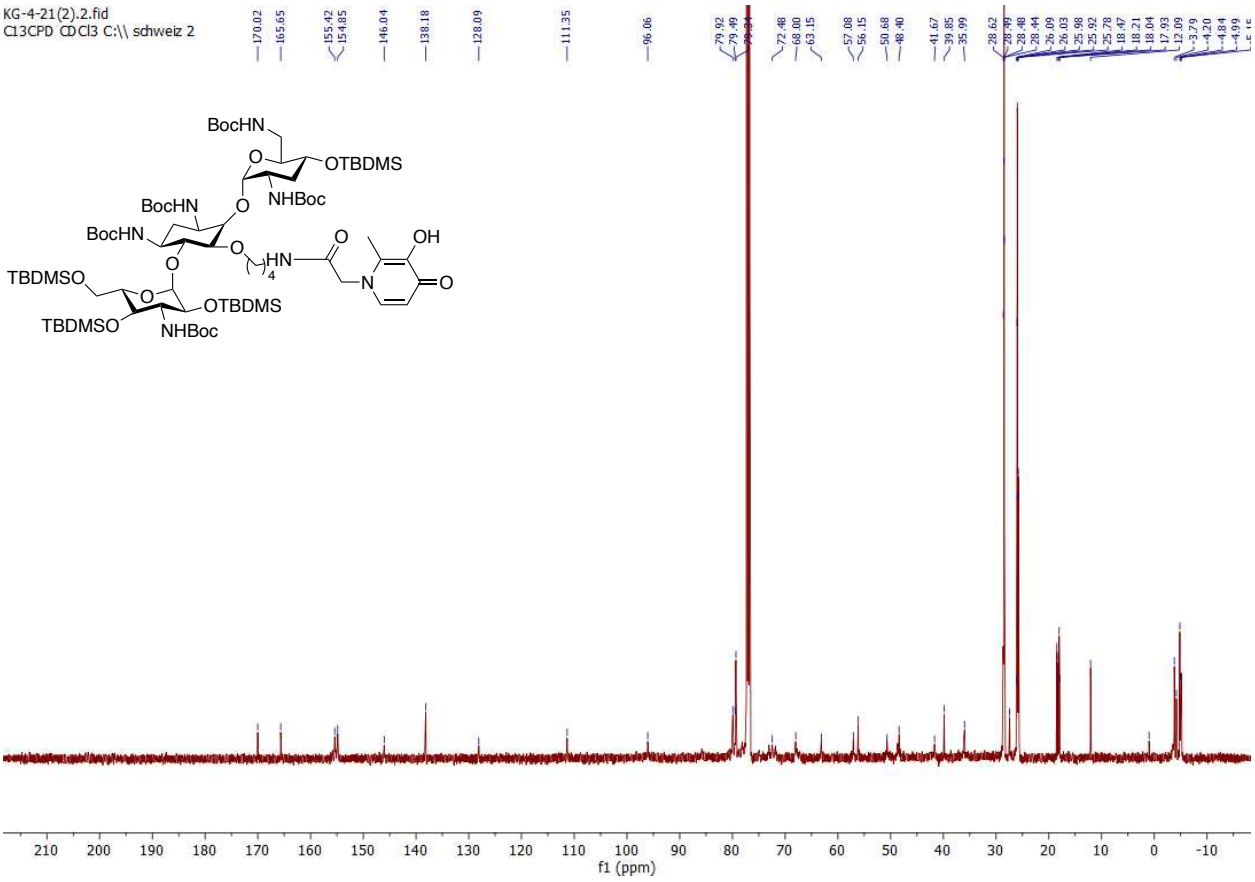
KG-4-21(2).2.fid
C13CPD CDCl3 C:\\ schweiz 2
BocHN
OTBDMS
NHBoc
BocHN
BocHN
HN
OH
TBDMSO
OTBDMS
TBDMSO
NHBoc
f1 (ppm)

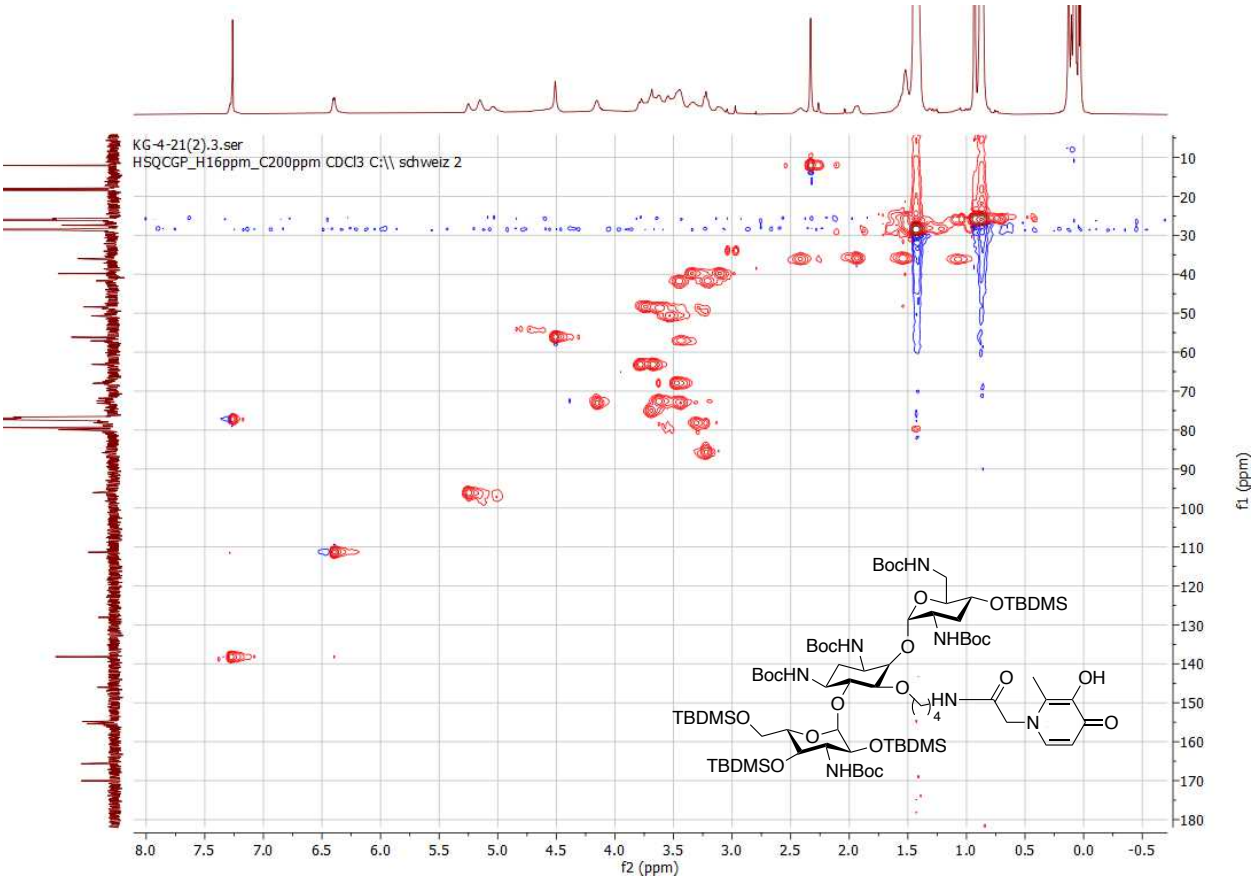
KG-4-21(2).3.ser
HSQCGP_H16ppm_C200ppm CDCl3 C:\\ schweiz 2
f2 (ppm)
f1 (ppm)
BocHN
OTBDMS
NHBoc
BocHN
BocHN
HN
OH
TBDMSO
OTBDMS
TBDMSO
NHBoc

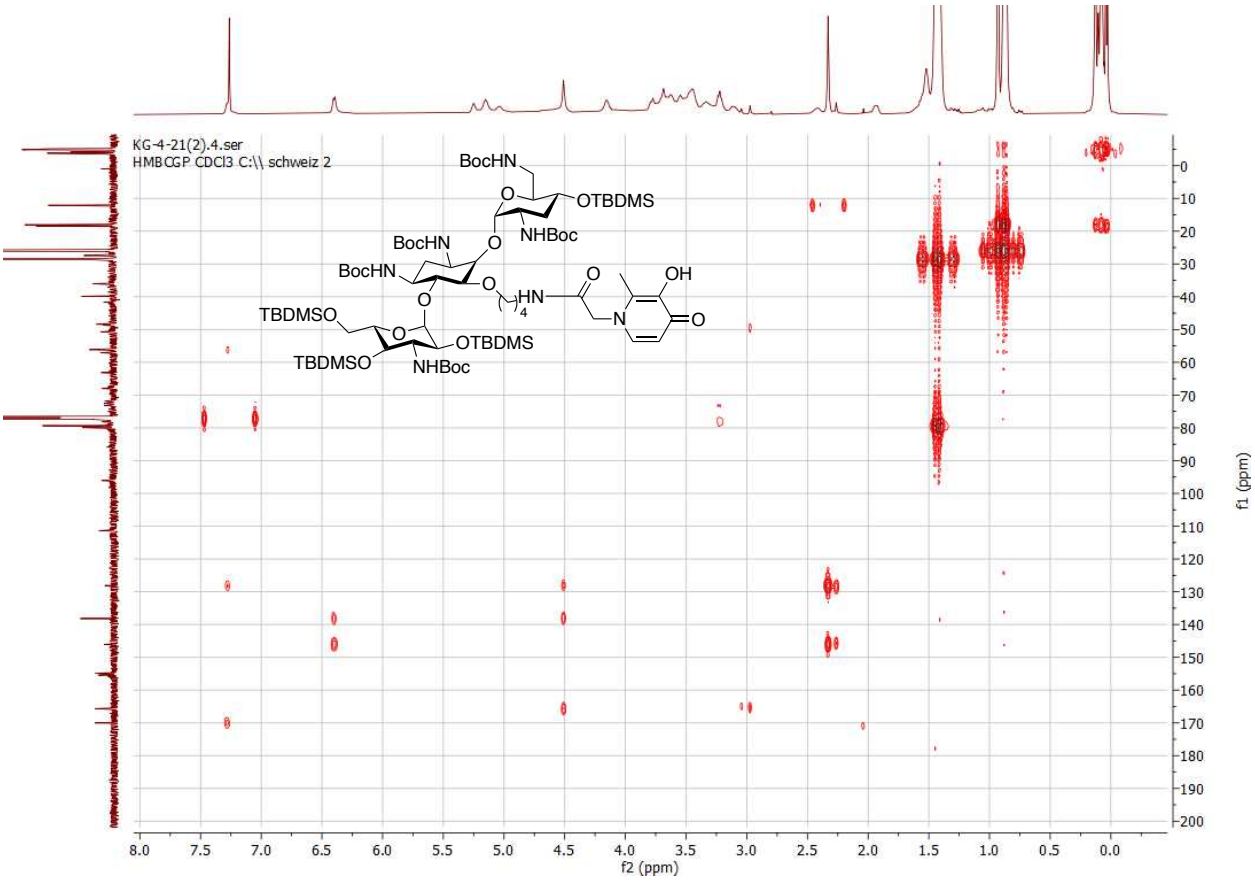
KG-4-21(2).4.ser
HMBCGP CDCl3 C:\\ schweiz 2
BocHN
OTBDMS
NHBoc
BocHN
BocHN
HN
4
OH
O
N
O
TBDMSO
TBDMSO
OTBDMS
NHBoc
f2 (ppm)
f1 (ppm)

Compound 36b

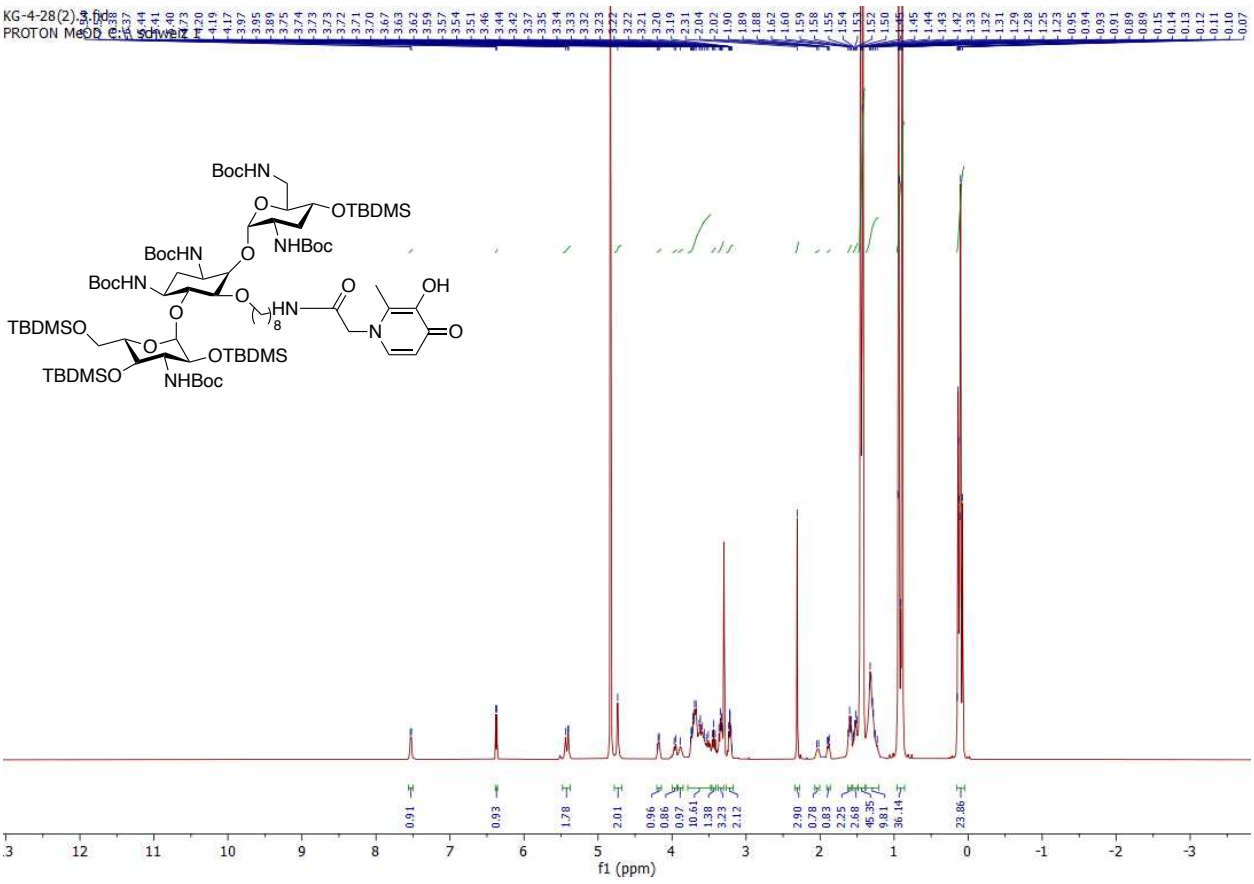

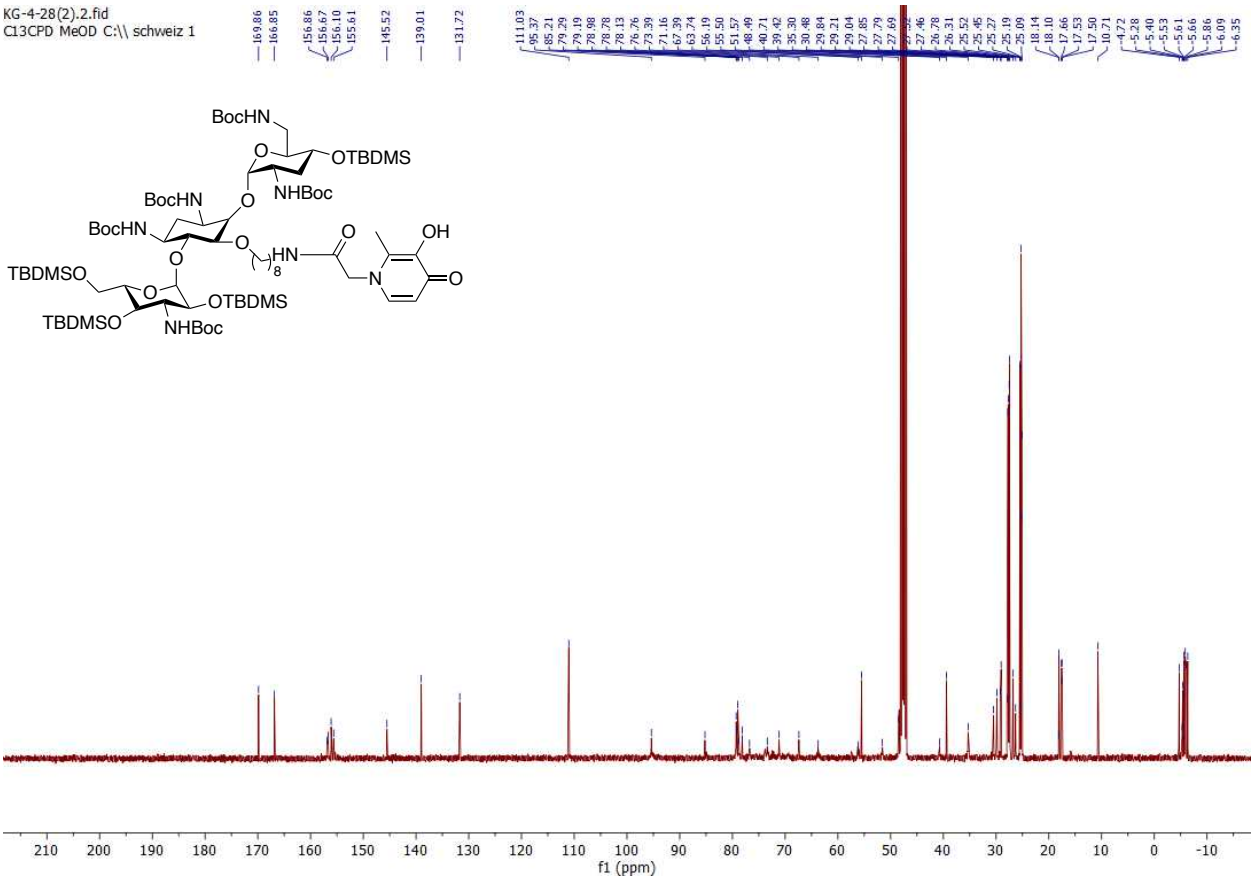
KG-4-28(2).2.fid
C13CPD MeOD C:\\ schweiz 1
BocHN
O
OTBDMS
NHBoc
BocHN
O
BocHN
O
O
HN
8
O
OH
N
O
TBDMSO
O
O
OTBDMS
TBDMSO
NHBoc
f1 (ppm)

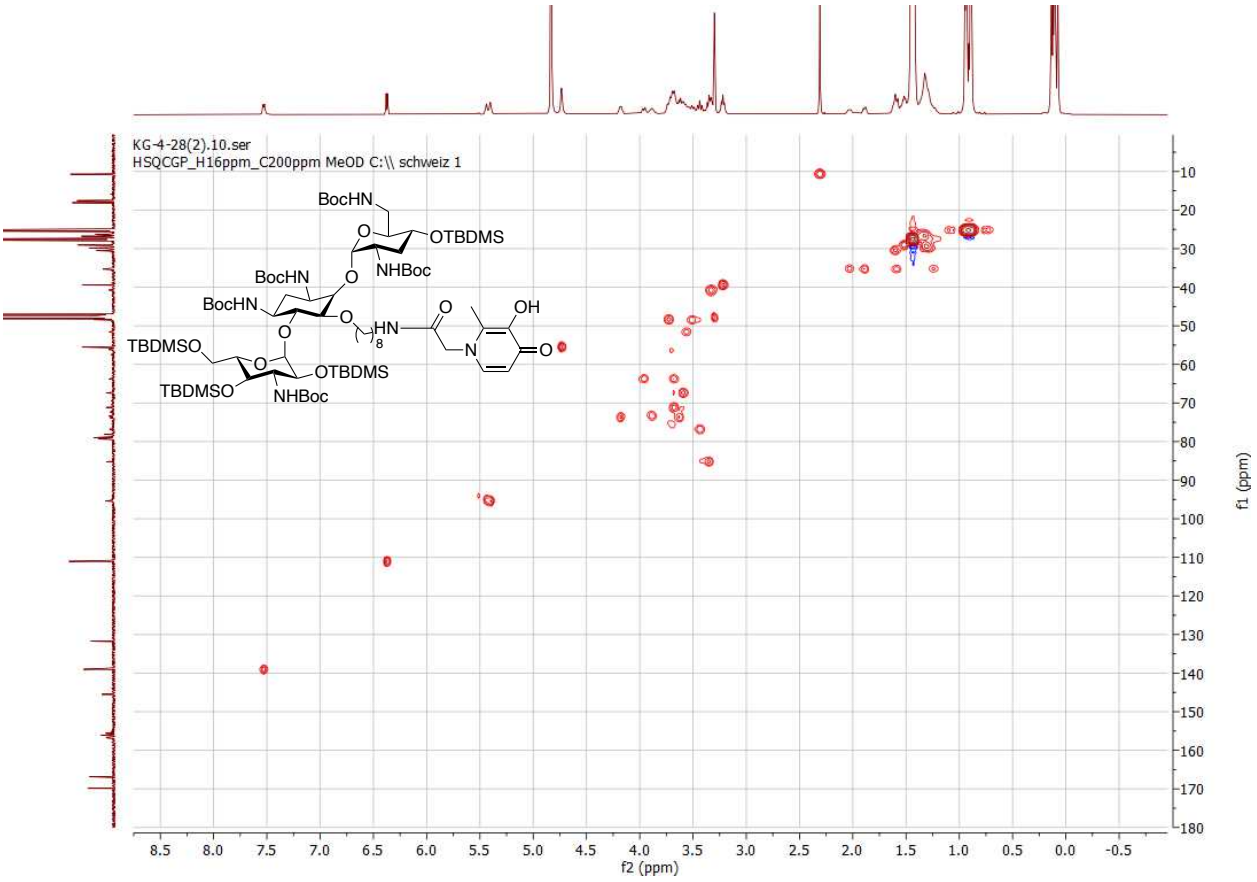
KG-4-28(2).10.ser
HSQCGP_H16ppm_C200ppm MeOD C:\\ schweiz 1
BocHN
OTBDMS
NHBoc
BocHN
BocHN
HN
8
OH
N
O
TBDMSO
OTBDMS
TBDMSO
NHBoc
f2 (ppm)
f1 (ppm)

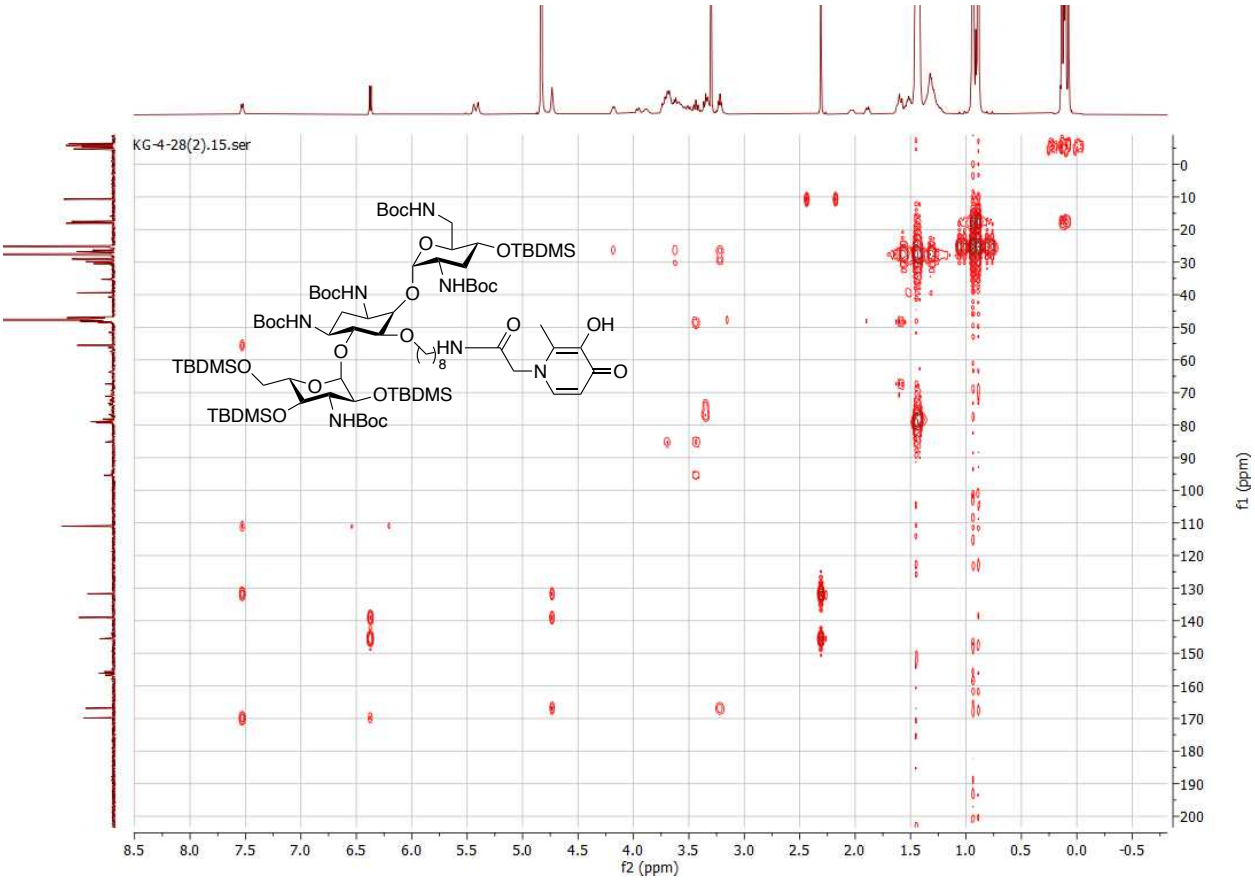
KG-4-28(2).15.ser
BocHN
O
OTBDMS
NHBoc
BocHN
O
BocHN
O
HN
8
O
OH
N
O
TBDMSO
O
OTBDMS
TBDMSO
NHBoc
f2 (ppm)
f1 (ppm)

Compound 36c

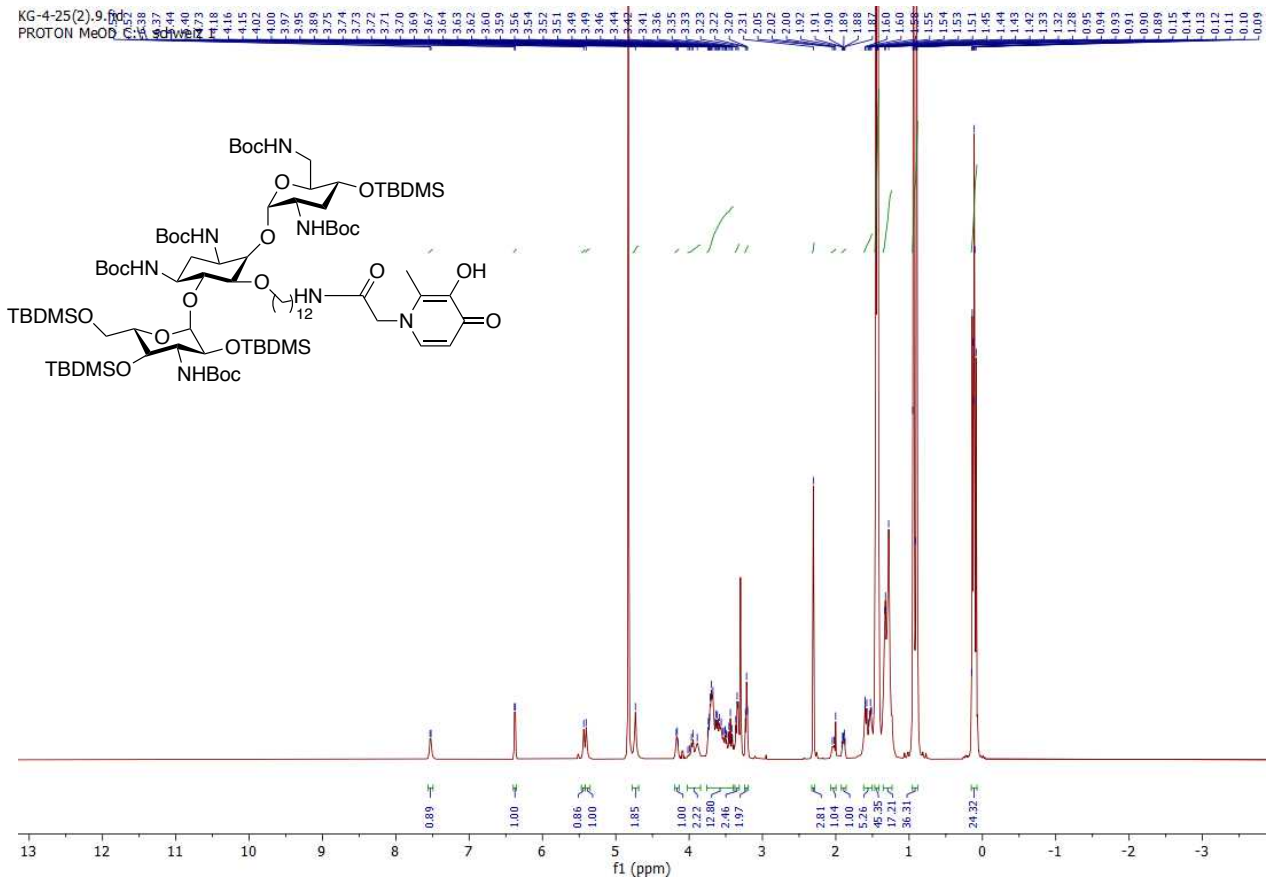

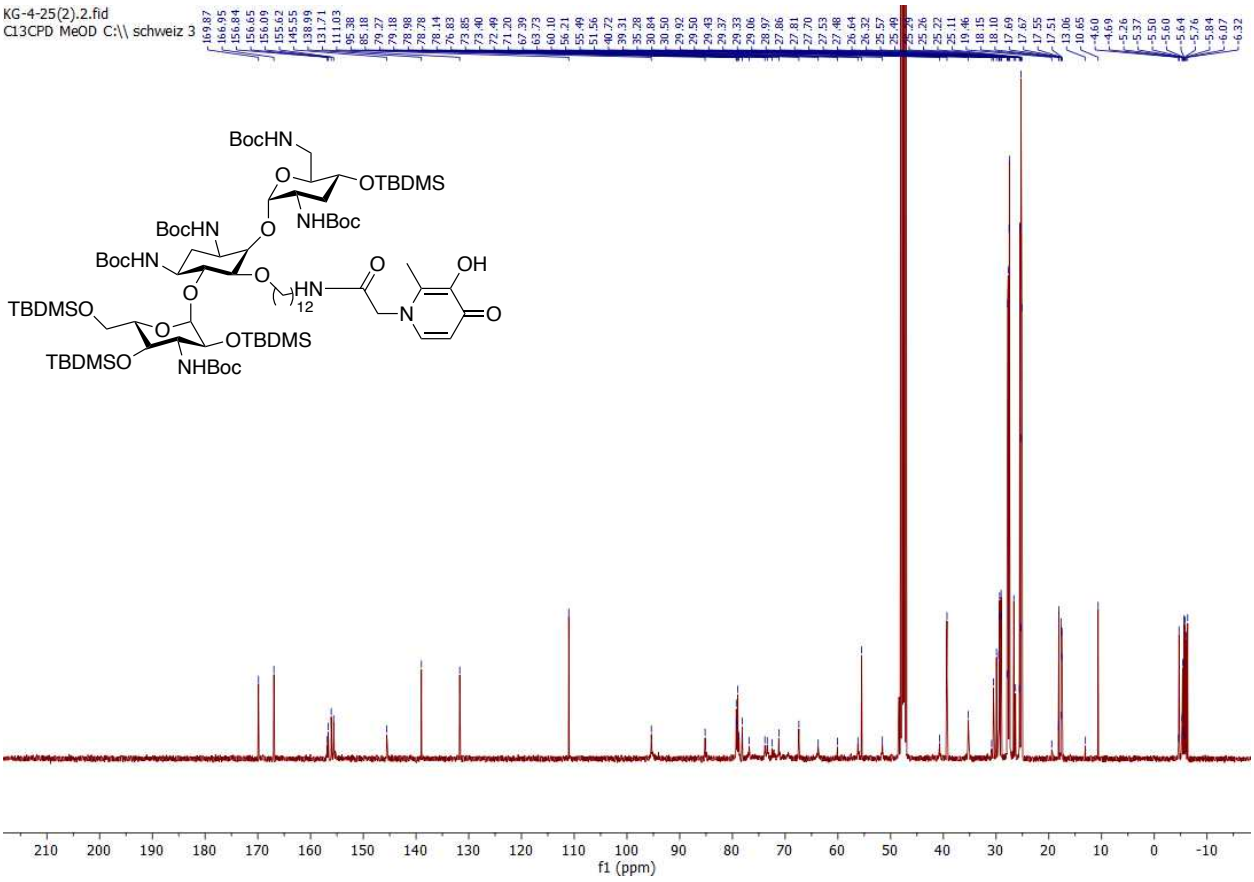
KG-4-25(2).2.fid
C13CPD MeOD C:\\ schweiz 3
BocHN
O
OTBDMS
NHBoc
BocHN
O
BocHN
O
HN
12
O
OH
N
O
TBDMSO
O
OTBDMS
TBDMSO
NHBoc
210
200
190
180
170
160
150
140
130
120
110
100
90
80
70
60
50
40
30
20
10
0
-10
f1 (ppm)

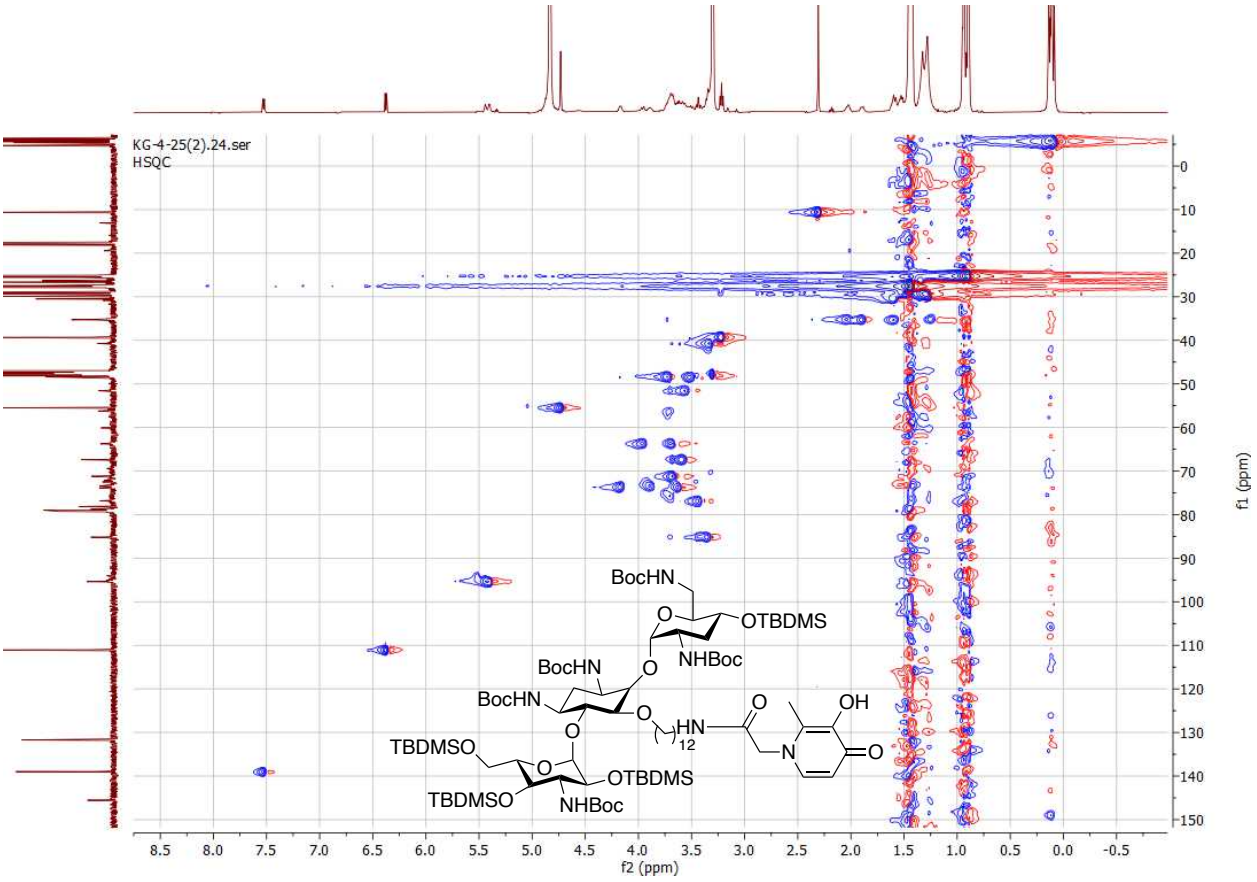
KG-4-25(2).24.ser
HSQC
f2 (ppm)
f1 (ppm)
BocHN
O
OTBDMS
NHBoc
BocHN
O
BocHN
O
O
HN
12
O
OH
N
O
TBDMSO
O
OTBDMS
TBDMSO
NHBoc

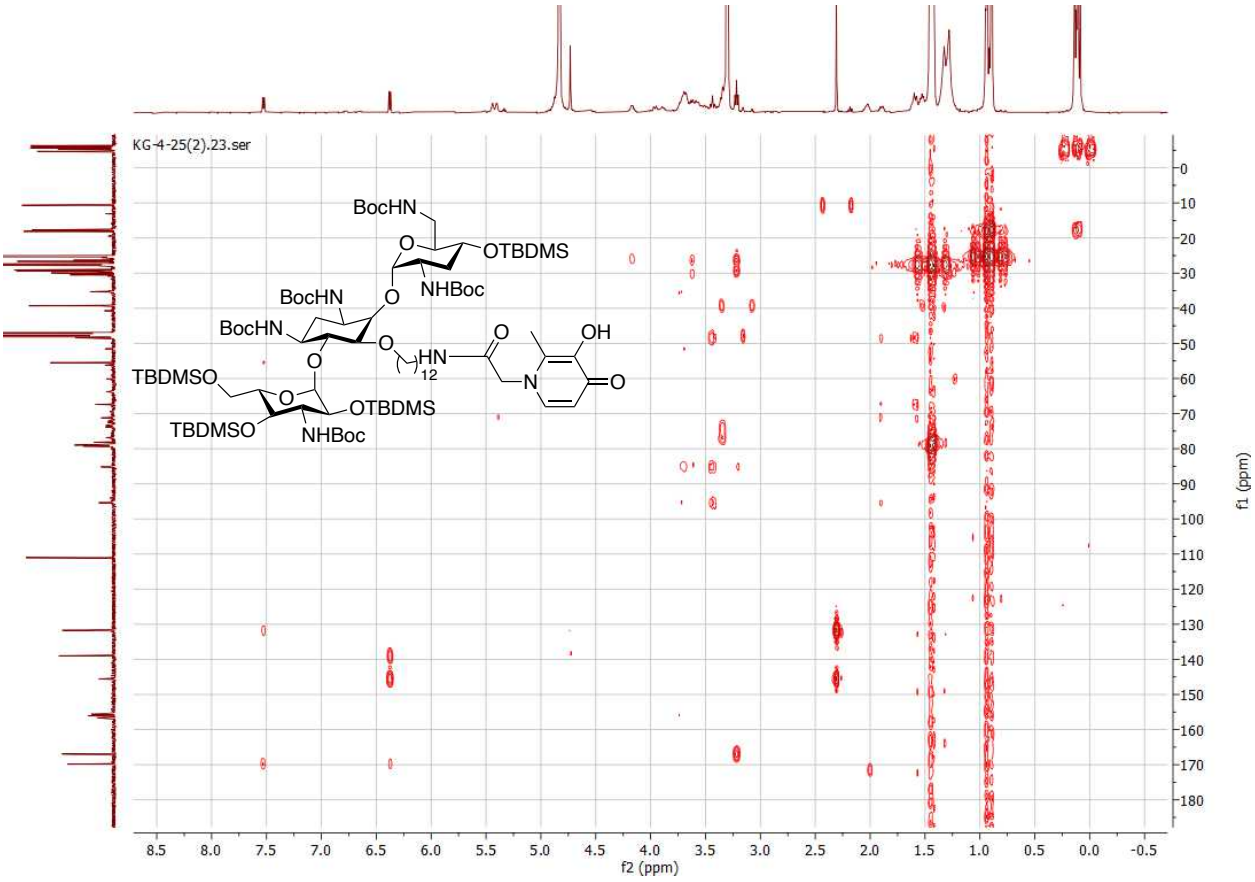
KG-4-25(2).23.ser
BocHN
O
OTBDMS
NHBoc
BocHN
O
BocHN
O
O
HN
12
O
OH
N
O
TBDMSO
O
OTBDMS
TBDMSO
NHBoc
f2 (ppm)
f1 (ppm)

Compound 26

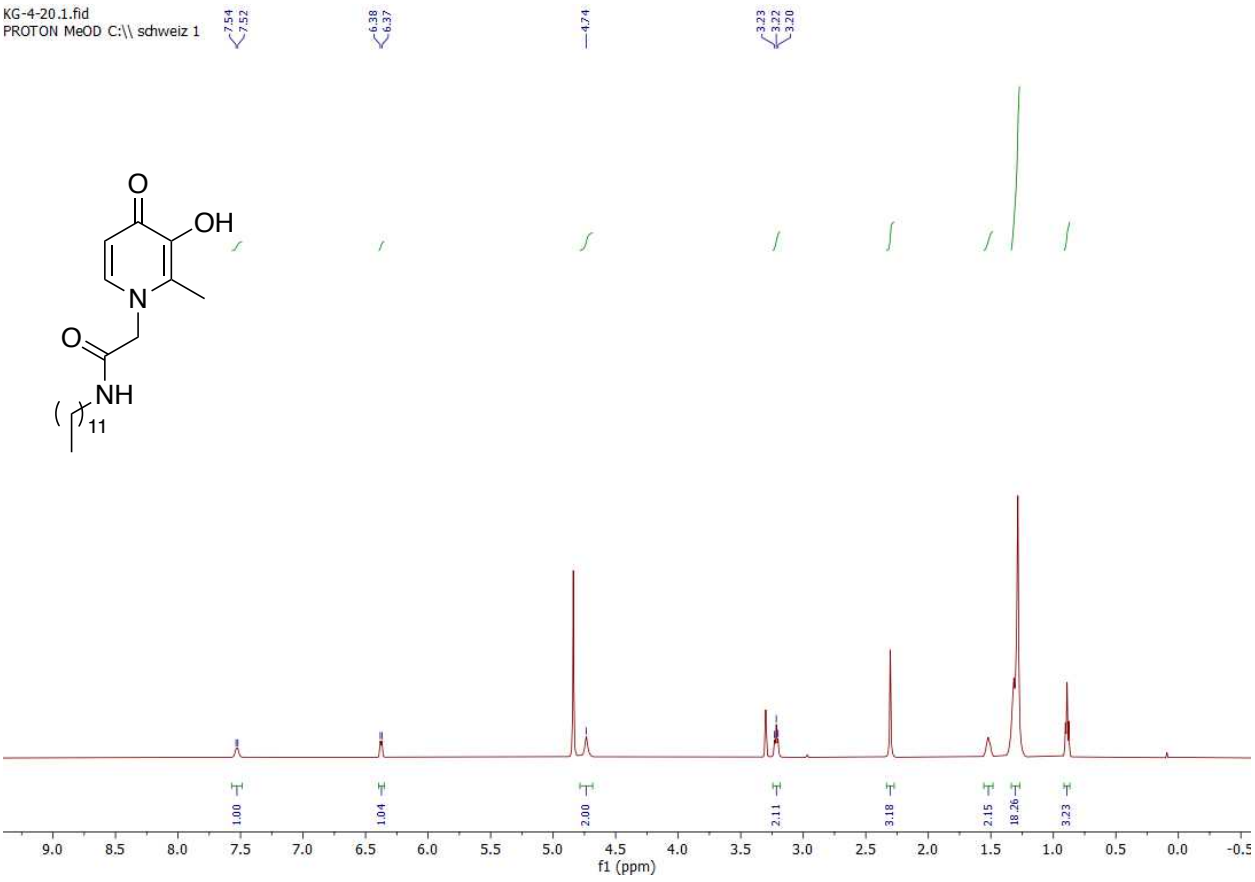
KG-4-20.1.fid
PROTON MeOD C:\\ schweiz 1
7.54
7.52
6.38
6.37
4.74
3.23
3.22
3.20
O
OH
N
O
NH
11
1.00
1.04
2.00
2.11
3.18
2.15
18.26
3.23
9.0
8.5
8.0
7.5
7.0
6.5
6.0
5.5
5.0
4.5
4.0
3.5
3.0
2.5
2.0
1.5
1.0
0.5
0.0
f1 (ppm)

Compound 25

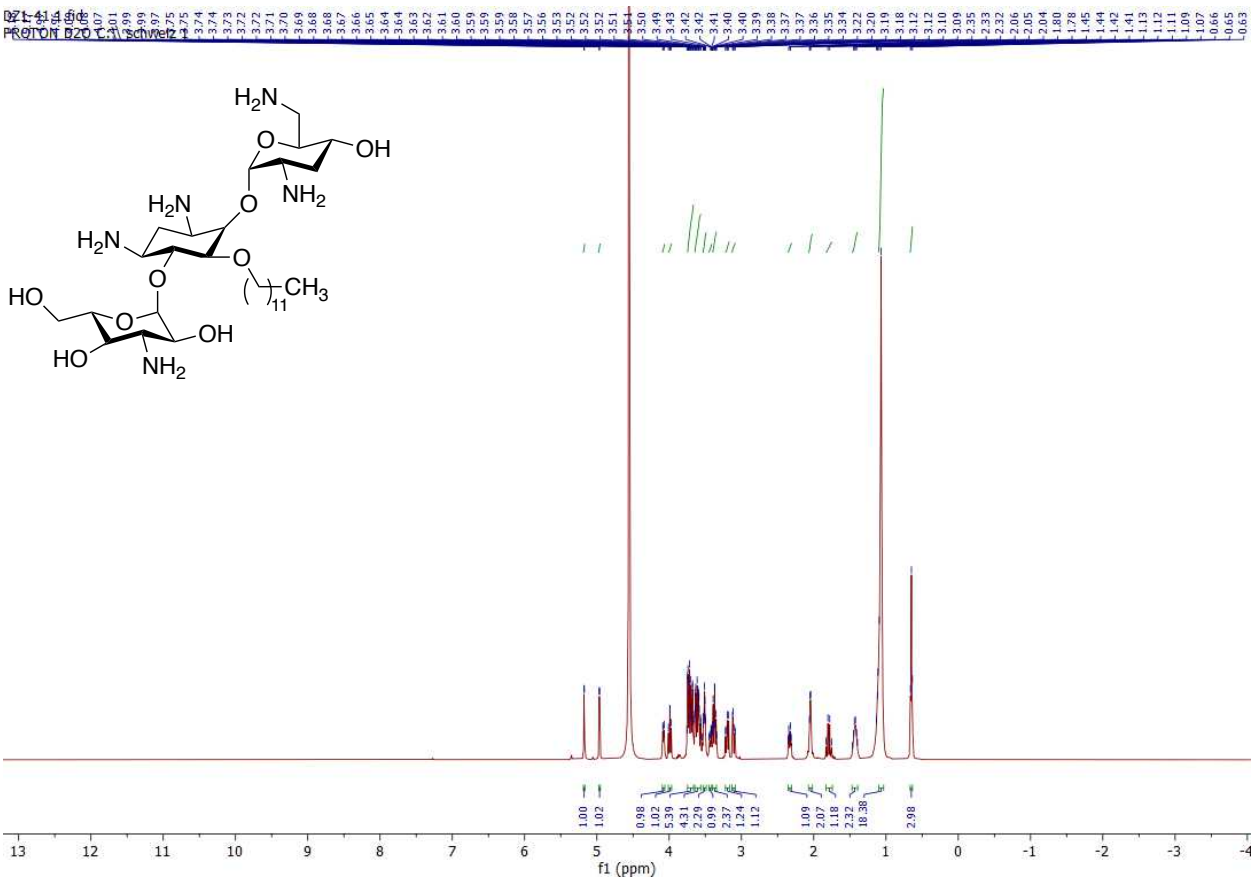
H2N
O
OH
NH2
H2N
O
H2N
O
O
CH3
11
HO
O
OH
HO
NH2
1.00
1.02
0.98
1.02
5.39
4.31
2.29
0.99
2.37
1.24
1.12
1.09
2.07
1.18
2.32
18.38
2.98
13
12
11
10
9
8
7
6
5
4
3
2
1
0
-1
-2
-3
-4
f1 (ppm)

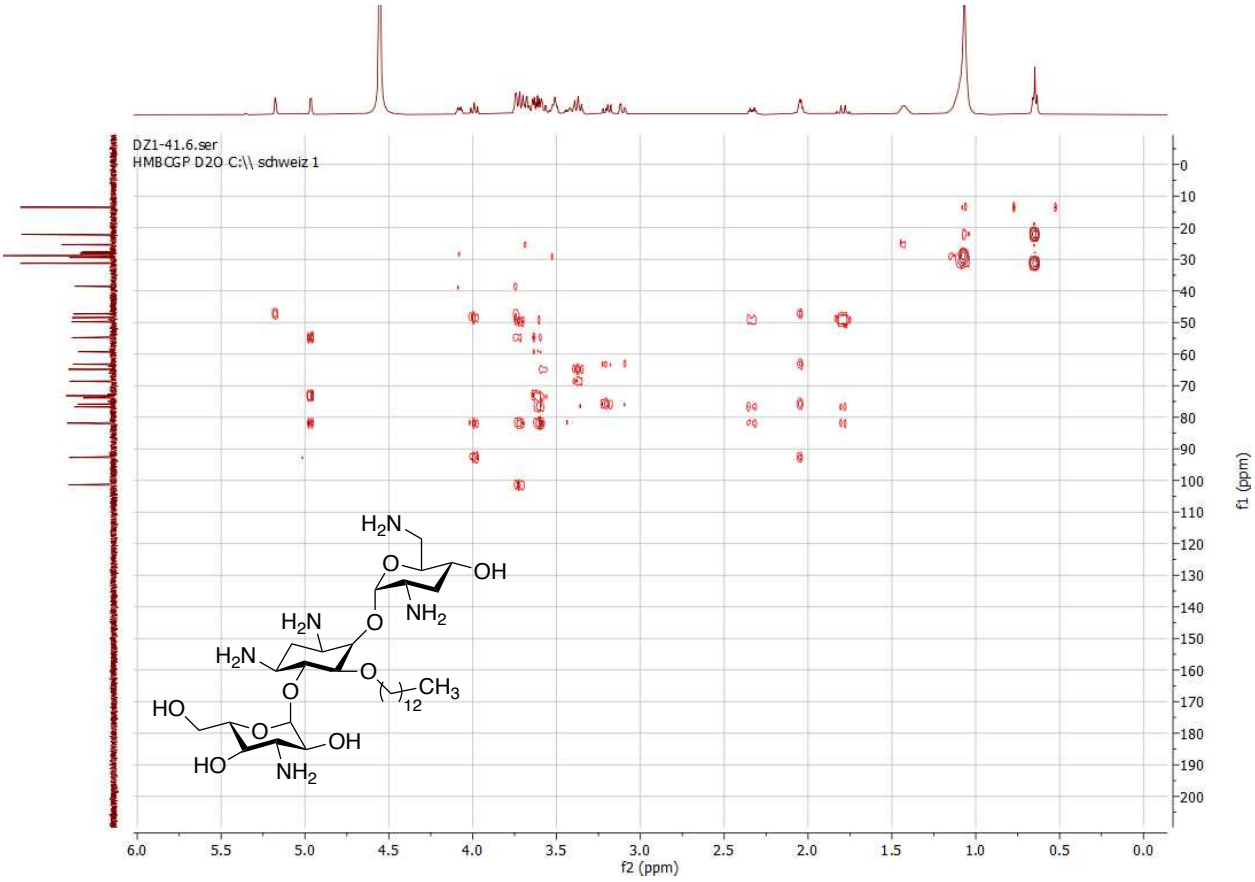
DZ1-41.6.ser
HMBCGP D2O C:\\ schweiz 1
f2 (ppm)
f1 (ppm)
H2N
O
OH
NH2
H2N
O
H2N
O
CH3
12
O
HO
O
OH
HO
NH2

HPLC analysis for purity determination of final compounds

Compound 24a

Chromatogram and Results

Injection Details

Injection Name:	**KG-4-24**	*Run Time (min):*	**8.93**
Vial Number:	**R:A3**	*Injection Volume:*	**3.00**
Injection Type:	**Unknown**	*Channel:*	**UV_VIS_1**
Calibration Level:		*Wavelength:*	**275**
Instrument Method:	**METHOD C (24-06-2022)**	*Bandwidth:*	**n.a.**
Processing Method:	**Basic Quantitative**	*Dilution Factor:*	**1.0000**
Injection Date/Time:	**25/Jun/22 16:36**	*Sample Weight:*	**1.0000**

Chromatogram

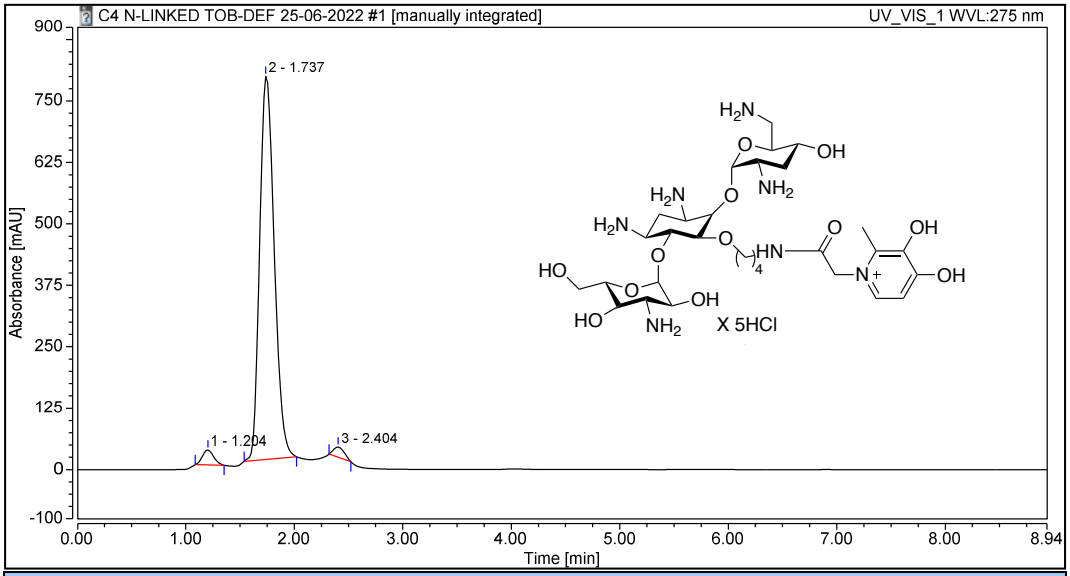

Integration Results

No.	Peak Name	Retention Time min	Area mAU*min	Height mAU	Relative Area %	Relative Height %	Amount n.a.
1		1.204	3.651	30.341	2.87	3.65	n.a.
2		1.737	120.955	779.312	95.22	93.83	n.a.
3		2.404	2.427	20.892	1.91	2.52	n.a.
Total:			**127.033**	**830.545**	**100.00**	**100.00**	

Compound 24b

Chromatogram and Results

Injection Details

Injection Name:	**KG-4-29-F**	*Run Time (min):*	**20.00**
Vial Number:	**R:A2**	*Injection Volume:*	**3.00**
Injection Type:	**Unknown**	*Channel:*	**UV_VIS_1**
Calibration Level:		*Wavelength:*	**275**
Instrument Method:	**METHOD B (25-06-2022) 3P 0.15FLOW**	*Bandwidth:*	**n.a.**
Processing Method:	**Basic Quantitative**	*Dilution Factor:*	**1.0000**
Injection Date/Time:	**25/Jun/22 15:27**	*Sample Weight:*	**1.0000**

Chromatogram

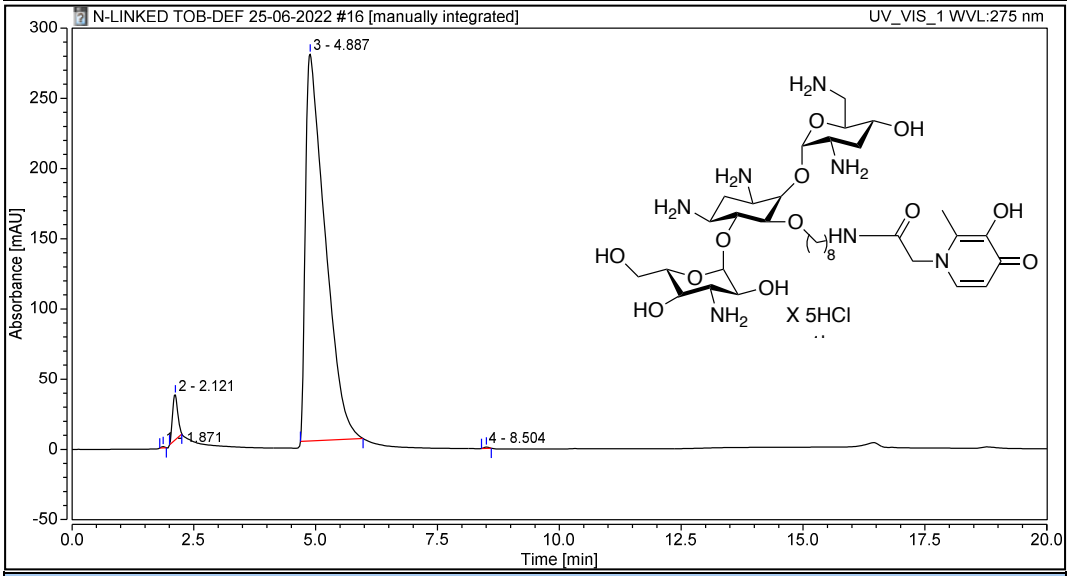

Integration Results

No.	Peak Name	Retention Time min	Area mAU*min	Height mAU	Relative Area %	Relative Height %	Amount n.a.
1		1.871	0.081	0.998	0.06	0.32	n.a.
2		2.121	4.060	31.946	3.06	10.33	n.a.
3		4.887	128.319	275.522	96.80	89.05	n.a.
4		8.504	0.106	0.928	0.08	0.30	n.a.
Total:			**132.567**	**309.394**	**100.00**	**100.00**	

Compound 24c

Chromatogram and Results

Injection Details

Injection Name:	**KG-4-30 FINAL**	*Run Time (min):*	**20.00**
Vial Number:	**R:A2**	*Injection Volume:*	**3.00**
Injection Type:	**Check Standard**	*Channel:*	**UV_VIS_1**
Calibration Level:		*Wavelength:*	**275**
Instrument Method:	**METHOD A (24-06-2022) FLOWRATE 0.3**	*Bandwidth:*	**n.a.**
Processing Method:	**Basic Quantitative**	*Dilution Factor:*	**1.0000**
Injection Date/Time:	**24/Jun/22 13:25**	*Sample Weight:*	**1.0000**

Chromatogram

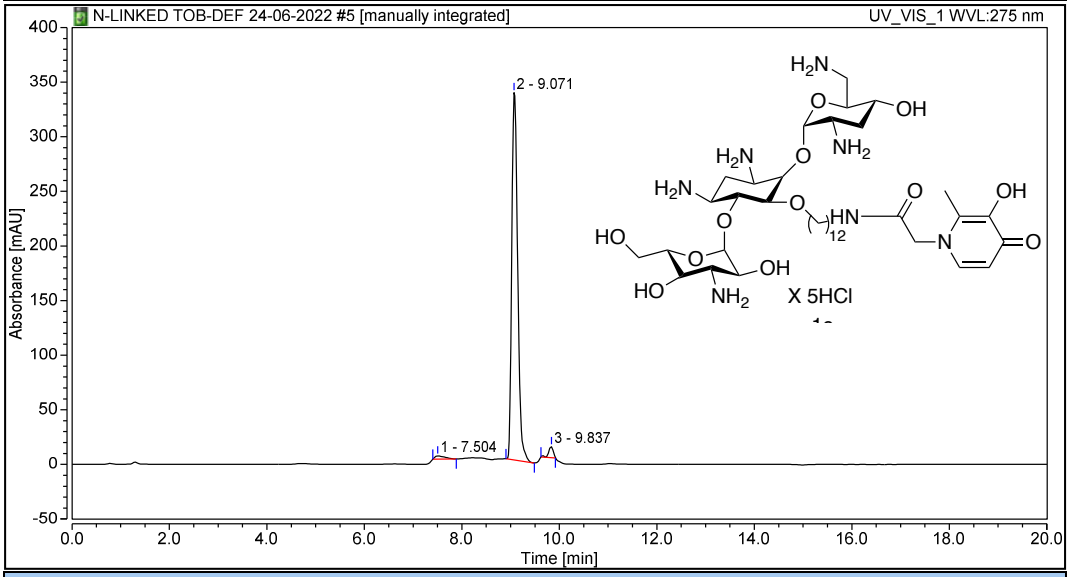

Integration Results

No.	Peak Name	Retention Time min	Area mAU*min	Height mAU	Relative Area %	Relative Height %	Amount n.a.
1		7.504	0.680	2.786	1.39	0.80	n.a.
2		9.071	47.056	336.270	96.29	96.32	n.a.
3		9.837	1.134	10.057	2.32	2.88	n.a.
Total:			**48.869**	**349.113**	**100.00**	**100.00**	

Compound 27a

Chromatogram and Results

Injection Details

Injection Name:	**KG-4-14**	*Run Time (min):*	**25.00**
Vial Number:	**G:D3**	*Injection Volume:*	**7.00**
Injection Type:	**Unknown**	*Channel:*	**UV_VIS_1**
Calibration Level:		*Wavelength:*	**280**
Instrument Method:	**TOB-DEF-9**	*Bandwidth:*	**n.a.**
Processing Method:	**Basic Quantitative**	*Dilution Factor:*	**1.0000**
Injection Date/Time:	**21/Jan/22 16:32**	*Sample Weight:*	**1.0000**

Chromatogram

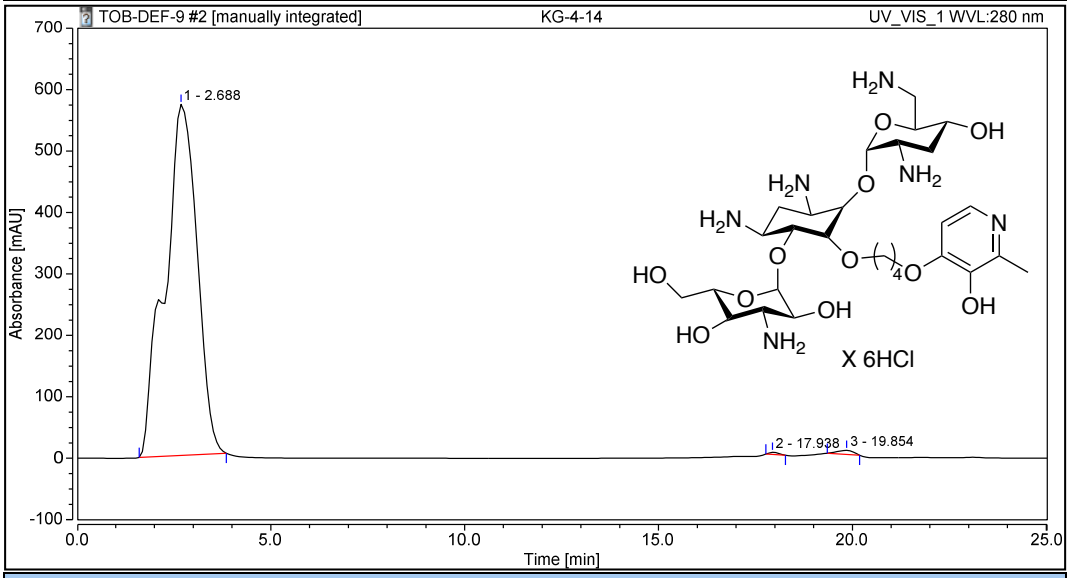

Integration Results

No.	Peak Name	Retention Time min	Area mAU*min	Height mAU	Relative Area %	Relative Height %	Amount n.a.
1		2.688	547.849	571.334	99.25	98.26	n.a.
2		17.938	1.017	3.430	0.18	0.59	n.a.
3		19.854	3.125	6.665	0.57	1.15	n.a.
Total:			**551.990**	**581.429**	**100.00**	**100.00**	

Compound 27b

Chromatogram and Results

Injection Details

Injection Name:	**KG-4-10**	*Run Time (min):*	**20.00**
Vial Number:	**G:D2**	*Injection Volume:*	**7.00**
Injection Type:	**Unknown**	*Channel:*	**UV_VIS_1**
Calibration Level:		*Wavelength:*	**280**
Instrument Method:	**TOB-DEF-7**	*Bandwidth:*	**n.a.**
Processing Method:	**Basic Quantitative**	*Dilution Factor:*	**1.0000**
Injection Date/Time:	**21/Jan/22 15:23**	*Sample Weight:*	**1.0000**

Chromatogram

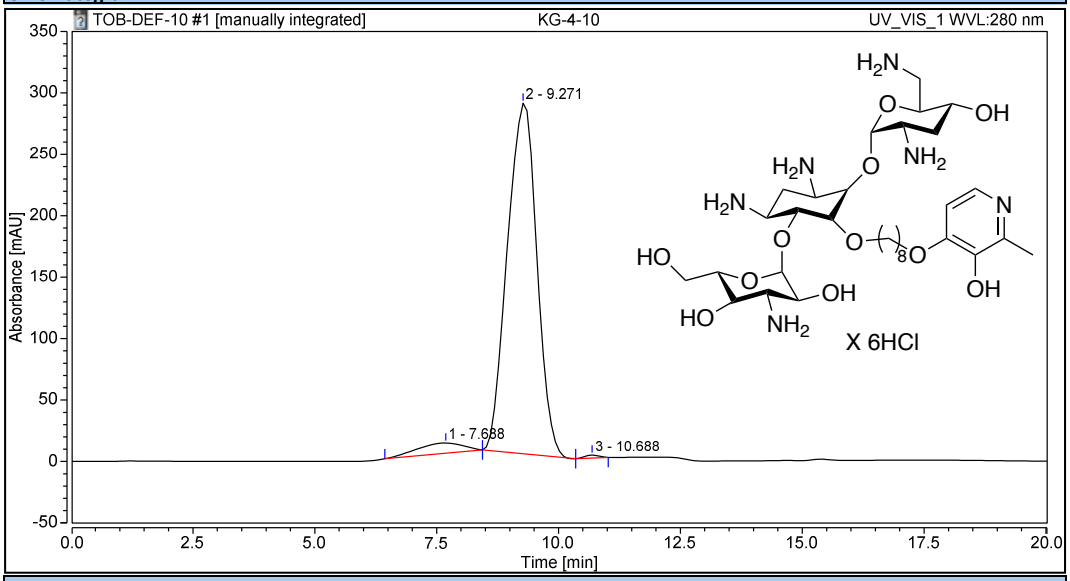

Integration Results

No.	Peak Name	Retention Time min	Area mAU*min	Height mAU	Relative Area %	Relative Height %	Amount n.a.
1		7.688	9.331	8.261	4.43	2.79	n.a.
2		9.271	200.376	285.309	95.17	96.40	n.a.
3		10.688	0.836	2.397	0.40	0.81	n.a.
Total:			**210.543**	**295.968**	**100.00**	**100.00**	

Compound 27c

Chromatogram and Results

Injection Details

Injection Name:	**KG-4-13**	*Run Time (min):*	**20.00**
Vial Number:	**G:D1**	*Injection Volume:*	**7.00**
Injection Type:	**Unknown**	*Channel:*	**UV_VIS_1**
Calibration Level:		*Wavelength:*	**280**
Instrument Method:	**TOB-DEF-1**	*Bandwidth:*	**n.a.**
Processing Method:	**Basic Quantitative**	*Dilution Factor:*	**1.0000**
Injection Date/Time:	**20/Jan/22 15:44**	*Sample Weight:*	**1.0000**

Chromatogram

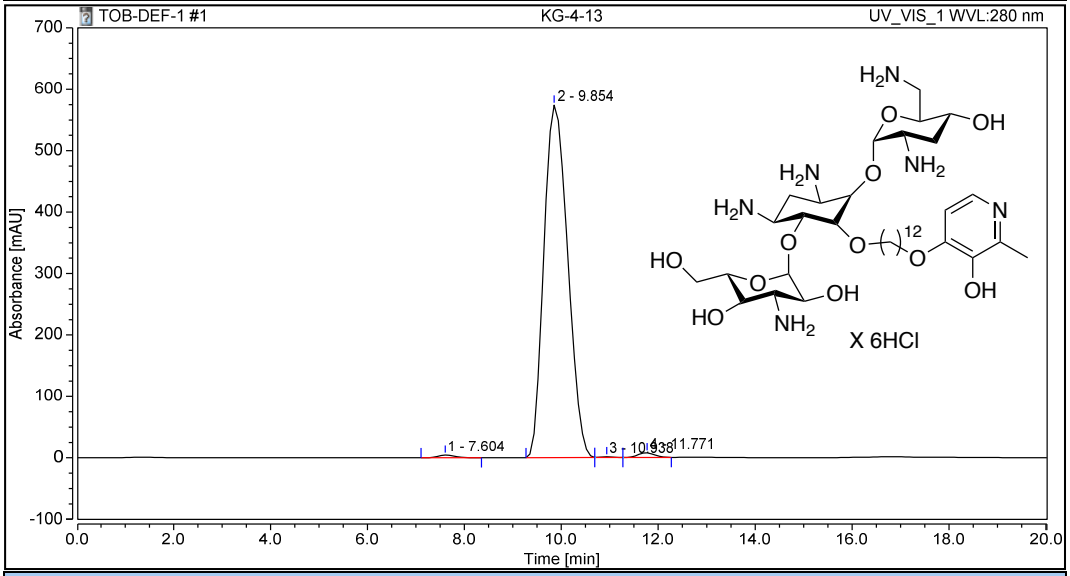

Integration Results

No.	Peak Name	Retention Time min	Area mAU*min	Height mAU	Relative Area %	Relative Height %	Amount n.a.
1		7.604	1.761	4.288	0.53	0.73	n.a.
2		9.854	326.527	573.927	98.48	97.84	n.a.
3		10.938	0.339	1.077	0.10	0.18	n.a.
4		11.771	2.923	7.325	0.88	1.25	n.a.
Total:			**331.551**	**586.618**	**100.00**	**100.00**	

HPLC method for **compound 24a**

Buffer A: 0.1% TFA in water; Buffer B: 0.1% TFA in acetonitrile

Flow rate: 0.15 ml/min; run time: 9 min; UV-Visible detection at 275 nm

Time duration (min)	% Buffer A	% Buffer B
0	99	1
1	99	1
2	95	5
3	95	5
4	75	25
5	75	25
6	50	50
7	50	50
8	99	1
9	99	1

HPLC method for **compound 24b**

Buffer A: 0.1% TFA in water; Buffer B: 0.1% TFA in acetonitrile

Flow rate: 0.15 ml/min; run time: 20 min; UV-Visible detection at 275 nm

Time duration (min)	% Buffer A	% Buffer B
0	95	5
3	95	5
4	90	10
6	90	10
7	85	15
9	85	15
10	75	25
13	75	25
14	50	50
15	50	50
18	95	5
20	95	5

HPLC method for **compound 24c**

Buffer A: 0.1% TFA in water; Buffer B: 0.1% TFA in acetonitrile

Flow rate: 0.3 ml/min; run time: 20 min; UV-Visible detection at 275 nm

Time duration (min)	% Buffer A	% Buffer B
0	90	10
3	90	10
4	85	15
6	85	15
7	60	20
9	60	20
10	70	30
13	70	30
14	50	50
15	50	50
18	90	10
20	90	10

HPLC method for **compound 27a**

Buffer A: 0.1% TFA in water; Buffer B: 0.1% TFA in acetonitrile

Flow rate: 0.1 ml/min; run time: 25 min; UV-Visible detection at 280 nm

Time duration (min)	% Buffer A	% Buffer B
0	98	2
3	98	2
4	97	3
6	97	3
7	95	5
8	95	5
9	85	15
10	85	15
12	70	30
14	70	30
16	50	50
18	50	50
20	70	30
22	98	2
25	98	2

HPLC method for **compound 27b**

Buffer A: 0.1% TFA in water; Buffer B: 0.1% TFA in acetonitrile

Flow rate: 0.2 ml/min; run time: 20 min; UV-Visible detection at 280 nm

Time duration (min)	% Buffer A	% Buffer B
0	97	3
3	97	3
4	95	5
6	95	5
7	70	30
9	70	30
10	60	40
13	60	40
14	50	50
15	50	50
18	97	3
20	97	3

HPLC method for **compound 27c**

Buffer A: 0.1% TFA in water; Buffer B: 0.1% TFA in acetonitrile

Flow rate: 0.2 ml/min; run time: 20 min; UV-Visible detection at 280 nm

Time duration (min)	% Buffer A	% Buffer B
0	90	10
3	90	10
4	85	15
6	85	15
7	60	20
9	60	20
10	70	30
13	70	30
14	50	50
15	50	50
18	90	10
20	90	10